Copy 31

NASA TM SX-531

TECHNICAL MEMORANDUM

SX-531

for the

U.S. Air Force

FLIGHT TESTS OF A 1/6-SCALE MODEL OF THE HAWKER P 1127 JET VTOL AIRPLANE

By Charles C. Smith, Jr.

Langley Research Center
Langley Field, Va.

NATIONAL AERONAUTICS AND SPACE ADMINISTRATION

WASHINGTON

MAR 16 1961

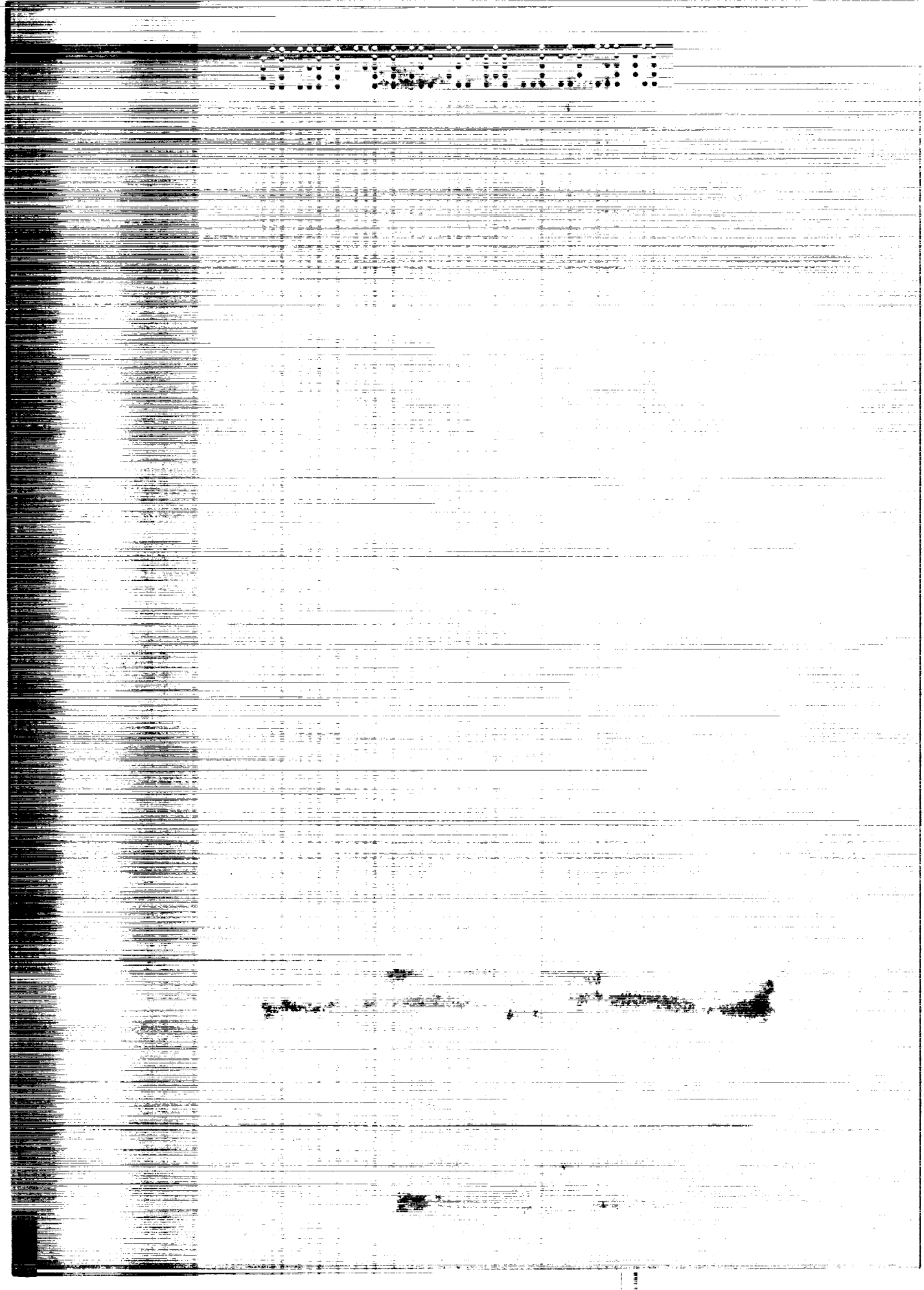

[redacted]

NATIONAL AERONAUTICS AND SPACE ADMINISTRATION

TECHNICAL MEMORANDUM SX-531

for the

U.S. Air Force

FLIGHT TESTS OF A 1/6-SCALE MODEL OF THE HAWKER P 1127 JET VTOL AIRPLANE*

By Charles C. Smith, Jr.

SUMMARY

An experimental investigation has been made to determine the dynamic stability and control characteristics of a 1/6-scale flying model of the Hawker P 1127 jet vertical-take-off-and-landing (VTOL) airplane in hovering and transition flight. The model was powered by a counter-rotating ducted fan driven by compressed-air jets at the tips of the fan blades. In hovering flight the model was controlled by jet-reaction controls which consisted of yaw and pitch jets at the extremities of the fuselage and a roll jet on each wing tip. In forward flight the model was controlled by conventional ailerons and rudder and an all-movable horizontal tail. In hovering flight the model could be flown smoothly and easily, but the roll control was considered too weak for rapid maneuvering or hovering in gusty air. Transitions from hovering to normal forward flight and back to hovering could be made smoothly and consistently and with only moderate changes in longitudinal trim. The model had a static longitudinal instability or pitch-up tendency throughout the transition range, but the rate of divergence in the pitch-up was moderate and the model could be controlled easily provided the angle of attack was not allowed to become too high. In both the transition and normal forward flight conditions the lateral motions of the model were difficult to control at high angles of attack, apparently because of low directional stability at small angles of sideslip. The longitudinal stability of the model in normal forward flight was generally satisfactory, but there was a decided pitch-up tendency for the flap-down condition at high angles of attack. In the VTOL landing approach condition, with the jets directed straight down or slightly forward, the nose-down pitch trim required was greater than in the transitions from hovering to forward flight, but the longitudinal instability was about the same. Take-offs and landings in still air could be made smoothly although there was a slight unfavorable ground effect on lift and a nose-down change in pitch trim near the ground. Short take-offs and landings could be made smoothly and consistently although the model experienced a decided nose-up change in pitching moment as it climbed out of ground effect.

---

*Title, [redacted]

[redacted]

INTRODUCTION

At the request of the Air Force an investigation has been made to determine the low-speed dynamic stability and control characteristics of a 1/6-scale flying model of the Hawker P 1127 jet vertical-take-off-and-landing (VTOL) airplane in hovering and transition flight. This airplane has a swept wing mounted high on the fuselage and is powered by a single Bristol Siddeley BS 53 turbofan engine exhausting through four rotatable nozzles, two on each side of the fuselage. Take-offs and landings with the airplane in a horizontal attitude are made with the nozzles rotated so that the exhaust of the engine is directed downward. In forward flight the nozzles are rotated so that the exhaust of the engine is directed to the rear. Control for hovering and low-speed flight is provided by jet-reaction controls located near the airplane extremities (the wing tips and the ends of the fuselage). Conventional aerodynamic controls consisting of ailerons, rudder, and an all-movable horizontal tail are provided for control in normal forward flight.

The investigation consisted of: (1) free-flight tests in still air for the study of the vertical-take-off-and-landing and hovering-flight conditions, (2) free-flight tests in the Langley full-scale tunnel for the study of slow constant-altitude transitions, and (3) control-line tests to study longitudinal stability and control in rapid transitions and short take-offs and landings. Force tests were also made, mainly as an aid in the interpretation of the flight-test results.

SYMBOLS

The forces and moments are referred to either the wind axes or the body axes, and the particular axis system used is indicated on each of the figures in which the data are presented. The wind axes are shown in figure 1 and the body axes, in figure 2. These figures also show the positive direction of forces, moments, and angles.

S	wing area, sq ft
b	wing span, ft
V	airspeed, knots
ρ	air density, slugs/cu ft
q	dynamic pressure, $\frac{\rho V^2}{2}$, lb/sq ft

c	chord, ft
α	angle of attack, deg
β	angle of sideslip, deg
F	thrust of jet control, lb
F_Y	lateral force, lb
M_X	rolling moment, ft-lb
M_Y	pitching moment, ft-lb
M_Z	yawing moment, ft-lb
C_Y	lateral-force coefficient, $\frac{F_Y}{qS}$
C_l	rolling-moment coefficient, $\frac{M_X}{qSb}$
C_n	yawing-moment coefficient, $\frac{M_Z}{qSb}$
C_{Y_β}	variation of lateral-force coefficient with angle of sideslip, $\frac{\partial C_Y}{\partial \beta}$, per deg
C_{l_β}	variation of rolling-moment coefficient with angle of sideslip, $\frac{\partial C_l}{\partial \beta}$, per deg
C_{n_β}	variation of yawing-moment coefficient with angle of sideslip, $\frac{\partial C_n}{\partial \beta}$, per deg
M_{Y_α}	variation of pitching moment with angle of attack, $\frac{\partial M_Y}{\partial \alpha}$, ft-lb/deg
F_{Y_β}	variation of lateral force with angle of sideslip, $\frac{\partial F_Y}{\partial \beta}$, lb/deg

[redacted]

M_{Z_β}	variation of yawing moment with angle of sideslip, $\frac{\partial M_Z}{\partial \beta}$, ft-lb/deg
M_{X_β}	variation of rolling moment with angle of sideslip, $\frac{\partial M_X}{\partial \beta}$, ft-lb/deg
δ_f	wing-flap deflection, deg
Δ	nozzle angle relative to fuselage reference line, deg
h	height of bottom of wheels of main landing gear above ground, in.
t/c	thickness-chord ratio
i_t	horizontal-tail incidence relative to fuselage reference line, deg
θ	angle of pitch of fuselage reference line relative to normal ground angle of airplane of 9°, deg
ϕ	angle of bank about fuselage X-axis, deg
I_X	moment of inertia about X-axis, slug-ft^2
I_Y	moment of inertia about Y-axis, slug-ft^2
I_Z	moment of inertia about Z-axis, slug-ft^2
X,Y,Z	longitudinal, lateral, and vertical axes

Subscript:

w	wind axis system

APPARATUS AND TESTS

Model

Photographs of the 1/6-scale model are presented in figures 3 and 4, and a sketch showing some of the more important model dimensions is presented in figure 5. It should be noted that, for some flight tests, the model was provided with an alternate wing flap with the revised planform

[redacted]

indicated by dashed lines in figure 5. A sketch showing the location of strakes and wing-tank pylons and an alternate horizontal-tail position on the model is presented as figure 6. The geometric characteristics of the model are presented in table I, and the mass characteristics are presented in table II. The engine exhaust nozzles on the sides of the fuselage rotated through angles as great as 100° for various phases of the transition and vertical take-offs and landing maneuvers.

The model was powered by a counter-rotating ducted fan powered by compressed-air jets at the tips of the fan blades. This power plant gave a reasonably accurate simulation of the engine of the full-scale airplane from an aerodynamic point of view. It was not possible, of course, to represent exactly the characteristics of the full-scale turbofan engine with the cold airflow of the model. In order to represent the jet interference properly, it was believed necessary to duplicate correctly the thrust of the individual nozzles and to represent approximately the proper size of the jet stream from each nozzle. Also, in order to represent the aerodynamic effects of the inlet, it was believed necessary to have the proper scaled-down inlet mass flow. For the exhaust simulation, therefore, the individual thrusts of the front and rear nozzles were correctly scaled and the total exhaust nozzle area was exactly the true scaled value. With these two characteristics set, the front nozzles were slightly larger than scale size, the rear nozzles were slightly smaller than scale size, and therefore the exhaust stream was approximately the correct scale size. With the exhaust flow represented in this manner, the inlet mass flow was about 90 percent of the correct scaled-down mass flow. The power simulation was set up in the foregoing manner for the static thrust condition. The adequacy of the simulation was not checked for forward flight conditions but the simulation must have been reasonably good since the conditions for flight required that the exhaust momentum, or thrust, be correctly represented.

Control for hovering flight was obtained by means of continuous-bleed air jets directed downward and located on the front and rear of the fuselage and on each wing tip. Roll control was obtained by reducing the thrust of one wing-tip jet and increasing the thrust of the other wing-tip jet. Pitch control was obtained by reducing the thrust of the jet at one end of the fuselage and increasing the thrust of the jet at the opposite end of the fuselage. Yaw control was obtained by rotating the pitch-control jets differentially about an axis parallel to the fuselage reference line with a maximum deflection of 20°. Each of the jet-reaction controls was adjusted to give approximately the scaled-down moment produced by the jet-reaction controls of the airplane in hovering flight. The moment produced by the jet-reaction controls varied with the power required to fly because the air for the reaction controls was obtained by bleeding the air supply to the ducted-fan power unit. The calibration of the pitch and roll jet controls is presented as figure 7.

[redacted]

The calibration shows the variation of F, the thrust of a single control jet in pounds, with the static thrust of the model power plant in pounds. The manner in which the jet control force varies with engine thrust for the full-scale airplane is not known; but, if it is presumed that the controls use a constant percentage of the high-pressure compressor airflow, as would seem to be the case, the true scaled-down variation would be that indicated by the dashed curve on figure 7 for comparison with the model characteristics. These data indicate that the model had slightly more than the correct scaled-down jet control forces at the hovering thrust of about 42 pounds and less than scale thrust at low power settings.

The aerodynamic controls for forward flight consisted of conventional ailerons, rudder, and an all-movable horizontal-tail. The ailerons and horizontal tail were always operated in conjunction with the roll and pitch jet controls. The rudder was used for directional trim in forward flight, but was not operated in conjunction with the jet yaw control, since the jet control, operated by the deflections required in hovering flight, provided all the yawing moment that was required in forward flight for the range of speeds covered in the tests.

All controls (aerodynamic and jet) were of the flicker type (full on or off) with integrating trimmers. These trimmers trimmed the control a small amount in the direction the control was moved each time a control deflection was applied. With actuators of this type, a model becomes accurately trimmed after flying a short time in a given flight condition. The aerodynamic-control deflections applied by a flick of the controls were as follows:

Horizontal-tail deflections, deg	±7
Rudder deflections	used for trim only
Aileron deflections, deg	±7 to ±14

The thrust of the ducted-fan power unit was adjusted by means of a valve in the air supply line, with approximately 35 feet of flexible hose between the valve and the model. This long length of hose between the throttling valve and the model motor, of course, caused considerable lag in the thrust control which was somewhat objectionable, but was no worse than the lag in other systems used to power free-flight models.

Test Equipment and Technique

Transition and landing approach flight tests were conducted in the test section of the Langley full-scale tunnel using the test setup illustrated in figure 8. This sketch shows the pitch pilot, the safety-cable operator, and the power operator on a balcony at the side of the test section. The roll and yaw pilots were located in an enclosure in the

lower rear part of the test section. The pitch, roll, and yaw pilots were located at the best available vantage points for observing and controlling the particular phase of the motion with which each was concerned. Motion-picture records were obtained with fixed cameras mounted near the pitch pilot and at the top rear of the test section.

The air for the ducted-fan power unit, jet controls, and control actuators was supplied through flexible plastic hoses while power for the electric trim motors and control solenoids was supplied through wires. These wires and tubes were suspended overhead and taped to a safety cable $\left(\frac{1}{16}\text{-inch braided aircraft cable}\right)$ from a point approximately 15 feet above the model down to the model. The safety cable, which was attached to the top of the wing over the center of gravity, was used to prevent crashes in the event of a power or control failure, or in the event that the pilots lost control of the model. During the flight the cable was kept slack so that it would not appreciably influence the motions of the model.

The test technique is best explained by describing a typical flight. The model hung from the safety cable and the power was increased until the model was in steady hovering flight. At this point the tunnel drive motors were turned on and the airspeed began to increase. As the airspeed increased, the controls and power were operated and the nozzles on the sides of the fuselage were rotated so that the jets were tilted progressively to maintain the fore-and-aft position of the model in the test section as the speed was increased and the transition to normal forward flight was performed. Transitions made in this manner were limited to very low rates of acceleration because of the slow rate at which the tunnel airspeed could be increased. Of course, it was also possible to hold the tunnel speed constant at various values in the transition range so that the model could be flown for extended periods of time at various stages in the transition range for detailed study of its behavior in these conditions. It was also possible to make slow-down transitions by reducing the airspeed in the tunnel, but there was little difference between the conditions for speed-up and slow-down transitions in the tunnel because of the low rates of change of tunnel speed that could be obtained. All these tests were made at effectively zero longitudinal acceleration. In most cases the flight was terminated by gradually taking up the slack in the safety cable while reducing the power to the model.

One of the proposed techniques for the landing approach and transition of the airplane is to start the approach in either level or gliding flight by reducing power to idle and rotating the nozzles to a deflection of 90° or 100°. As the airspeed drops off or is reduced in a flare, and the wings are no longer capable of supporting the airplane, the engine thrust is gradually increased to maintain the necessary lift until the

airplane comes to a stop in hovering flight. In order to simulate this condition in the tunnel, the model was propelled with a compressed-air jet exhausting rearward from the rear of the fuselage so that the model could be flown in steady level flight with the engine nozzles at an arbitrary deflection and thrust setting that would not propel the model in level flight. The thrust of this jet effectively represented the forward component of the weight of the airplane in a gliding descent or the force due to longitudinal deceleration. This device therefore made it possible to duplicate the aerodynamic forces and engine thrust and nozzle deflection conditions corresponding to descent or deceleration conditions with the model flying in level constant-speed flight in the tunnel.

For these landing-approach and transition tests the model was towed by the safety cable as the airspeed of the tunnel was increased to the test condition. The angle of attack was then increased to the condition desired for the test, the engine thrust was brought up to supply the remainder of the lift necessary to support the model, and the thrust of the propulsion jet at the rear of the fuselage was increased to balance the drag of the model. Once the test condition had been established the model could be flown steadily at this condition or the tunnel airspeed could be gradually reduced to zero and the landing, or slow-down, transition performed.

The vertical take-off, landing, and hovering flight tests were made by using the same general setup and test technique used for the transition tests except that these tests were conducted in the return passage of the full-scale tunnel for convenience and to provide protection from weather and from the random effects of outside air gusts. The air in the return passage of the tunnel was not completely still after a short period of flight, however, because of the random recirculation of the model exhaust.

The control-line facility is illustrated in figure 9 and described in detail in reference 1. Basically the control-line facility consists of a crane with a jib boom to provide an overhead support for the safety cable. The pilot and operators ride in the cab of the crane so that they will always face the model as it flies in a circle at the end of a restraining line which opposed the centrifugal force. The restraining line entered the model at the center of gravity and provided some restraint of the lateral freedom of the model but did not affect the longitudinal degrees of freedom. The facility is mounted on a pedestal in the middle of a large concrete apron located in a wooded area which serves as a wind break. With this facility rapid transition flights from hovering to normal forward flight, or vice versa, can be made since the crane has a high rate of acceleration. Actually the crane can accelerate rapidly enough to keep up with a forward or rearward model acceleration of 1 g. Running take-offs and landings can also be performed with this facility.

Tests

The investigation consisted mostly of flight tests to study the stability and control characteristics of the model. The stability and controllability were determined in various tests either qualitatively from pilots' observations or quantitatively from motion-picture records of the flights.

Flight tests were made in the test section of the full-scale tunnel to determine the overall stability and control characteristics of the model in transition flight from hovering to forward flight. These flights were slow constant-altitude transitions covering a speed range from about 0 to 48 knots (full-scale airspeeds from 0 to 118 knots). Since small adjustments or corrections in the tunnel airspeed could not be made readily, the pitch pilot and the power operator had to make adjustments continually to hold the model in the center of the test section. Flights were also made in which the airspeed was held constant at intermediate speeds so that the stability and control characteristics at a particular speed could be studied. The transition tests also included flights to represent the proposed landing-approach condition for the airplane in which the nozzles are kept at approximately 100° incidence during the approach and transition.

In order to study the stability and control characteristics of the model in rapid transitions and short take-offs and landings, flight tests were also made on the control-line facility. This part of the investigation was limited to a study of longitudinal stability and control since the model is restrained in the lateral degrees of freedom by the control line.

Hovering flight tests were made with the model hovering at heights of 5 to 15 feet above the ground to determine the basic stability and controllability of the model. Hovering flight tests were also made at very low heights in order to study the effects of ground proximity on stability and control. Vertical take-offs and landings were also made to study the behavior of the model in these transient conditions. These take-off and landing and ground-effect tests were made both with and without the strakes shown in figure 6 and with and without the wing-tank pylons.

Some preliminary force tests were made in a low-speed tunnel with a 12-foot octagonal test section in an effort to determine some of the stability and control characteristics of the model in transition flight. The longitudinal force tests were made at various nozzle angles for a range of power settings. The lateral tests were made at various nozzle angles with power on at the setting required to balance the drag along the wind axis for the zero sideslip condition. These lateral tests,

therefore, duplicated the condition of flight at zero longitudinal acceleration which was the condition for the free-flight tests in the Langley full-scale tunnel. Practically all the force tests were made with the model in the original, or basic, condition, but a few tests were made with the horizontal tail in the alternate position to study the effect of this change in tail location on static longitudinal stability. A few force tests were also made to determine the variation of pitching moment, rolling moment, and lift with height of the model above the ground. These tests were made inside where the model was free from the random effects of outside air gusts.

All the force tests and most of the flight tests were made with the flap shown in solid lines in figure 5 used for the flap-down conditions. It should be understood that the symbol δ_f or the term "flap-down" refers to the use of this flap except in the case of a few slow transition flight tests in the full-scale tunnel where the use of the alternate flap, shown by dotted lines in figure 5, is specifically mentioned.

RESULTS AND DISCUSSION

A motion-picture film supplement illustrating the flight-test results has been prepared and is available on loan. A request card form and a description of the film will be found at the back of this paper, on the page immediately preceding the abstract and index pages.

Hovering Flight

The model could be flown successfully in hovering flight in relatively still air. It could be flown smoothly and could be maneuvered readily from one position to another. The main difficulty encountered in the tests was that the roll control was undesirably weak when the jet-reaction control power was set at the proper value to represent the design value for the full-scale airplane.

As pointed out previously, the roll jet-reaction controls were not as strong as might be desired, and it was sometimes difficult for the pilots to restore the model to a steady-flight condition after it had been allowed to move about quickly or after it had been disturbed by a violent motion of the flight cable or by turbulence in the air induced by recirculation of the exhaust air from the model. With the thrust of the roll jet-reaction control increased to give approximately 1.5 times the scaled-down control moment of the airplane, the model could be maneuvered fairly easily and could be settled down quickly after fairly violent disturbances. Even when the model was provided with this amount

of control, however, its motions were not as smooth and steady and it was not as easy to control as might be desired, evidently because of the absence of damping in roll. The results of the tests, therefore, indicate that the pilot would have sufficient jet-reaction control for hovering the full-scale airplane in still air but a stronger control would be desirable to overcome disturbances such as might be experienced in gusty air, and that some form of roll-rate stabilization would also be desirable.

The pitching motions of the model seemed to be about neutrally stable as would ordinarily be expected for a jet VTOL configuration. The pitching motions were relatively slow and were not easily excited by outside effects such as gust disturbances or movements of the control and power cable because of the relatively high moment of inertia of the model in pitch. The jet-reaction pitch control seemed entirely adequate for control of the model in any condition encountered in the tests; it was strong enough to give adequate rates of acceleration for adequate control, but not overly powerful so that it would tend to lead to overcontrol and a waste of power.

The yaw control of the model seemed adequate for safe visual flight although it was much less than is recommended by suggested control criteria of reference 2 as being desirable for helicopters and VTOL aircraft in hovering and low-speed forward flight.

Vertical Take-Offs and Landings and Ground Effect

Vertical take-offs and landings could be performed smoothly and consistently in still air. For the model in the basic configuration there appeared to be a slight adverse ground effect on the lift and a slight nose-down trim change when the model was near the ground. The use of longitudinal strakes on the underside of the fuselage as suggested by the manufacturer and shown in figure 6 caused the ground effect on lift to become slightly favorable, but also caused an increase in the nose-down trim change. The use of wing-tank pylons with the strakes appeared to cancel the effects of the strakes in that there was no apparent difference in the flying characteristics between this configuration and the basic model. Deflecting the flaps down 50° on the basic model made no change in the effect of the proximity of the ground on lift and pitch that was noticeable in the flight tests. Although the model experienced changes in pitch trim with height above the ground in all of the take-off and landing tests, the pilot had no difficulty in controlling the model by using approximately one-half the scaled-down pitch and yaw jet control forces. The scaled-down roll-jet control force was used in all of the take-off and landing tests and was considered weak as it had been considered in the hovering flight tests.

[redacted]

The results of some preliminary force tests made to determine the effect of the proximity of the ground on the lift and the static lateral and longitudinal stability of the model are presented as figures 10 to 13. The data presented in figure 10 show that, for the basic model, there was about a 2-percent adverse effect on lift and a nose-down trim change when the model was near the ground. The use of strakes on the underside of the fuselage caused the ground effect on lift to become favorable but also increased the nose-down trim change. The addition of wing-tank pylons to this configuration made the ground effect on lift more adverse and reduced the trim change to that of the basic model. In general, the variation of pitching moment with height above the ground was about the same for the flap-down condition as for the flap-up condition. The force tests indicated that the effect of ground proximity on lift, however, was somewhat more adverse for flap-down condition than the flap-up condition; but, as previously indicated, this difference was not sufficient to be noticeable in the flight tests.

The effect of the proximity of the ground on the static longitudinal stability of the model is shown by the data presented in figure 11. The data show that the basic model has neutral static longitudinal stability when out of ground effect, as would be expected, and becomes generally unstable as it approaches the ground. At heights below about 12 inches the model is about neutrally stable for nose-down changes and unstable for nose-up changes in pitch attitude. (Note that the pitch angle indicated in fig. 11 is measured relative to the normal 9° ground angle of the model.) This instability for nose-up changes is presumed to result from a change in the reflection of the downwardly deflected jets back up around the horizontal tail as a result of changes in pitch attitudes of the model. A comparison of the data presented in figures 11(a) to 11(d) shows that the use of strakes, flaps, extension of the landing-gear doors, did not have any great effect on the static longitudinal stability of the model. The data presented in figures 11(e) to 11(h) show that the pitch jet-reaction controls had an appreciable effect on the longitudinal stability particularly when the model was close to the ground. With the jet controls on, the model becomes stable for nose-down changes in pitch attitude when close to the ground.

The data presented in figures 12 and 13 show that the model is statically unstable in roll when near the ground. The use of strakes, wing-tank pylons, or flaps had no appreciable effect on the static lateral stability as shown by the data presented in figures 12(a) to 12(f). The data of figures 12 and 13 show that the roll jet-reaction controls caused no appreciable change in the stability of the basic model or of model with flaps deflected, but for the strakes-on case the model was slightly less unstable close to the ground.

Transition Flight

Longitudinal characteristics in slow transitions.- Slow constant-altitude transitions from hovering to forward flight or steady flight at more-or-less constant airspeeds in the transition range could be made smoothly and consistently on the control-line facility or in the test section of the full-scale tunnel. At low angles of attack the model appeared to be neutrally stable or slightly unstable and at the high angles of attack it had a decided pitch-up tendency in the transition range. The rate of divergence of the pitch-up was moderate because of the low airspeeds involved and could be controlled easily provided the angle of attack was not allowed to become too high. In order to provide adequate nose-down moment for trim and control in the transition range, however, it was necessary to change to a range of stabilizer incidence of -2° to $+12^\circ$ instead of the range of -12° to $+3^\circ$ which was originally specified by the manufacturer. This change in stabilizer incidence range was obtained by changing the linkage between the stabilizer and the pitch control jet so that the stabilizer was at $4\frac{1}{2}^\circ$ when the pitch jet was in the neutral position for hovering flight instead of being at -4° when the pitch jet was neutral. The actual range of stabilizer incidence used for trim at various conditions is shown in table III. These data show that with the revised tail-incidence range, there was very little change in trim during the transition, the maximum change being from $4\frac{1}{2}^\circ$ incidence for hovering to 8° incidence for intermediate transition speeds. This change corresponds to a trim change from neutral control to one-half of the maximum available nose-down control during the transition. It should be realized that in all the tests the pitch jet was operating in conjunction with the stabilizer in such a manner that it reached maximum moment in one direction or the other at the same time that the stabilizer reached the end of its range.

The results of some preliminary force tests to determine the static longitudinal stability of the model are presented as figures 14 to 20 and a plot of $-M_{Y_\alpha}$ for angles of attack of 5°, 10°, 15°, and 20° against forward airspeed for the condition of zero drag is presented as figure 21. The data presented in this figure, both values of $-M_{Y_\alpha}$ and V, have been scaled up from the basic data to a lift of 41 pounds which was the actual weight of the model during the flight tests in the full-scale tunnel. At this weight the model represented the full-scale airplane at a weight of 8,856 pounds. These data show that for both flap conditions the model is statically unstable in the transition range and slightly stable in forward flight ($\Delta = 0^\circ$), and that the instability in the transition range becomes greater with increased angle of attack. The increased instability at the higher angles of attack was very apparent in the transition tests made in the test section of the full-scale tunnel because the

[redacted]

limited airspeed used in these tests (48 knots) caused the model to be at too high an angle of attack to complete the transition consistently for the flap-up condition. A limit of 48 knots on the tunnel airspeed was selected because it is the point where a pole change on the tunnel drive motors is required for higher speeds. This pole change causes a decided lag in the build-up of airspeed which is inconvenient and was avoided in the present tests by completing the transition at 48 knots. The model could be flown up to this speed very satisfactorily at low angles of attack and high jet deflections with the flaps at a deflection of either 0° or 50°. During the process of rotating the nozzles further to get the model completely wing-borne at this speed with flaps up, however, it was necessary to increase the angle of attack to about 18°. The pitch-up instability was very strong in this condition and the model frequently pitched up out of control. For the flap-down condition, by way of comparison, the angle of attack never exceeded 13° during the process of making the transition to wing-borne flight at the same speed, and the instability was never great enough to cause an uncontrollable pitch-up. Analysis of the force-test data indicate that this apparent difference between stability for the flap-up and flap-down conditions was simply the result of the arbitrary limitation on airspeed imposed in the wind-tunnel flight tests, and there was no reason to expect any significant difference if the transition to completely wing-borne flight were delayed to a higher airspeed, for example, to 65 or 70 knots. This analysis was supported by the results of the control-line tests in which no significant difference between the flap-up and flap-down conditions was found except in steady flight at an angle of attack of about 15° with nozzle deflections of about 45°. In this condition with flaps up, the model was considerably more unstable than in the corresponding flap-down condition.

In the slow transition tests, the model was also flown with the alternate flap, shown by the dashed lines in figure 5, as well as with the basic flap. There was no noticeable difference in the longitudinal stability and control characteristics of the model with these two flaps.

In an effort to find a "fix" for the static longitudinal instability of the model, force tests were made with the horizontal tail moved to the low position shown in figure 6. The basic data from these tests are presented in figure 20 and the results are summarized in figure 21(c). These data show that the use of the low horizontal-tail location greatly improved the static longitudinal stability. No flight tests were made with the horizontal tail in the low position, however, because the model was flyable with the original tail position and because it did not seem very practical to put the tail of the actual airplane in the low position where it would be swept by the engine exhaust as the nozzles were rotated in performing the transition.

In the landing-approach and transition tests made in the full-scale tunnel by the method previously described for simulating descent and

deceleration conditions, a range of angles of attack from 4° to 11° and forward speeds of 92 to 130 knots (full scale) were covered for nozzle angles of 90° to 100°. In these tests it was found that the model had about the same longitudinal and lateral stability and control characteristics as it did in the slow transitions from hovering to forward flight. The only significant difference between the VTOL landing-approach condition and the slow transitions was that there was an increased nose-up pitching moment which, of course, required an increased nose-down pitching moment for trim. For example, a horizontal-tail incidence of about 10° was required for the approach condition as compared with 5° for the slow transition condition.

Longitudinal characteristics in rapid transitions.- Rapid transitions from hovering to forward flight were made in the control-line tests in as little as 7 seconds (17 seconds full scale). This time was as rapid as the transition could be made without the loss of a significant amount of altitude. In general the pilot much preferred to perform the transition quickly instead of slowly since he was then not required to control the model for as long a period of time in the transition range where it was generally longitudinally unstable.

Slow-down transitions were made by starting with the model in normal unaccelerated forward flight with the nozzles pointed straight back (0° deflection) at an angle of attack of about 5°. The nozzles were then rotated to 100° deflection at a rate of 12° per second without changing the throttle setting. It was, of course, necessary to reduce the angle of attack somewhat as the nozzles rotated to prevent the model from climbing. Then, as the model slowed down, the angle of attack was gradually increased to about 10° to keep the lift constant as the speed dropped off. As the model slowed down further, the throttle was advanced to maintain the necessary lift without further increase in angle of attack. These transitions were made in about 13 seconds (32 seconds full scale). It was found that slow-down transitions could be performed very easily and consistently in this manner and that the control power was adequate with the revised stabilizer incidence range (-2° to +12°).

The total pitch jet control force (sum of force of front and rear jets) for the model for the power condition at the start of the slow-down transition was 0.52 pound (112 pounds full scale). This force, of course, increased as the thrust was increased during the transition until at hovering it was 2.26 pounds (490 pounds full scale) for a model weight of 45 pounds (9,700 pounds full scale). As pointed out previously, the manner in which the jet control force varies with engine thrust is not known for certain, but is likely to be greater than that of the model at low thrust settings as shown in figure 7. In any event, the control-line tests showed that the slow-down transition was quite easy to perform by using the foregoing amount of control and the technique just

described. This technique was not especially developed; it was a very natural procedure and was the only one tried in the tests.

Lateral characteristics.- The lateral motions of the model could be controlled successfully but considerable effort on the part of the roll pilot was required to keep the model positioned in the test section of the tunnel. At low airspeeds these difficulties seemed to be an extension of the difficulties experienced in hovering flight because of low control power and low damping in roll. At higher speeds, particularly at 48 knots where the transition to completely wing-borne flight was being made, it seems likely that the difficulty resulted from low directional stability. This low directional stability is shown in the force-test data of figures 22 and 23. These data show that for the higher angles of attack (10° to 20°) the model was directionally unstable, or neutrally stable, for small angles of sideslip. The force-test data also show that, in these conditions, the model had considerable positive dihedral effect $\left(-C_{l_\beta}\right)$. During the flight tests the low directional stability probably allowed the model to yaw around considerably at the higher angles of attack so that the dihedral effect could produce rolling moments which were difficult to control and keep trimmed. On the basis of the force-test data and analysis of the flight results, it seems that steps should be taken to improve the directional stability of the airplane at high angles of attack.

This investigation of the lateral stability and control characteristics of the model was made with the alternate flap shown by the dashed lines in figure 5 as well as with the basic flap. There was, however, no noticeable difference in the lateral behavior of the model with these two flaps.

Short Take-Offs and Landings

Short take-offs were made for a number of fixed nozzle angles from 0° (straight back) to 75°. From a performance standpoint these take-offs did not represent the airplane very well. First, they were made at fixed nozzle settings since the nozzles could not be rotated rapidly. Second, the model did not have brakes to permit the engine thrust to be brought up to a high value before the ground roll was started. Finally, it took about 7 seconds (17 seconds full scale) for the engine to reach the full-power condition which was arbitrarily limited in these tests to the value that gave a static thrust-weight ratio of 0.9. Even with these limitations, only about 100 feet (600 feet full scale) was required for the model to take off and reach a height of 8 feet (50 feet full scale) for nozzle angles in the 30° to 60° range. From a stability and control standpoint, these take-offs were quite easy to perform and there was no

particular characteristic to note except that the model experienced a decided nose-up change in pitching moment as it climbed out of ground effect.

A few short landings were also made with a nozzle angle of 60°. In these landings the effect of the ground in causing a nose-down pitching moment was not as evident as it had been in the take-off tests since the pilot was pulling the elevator up anyway as the model neared the ground to execute a flare. It is likely, therefore, that the nose-down pitching moment due to ground effect, if there was one, simply seemed like an increase in stick-position stability. It is also likely that the ground effect on trim was much less for the landing condition than for the take-off condition because of the lower power setting, since the ground effect on pitching moment is presumed to result from the reflection of the downwardly deflected jet back up around the tail plane.

Normal Forward Flight

In normal forward flight (nozzles at 0°), in either the wind-tunnel or control-line flight tests, the model was generally longitudinally stable over the small speed range covered in the tests (speeds from 55 knots down to the stall). In the flap-down condition, however, the model had a pitch-up tendency at the stall. This observation is confirmed by the force-test data of figure 21 which show unstable values of $-My_{\alpha}$ for angles of attack above about 18° with flaps down.

Both the flight tests and the force-test data of figure 21 also show that at an angle of attack of about 20°, the model flew at about 45 knots with flaps up and about 30 knots with flaps down. For a flying weight of 41 pounds, these speeds correspond to lift coefficients of 1.2 for flaps up and 2.6 for flaps down. This very high lift coefficient for the flap-down condition with a very modest-sized flap indicates that there was a very considerable thrust redirection and jet-flap effect caused by the jet exhaust impinging on and being turned downward by the lower surface of the flap. From an inspection of the geometry of the jet nozzles and flap, it seems very likely that the exhaust from both jets was impinging on the flap when the nozzles were in the normal forward flight position of 0° deflection.

In general, the lateral stability and control characteristics of the model were satisfactory over the limited speed range covered in the tests for the normal forward flight conditions except at high angles of attack (angles of approximately 10° to 20°) where the pilot had difficulty in controlling the model in roll. This difficulty undoubtedly resulted partly from the low or negative directional stability shown by the force-test data of figure 23 which permitted the model to sideslip

in random fashion so that the dihedral effect could cause considerable random rolling moments. The difficulty of controlling the lateral motions at high angles of attack might also have been caused by a reduction in aileron effectiveness as the wing neared the stall. No measurements of aileron effectiveness were made to investigate this possibility, however,

SUMMARY OF RESULTS

The results of a free-flight investigation of the stability and control characteristics of a 1/6-scale model of the Hawker P 1127 VTOL airplane can be summarized as follows:

1. In hovering flight in still air the model could be flown smoothly and moved easily from one position to another. The pitch and yaw jet-reaction controls had adequate power but the roll jet-reaction control was about two-thirds as strong as desired for restoring the model to steady flight after it had been disturbed.

2. Transitions from hovering to normal forward flight and back to hovering could be made smoothly and consistently and with only moderate changes in longitudinal trim. The model had a static longitudinal instability or pitch-up tendency throughout the transition range, but the rate of divergence was moderate and the model could be controlled easily provided the angle of attack were not allowed to become too high. The lateral motions of the model at high angles of attack (10° to 20°) during the transition were difficult to control, apparently because of low or negative directional stability at small angles of sideslip.

3. In the VTOL landing approach with the engine exhaust nozzles deflected 90° to 100°, the nose-down trim required was greater than in the transition from hovering to forward flight whereas the instability was about the same.

4. Vertical take-offs and landings in still air could be made smoothly although there was a slight unfavorable ground effect on lift and there was a nose-down change in pitch trim near the ground. The use of strakes on the underside of the fuselage made the ground effect on lift favorable but increased the nose-down change in pitch trim.

5. Short take-offs and landings could be made smoothly and consistently, and there was no particular characteristic to note except that the model experienced a decided nose-up change in pitching moment as it climbed out of ground effect. This trim change was not noticeable on landing, however.

6. In normal forward flight the model was generally longitudinally stable, but was unstable at the stall for the flaps-down case at the higher angles of attack. The lateral motions of the model in the normal forward flight condition were difficult to control at high angles of attack (10° to 20°), just as they were in the transition range, apparently because of low or negative directional stability at small angles of sideslip.

Langley Research Center,
National Aeronautics and Space Administration,
Langley Field, Va., February 28, 1961.

REFERENCES

1. Schade, Robert O.: Flight-Test Investigation on the Langley Control-Line Facility of a Model of a Propeller-Driven Tail-Sitter-Type Vertical-Take-Off Airplane With Delta Wing During Rapid Transitions. NACA TN 4070, 1957.

2. Tapscott, Robert J.: Criteria for Control and Response Characteristics of Helicopters and VTOL Aircraft in Hovering and Low-Speed Flight. Paper No. 60-51, Inst. Aero. Sci., Jan. 1960.

[redacted]

[redacted]

TABLE I.- GEOMETRIC CHARACTERISTICS OF MODEL

Wing:	
Sweepback of leading edge, deg	40
Airfoil section	Hawker symmetrical, t/c = 0.085 root, 0.07 tip
Aspect ratio	3.1
Area, sq ft	5.32
Span, ft	4
Mean aerodynamic chord, ft	1.31
Incidence angle, deg	1
Dihedral angle, deg	-10
Overall length of model, ft	7.58
Vertical tail:	
Sweepback of leading edge, deg	52
Airfoil section	Hawker symmetrical, t/c = 0.08 constant
Aspect ratio	0.72
Area, sq ft	1.11
Height, ft	0.84
Horizontal tail (all movable):	
Sweepback of leading edge, deg	45
Airfoil section	Hawker symmetrical, t/c = 0.06 constant
Aspect ratio	2.76
Area, sq ft	1.005
Span, ft	1.67
Jet controls:	
Distance of roll jets from fuselage center line, ft	2
Distance of forward pitch-yaw jet from center of gravity, ft	2.86
Distance of rear pitch-yaw jet from center of gravity, ft	3.58
Engine exhaust nozzles:	
Total area of forward nozzles, sq in.	15.10
Total area of rear nozzles, sq in.	13.20

[redacted]

TABLE II.- MASS CHARACTERISTICS OF MODEL

Weight:	
With landing gear, lb	43
Without landing gear, lb	41
Control-line tests, with landing gear, lb	45
Distance of c.g. from leading edge of M.A.C., percent M.A.C.	22
Moments of inertia:	
I_X, slug-ft^2	0.451
I_Y, slug-ft^2	2.461
I_Z, slug-ft^2	2.832

[redacted]

TABLE III.- HORIZONTAL-STABILIZER INCIDENCES USED FOR TRIM AT VARIOUS CONDITIONS

V, knots	α, deg	Δ, deg	i_t, deg (a)
$\delta_f = 50^\circ$			
0	0	90	$4\frac{1}{2}$
22	0	85	$5\frac{1}{2}$
22	5	75	6
22	10	65	7
22	15	60	7
33	5	65	$6\frac{1}{2}$
33	10	55	7
33	15	45	7
44.5	5	45	5
44.5	10	30	$5\frac{1}{2}$
44.5	15	10	3
$\delta_f = 0^\circ$			
0	0	90	$4\frac{1}{2}$
22	5	75	6
22	10	65	6
22	15	60	8
33	5	70	$5\frac{1}{2}$
33	10	60	7
33	15	55	8
44.5	10	50	7
44.5	15	35	7

[a]The jet controls and horizontal stabilizer were operated together, with the maximum jet control force being obtained at the maximum and minimum horizontal-stabilizer incidences of 13° and 0°.

[redacted]

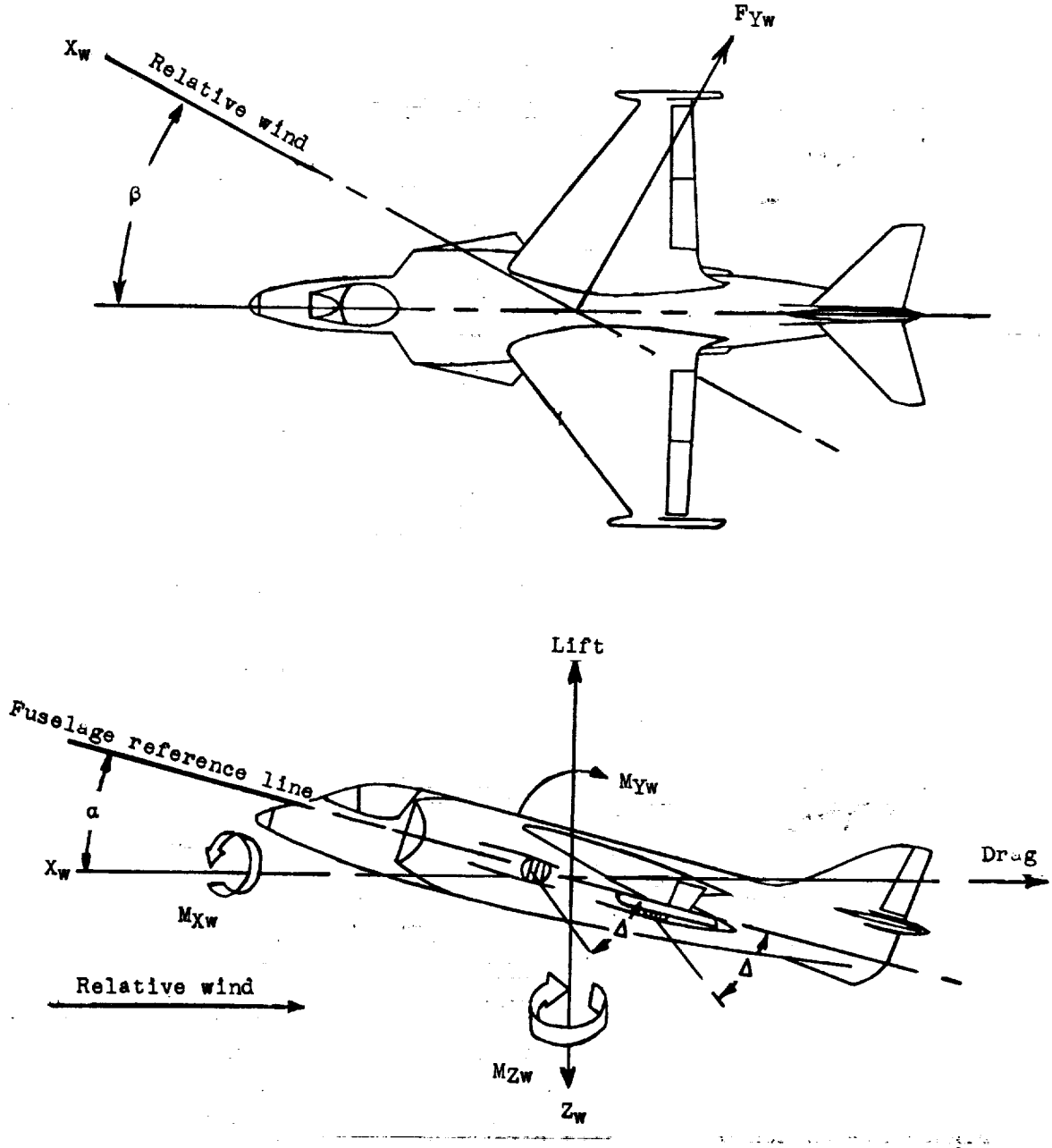

Figure 1.- Sketch of wind axis system showing positive direction of forces, moments, and angles.

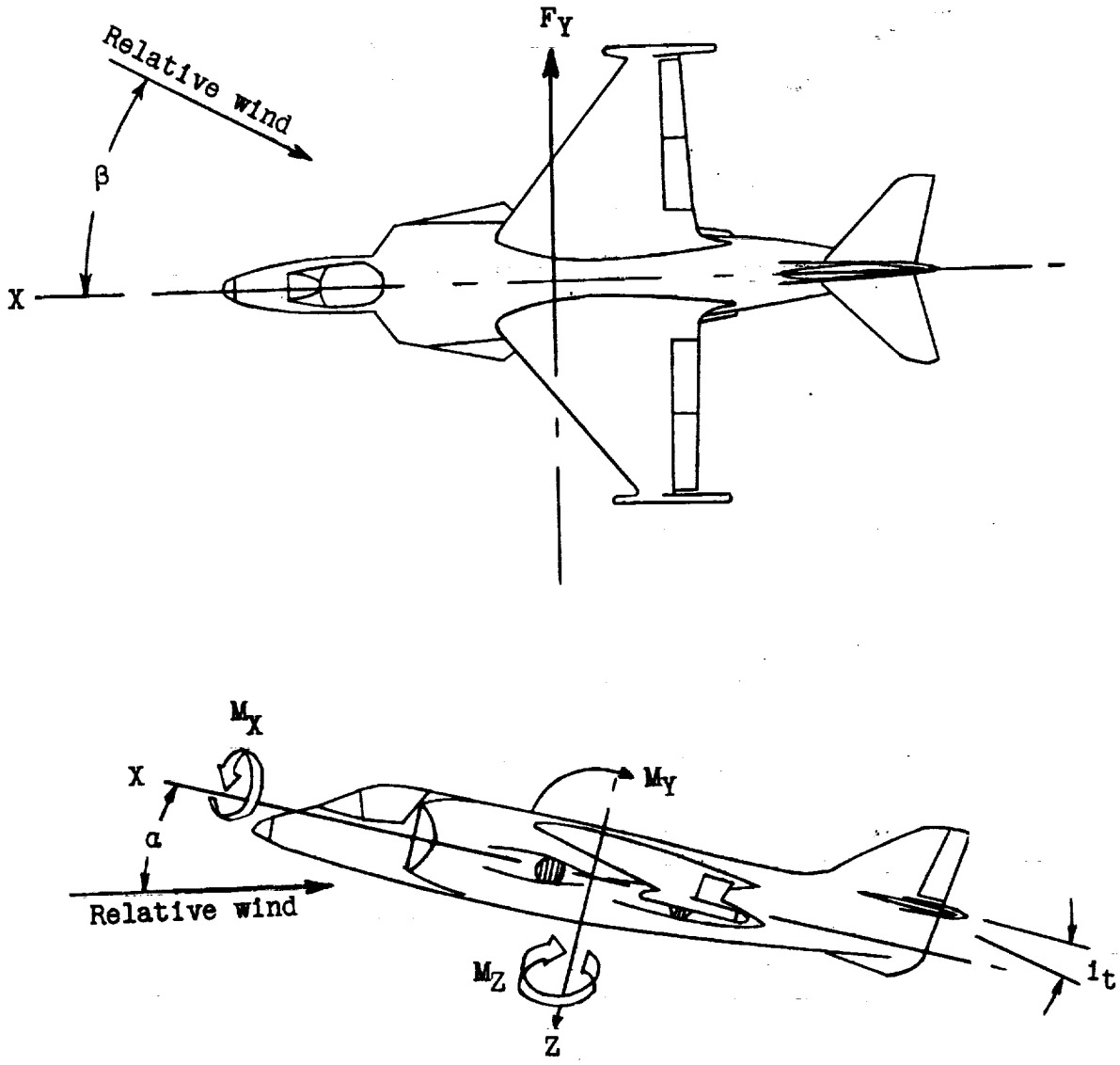

Figure 2.- Sketch of body axis system showing positive direction of forces, moments, and angles.

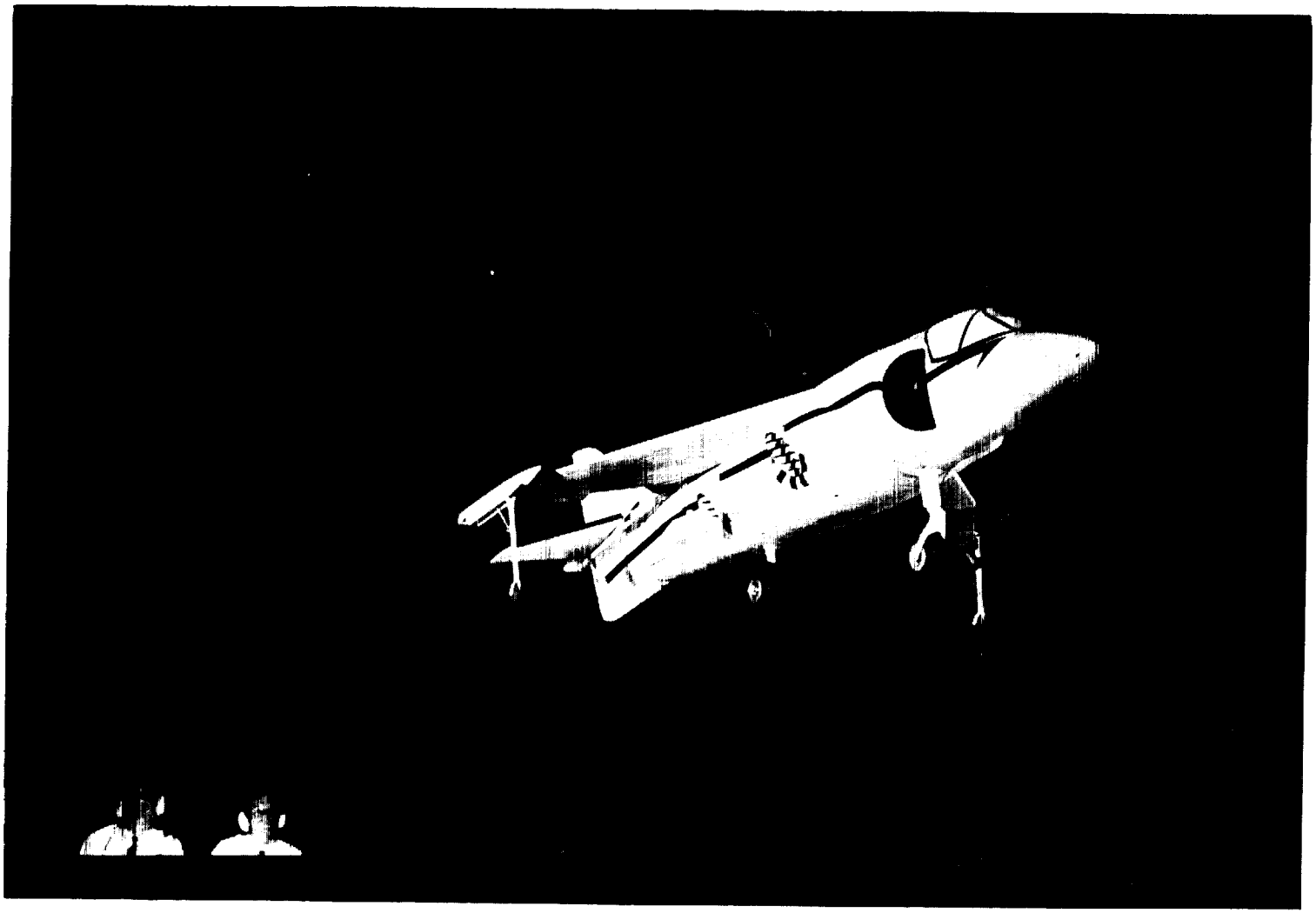

Figure 3.- Three-quarter-front view of the model in hovering flight. L-60-2543

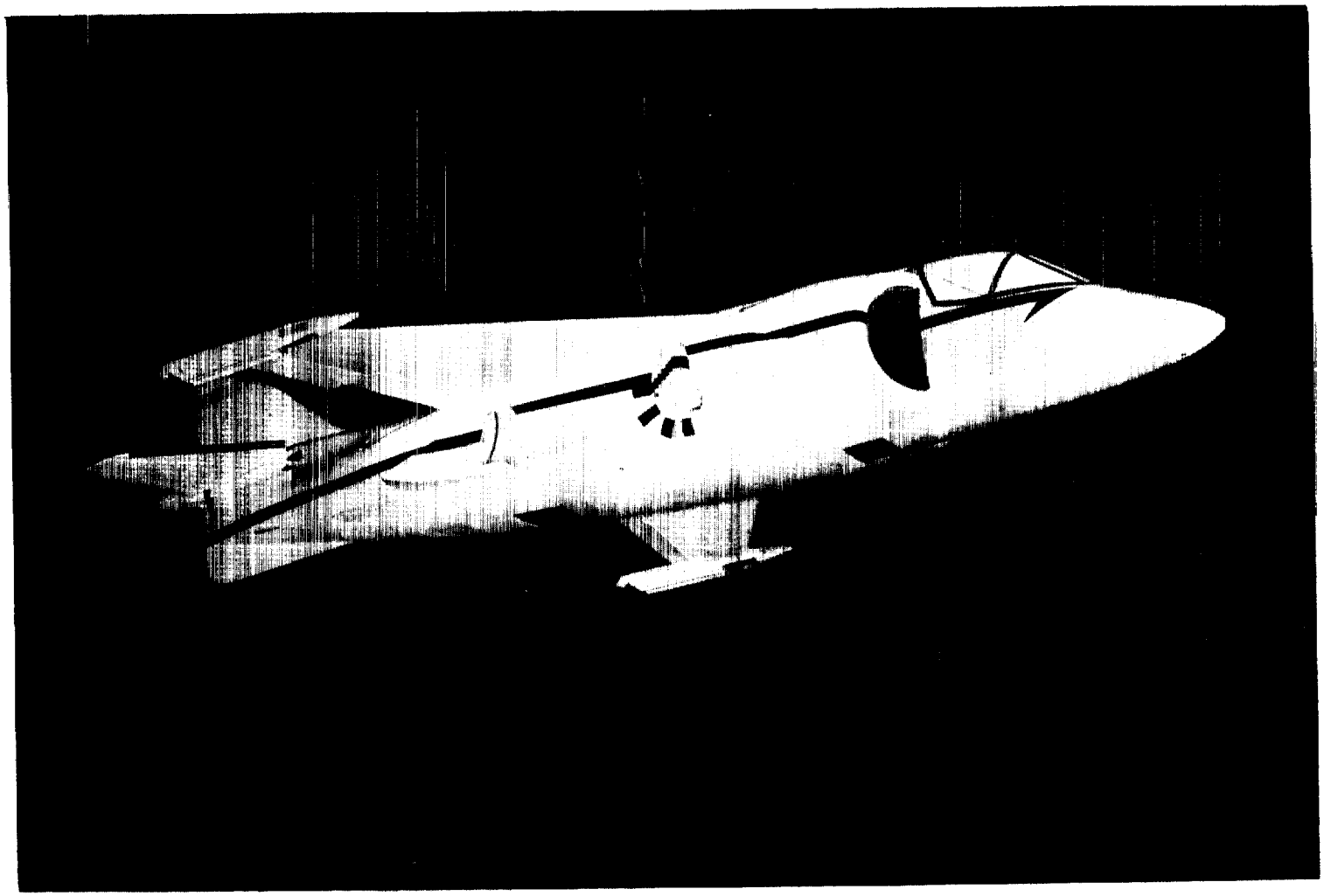

Figure 4.- Three-quarter-front view of the model in forward flight. L-60-1792

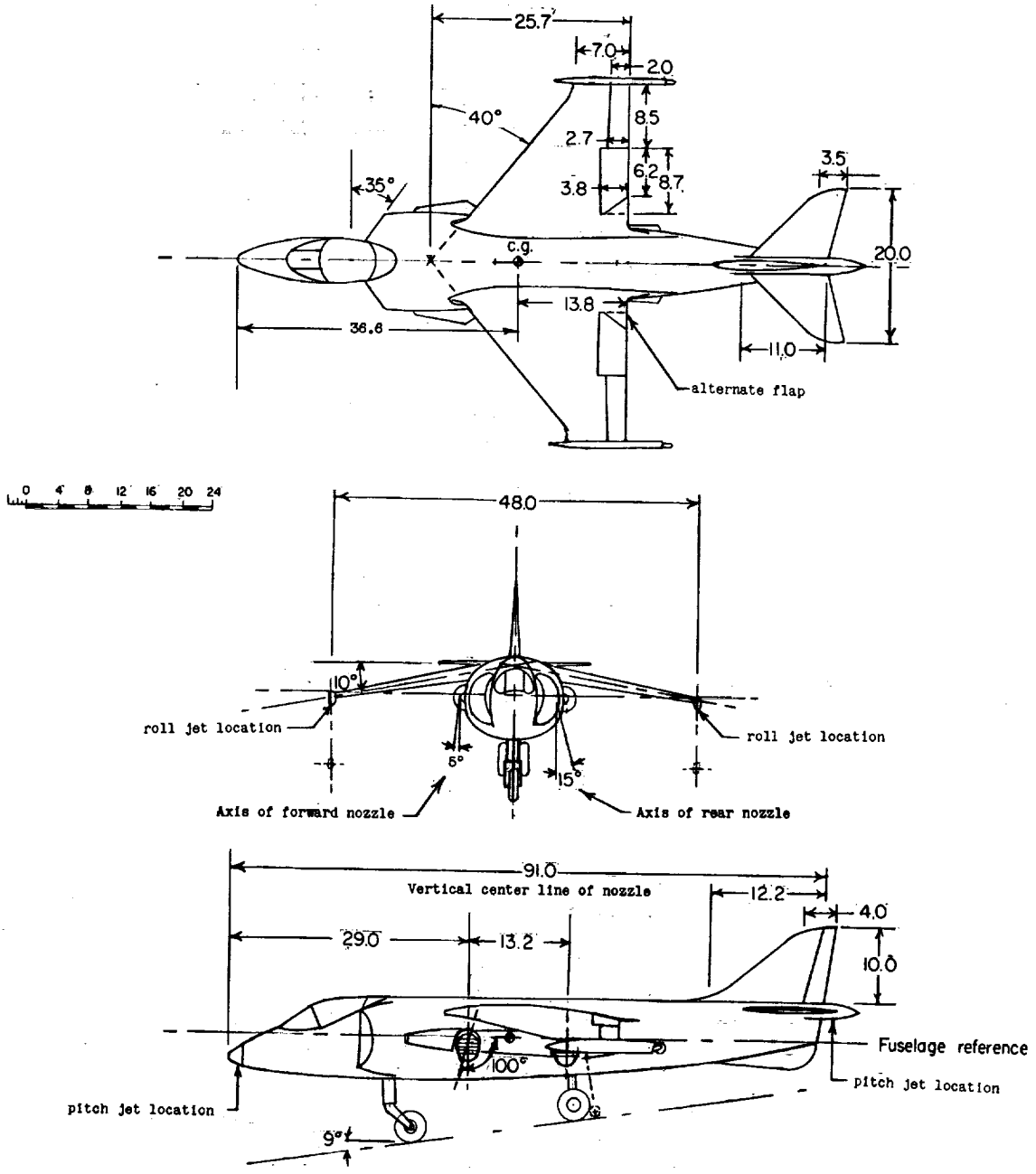

Figure 5.- Three-view sketch of the model used in the tests. All dimensions are in inches.

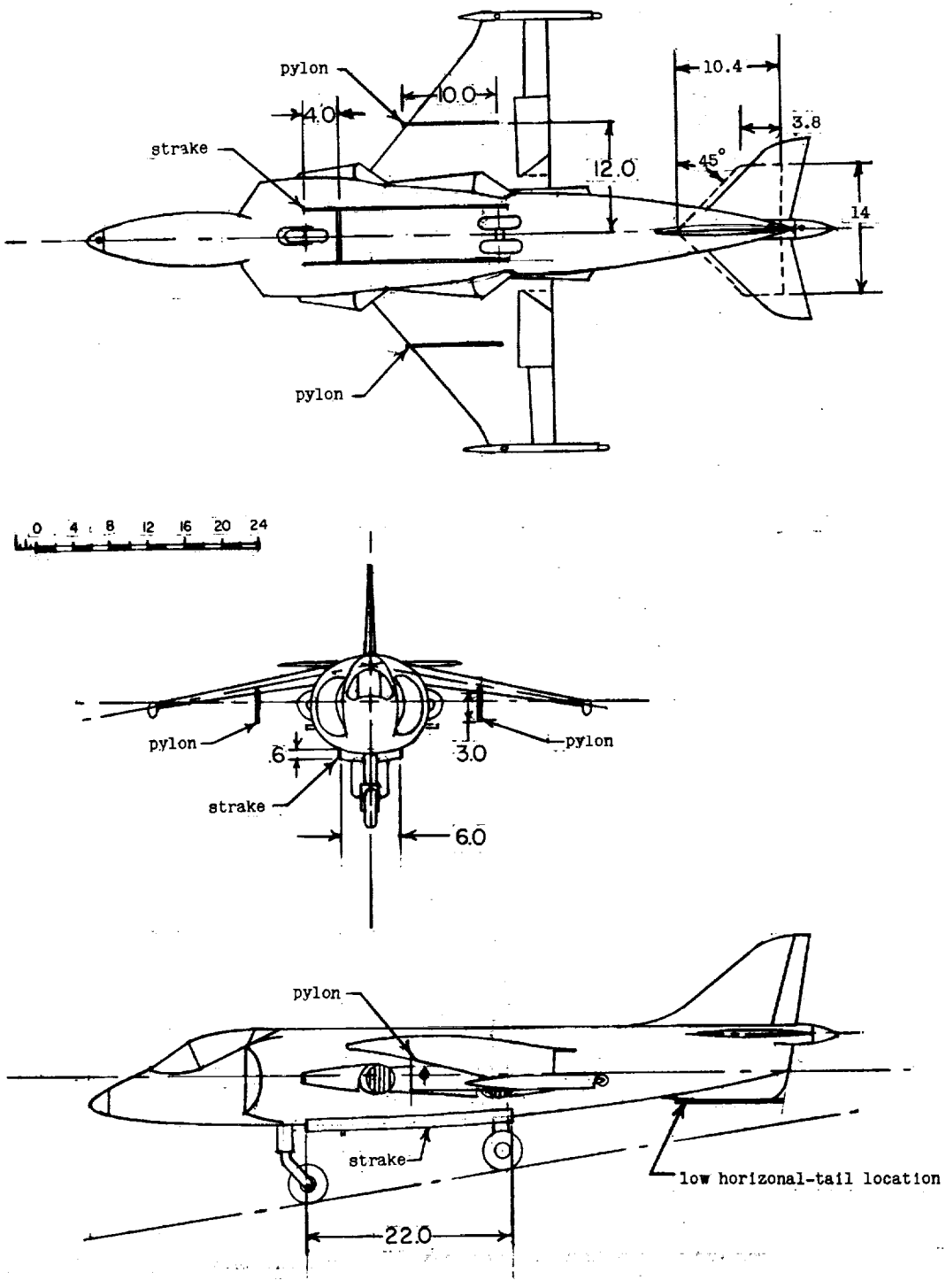

Figure 6.- Three-view sketch of the model showing the location of strakes and wing-tank pylons. All dimensions in inches.

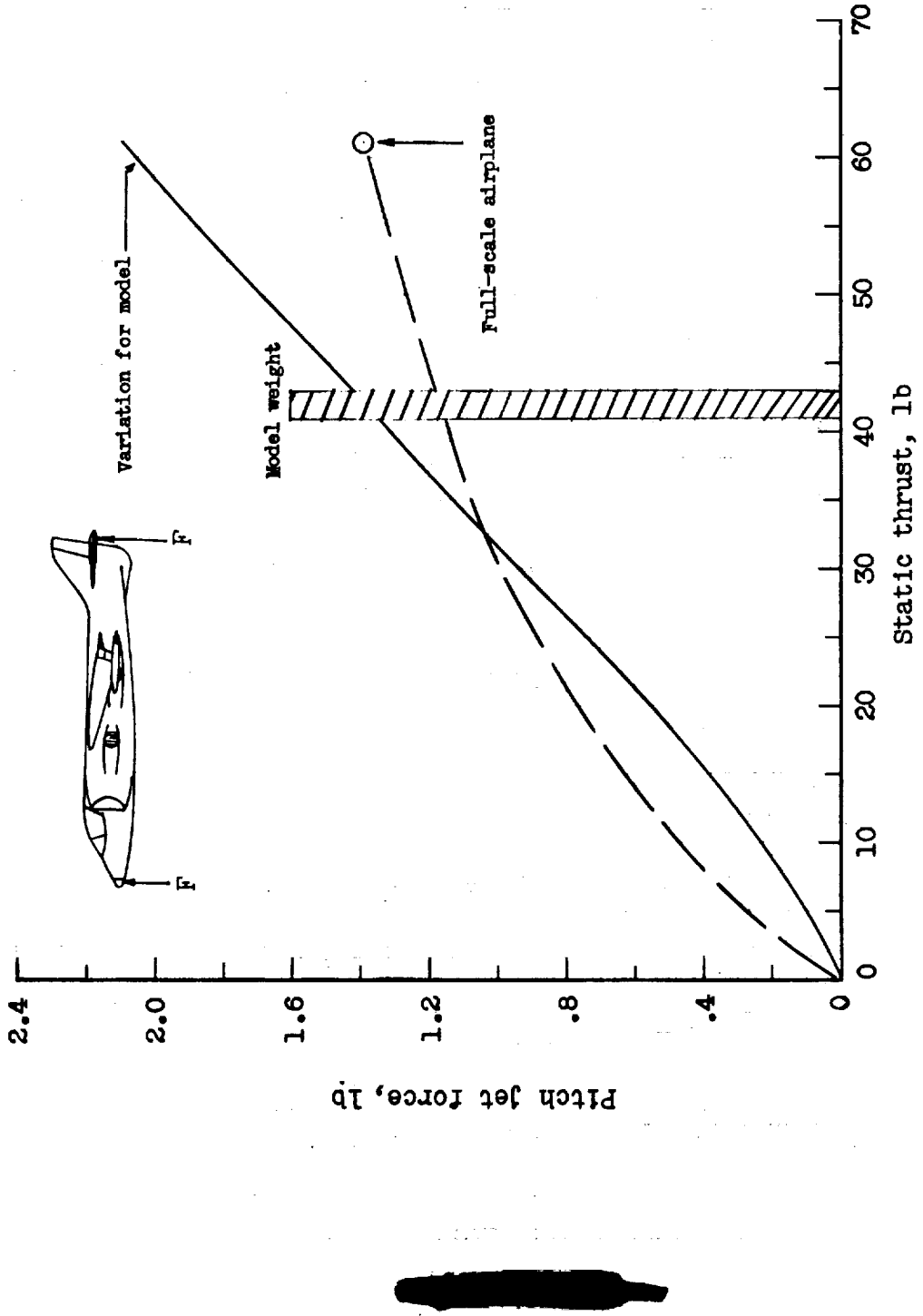

(a) Pitch jet.

Figure 7.- Variation of the jet control force with the static thrust of the model power plant.

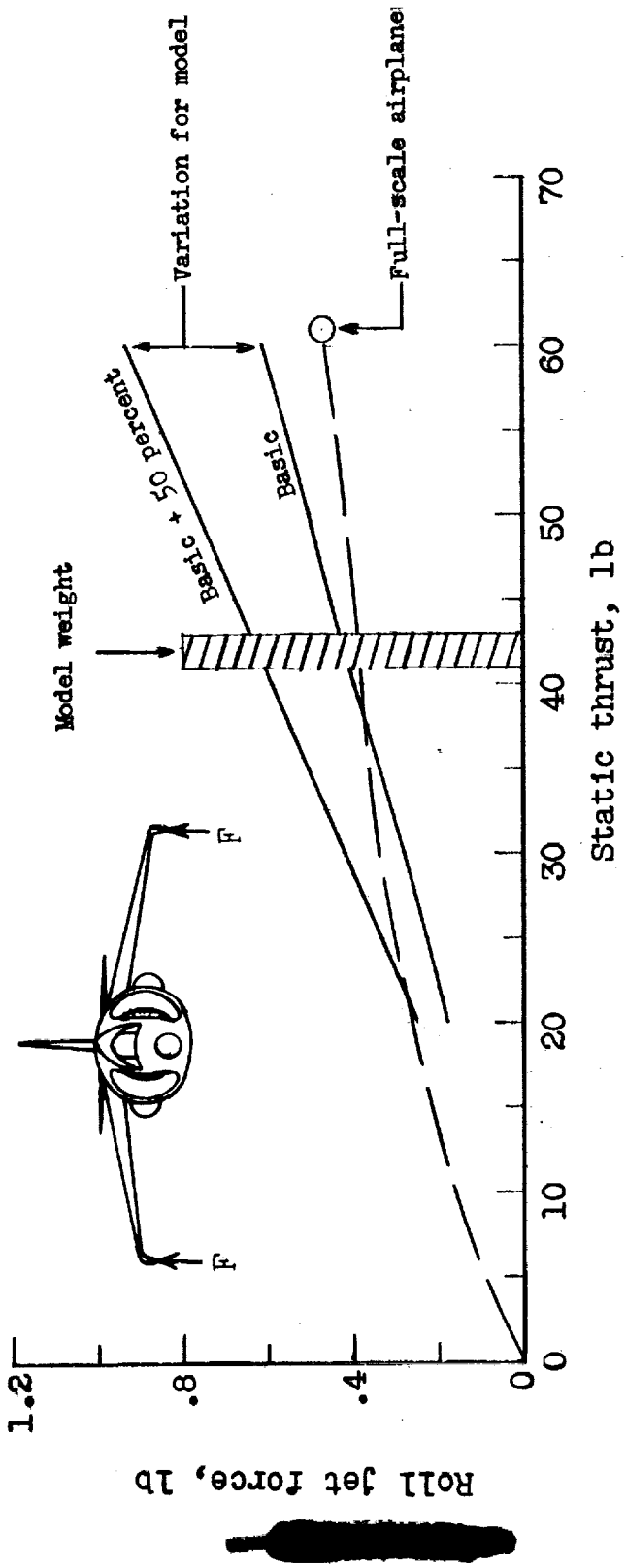

(b) Roll jet.

Figure 7.- Concluded.

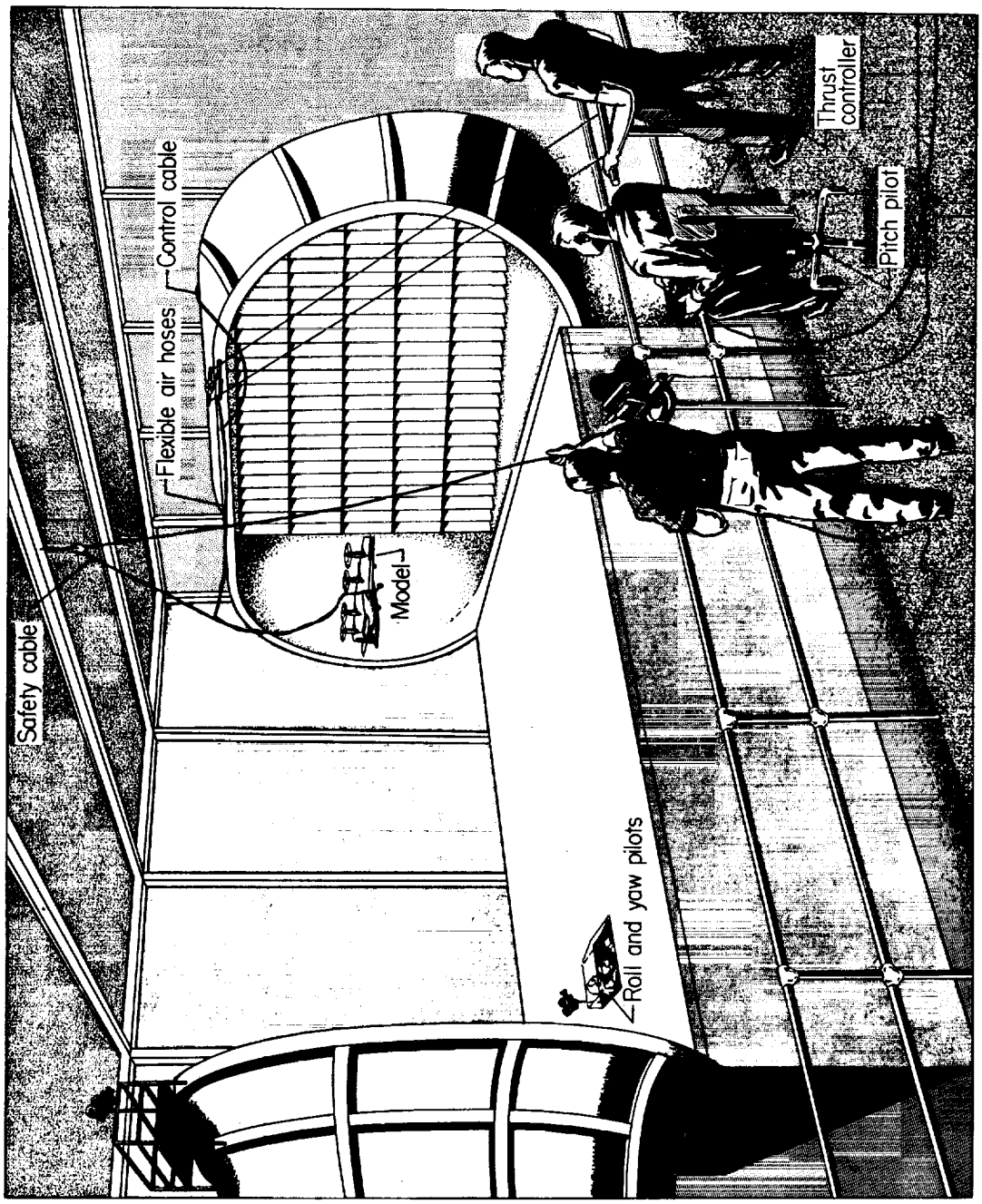

Figure 8.- Test setup for flight tests in the Langley full-scale tunnel.

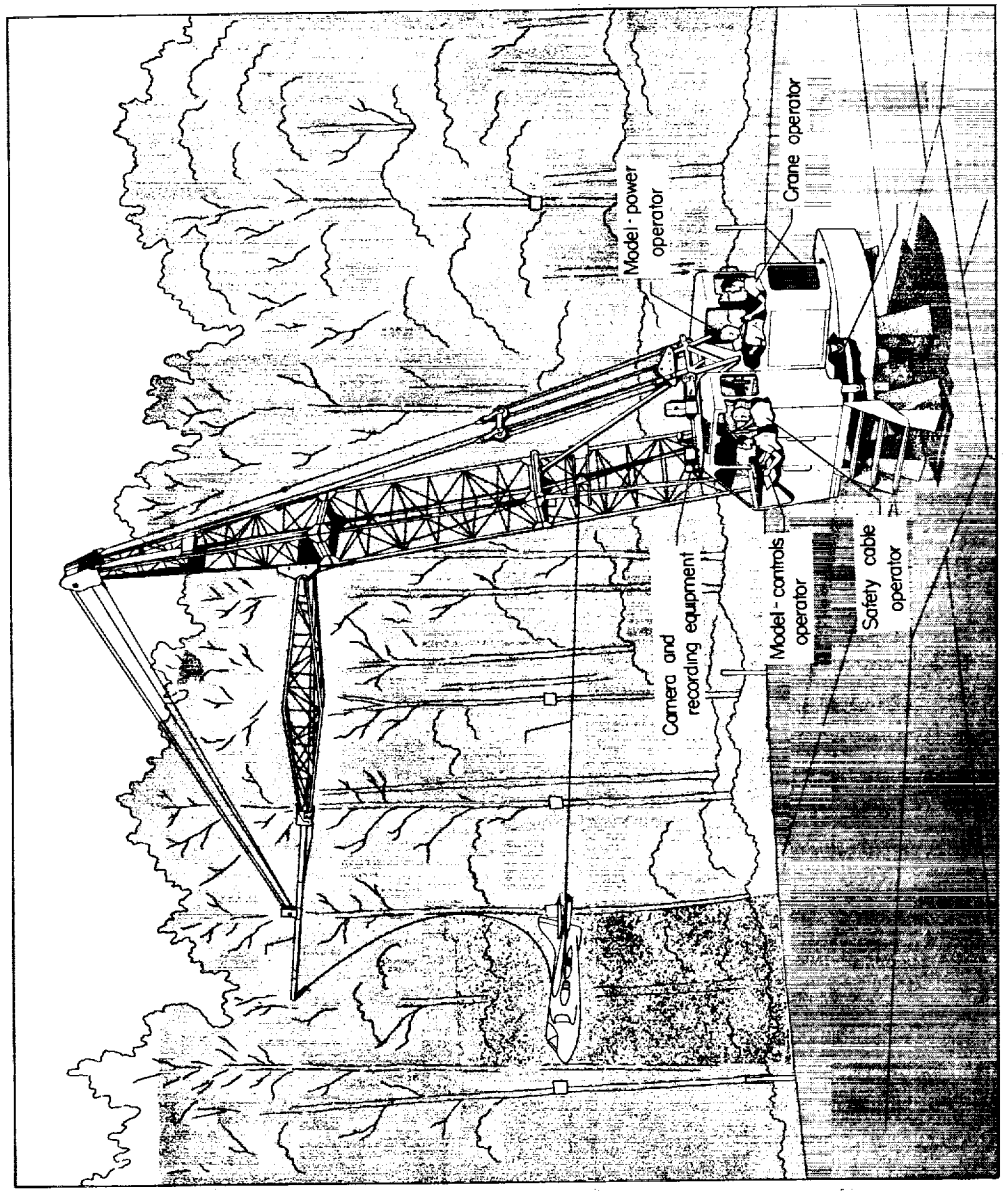

Figure 9.- The Langley control-line facility.

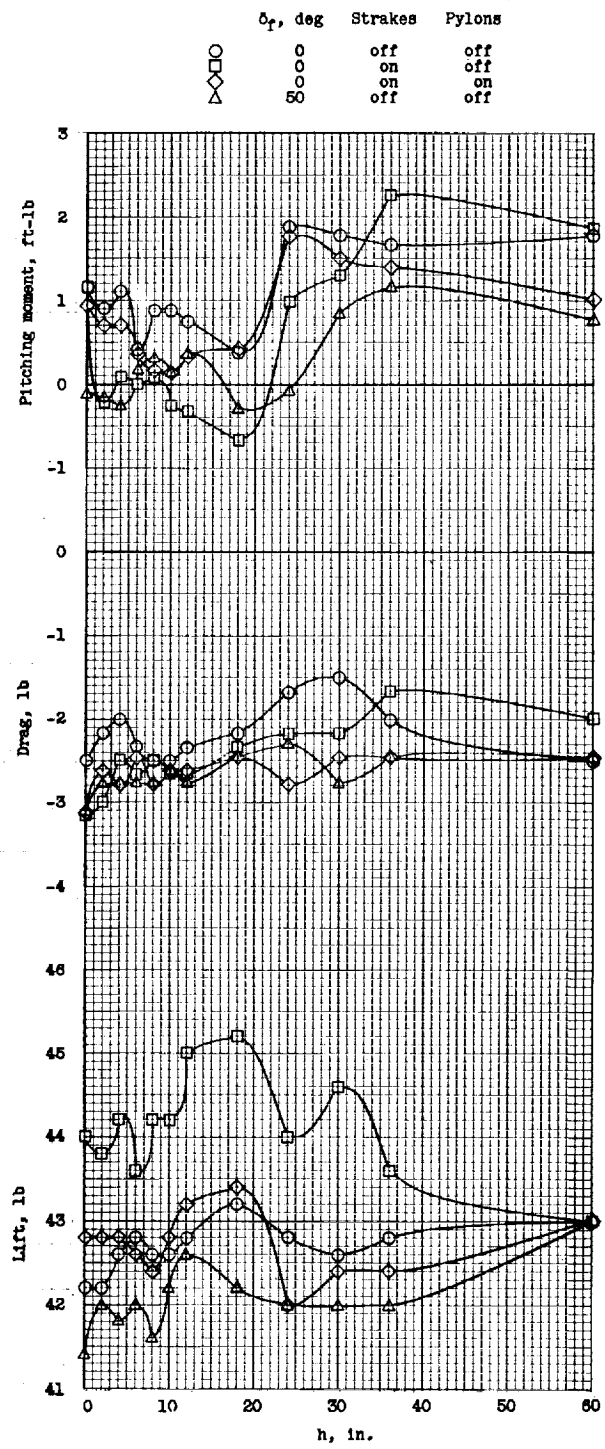

Figure 10.- Effect of ground proximity on the lift and longitudinal trim of the model. Referred to the body axes.

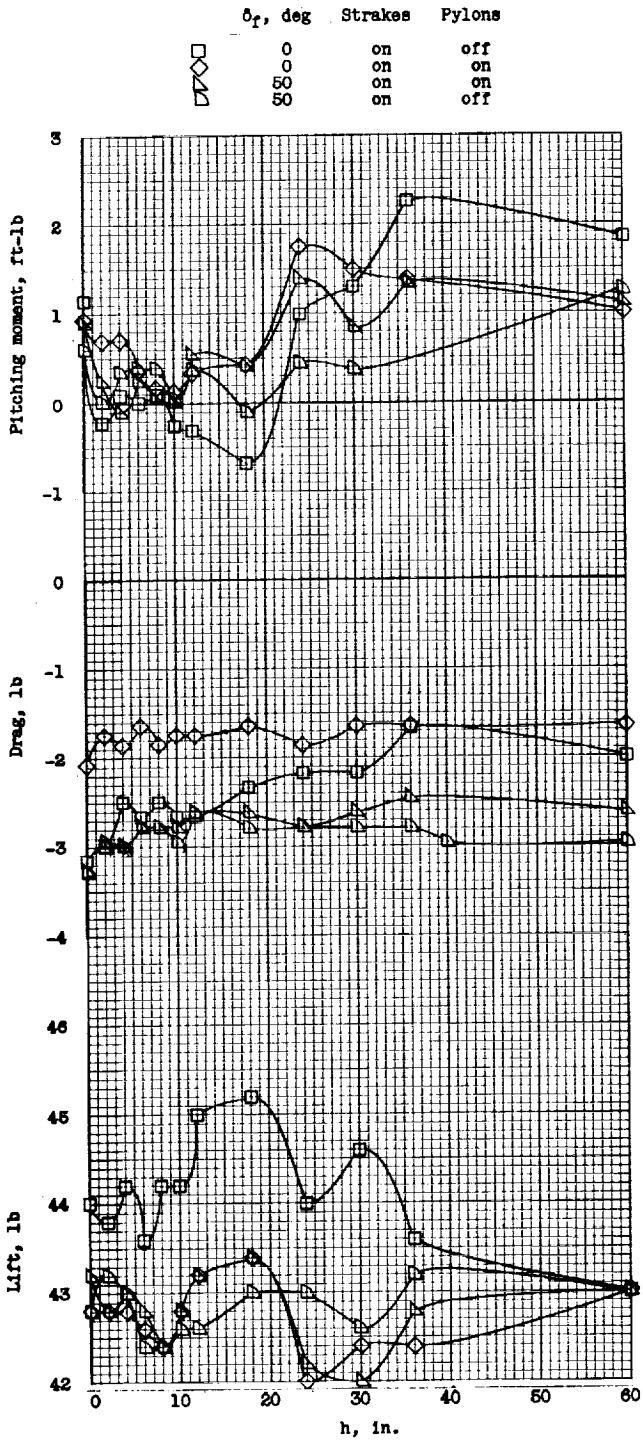

Figure 10. - Concluded.

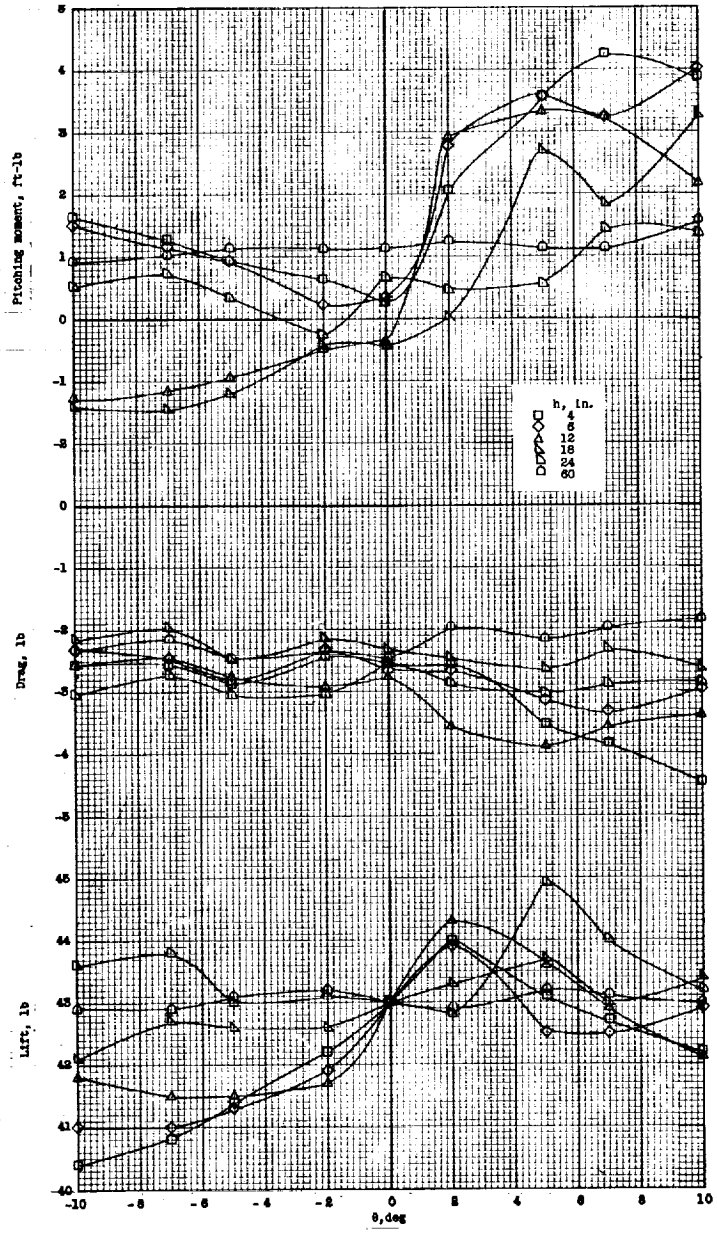

(a) Basic model with control jets off and $\delta_f = 0^\circ$.

Figure 11.- Variation of static longitudinal stability of the model with height above the ground. The main jet nozzles are fixed with respect to the airplane and are perpendicular to the ground at $\theta = 0^\circ$. θ is measured relative to a ground angle of 9°. Referred to the body axes. $i_t = 5^\circ$.

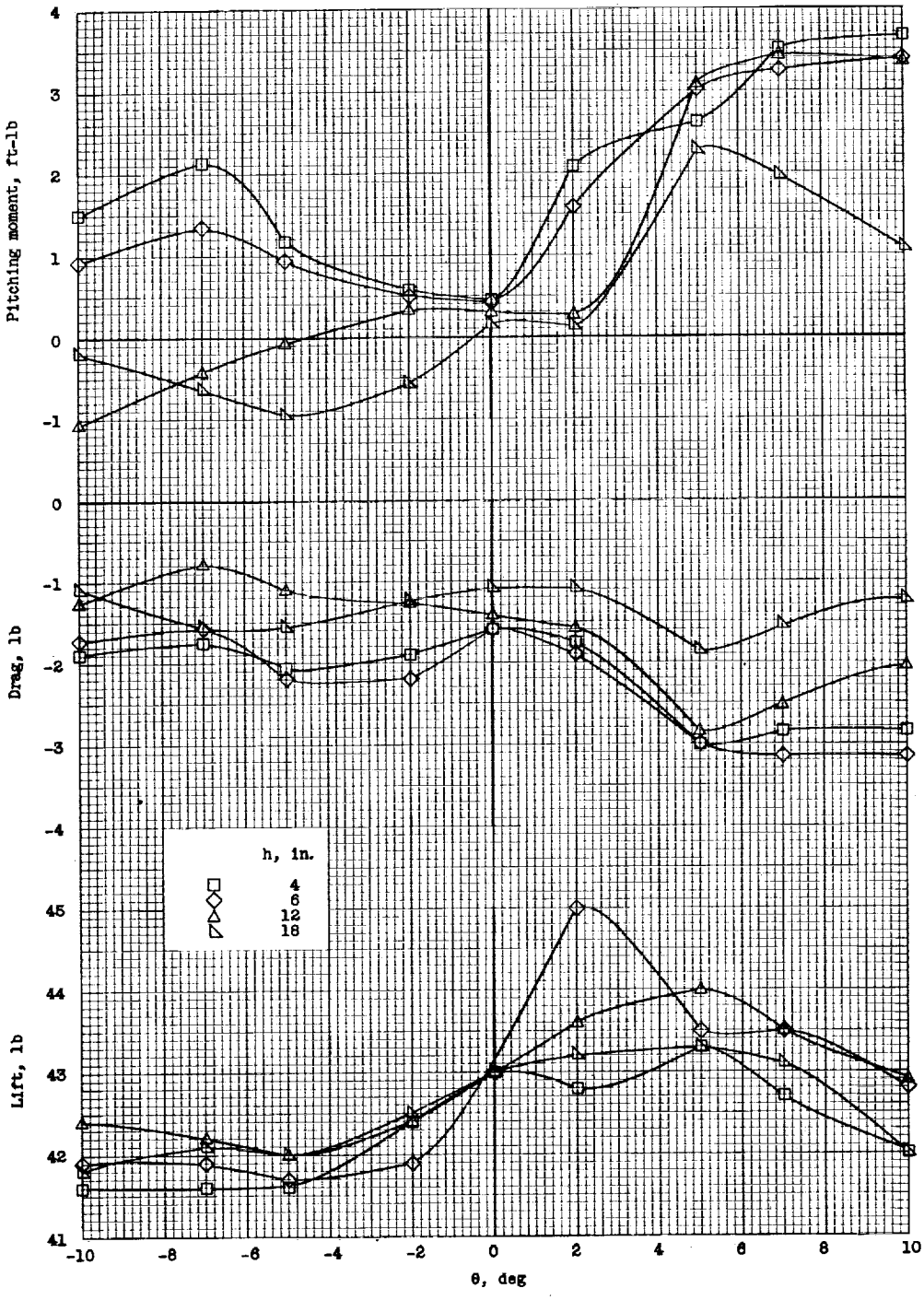

(b) Model with control jets off, $\delta_f = 0^o$, and strakes on.

Figure 11.- Continued.

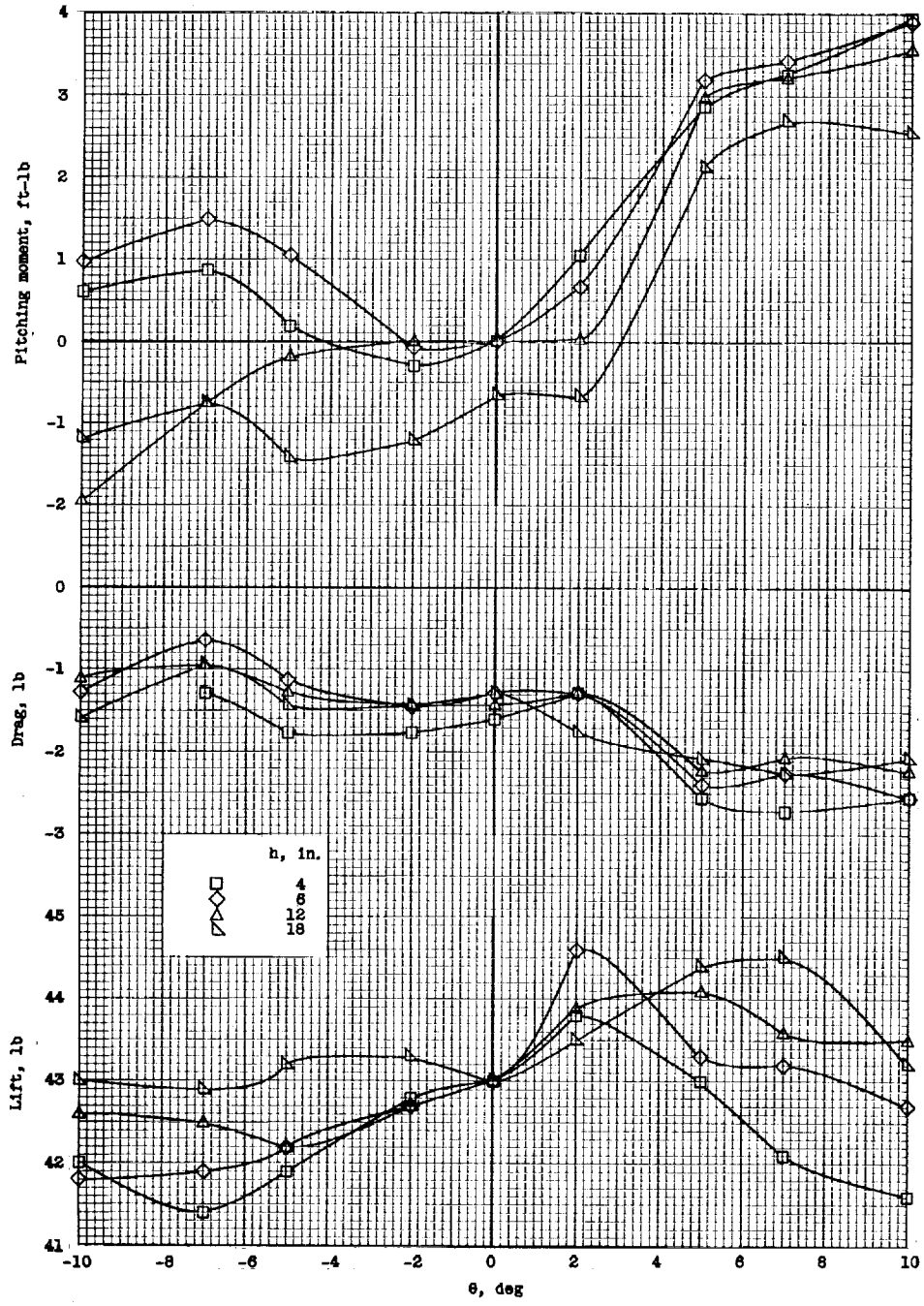

(c) Model with control jets off, $\delta_f = 0^\circ$, and landing-gear doors extended.

Figure 11.- Continued.

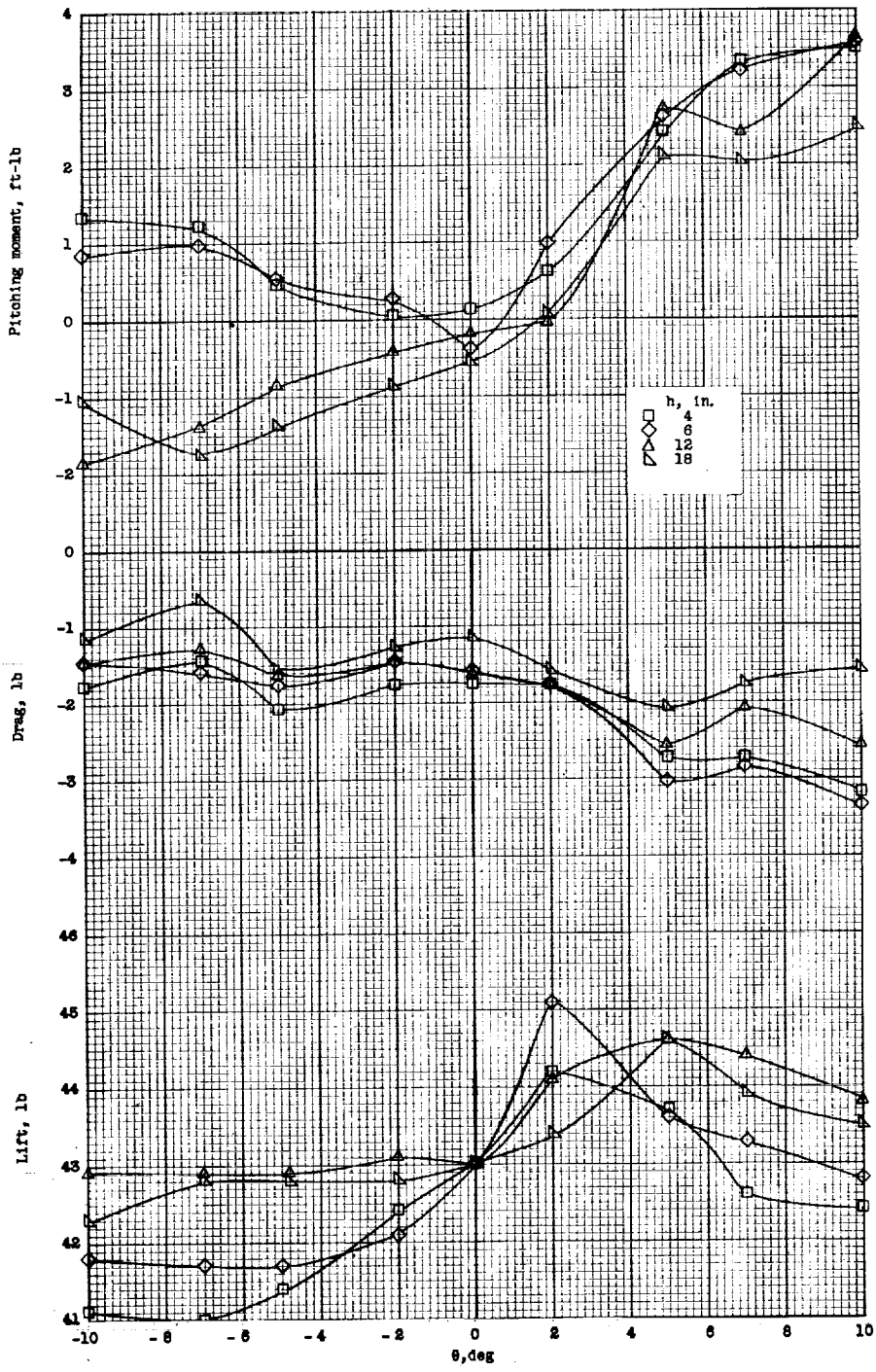

(d) Model with control jets off and $\delta_f = 50^\circ$.

Figure 11.- Continued.

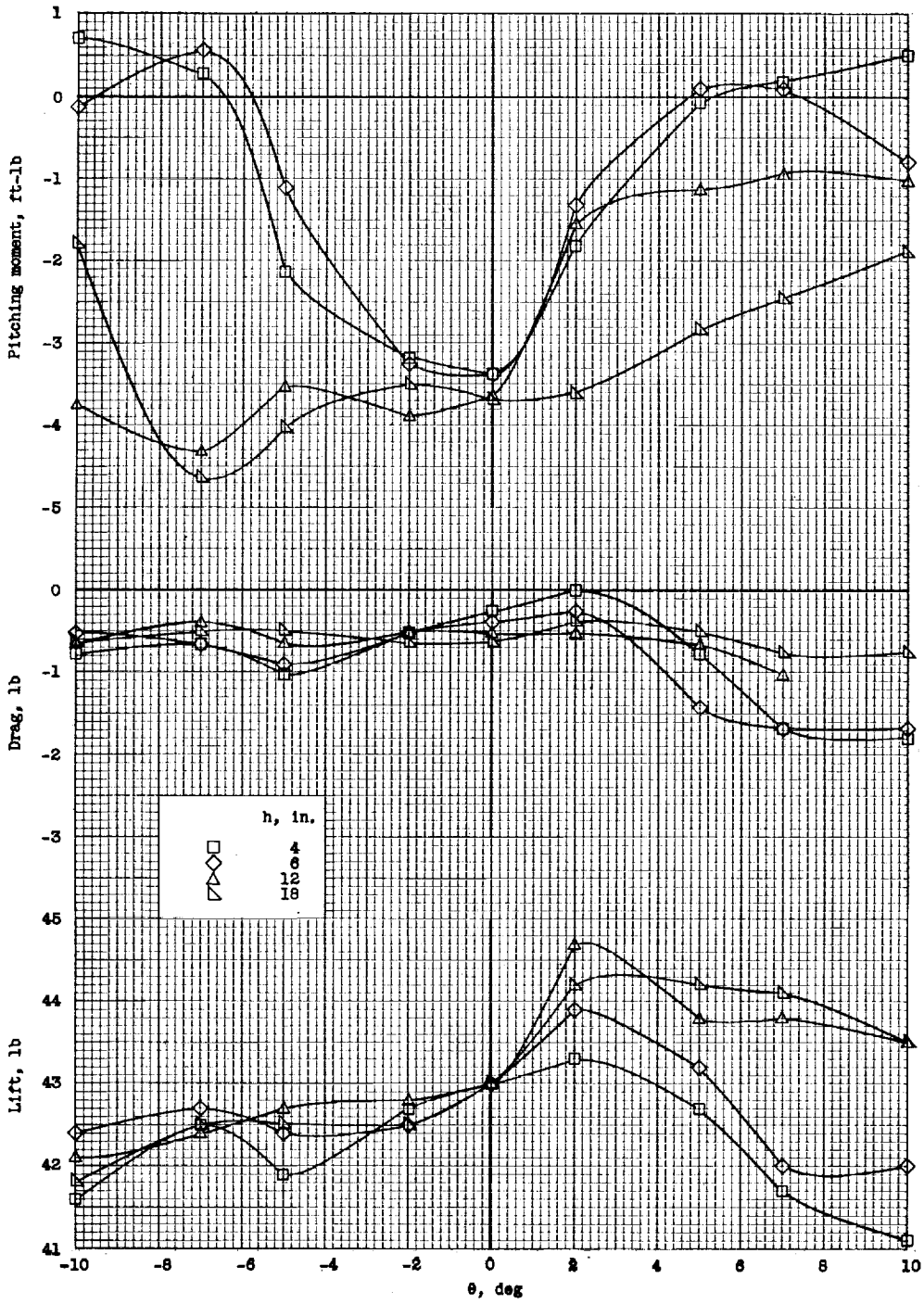

(e) Basic model with control jets on and $\delta_f = 0^\circ$.

Figure 11.- Continued.

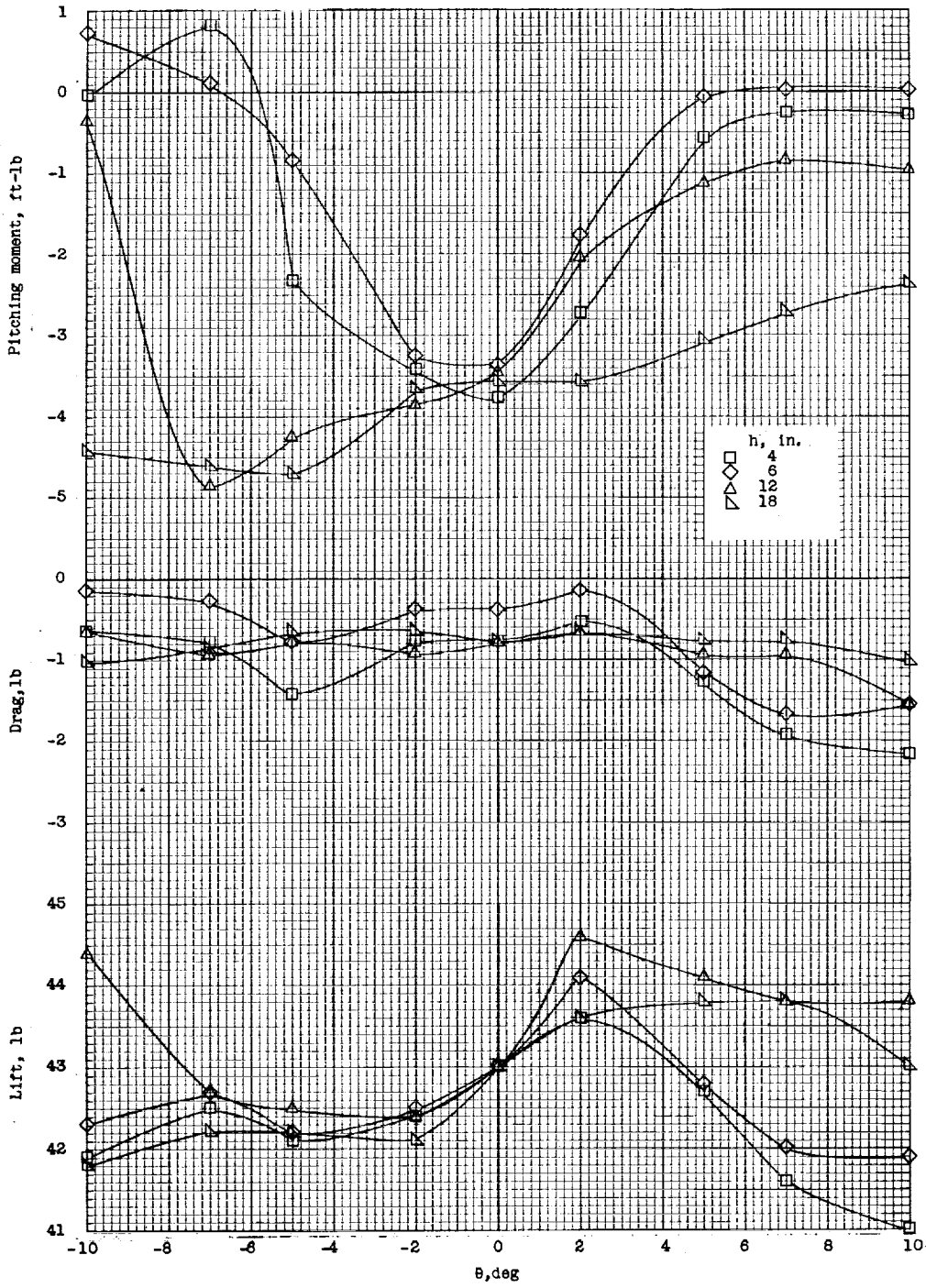

(f) Model with control jets on and $\delta_f = 50^o$.

Figure 11.- Continued.

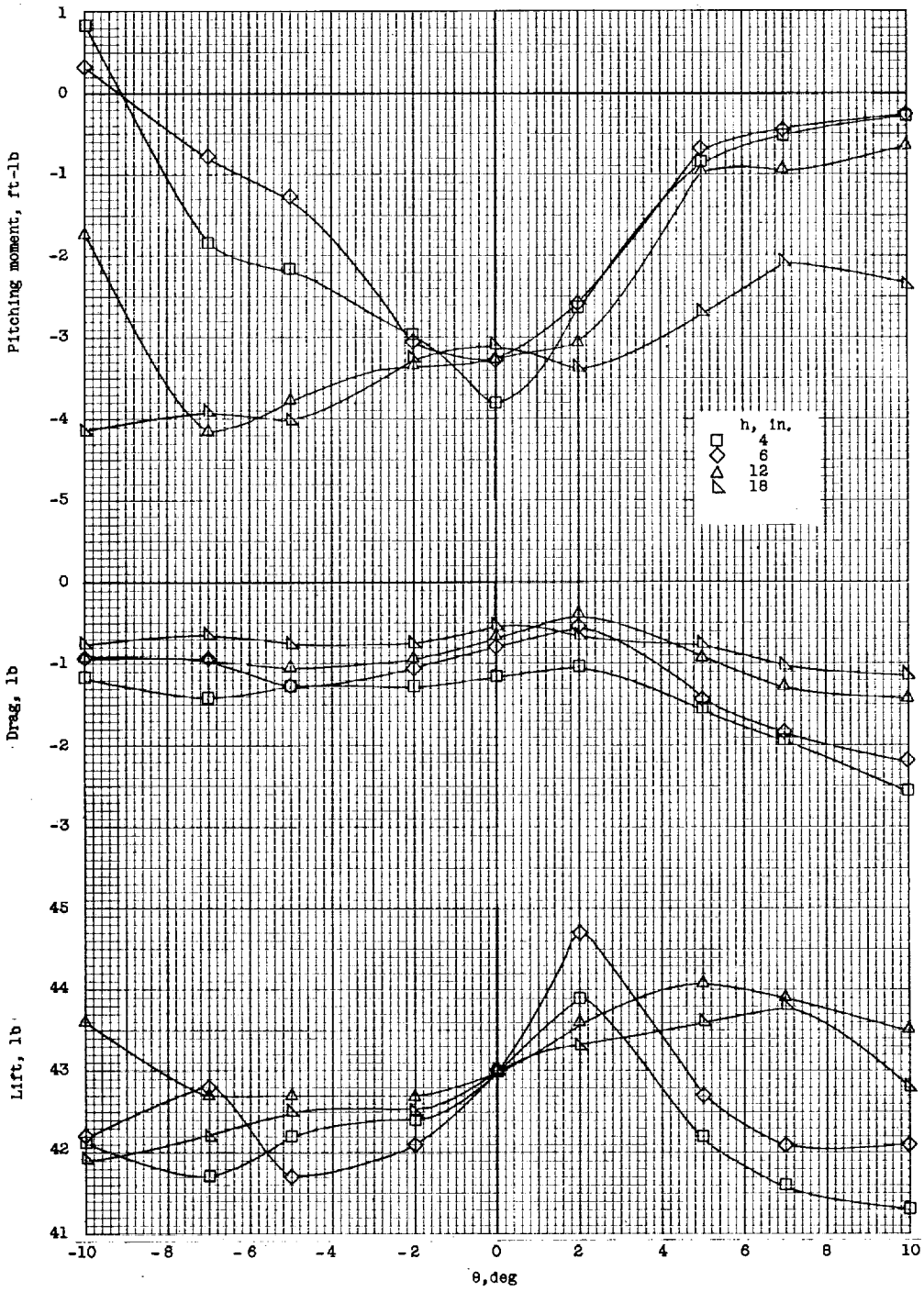

(g) Model with control jets on, $\delta_f = 0^o$, and strakes on.

Figure 11.- Continued.

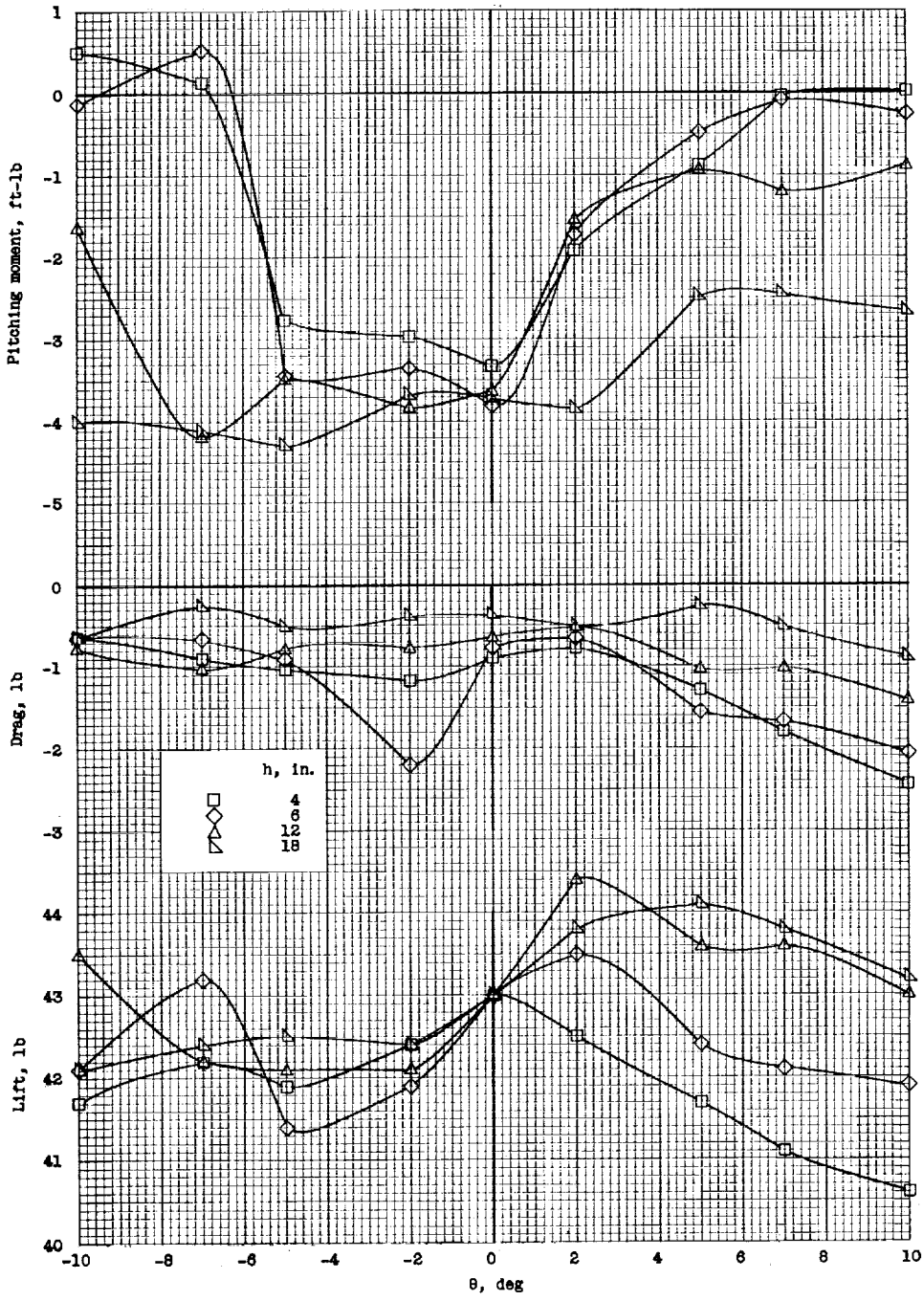

(h) Model with control jets on, $\delta_f = 0^o$, and landing-gear doors extended.

Figure 11.- Concluded.

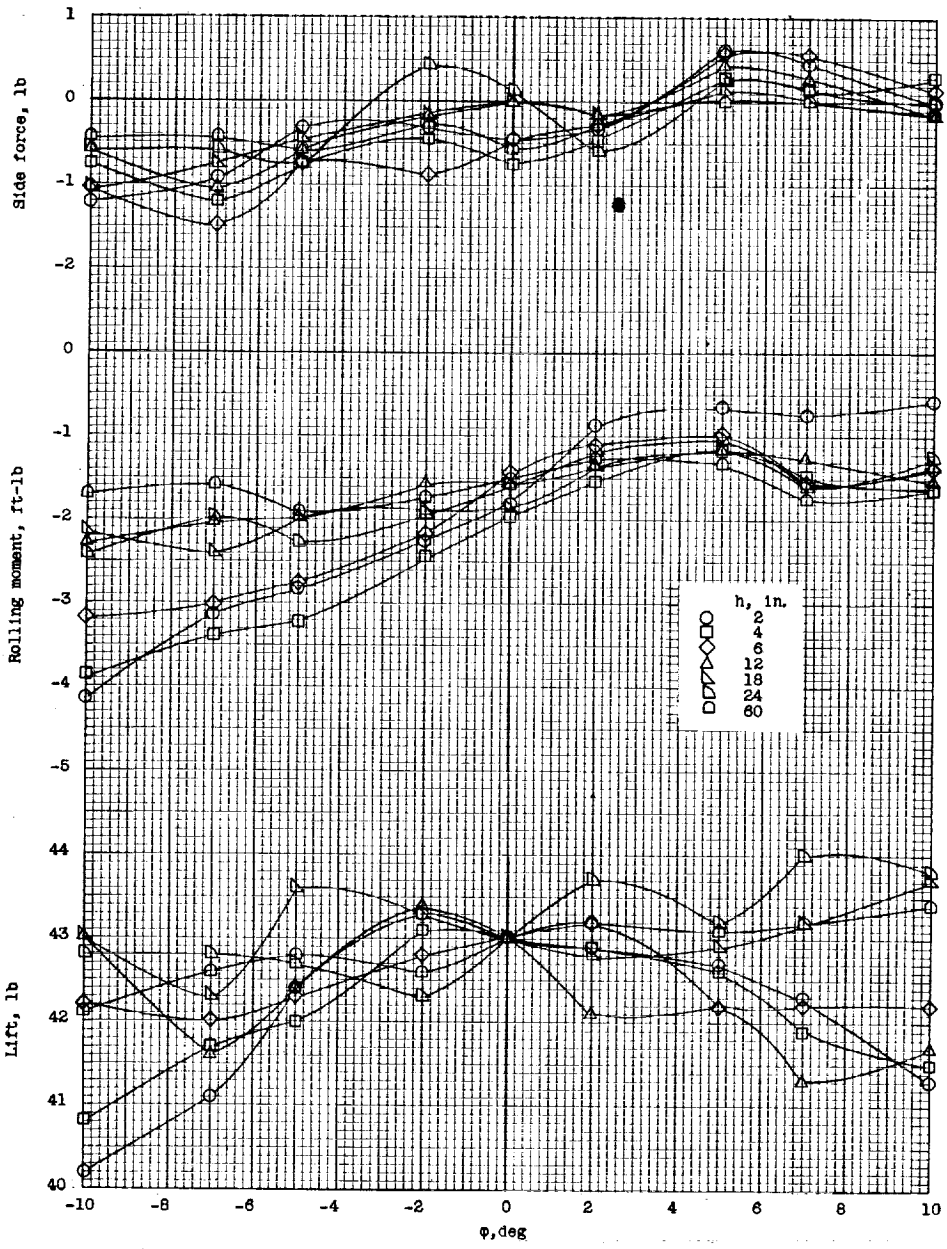

(a) Basic model with control jets off and $\delta_f = 0^\circ$.

Figure 12.- Variation of static lateral stability of the model with height above the ground. The main jet nozzles are fixed with respect to the airplane and are perpendicular to the ground at $\theta = 0^\circ$. θ is measured relative to a ground angle of 9°. Referred to the body axes. $i_t = 5^\circ$.

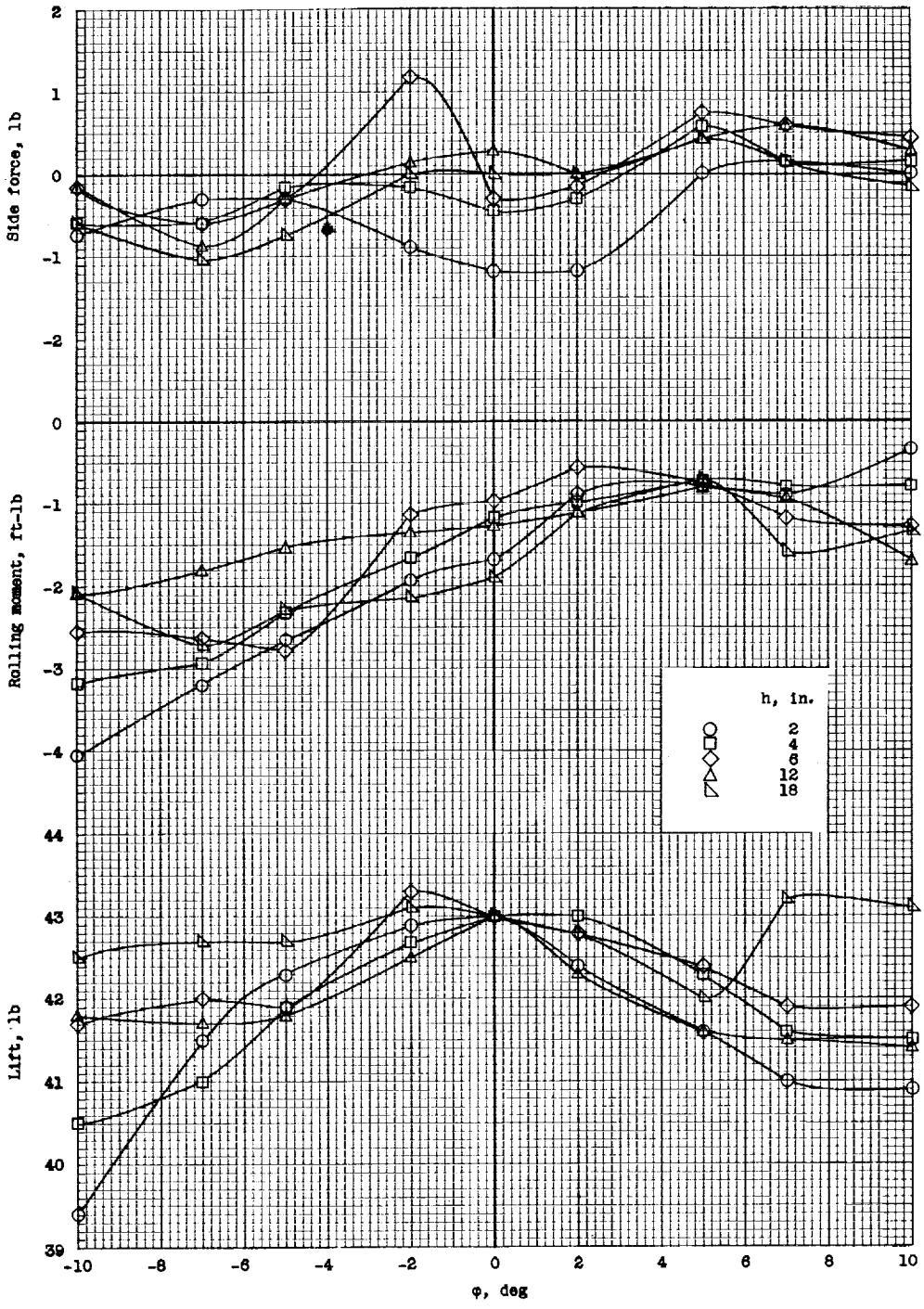

(b) Model with control jets off, $\delta_f = 0^o$, and strakes on.

Figure 12.- Continued.

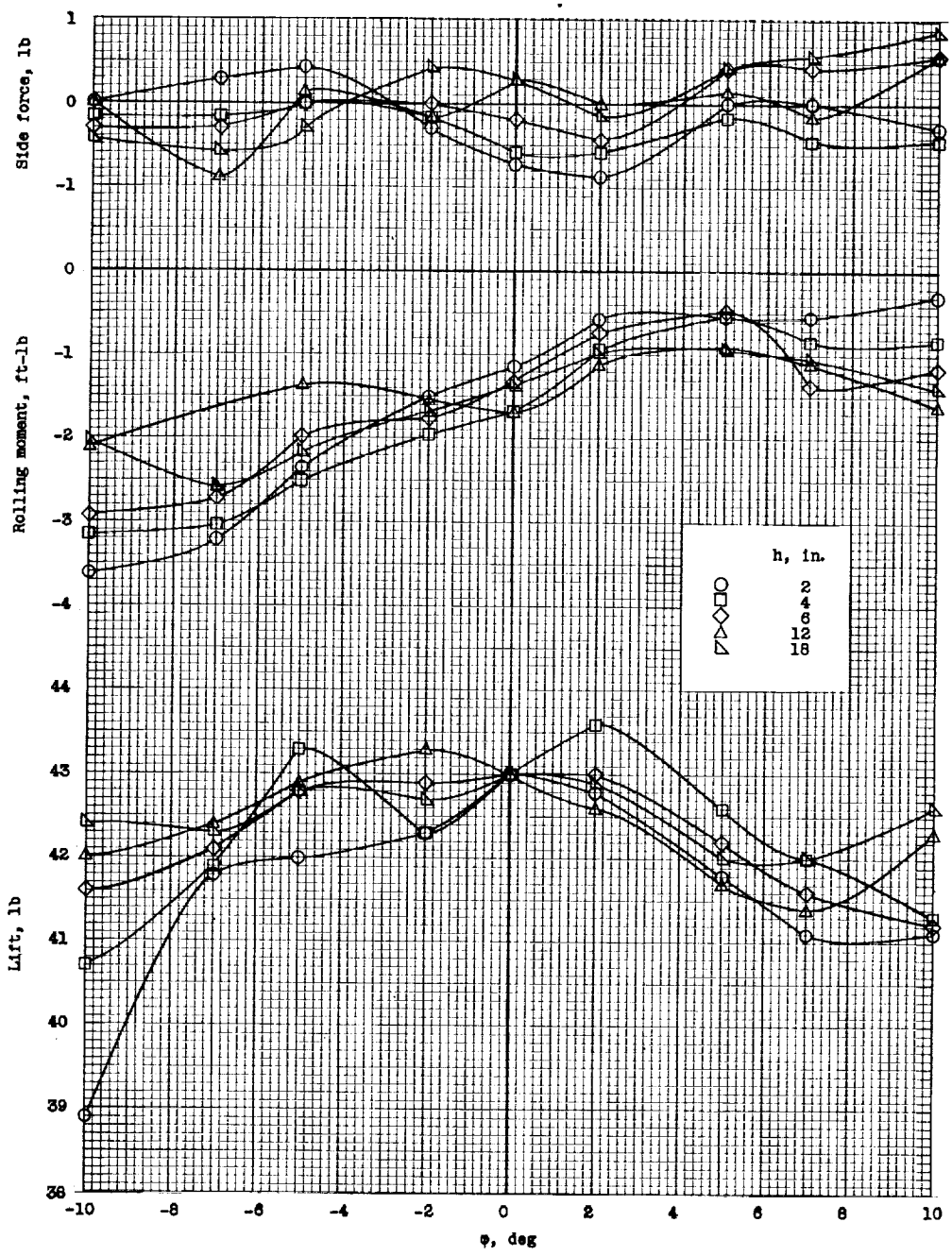

(c) Model with control jets off, $\delta_f = 0^o$, strakes and wing-tank pylons on.

Figure 12.- Continued.

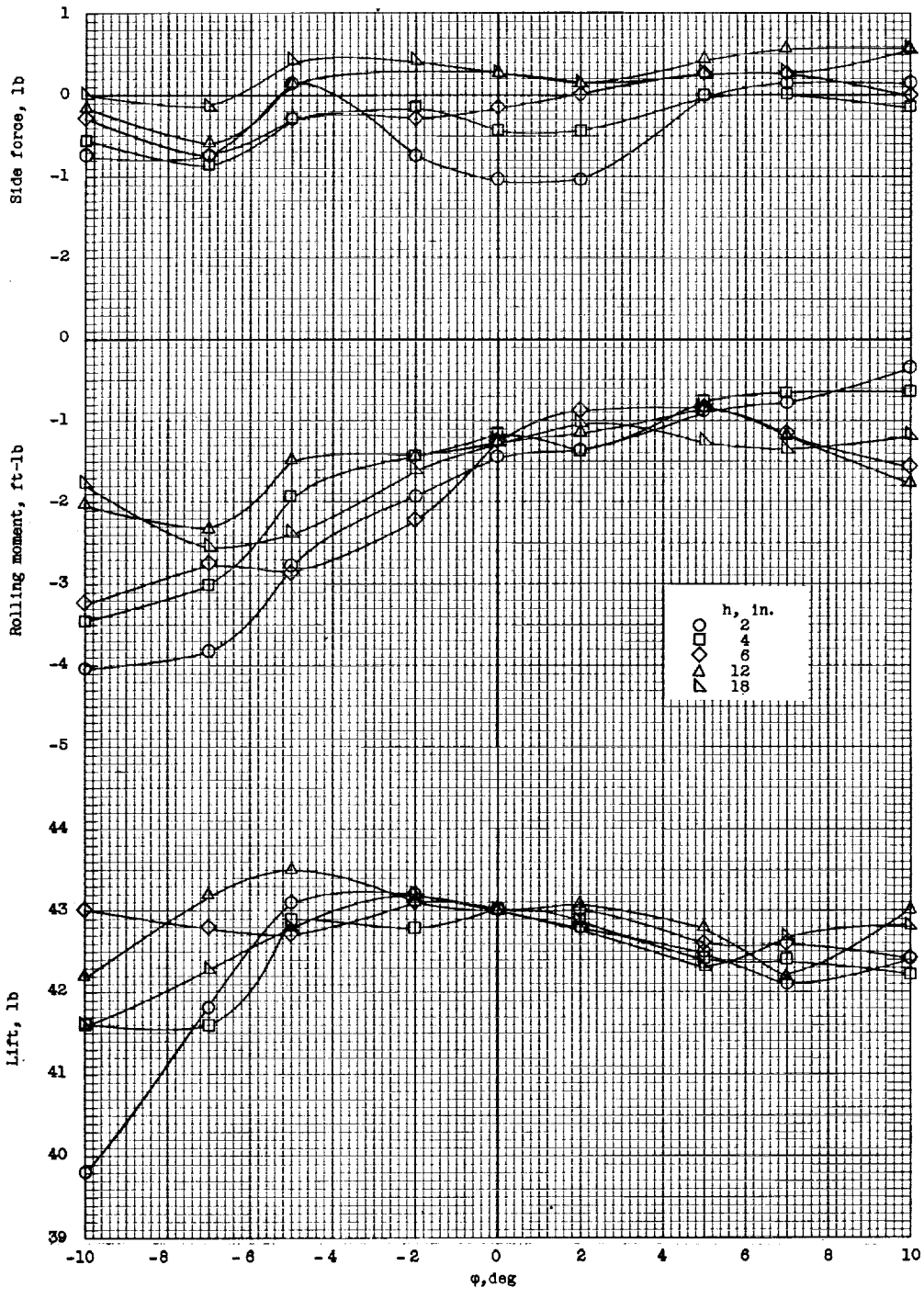

(d) Model with control jets off, $\delta_f = 50^o$, and strakes on.

Figure 12.- Continued.

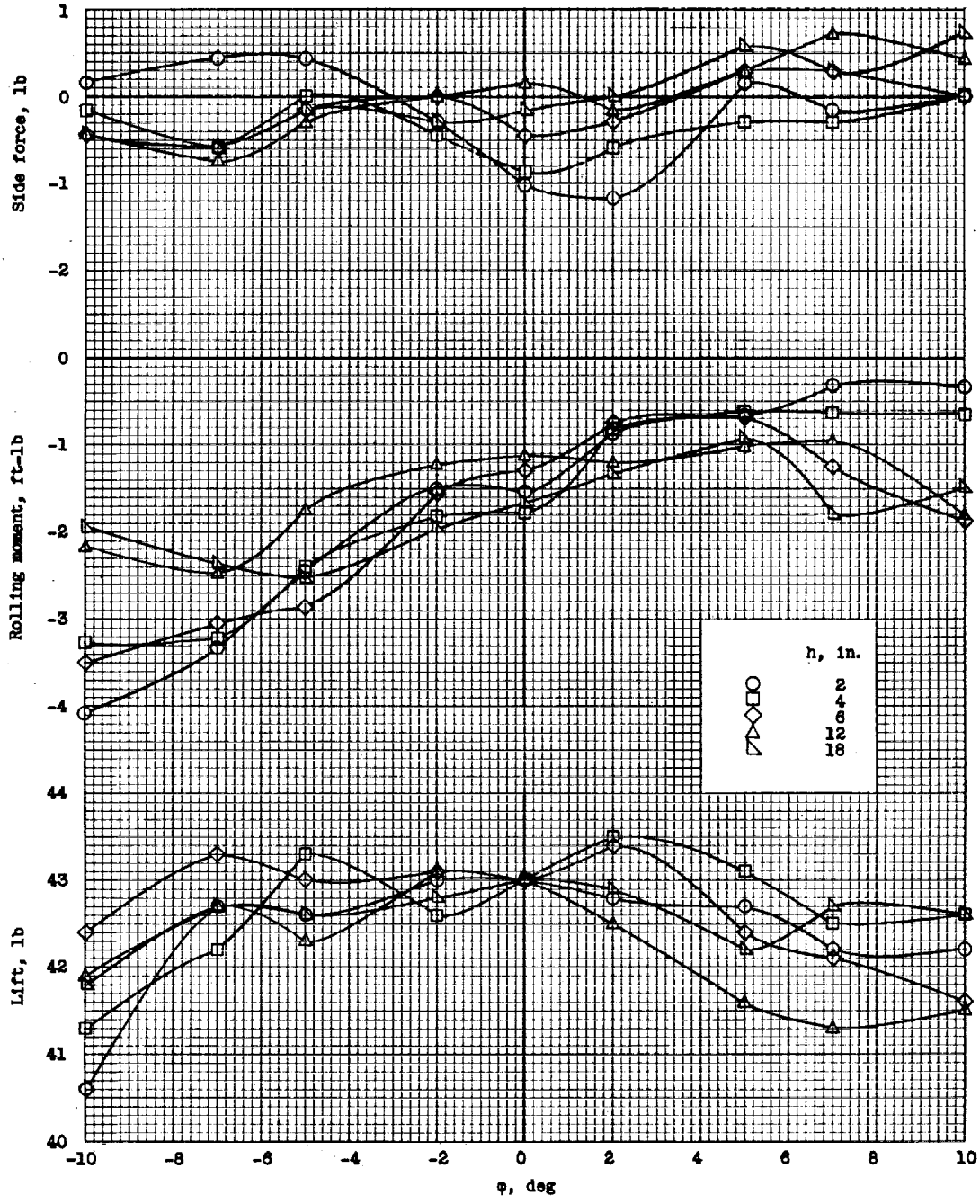

(e) Model with control jets off, $\delta_f = 50^\circ$, strakes and wing-tank pylons on.

Figure 12.- Continued.

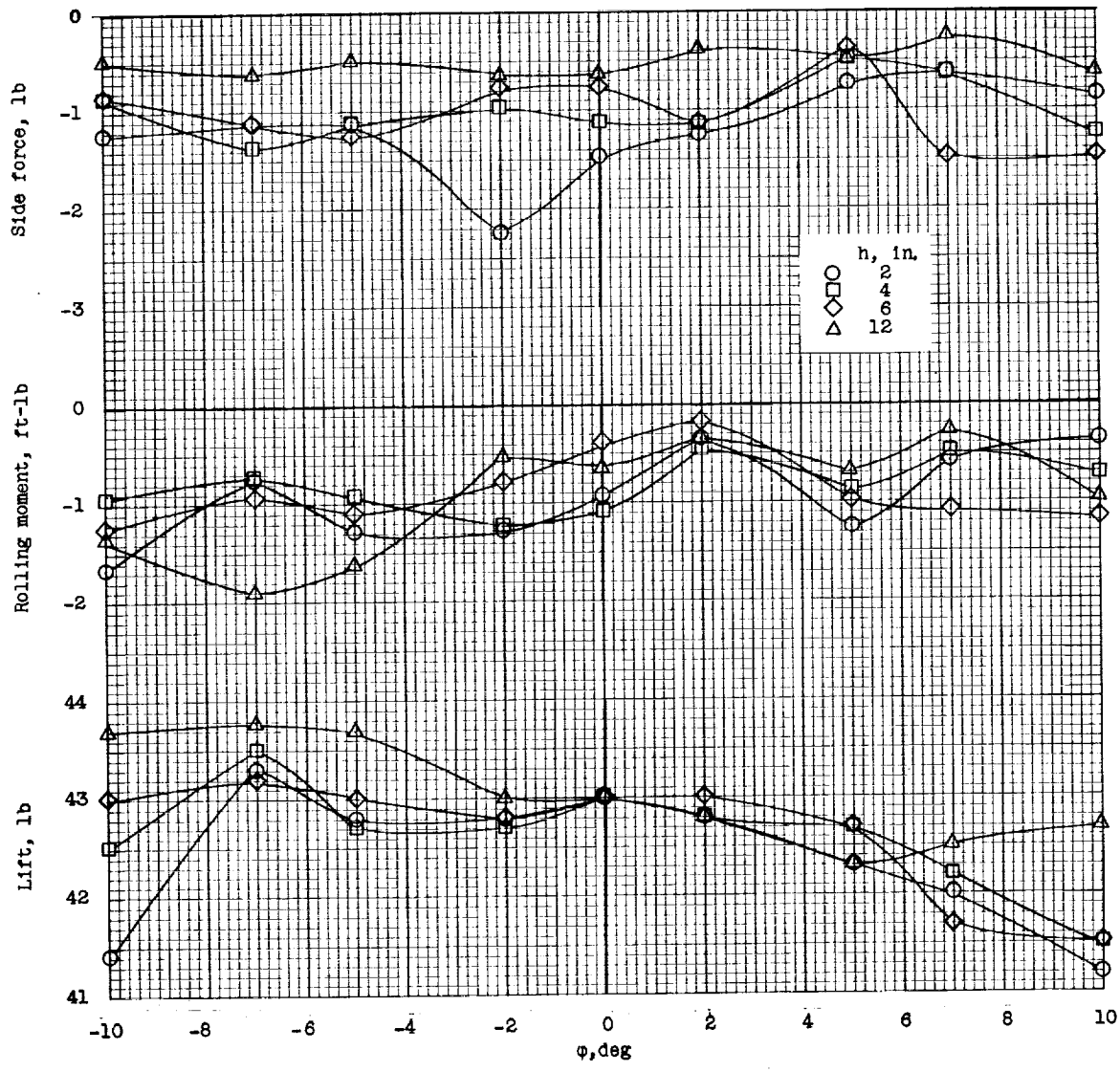

(f) Model with control jets on, $\delta_f = 0^o$, and strakes on.

Figure 12.- Concluded.

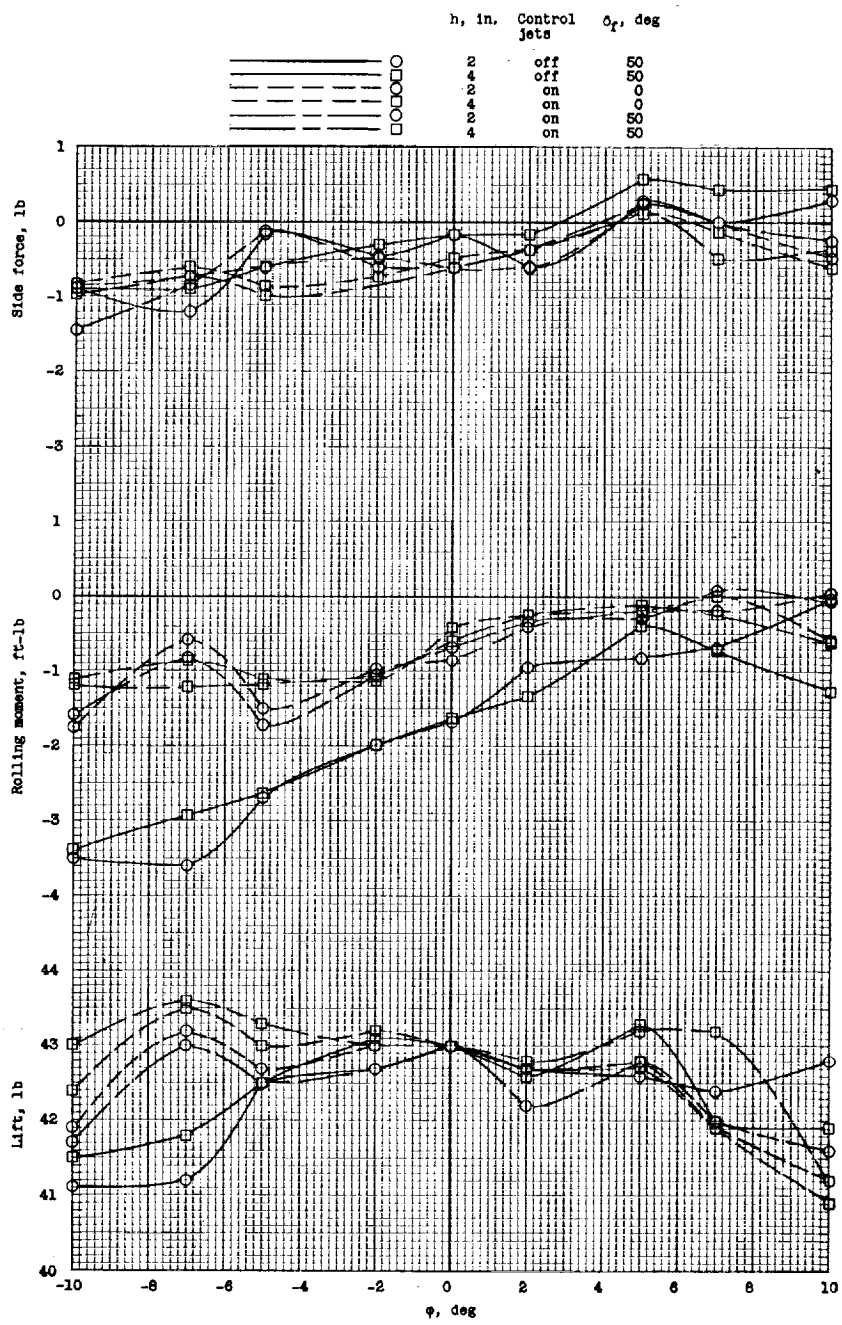

Figure 13.- Effect of flaps and control jets on the static lateral stability of the model when close to the ground. The main jet nozzles are fixed with respect to the airplane and are perpendicular to the ground at $\theta = 0^\circ$. θ is measured relative to a ground angle of 9°. Referred to the body axes. $i_t = 5^\circ$.

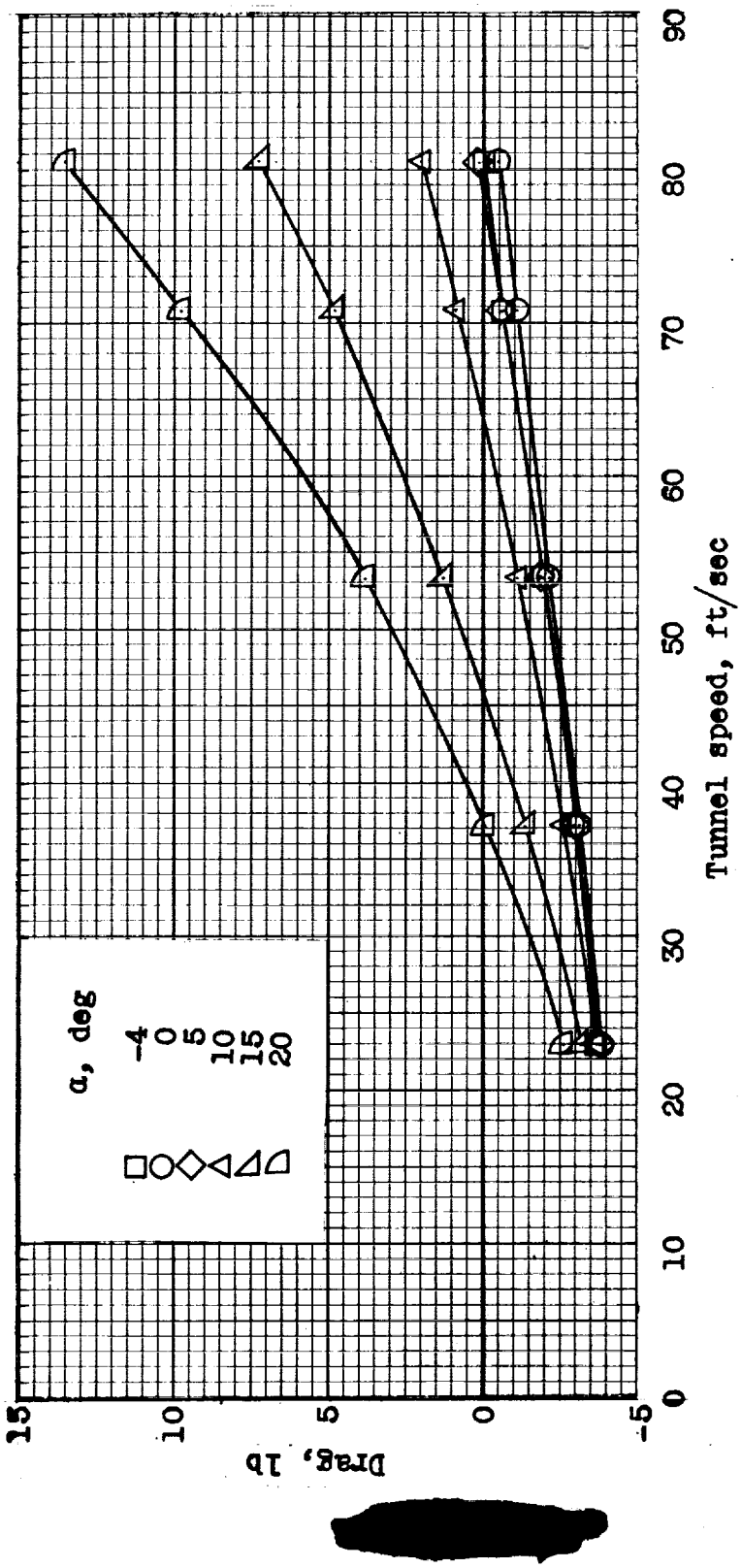

(a) $\Delta = 0^{\circ}$.

Figure 14.- Longitudinal force-test data for the basic model. Referred to the wind axes. $i_t = 0^{\circ}$ and $\delta_f = 0^{\circ}$.

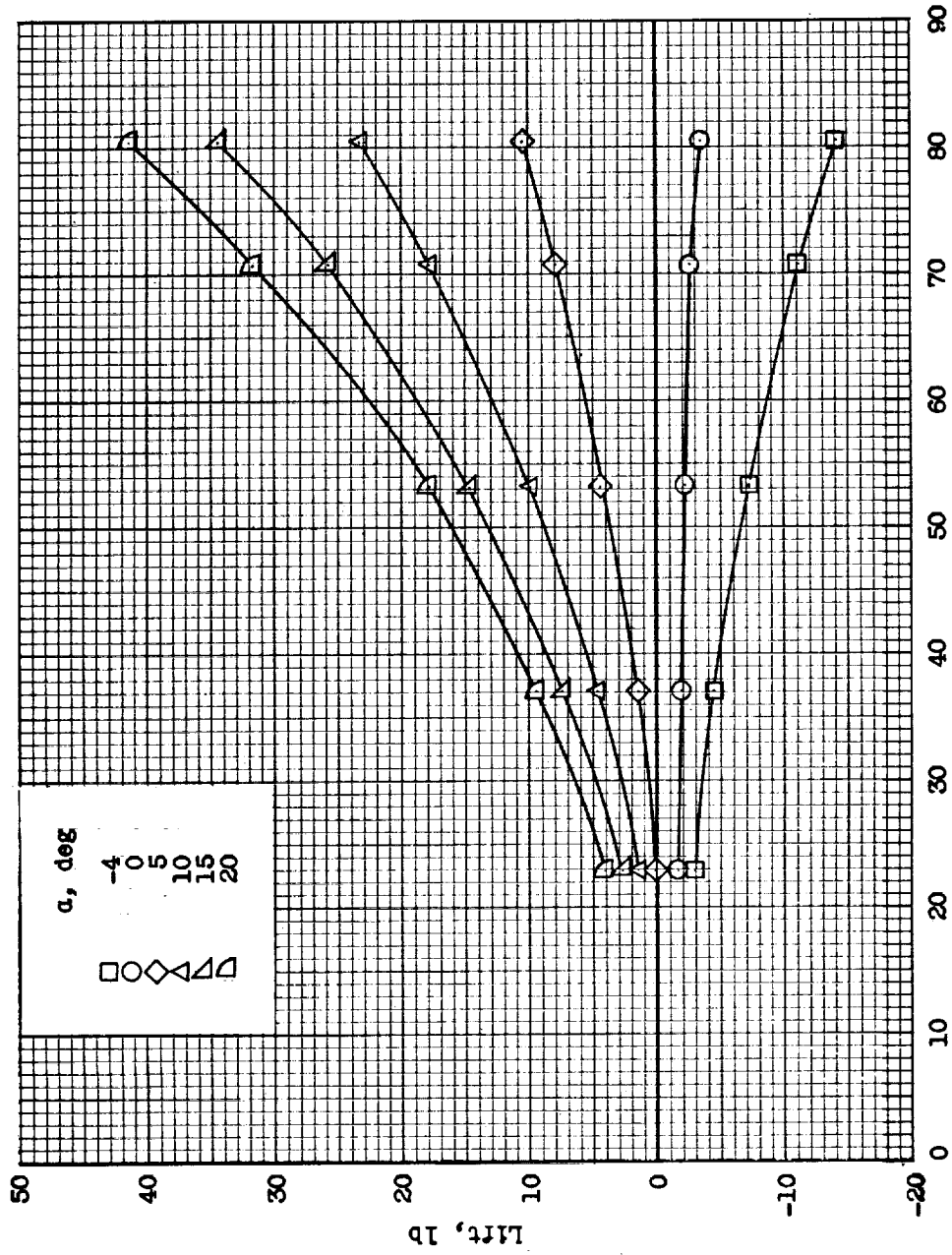

(a) Continued. $\Delta = 0^{\circ}$.

Figure 14.- Continued.

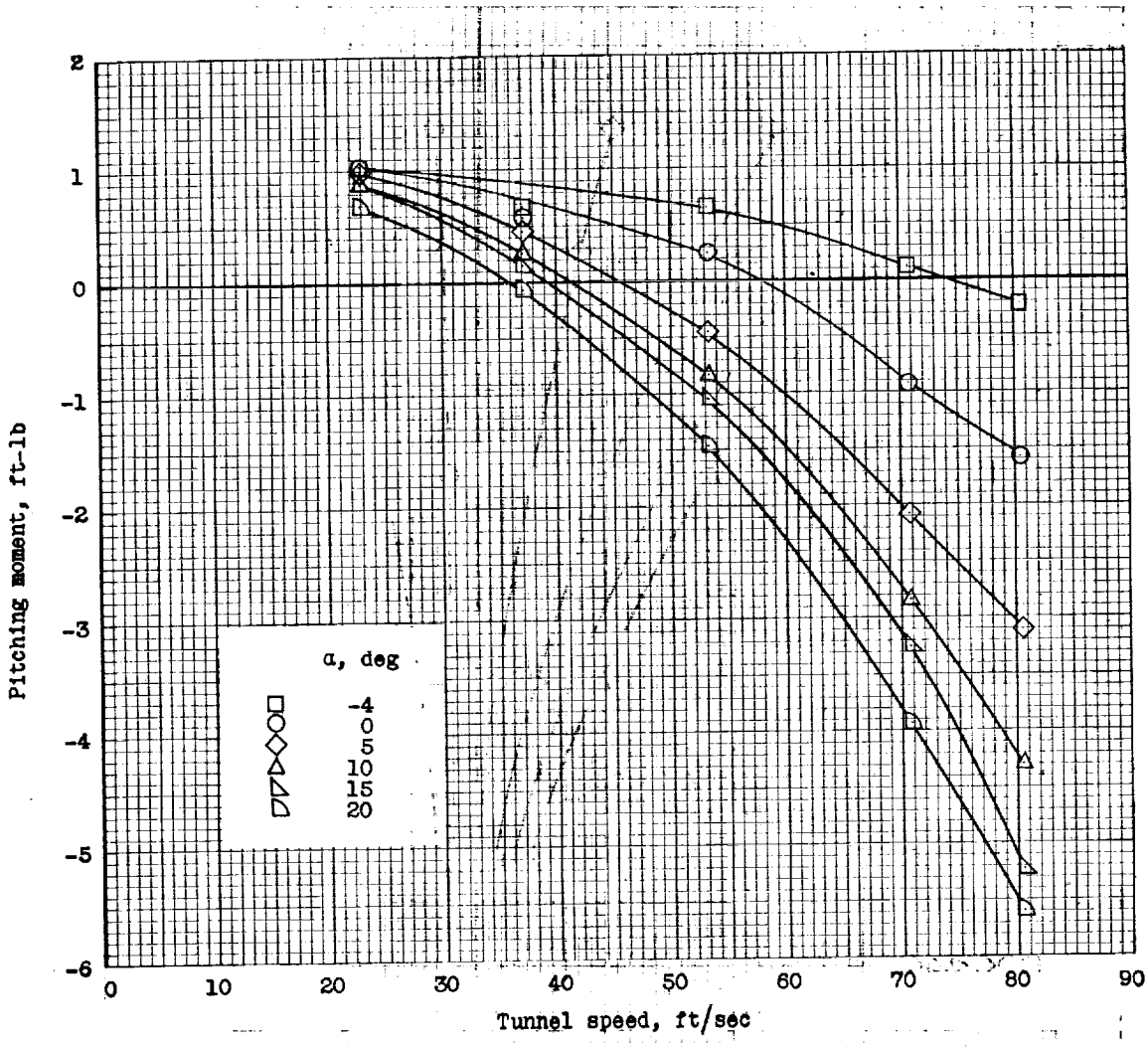

(a) Concluded. $\Delta = 0^{\circ}$.

Figure 14.- Continued.

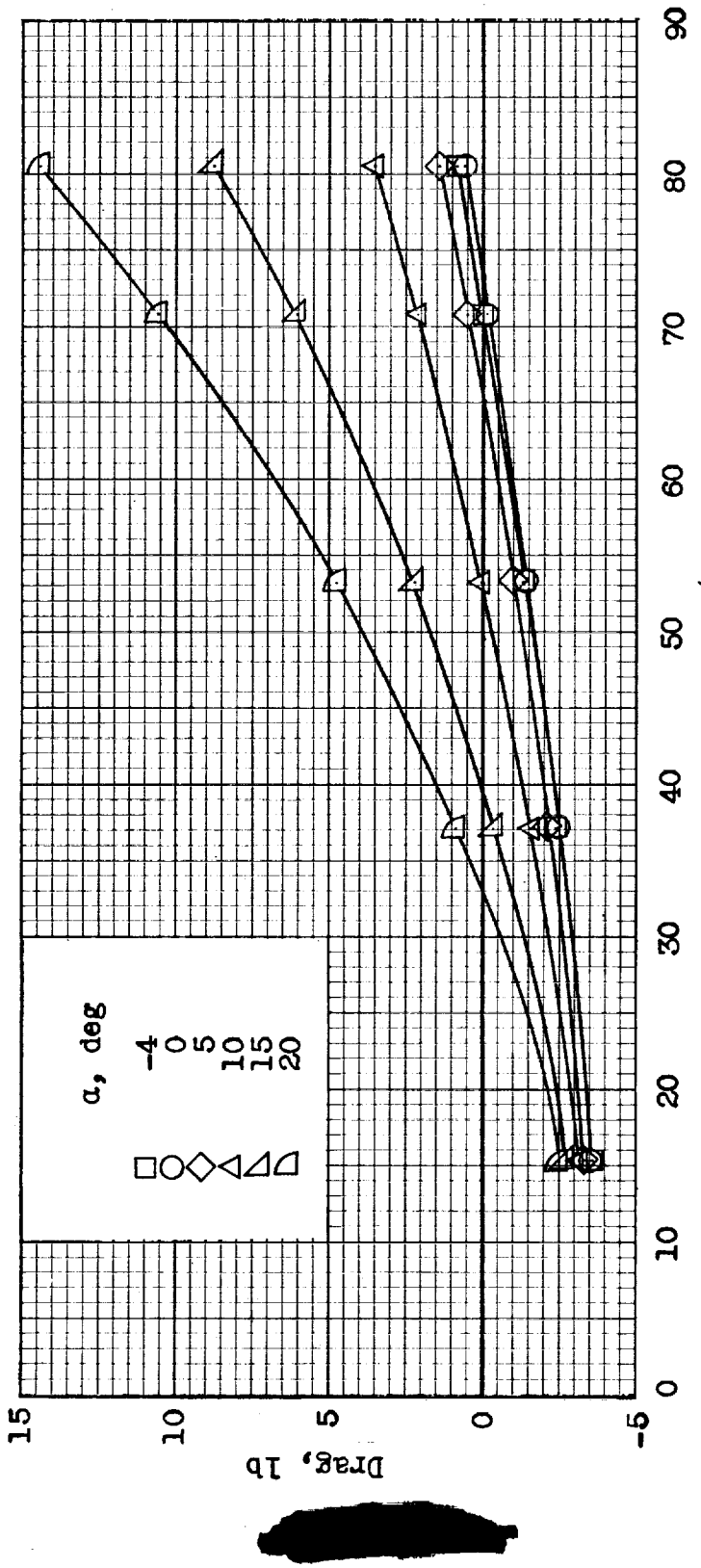

(b) $\Delta = 30^{\circ}$.

Figure 14.- Continued.

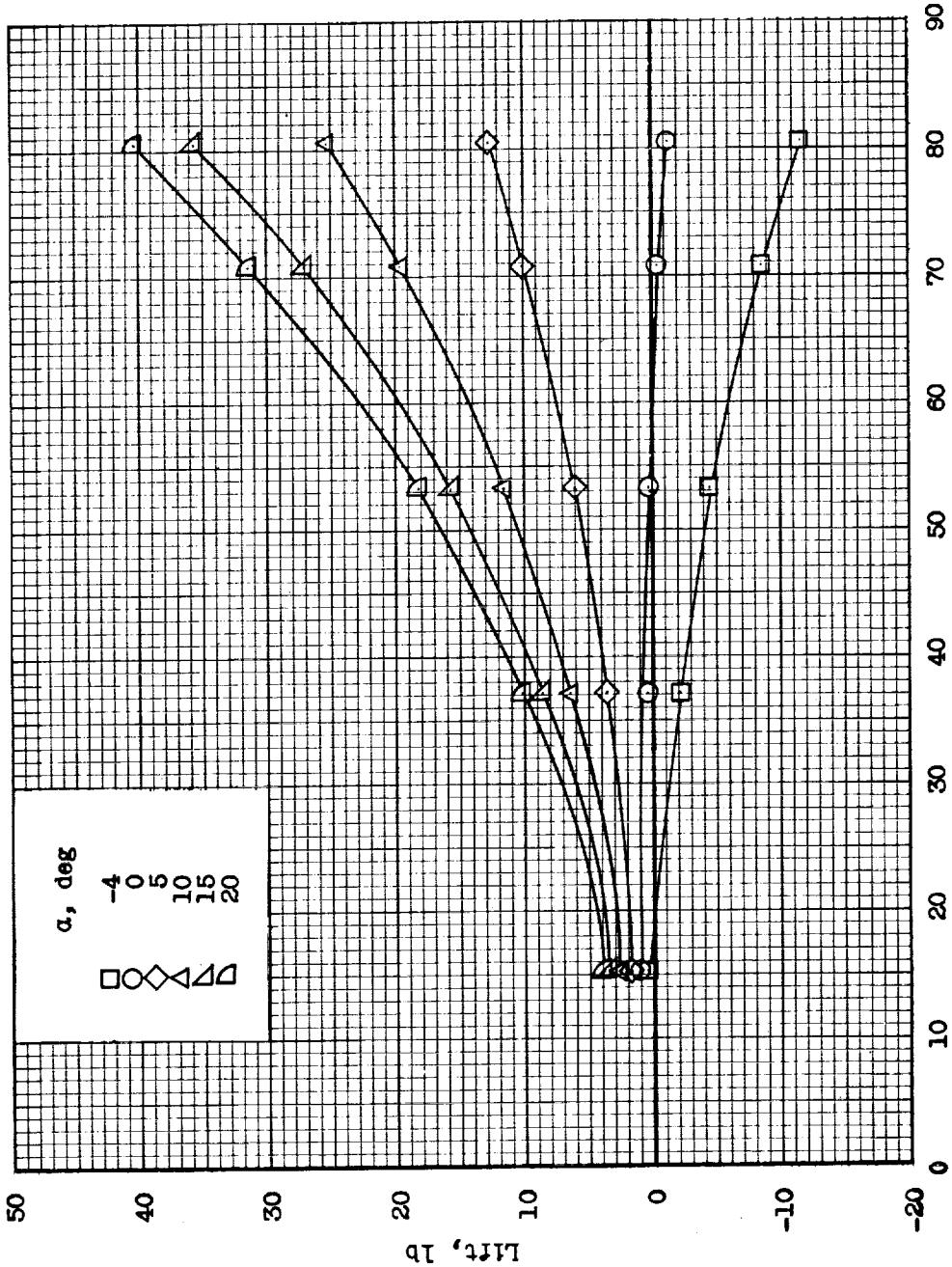

(b) Continued. $\Delta = 30°$.

Figure 14.- Continued.

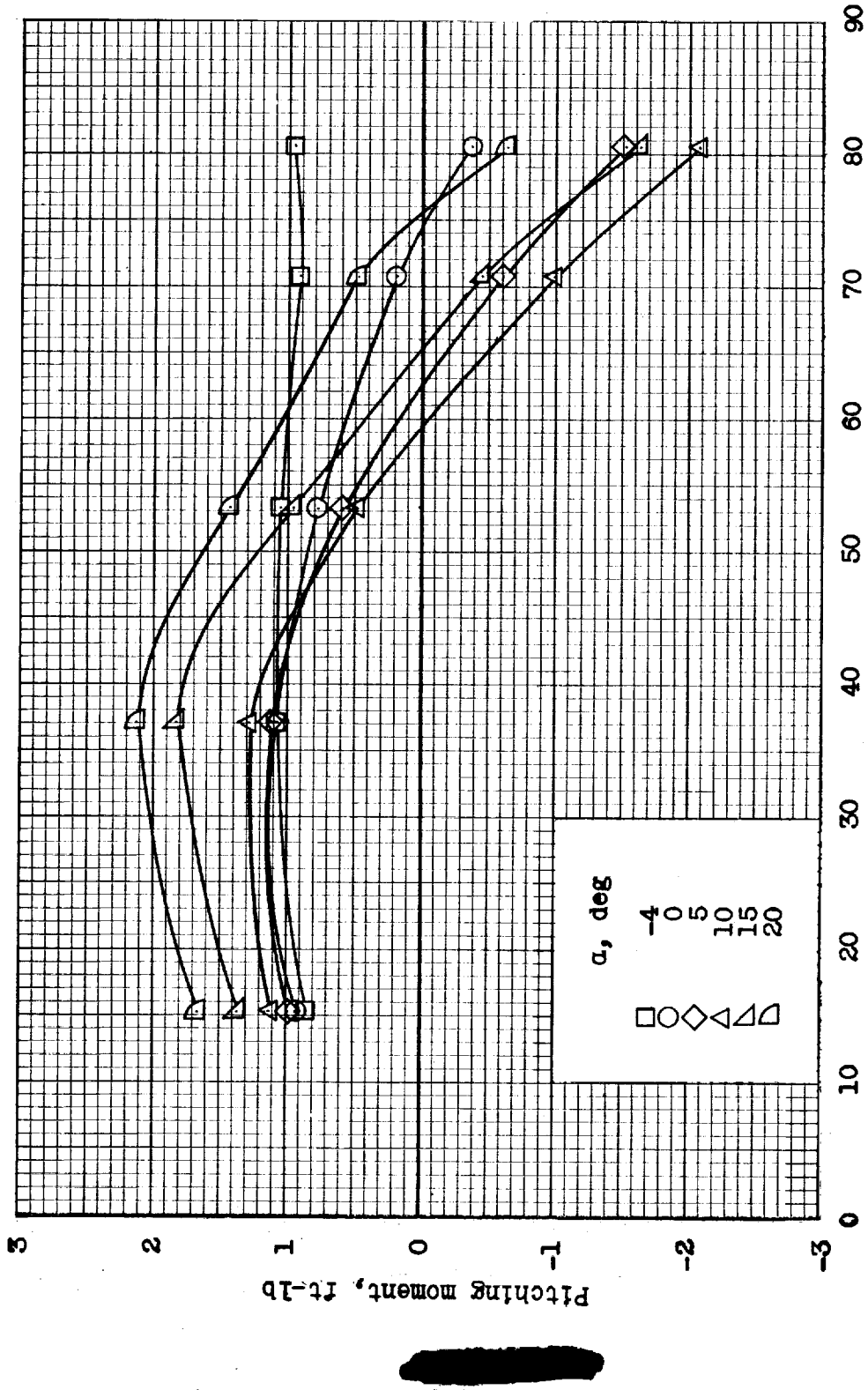

(b) Concluded. $\Delta = 30^{\circ}$.

Figure 14.- Continued.

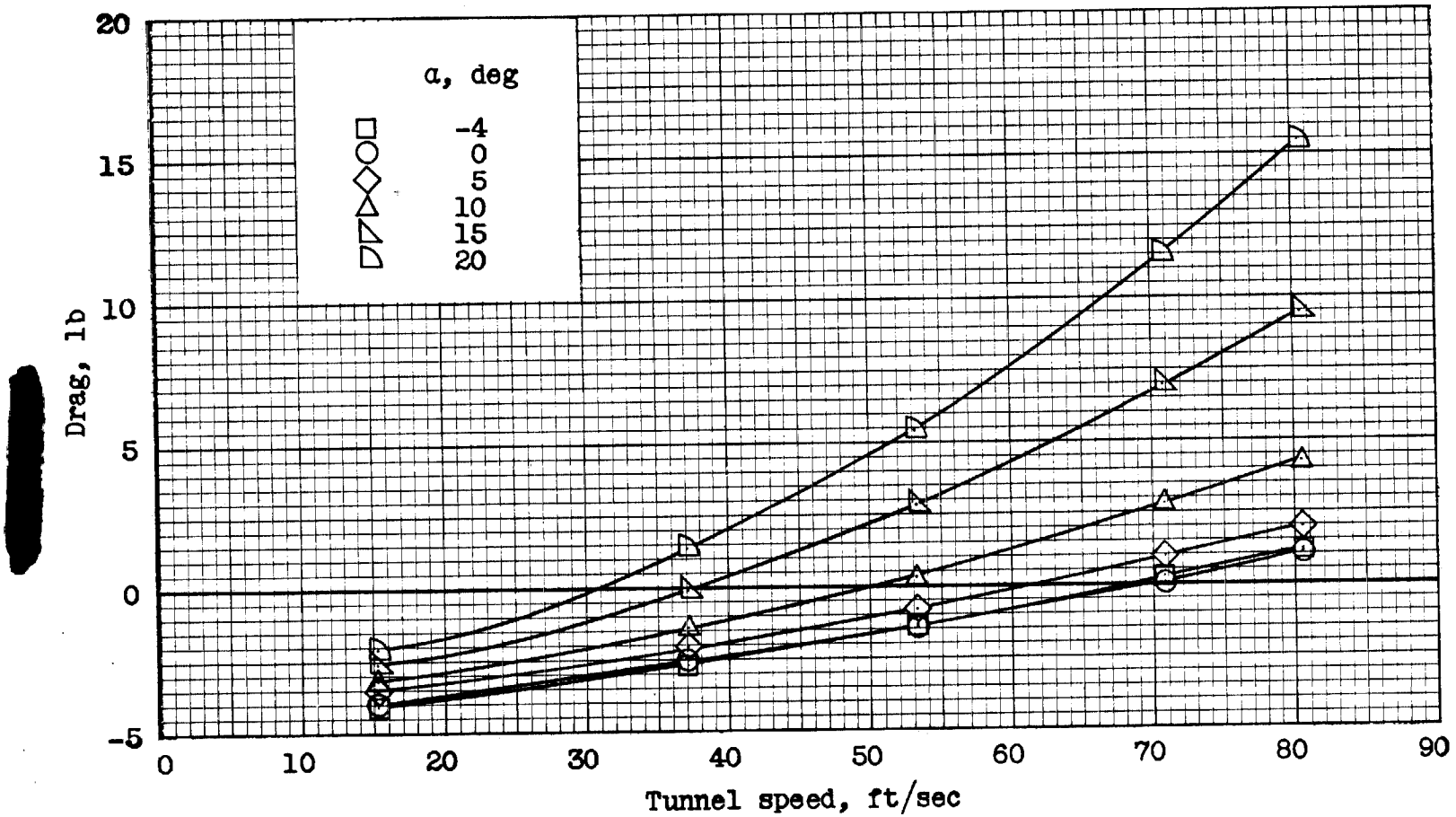

(c) $\Delta = 45^{\circ}$.

Figure 14.- Continued.

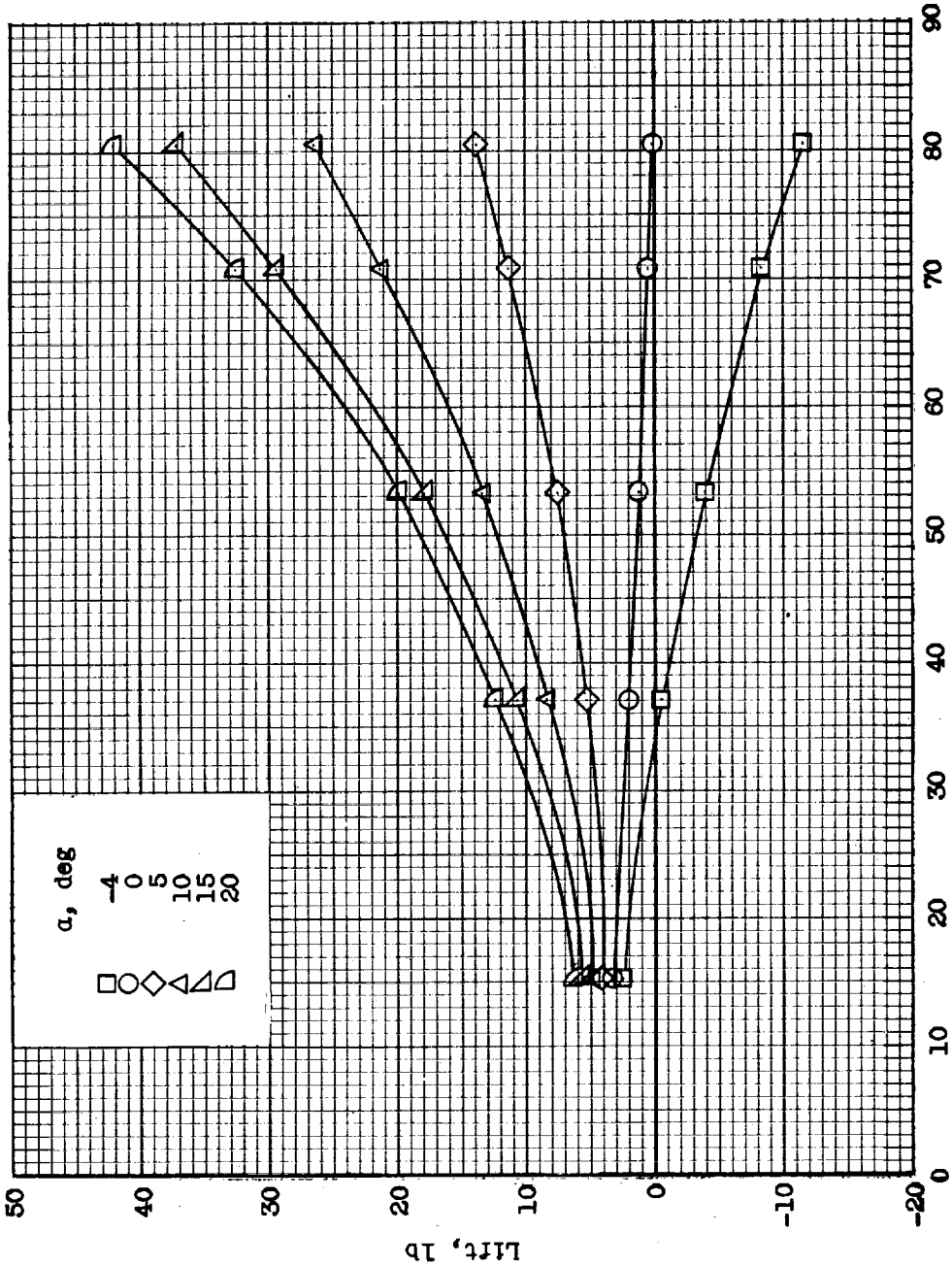

(c) Continued. $\Delta = 45°$.

Figure 14.- Continued.

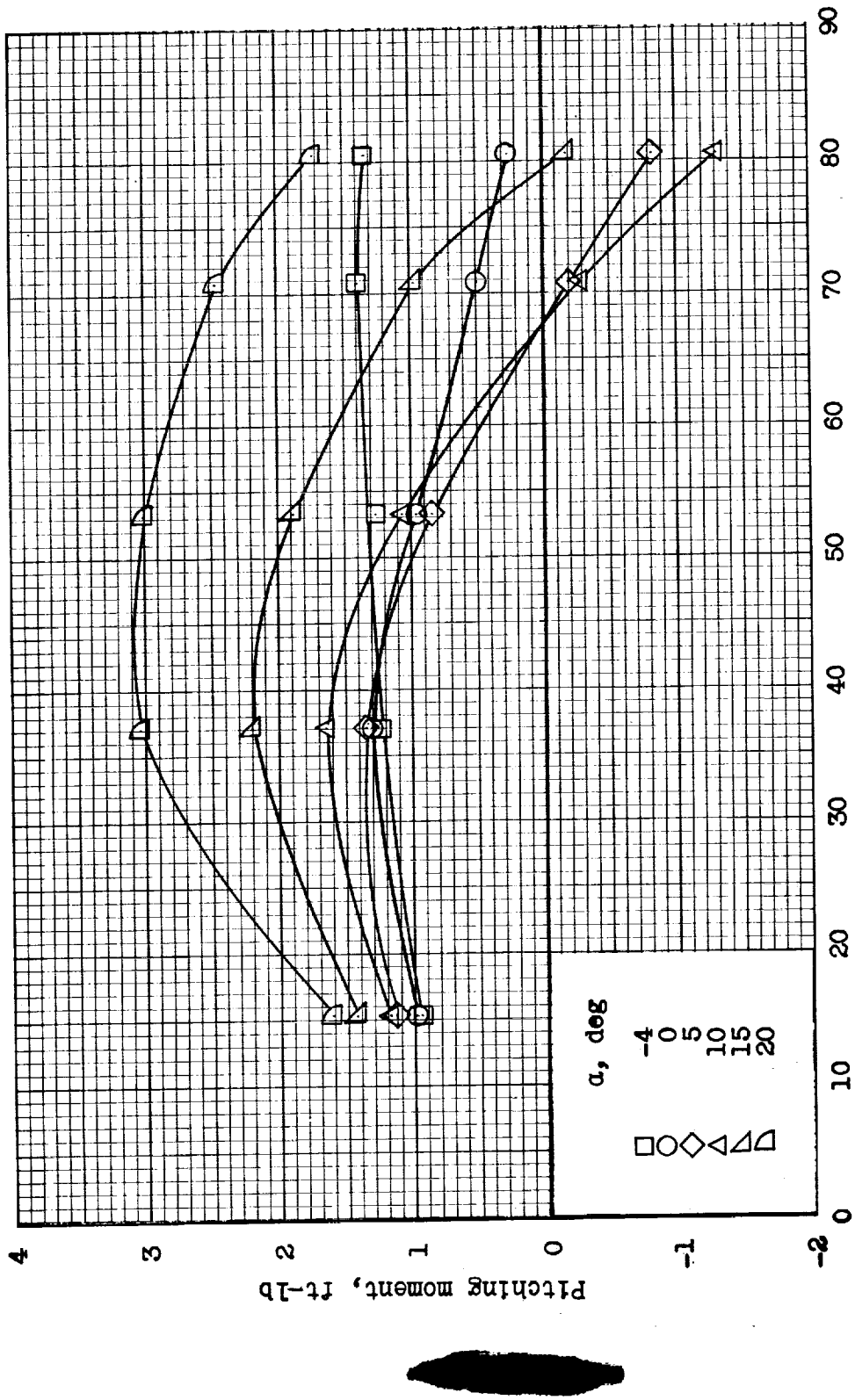

(c) Concluded. $\Delta = 45°$.

Figure 14.- Continued.

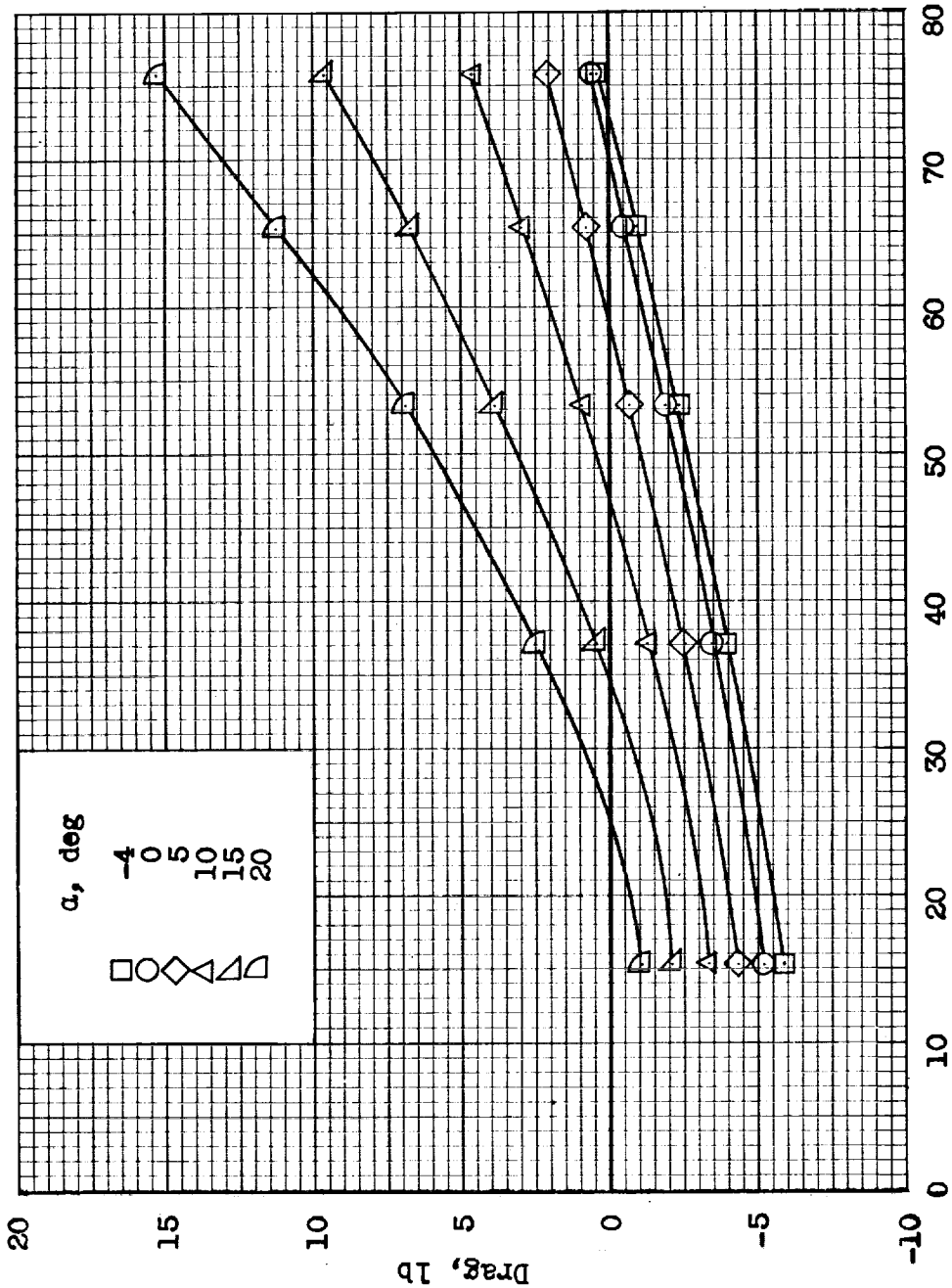

(d) $\Delta = 60^{\circ}$.

Figure 14.- Continued.

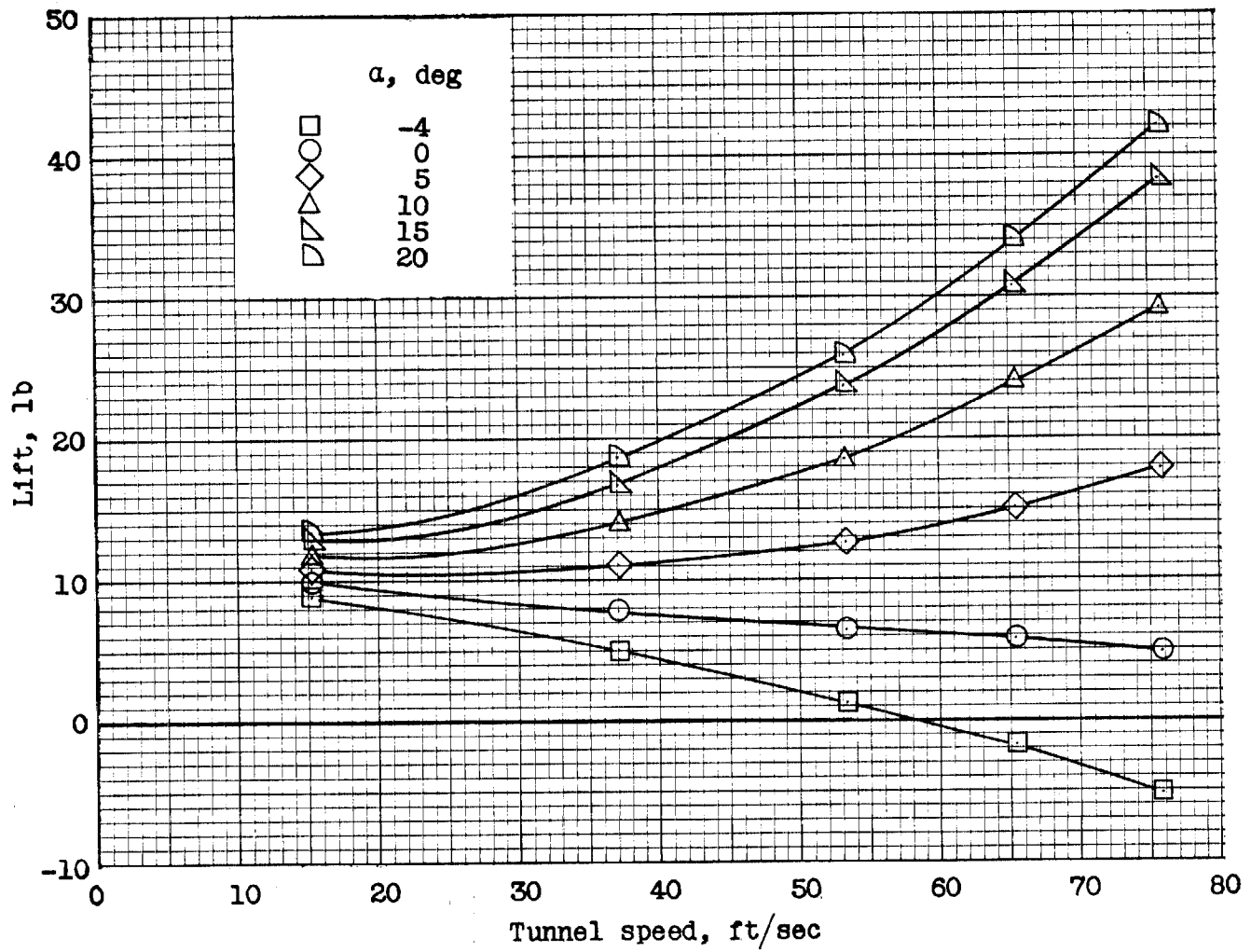

(d) Continued. $\Delta = 60^{\circ}$.

Figure 14.- Continued.

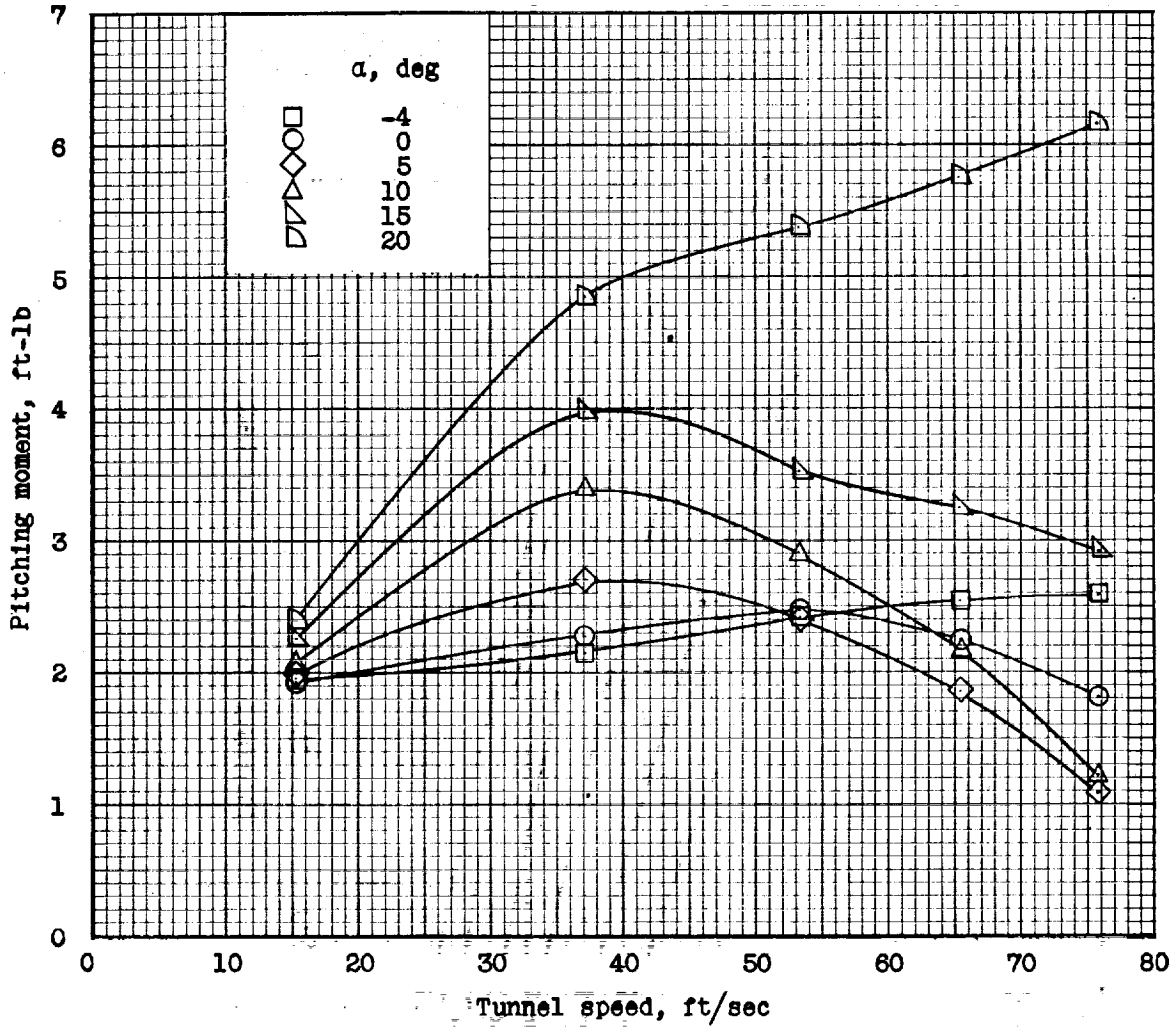

(d) Concluded. $\Delta = 60^{\circ}$.

Figure 14.- Continued.

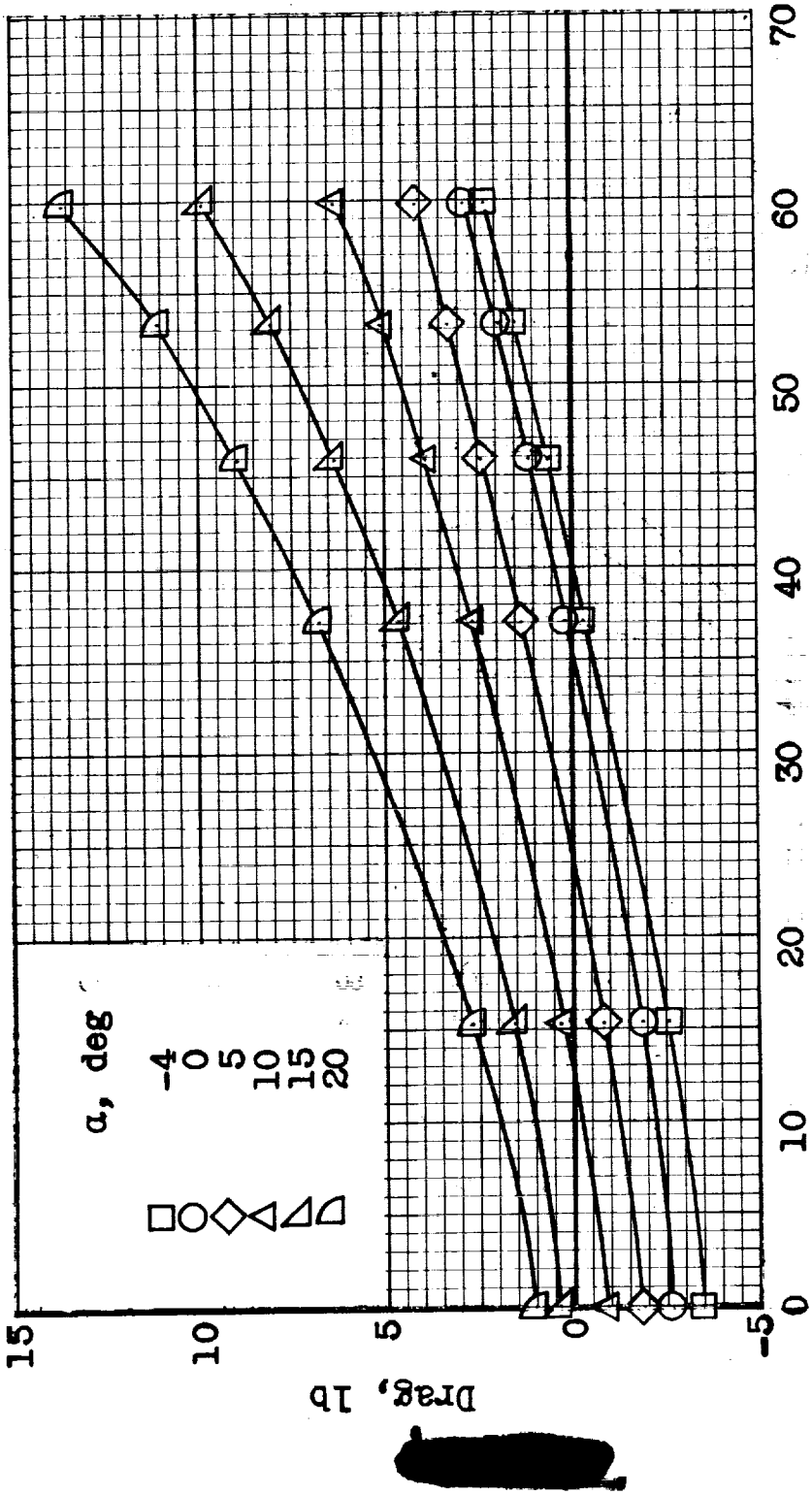

(e) $\Delta = 75°$.

Figure 14.- Continued.

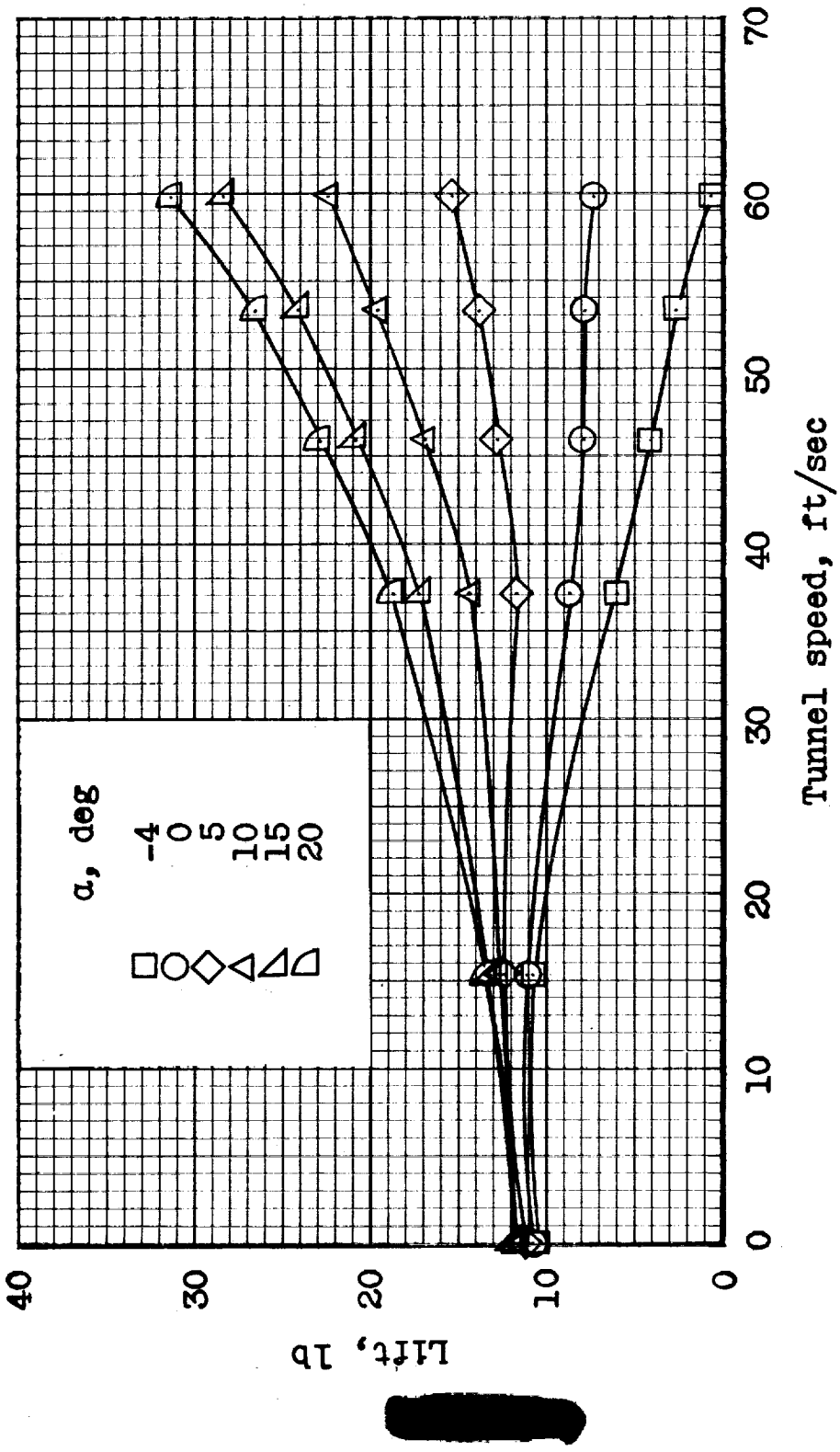

(e) Continued. $\Delta = 75^{\circ}$.

Figure 14.- Continued.

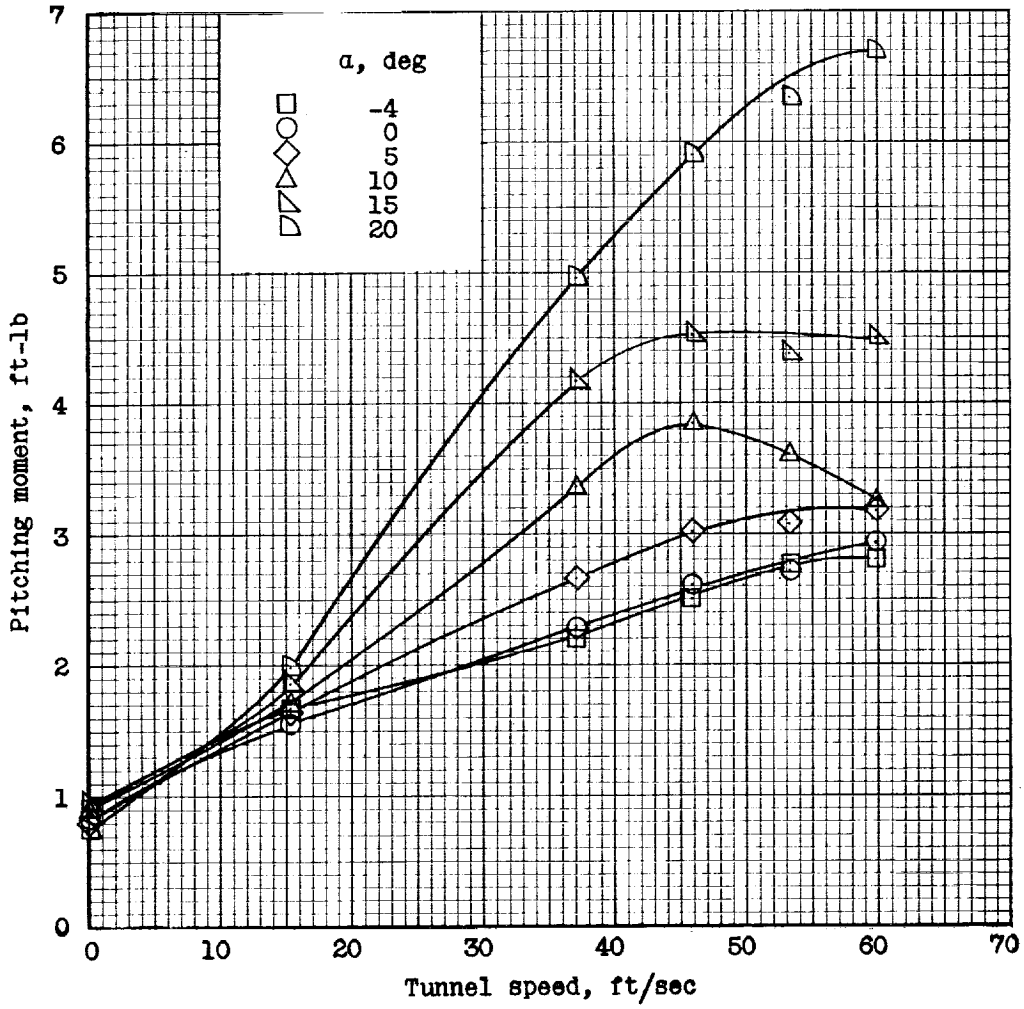

(e) Concluded. $\Delta = 75^{\circ}$.

Figure 14.- Concluded.

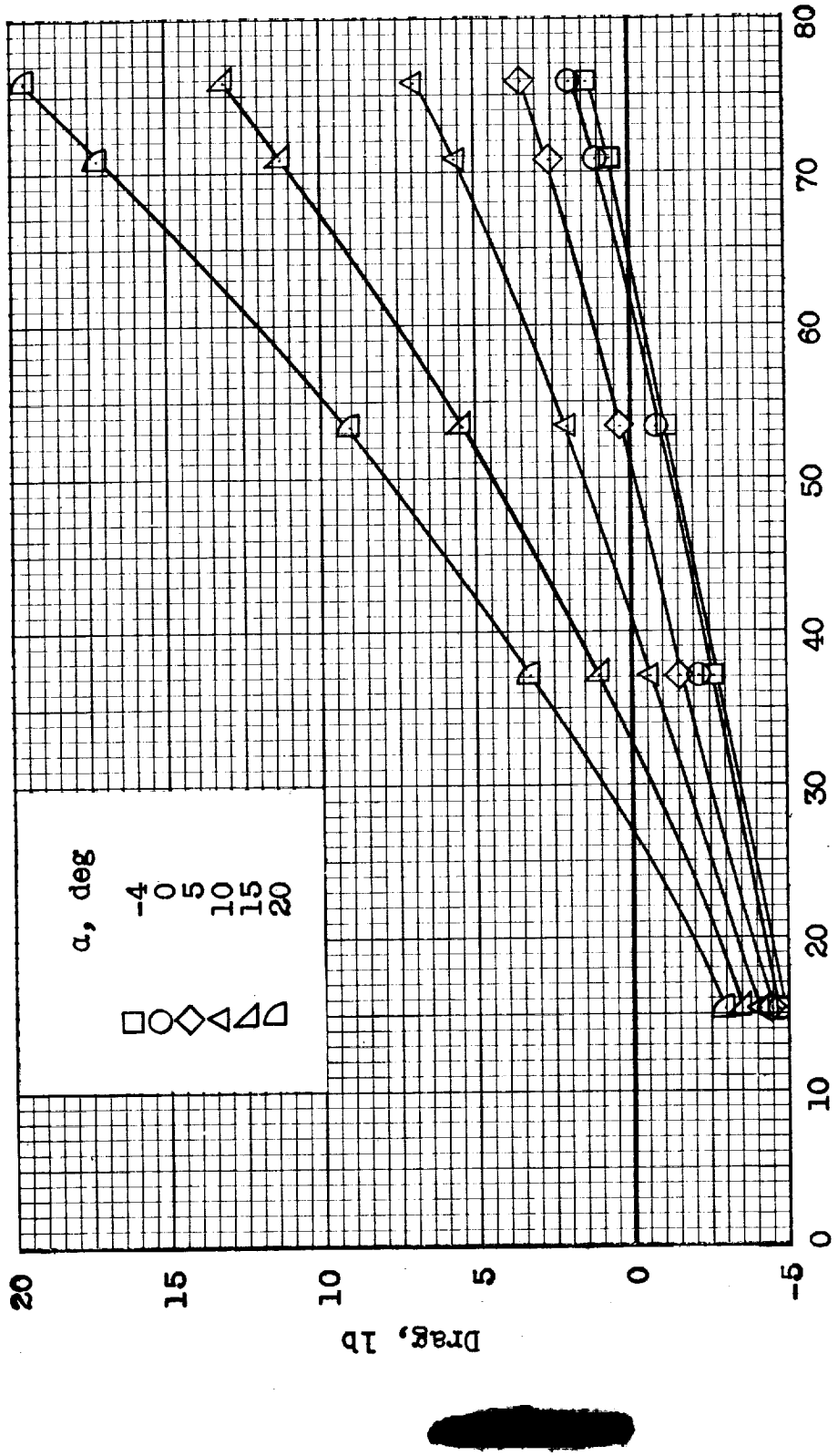

(a) $\Delta = 0^{\circ}$.

Figure 15.- Longitudinal force-test data for the model with the flaps deflected and $i_t = 0^{\circ}$. Referred to the wind axes. $\delta_f = 50^{\circ}$; $i_t = 0^{\circ}$.

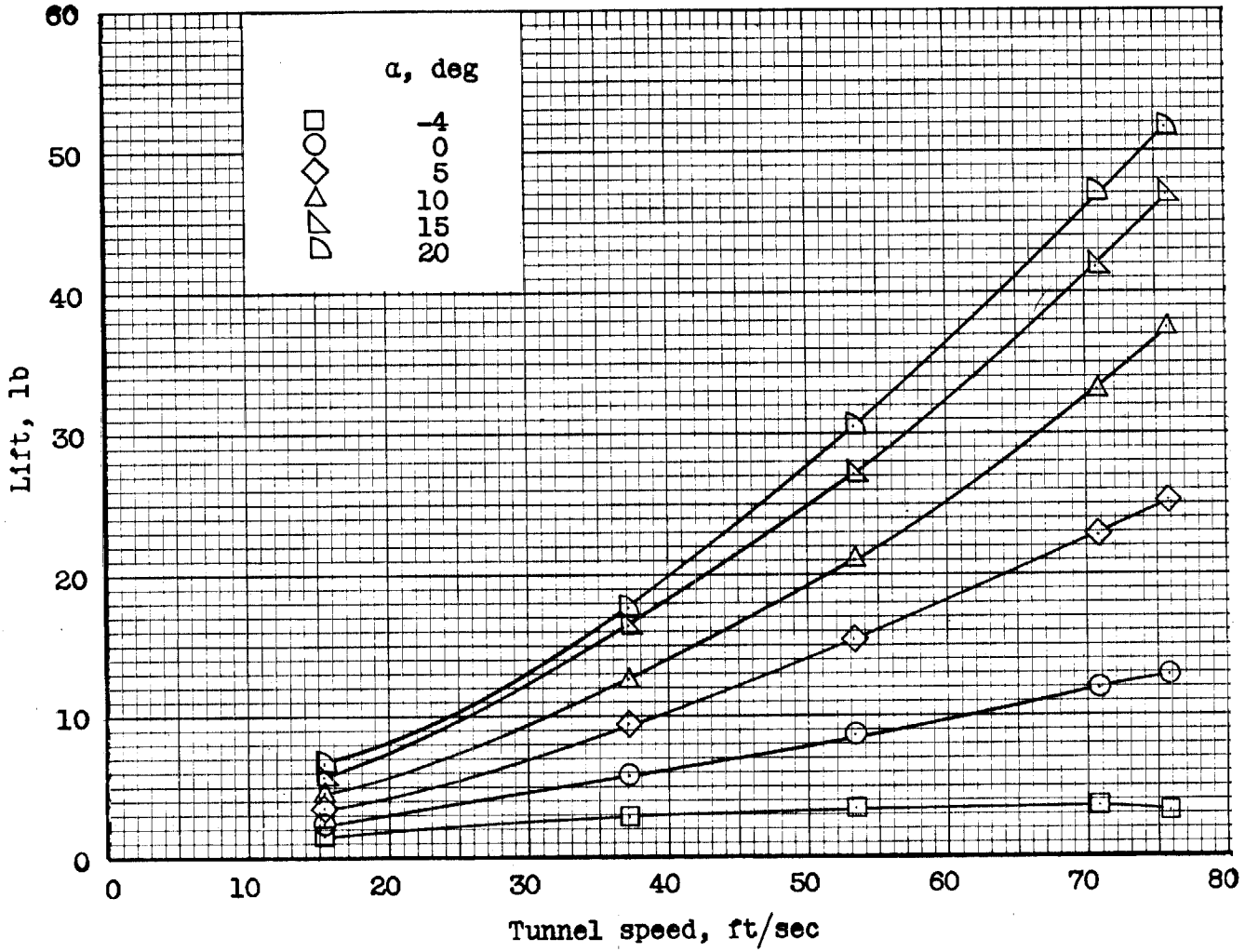

(a) Continued. $\Delta = 0^{\circ}$.

Figure 15.- Continued.

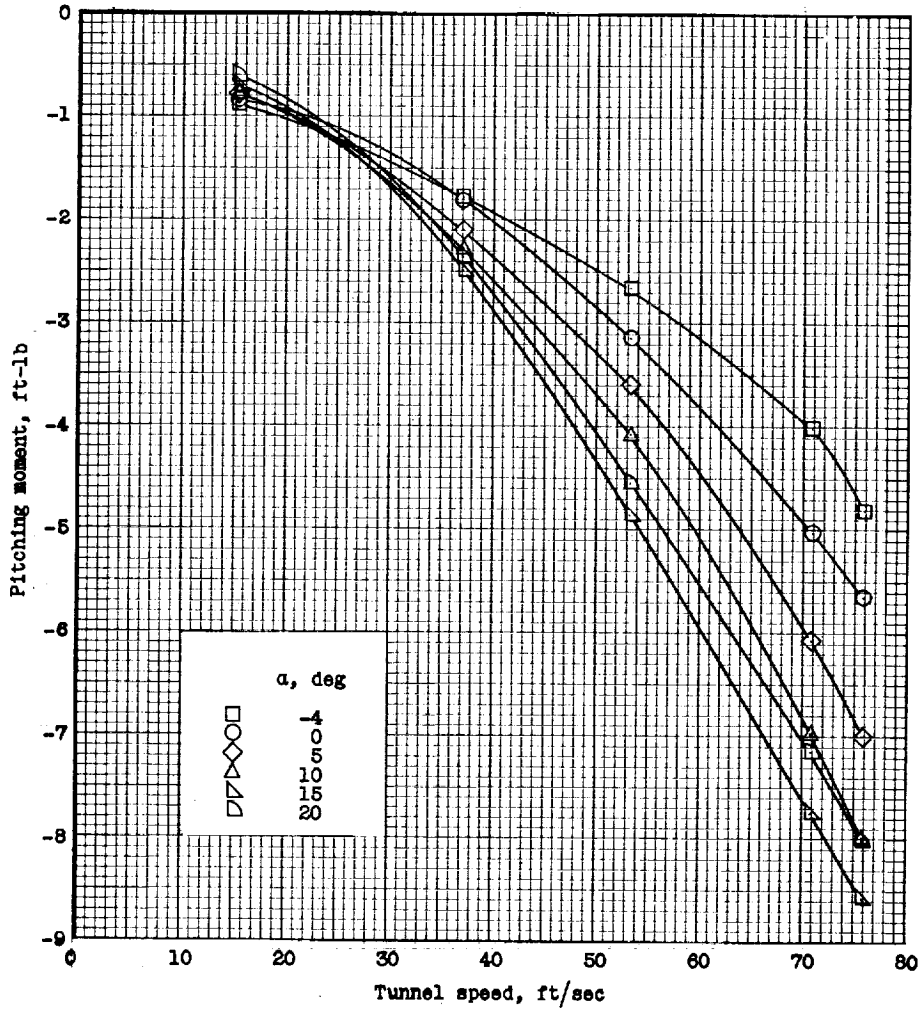

(a) Concluded. $\Delta = 0^{\circ}$.

Figure 15.- Continued.

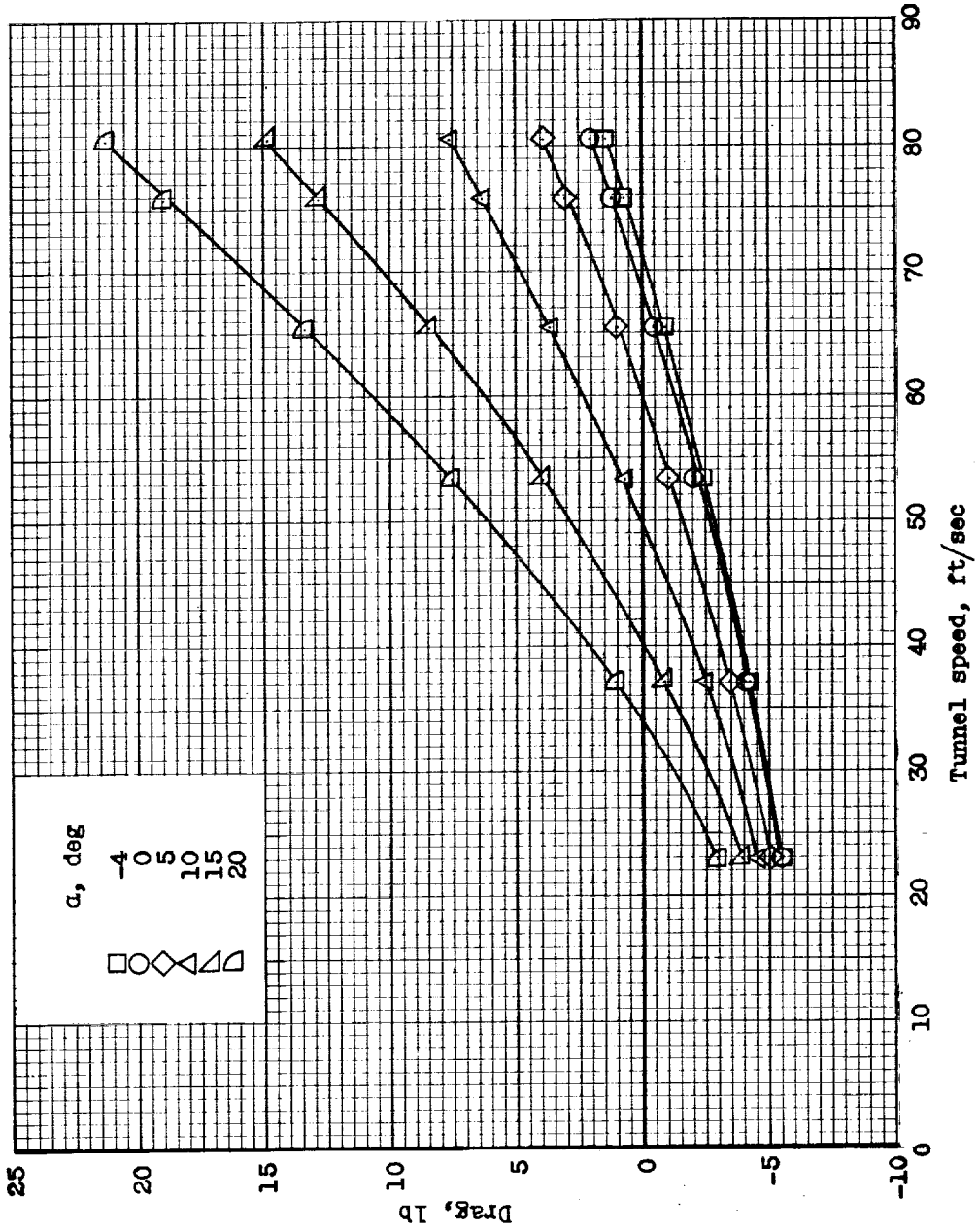

(b) $\Delta = 30^{\circ}$.

Figure 15.- Continued.

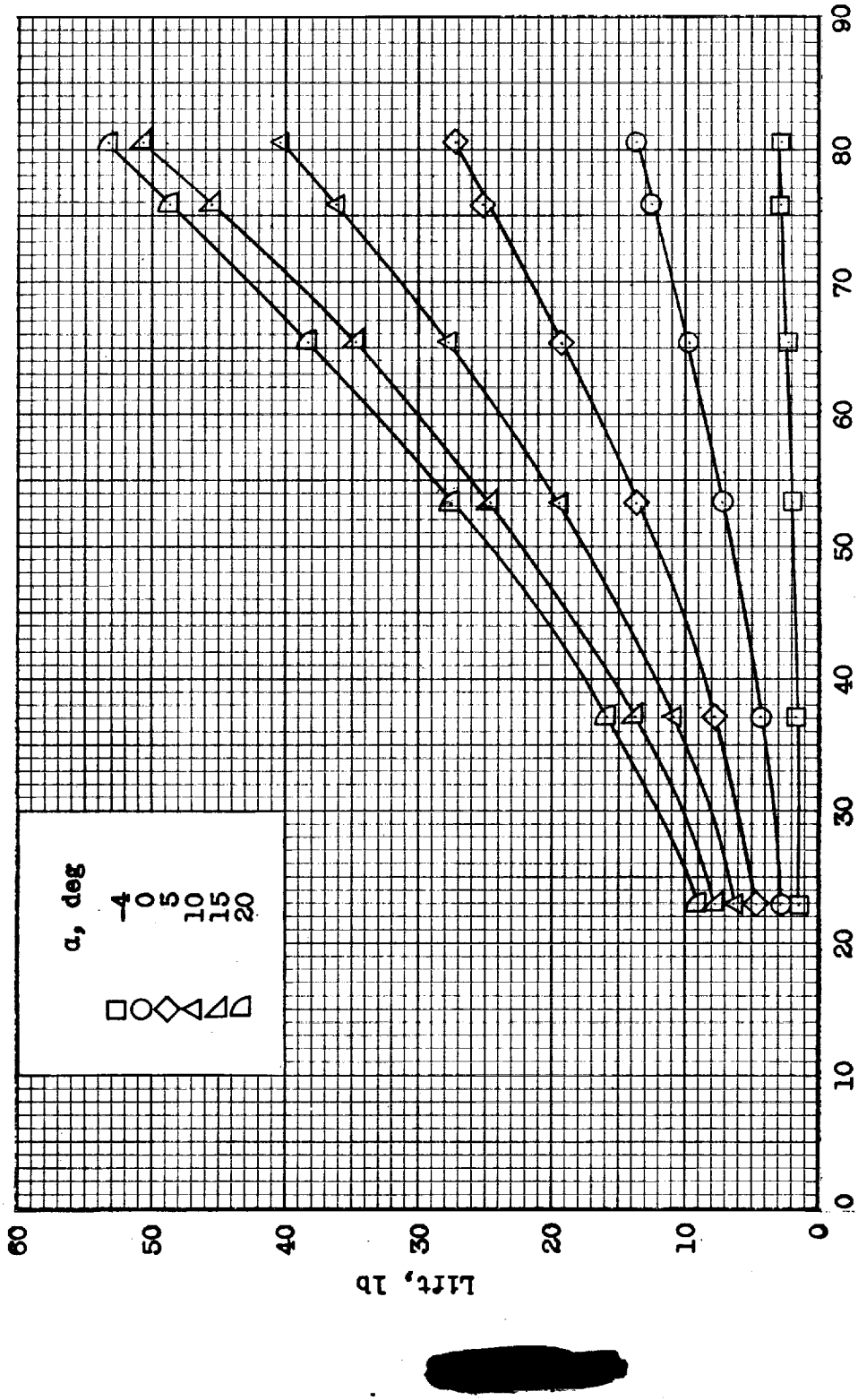

(b) Continued. $\Delta = 30^{\circ}$.

Figure 15.- Continued.

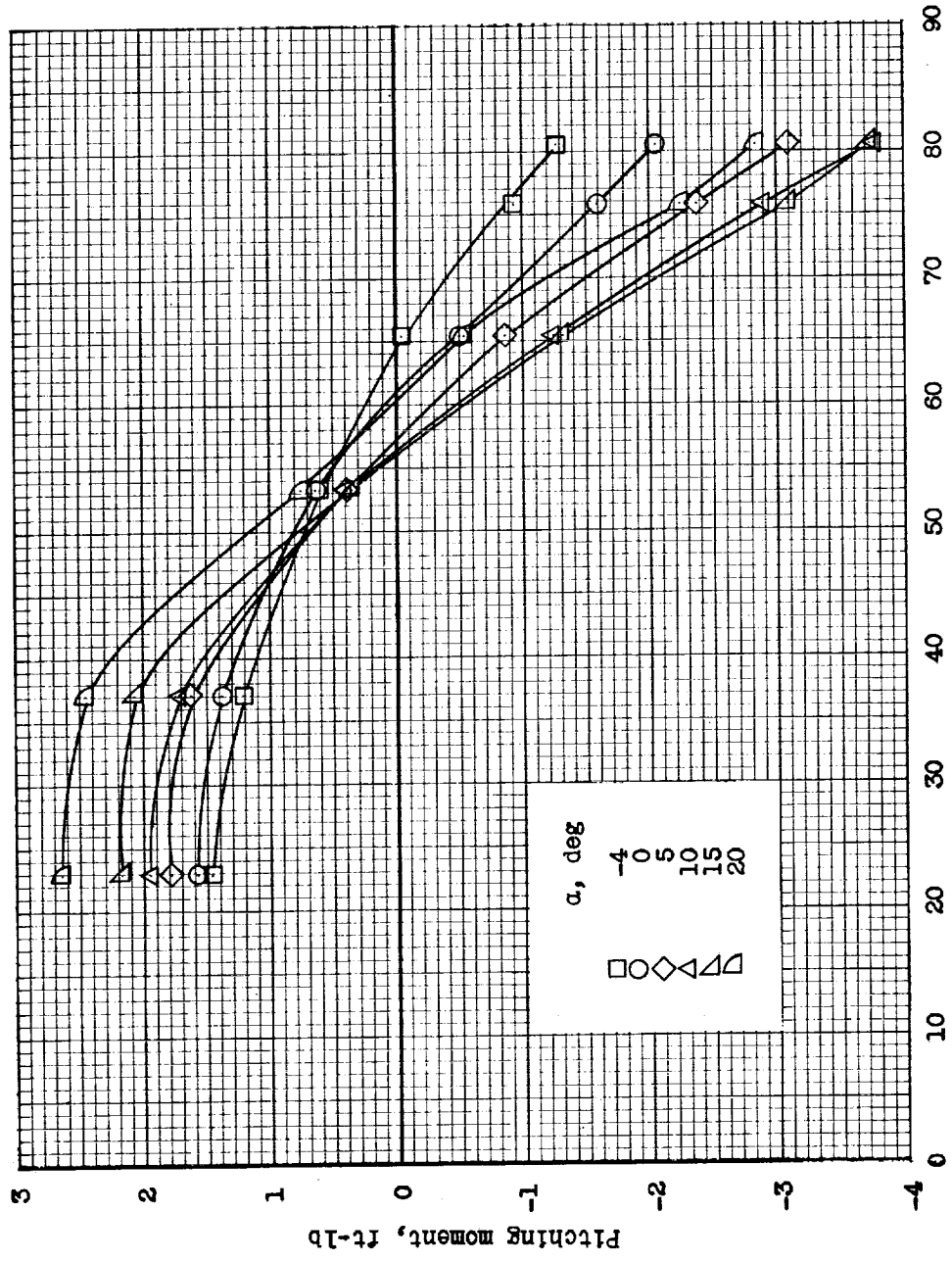

(b) Concluded. $\Delta = 30^{\circ}$.

Figure 15.- Continued.

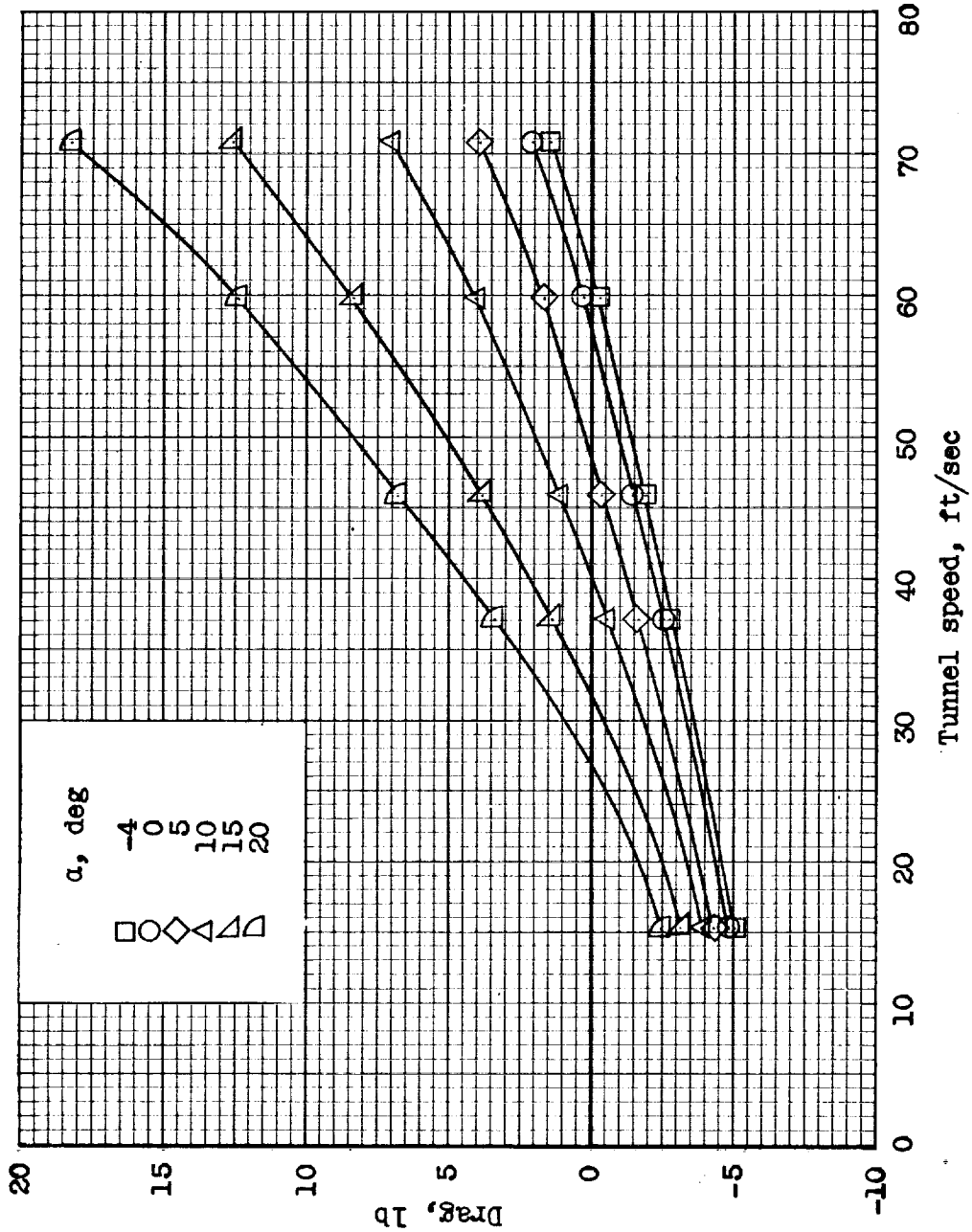

(c) $\Delta = 45^{\circ}$.

Figure 15.- Continued.

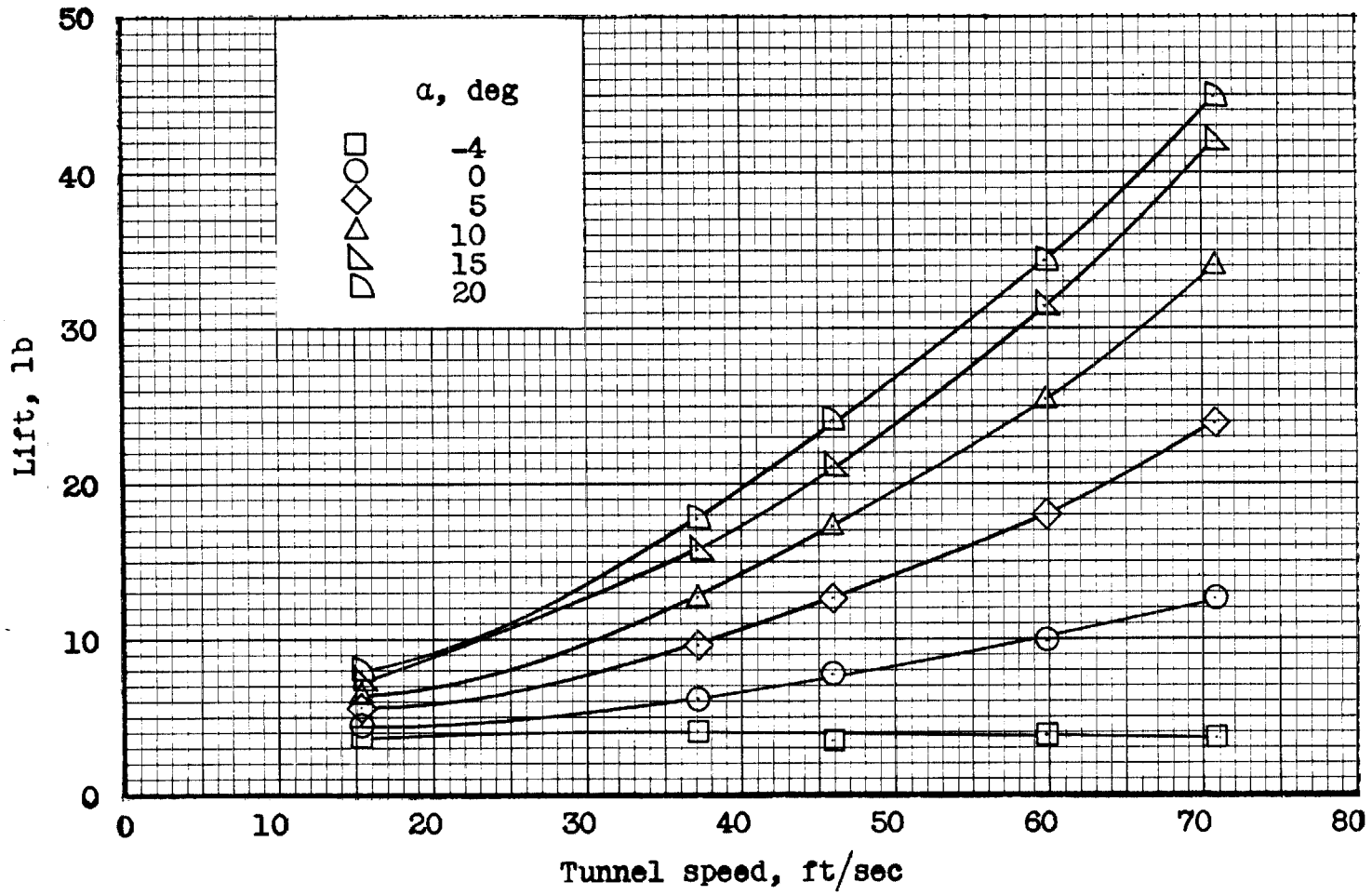

(c) Continued. $\Delta = 45^{\circ}$.

Figure 15.- Continued.

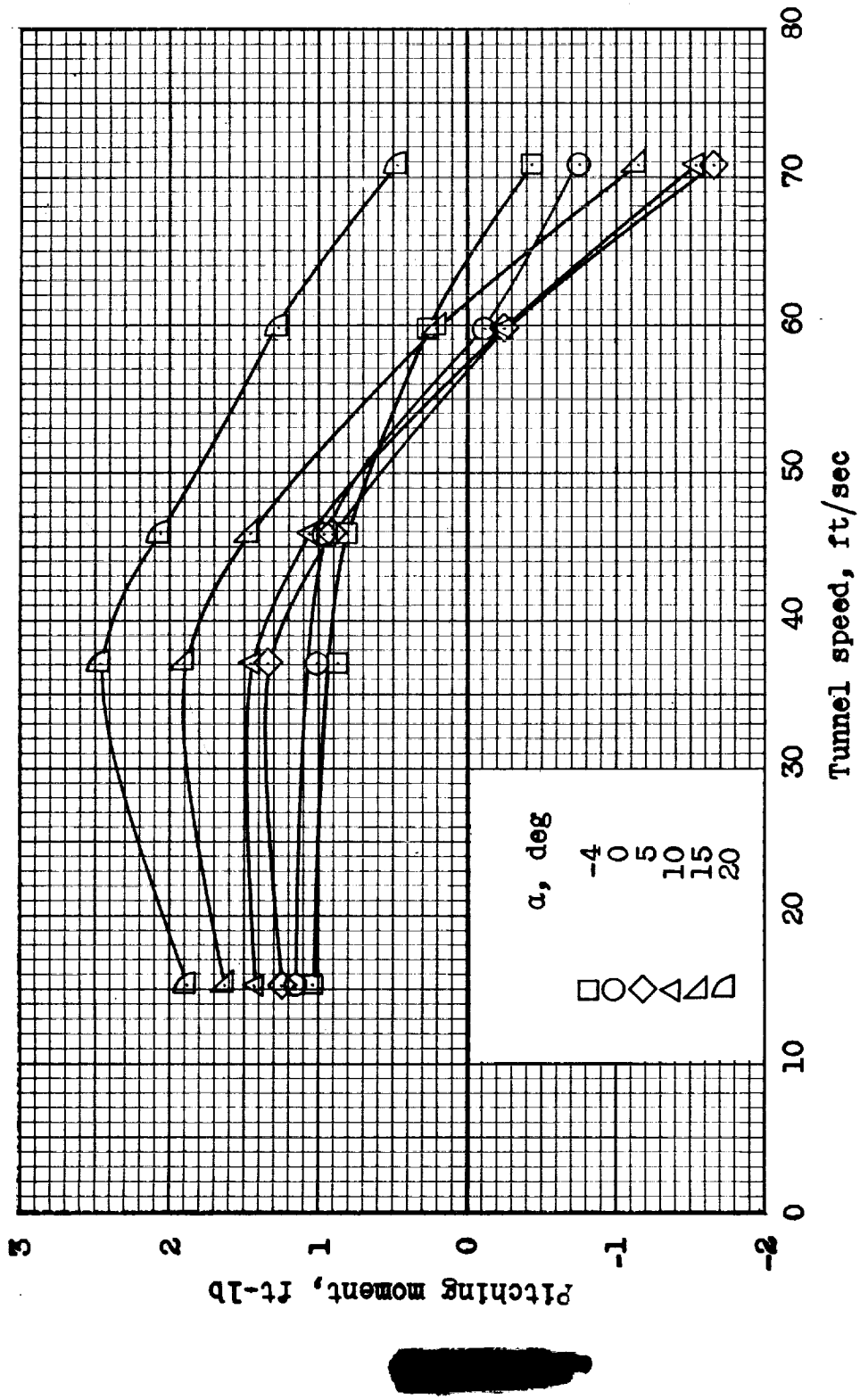

(c) Concluded. $\Delta = 45^{\circ}$.

Figure 15.- Continued.

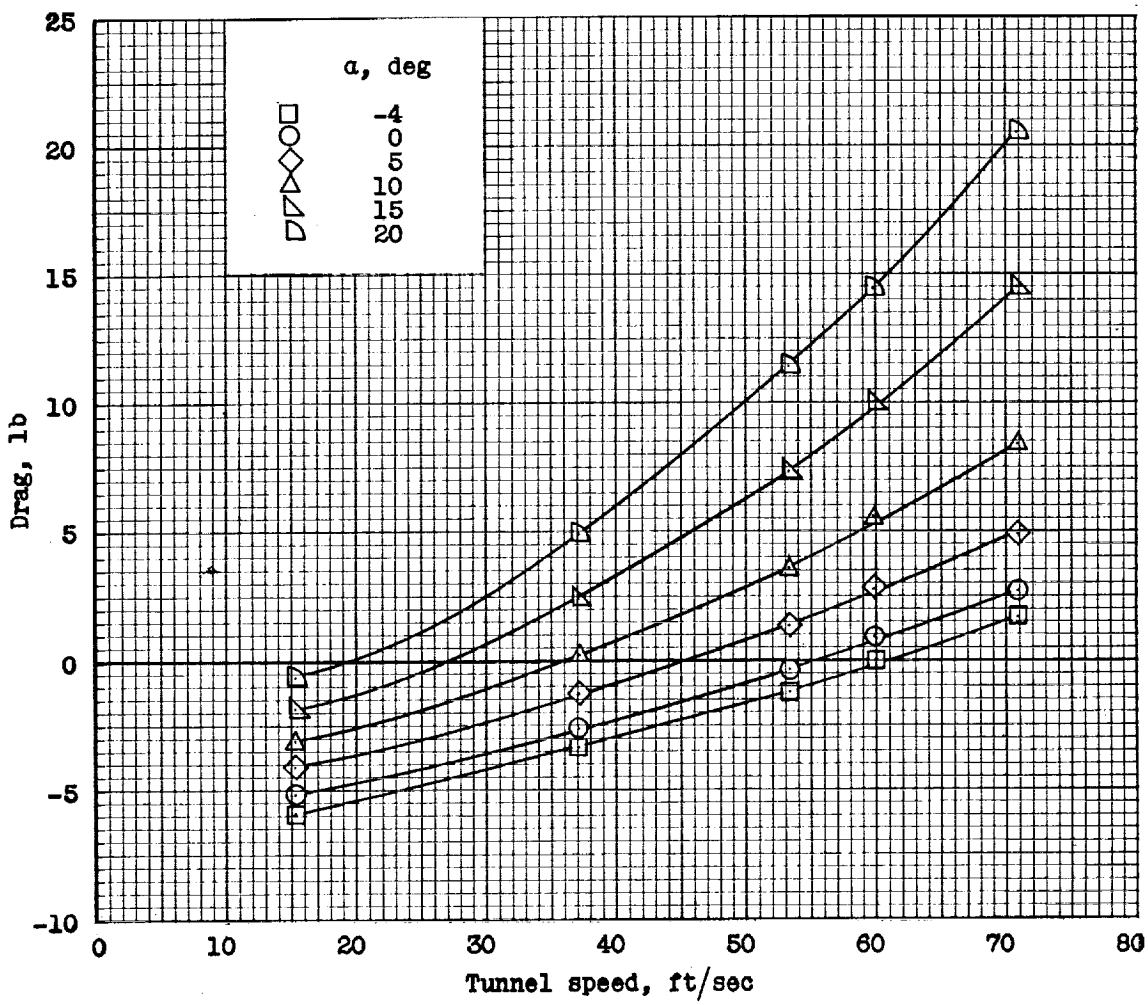

(d) $\Delta = 60^{\circ}$.

Figure 15.- Continued.

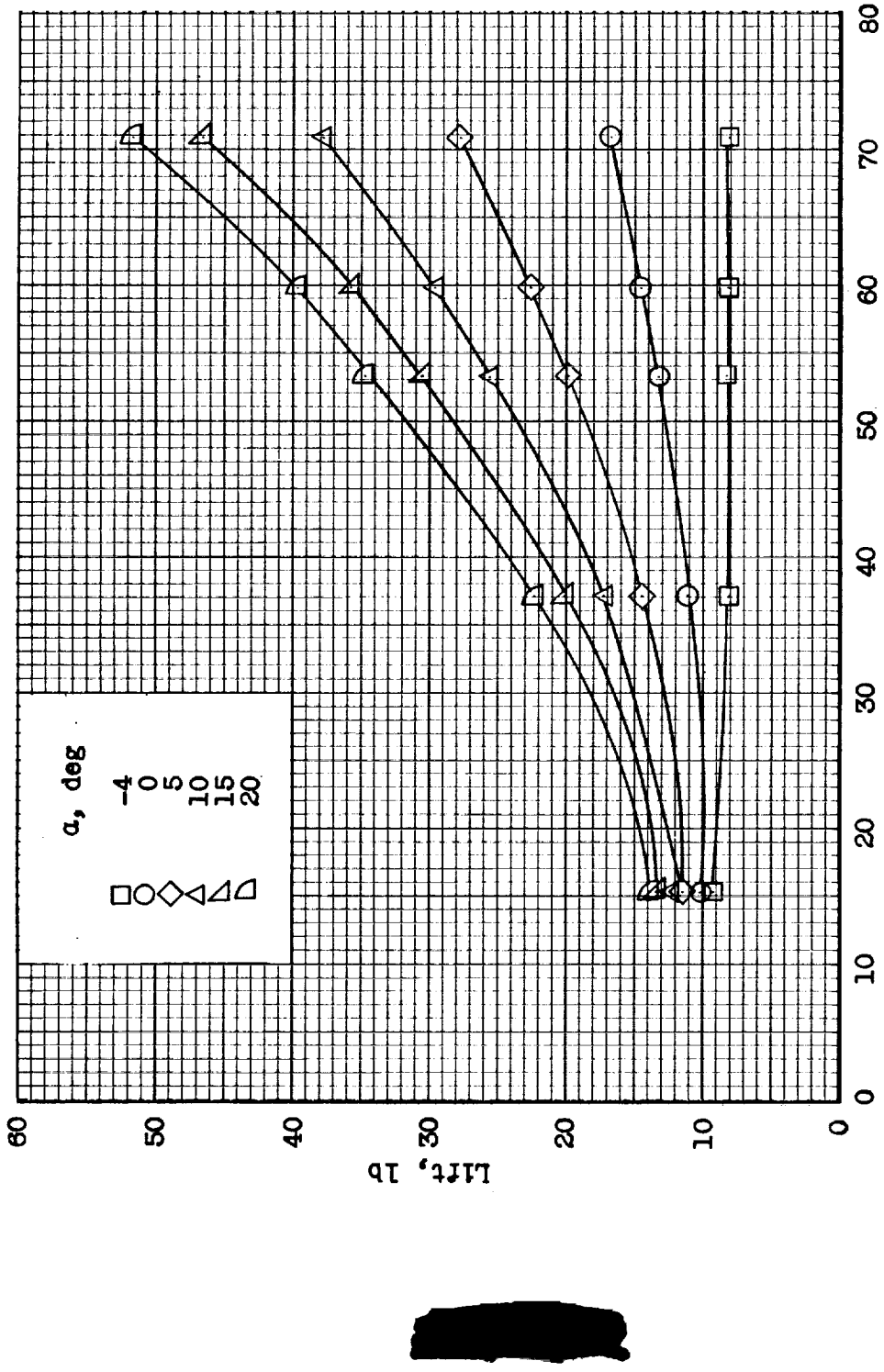

(d) Continued. $\Delta = 60°$.

Figure 15.- Continued.

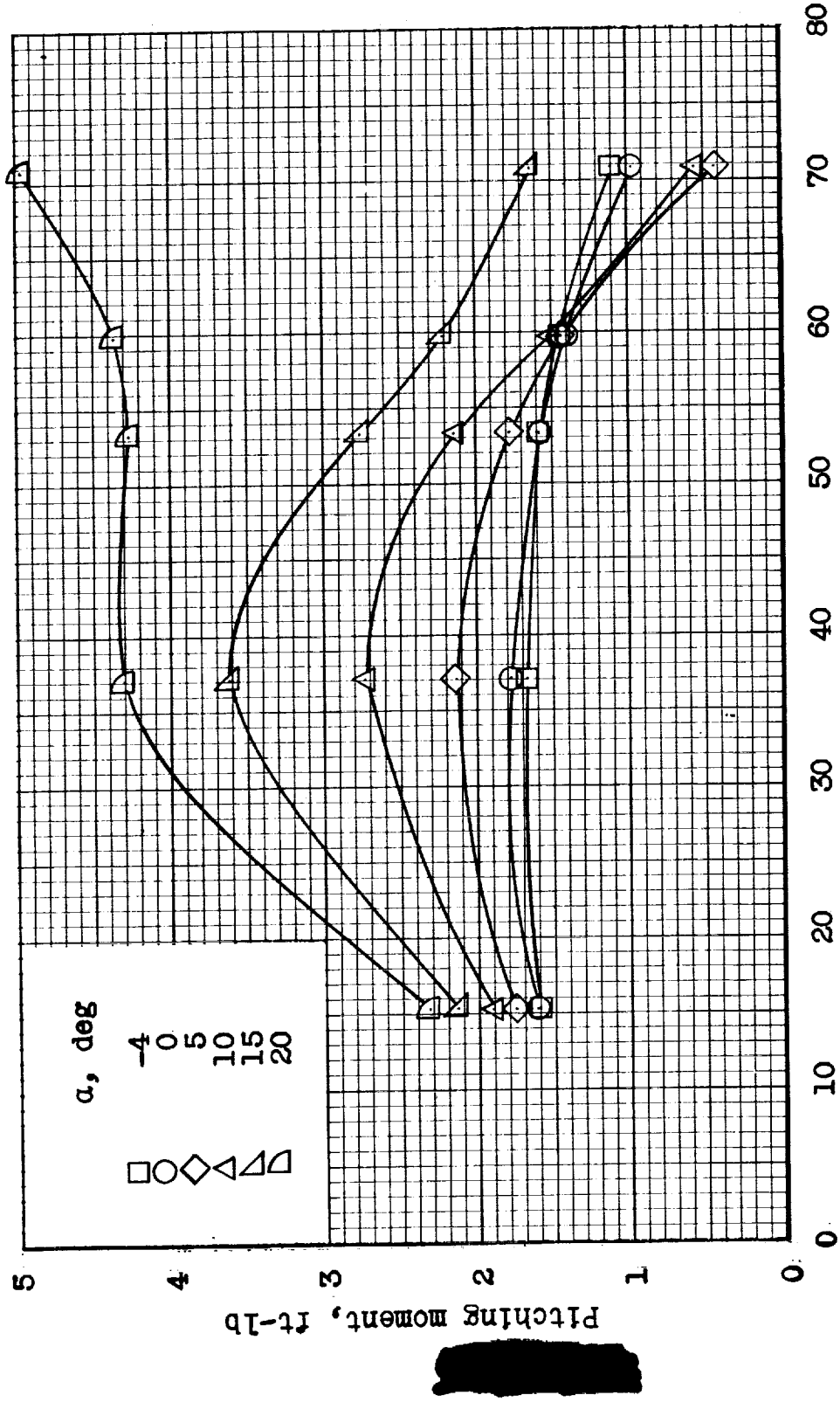

(d) Concluded. $\Delta = 60^{\circ}$.

Figure 15.- Continued.

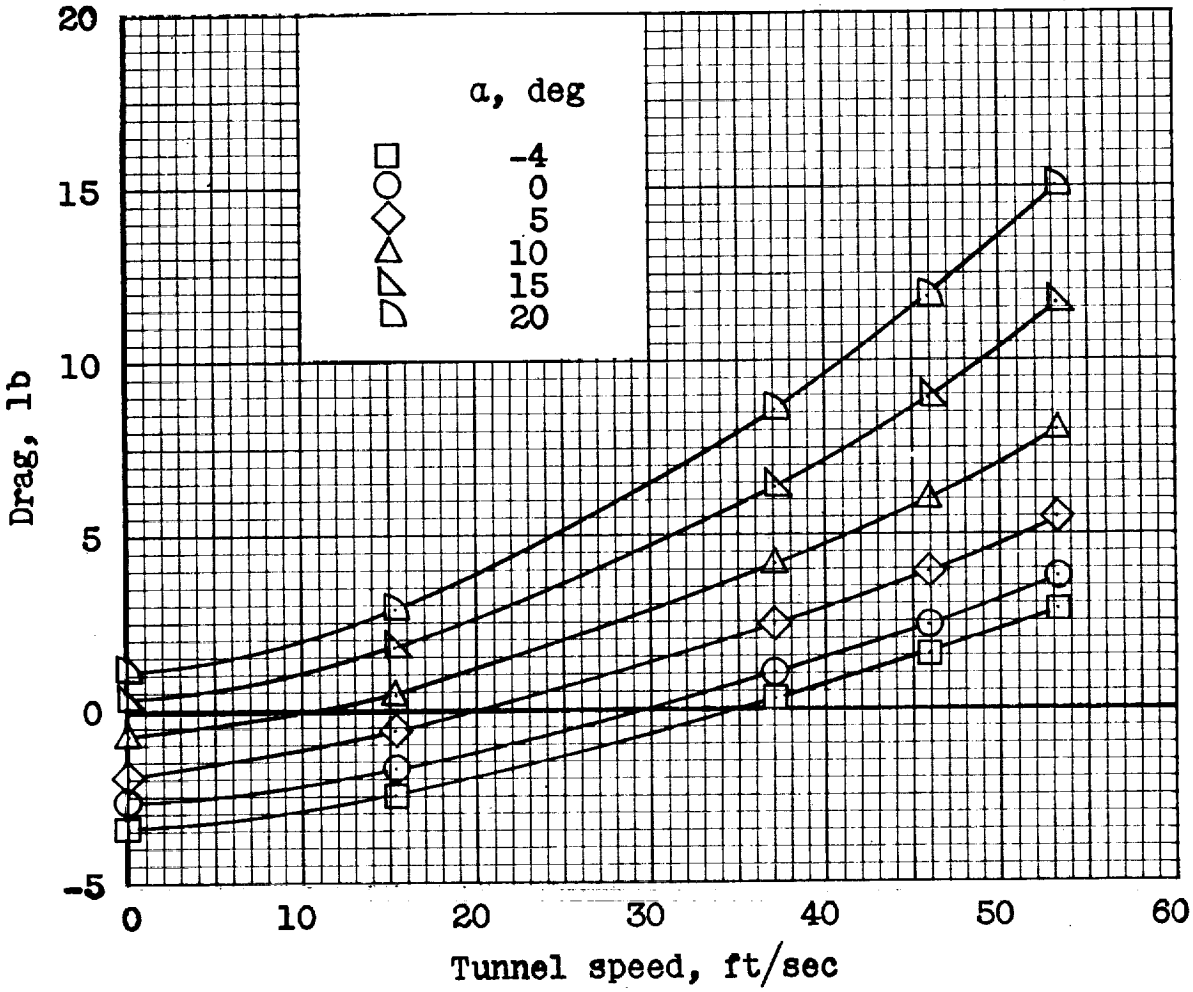

(e) $\Delta = 75^{\circ}$.

Figure 15.- Continued.

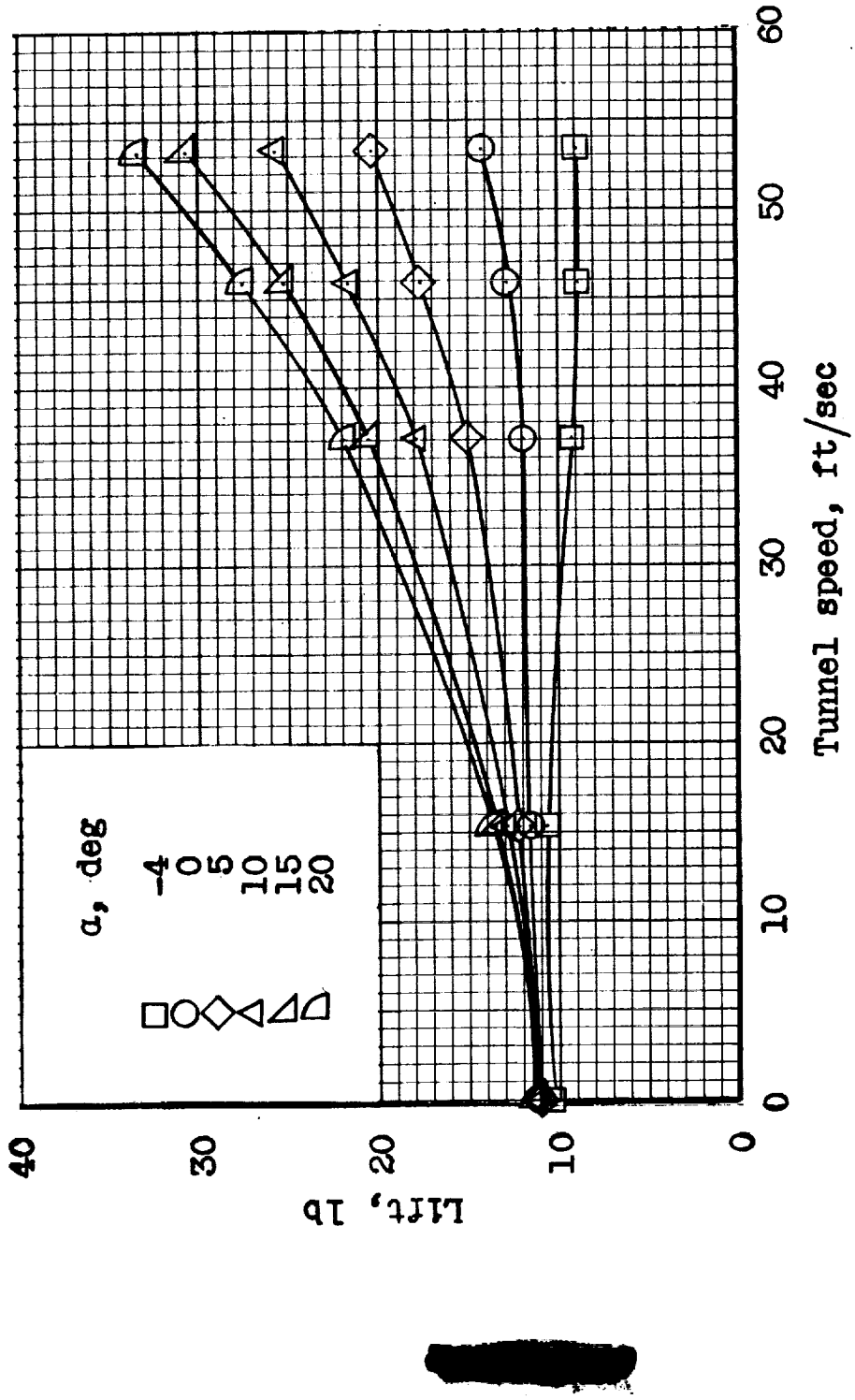

(e) Continued. $\Delta = 75^{\circ}$.

Figure 15.- Continued.

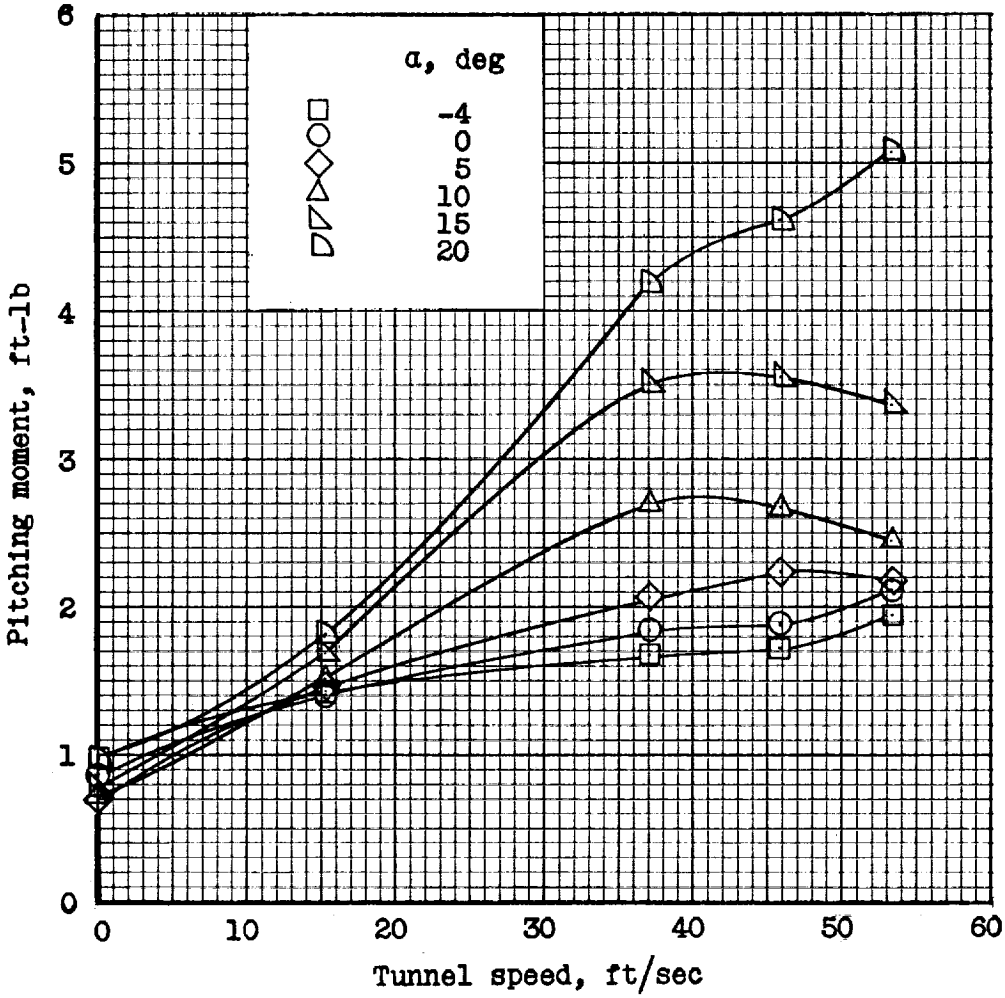

(e) Concluded. $\Delta = 75^{\circ}$.

Figure 15.- Concluded.

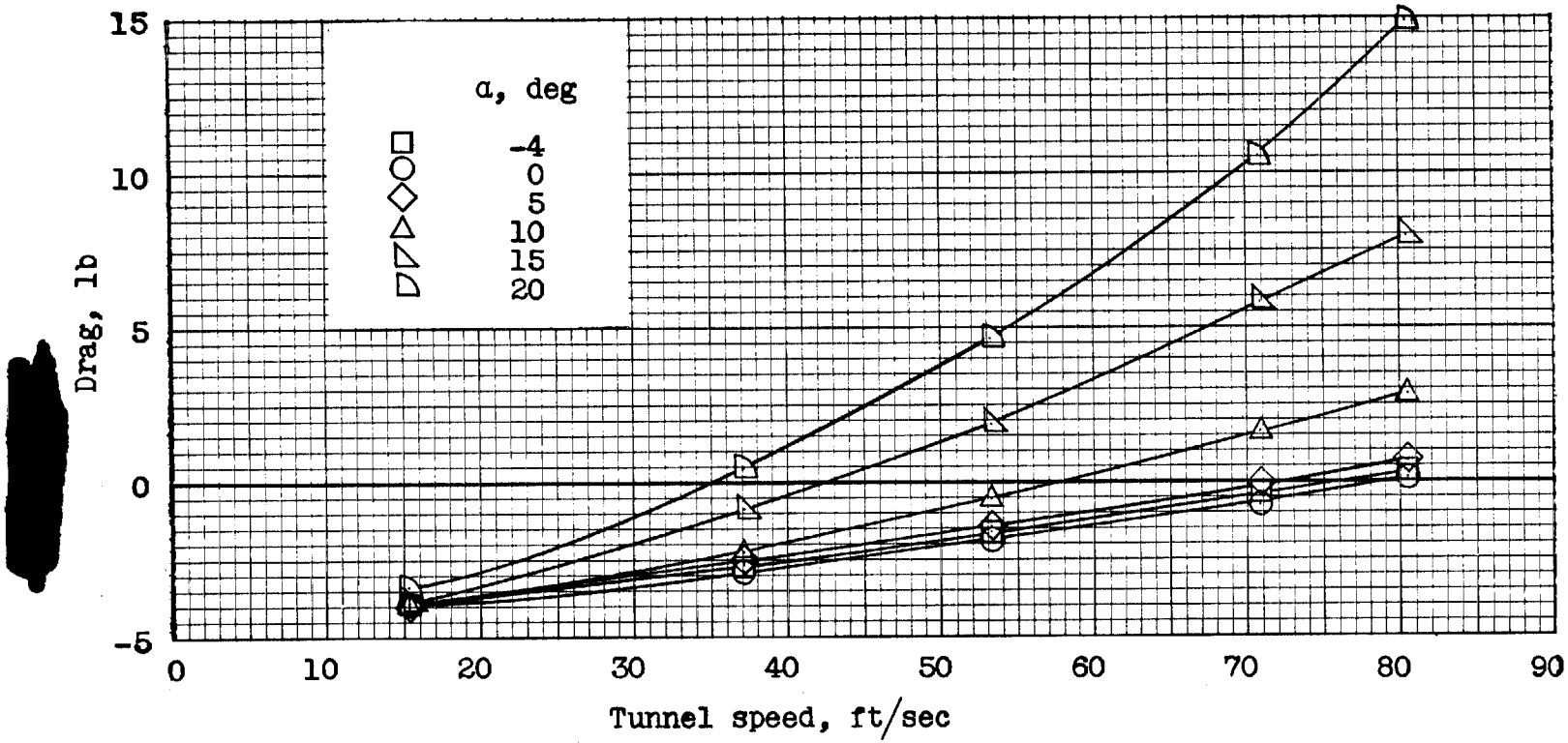

(a) $\Delta = 0^{\circ}$.

Figure 16.- Longitudinal force-test data for the model with $i_t = 5^{\circ}$ and $\delta_f = 0^{\circ}$. Referred to the wind axes

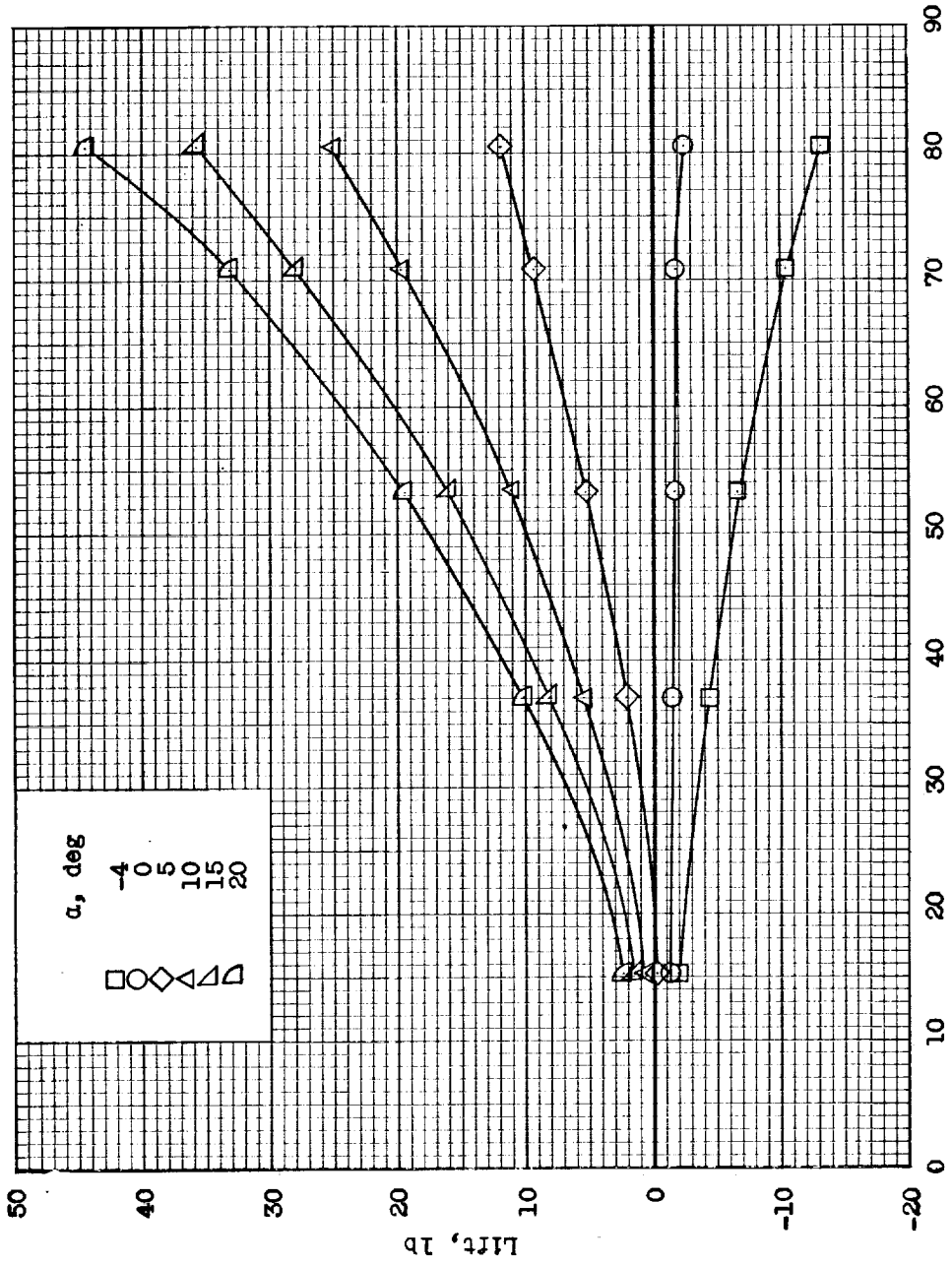

(a) Continued. $\Delta = 0^{o}$.

Figure 16.- Continued.

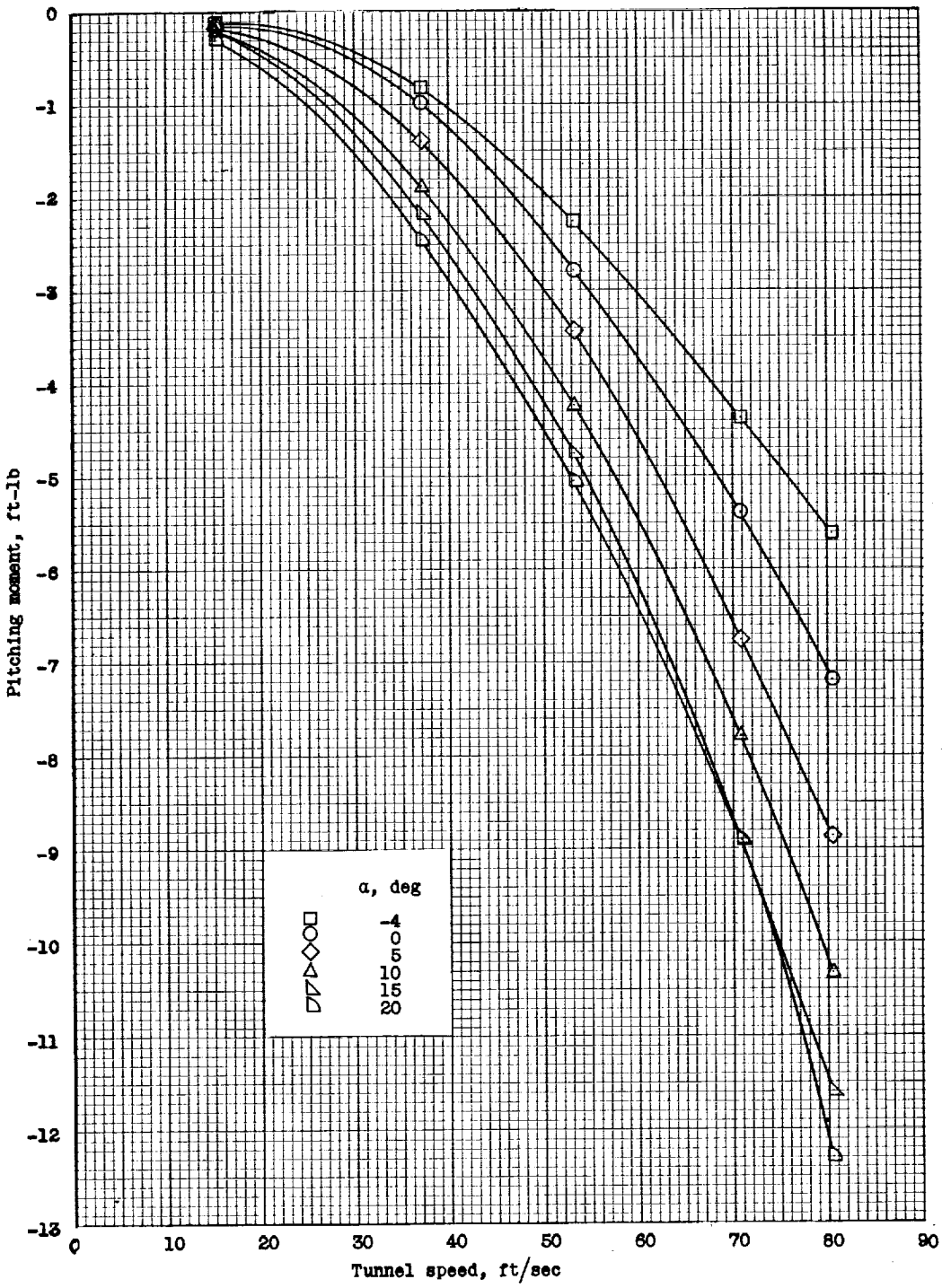

(a) Concluded. $\Delta = 0^{\circ}$.

Figure 16.- Continued.

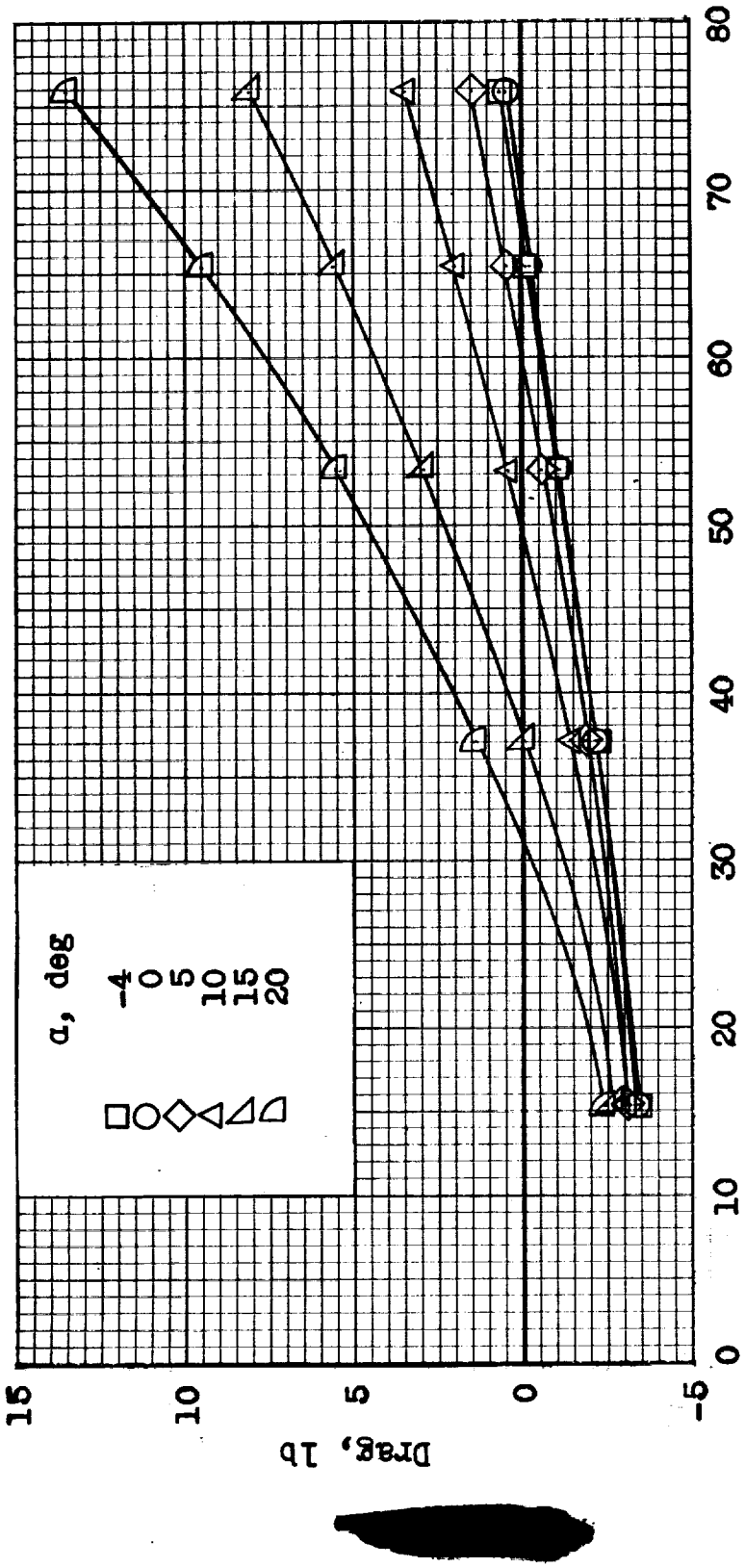

(b) $\Delta = 30^{\circ}$.

Figure 16.- Continued.

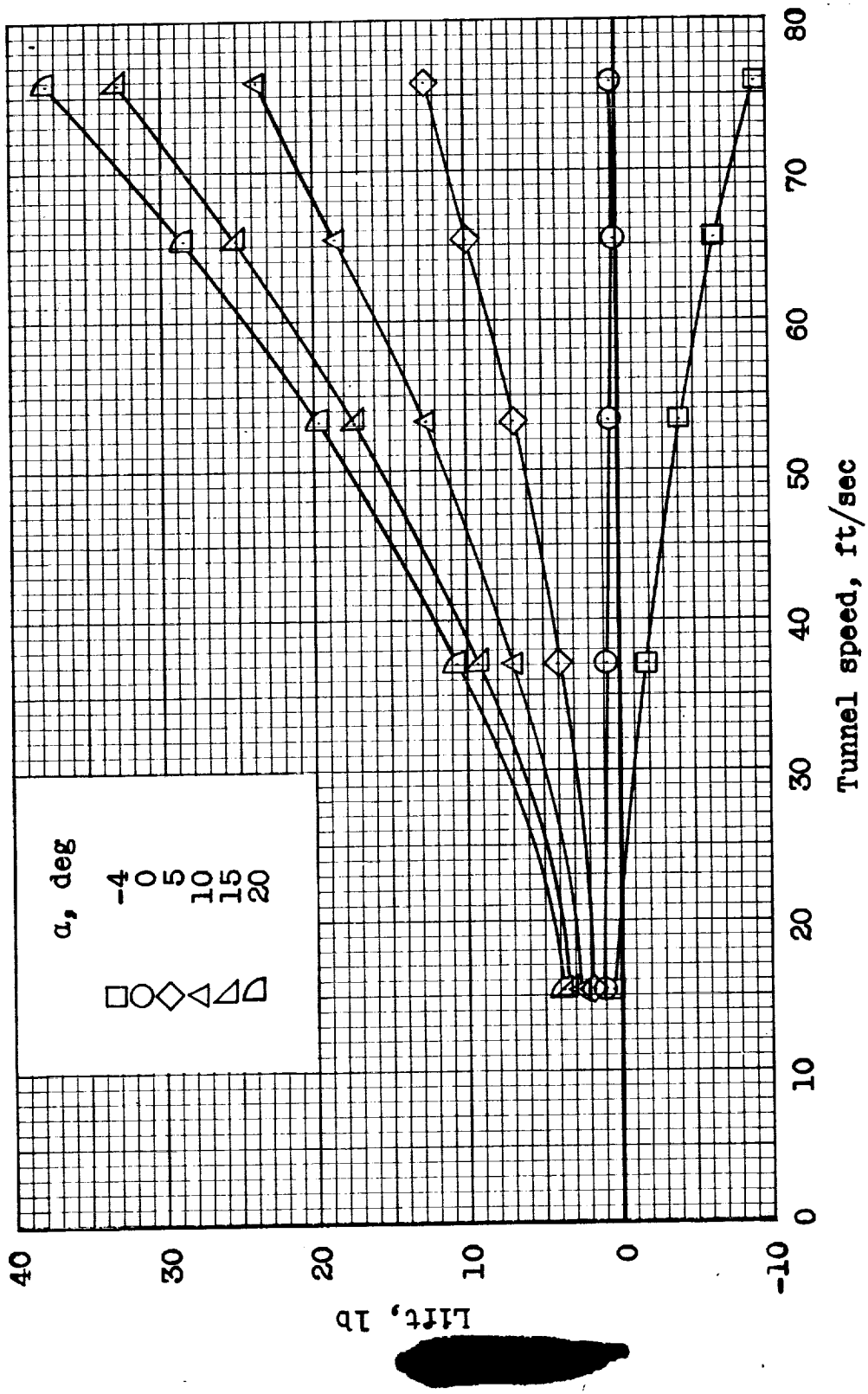

(b) Continued. $\Delta = 30^{\circ}$.

Figure 16.- Continued.

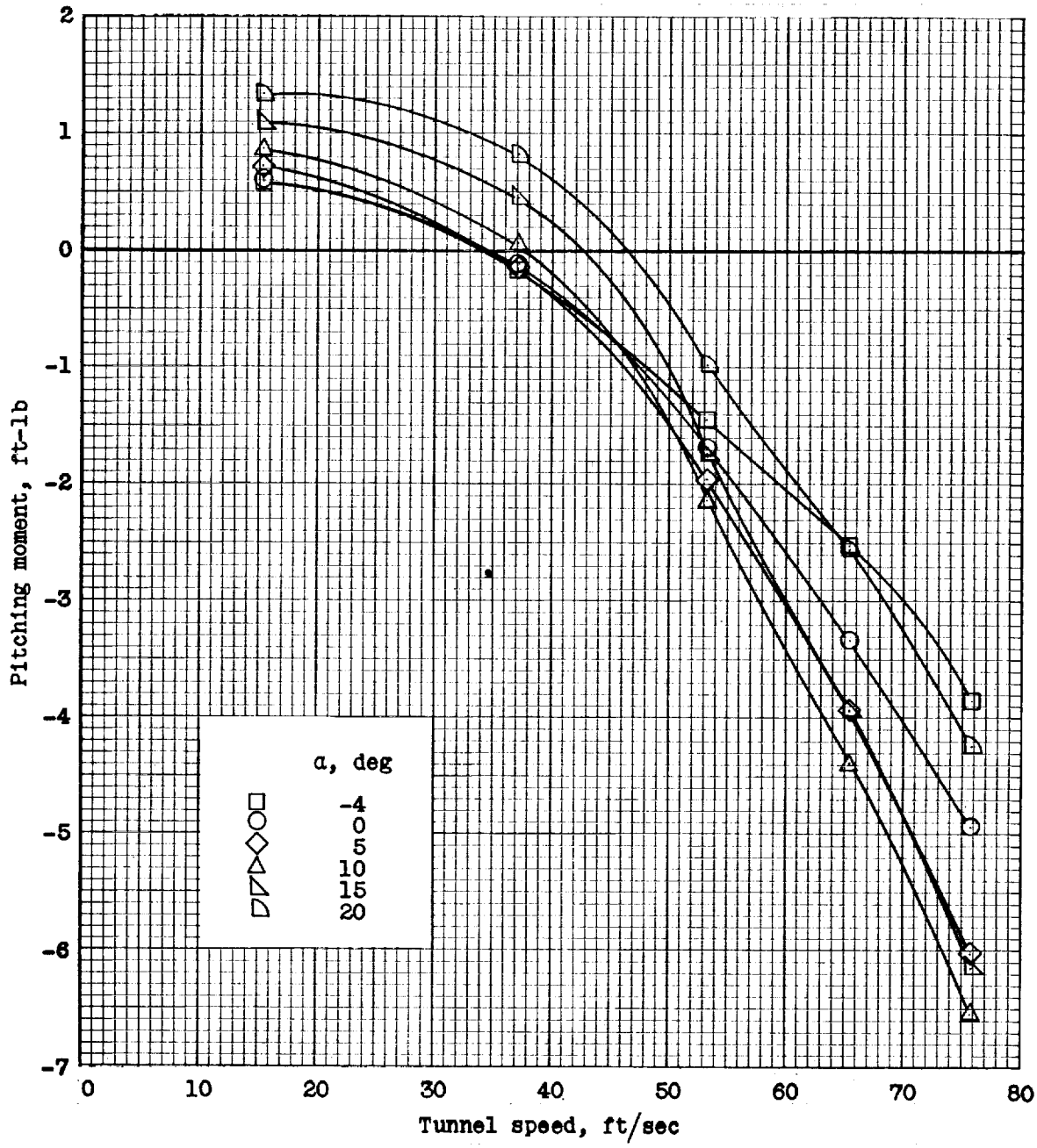

(b) Concluded. $\Delta = 30^{\circ}$.

Figure 16.- Continued.

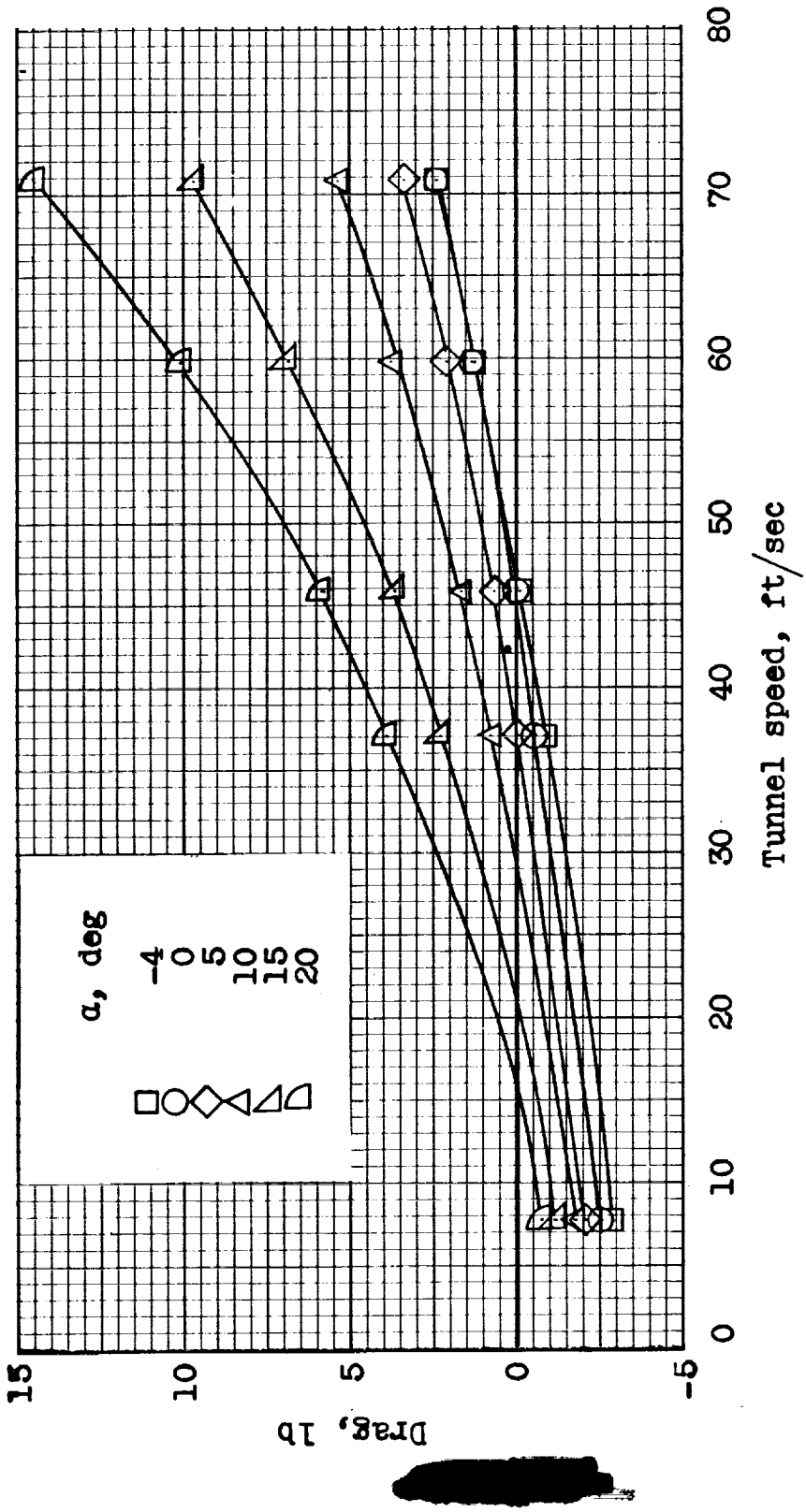

(c) $\Delta = 60°$.

Figure 16.- Continued.

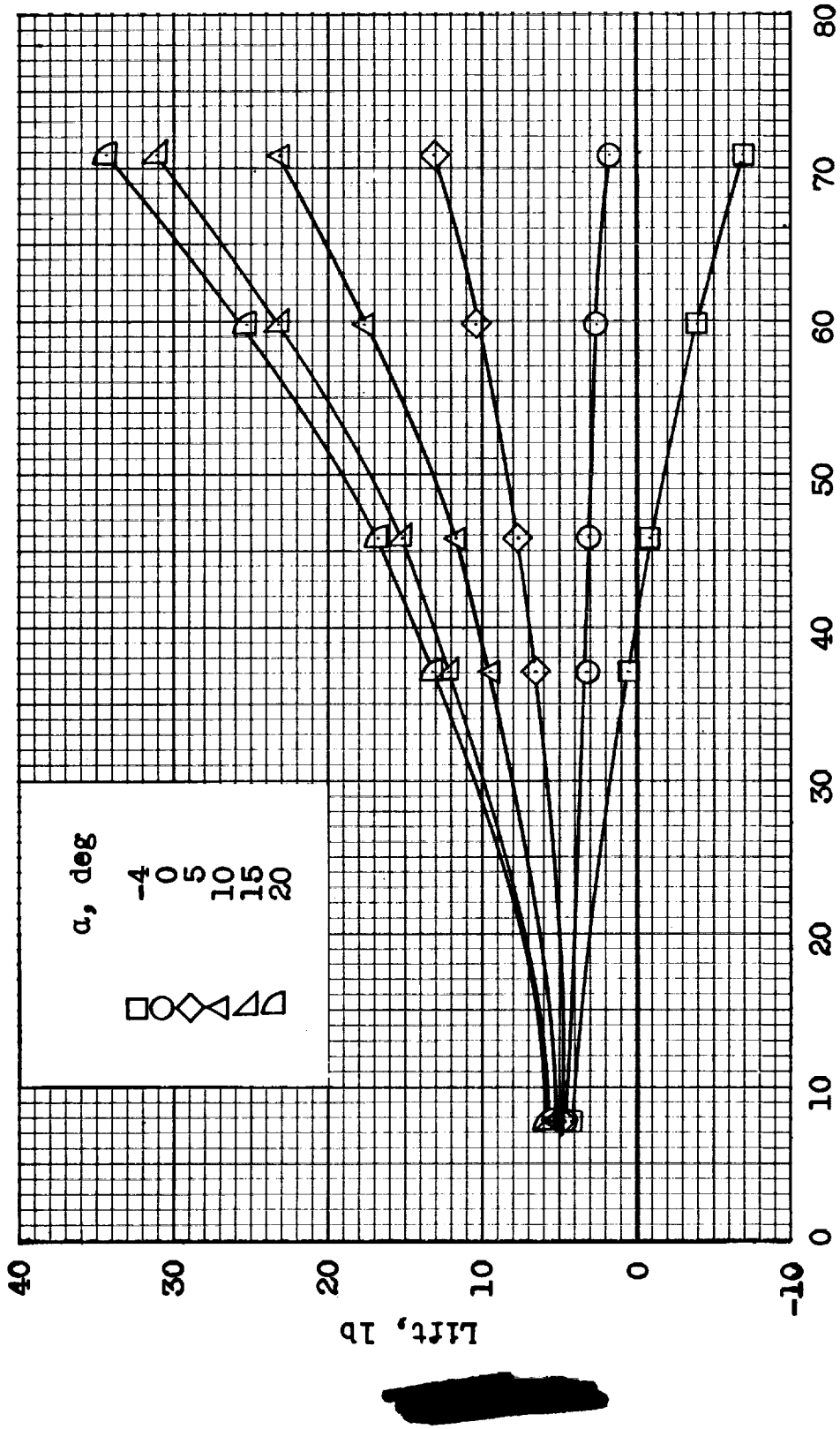

(c) Continued. $\Delta = 60^{\circ}$.

Figure 16.- Continued.

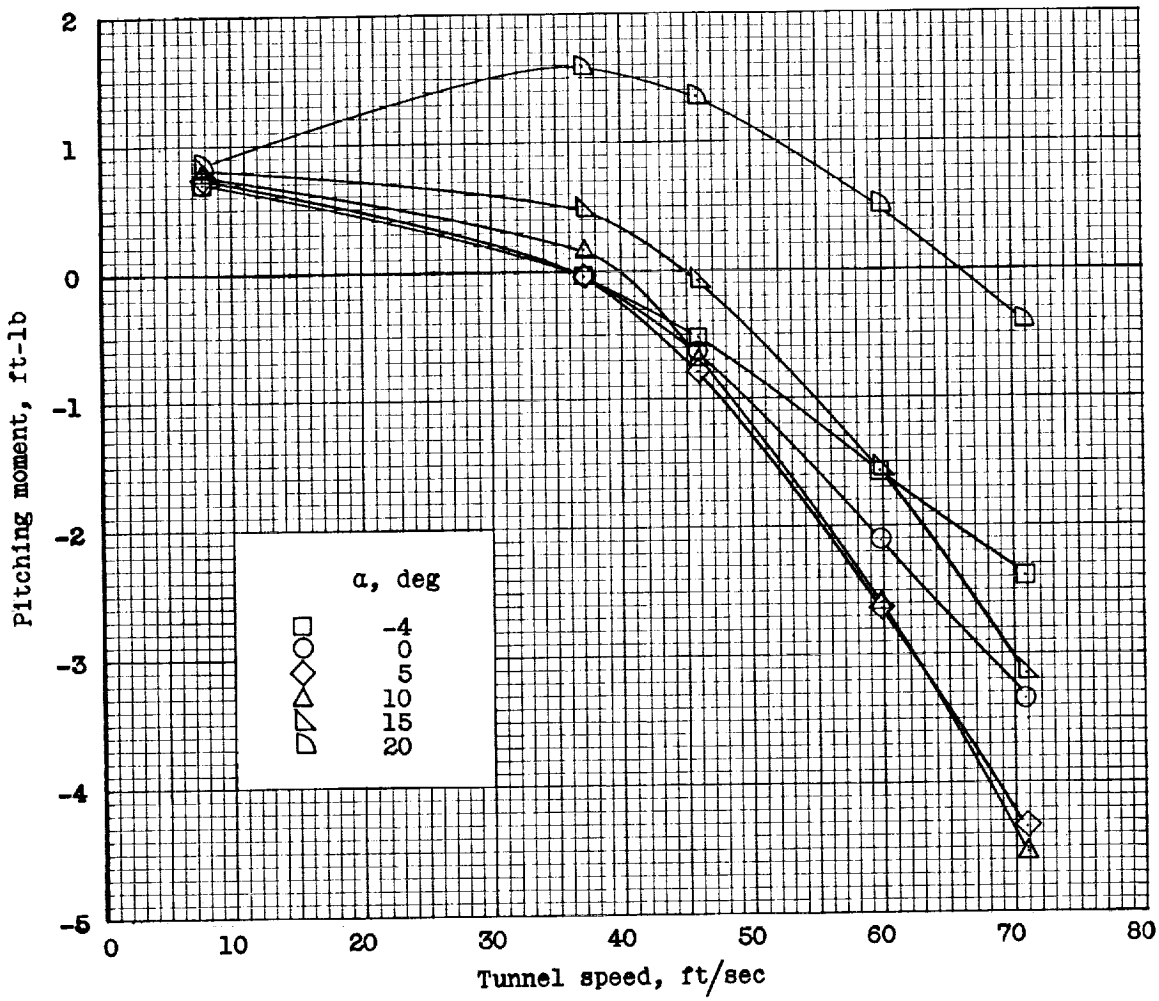

(c) Concluded. $\Delta = 60^{o}$.

Figure 16.- Concluded.

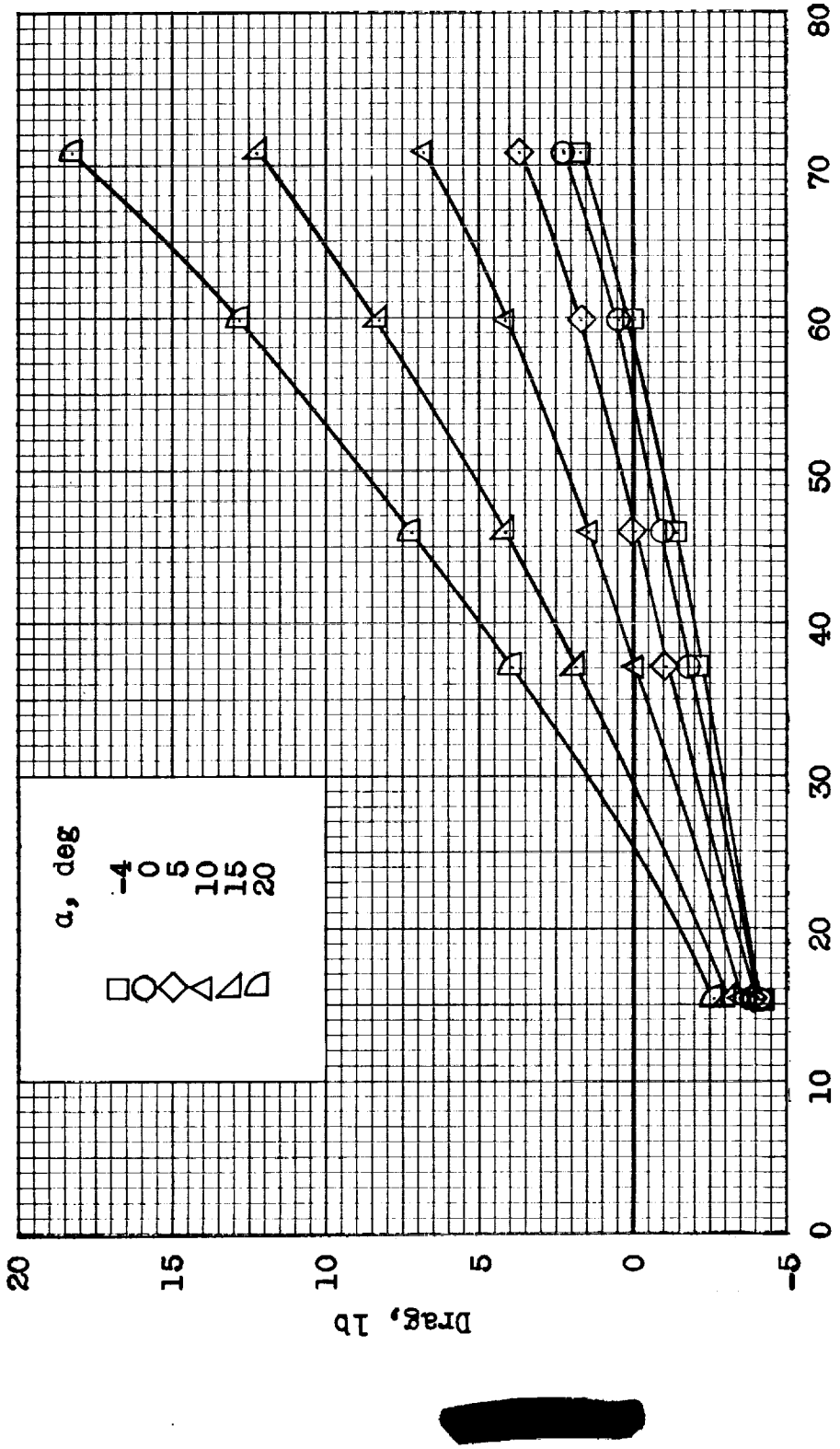

(a) $\Delta = 0^{\circ}$.

Figure 17.- Longitudinal force-test data for the model with the flaps deflected 50° and $i_t = 5^{\circ}$. Referred to the wind axes.

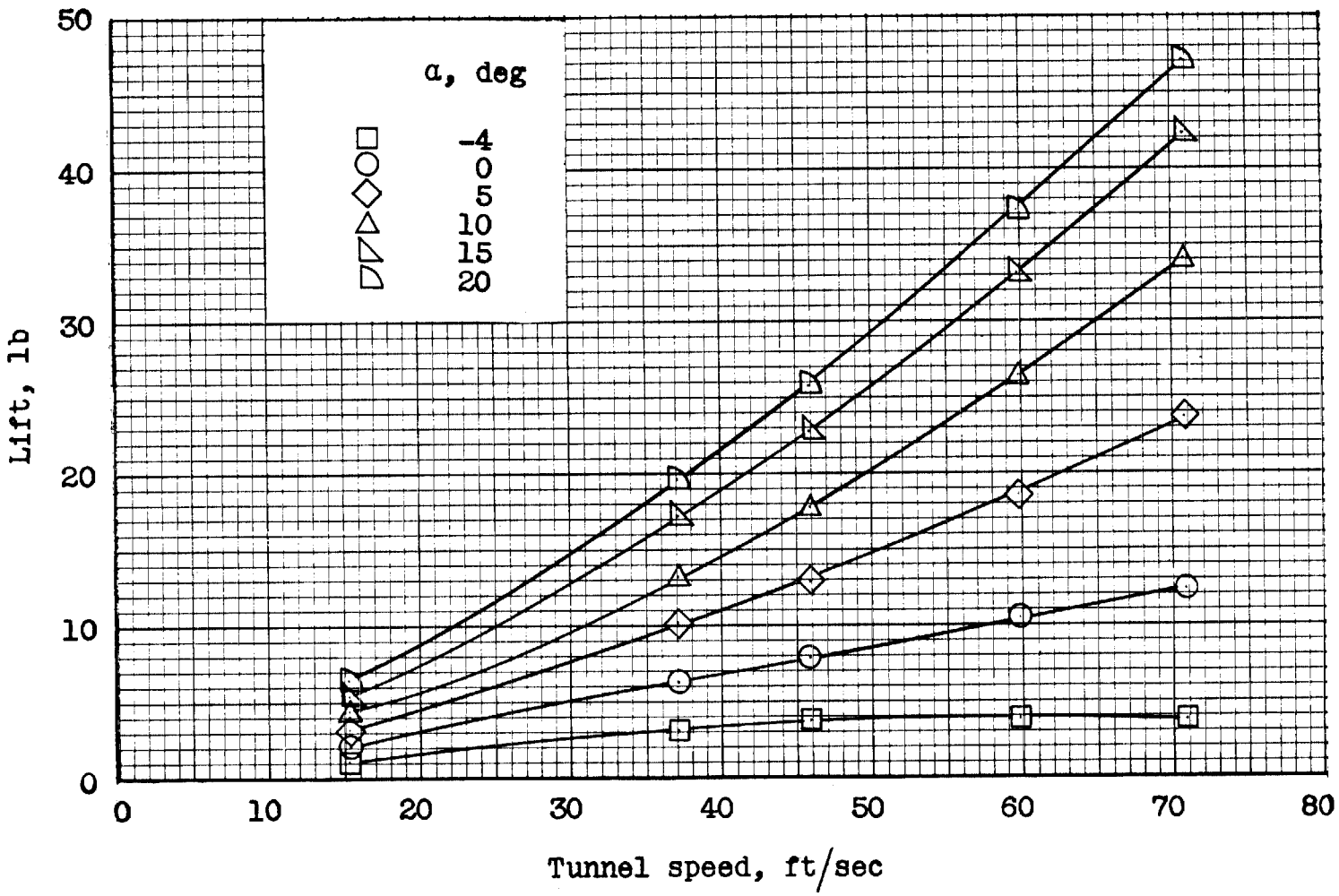

(a) Continued. $\Delta = 0^{\circ}$.

Figure 17.- Continued.

(a) Concluded. $\Delta = 0^{\circ}$.

Figure 17.- Continued.

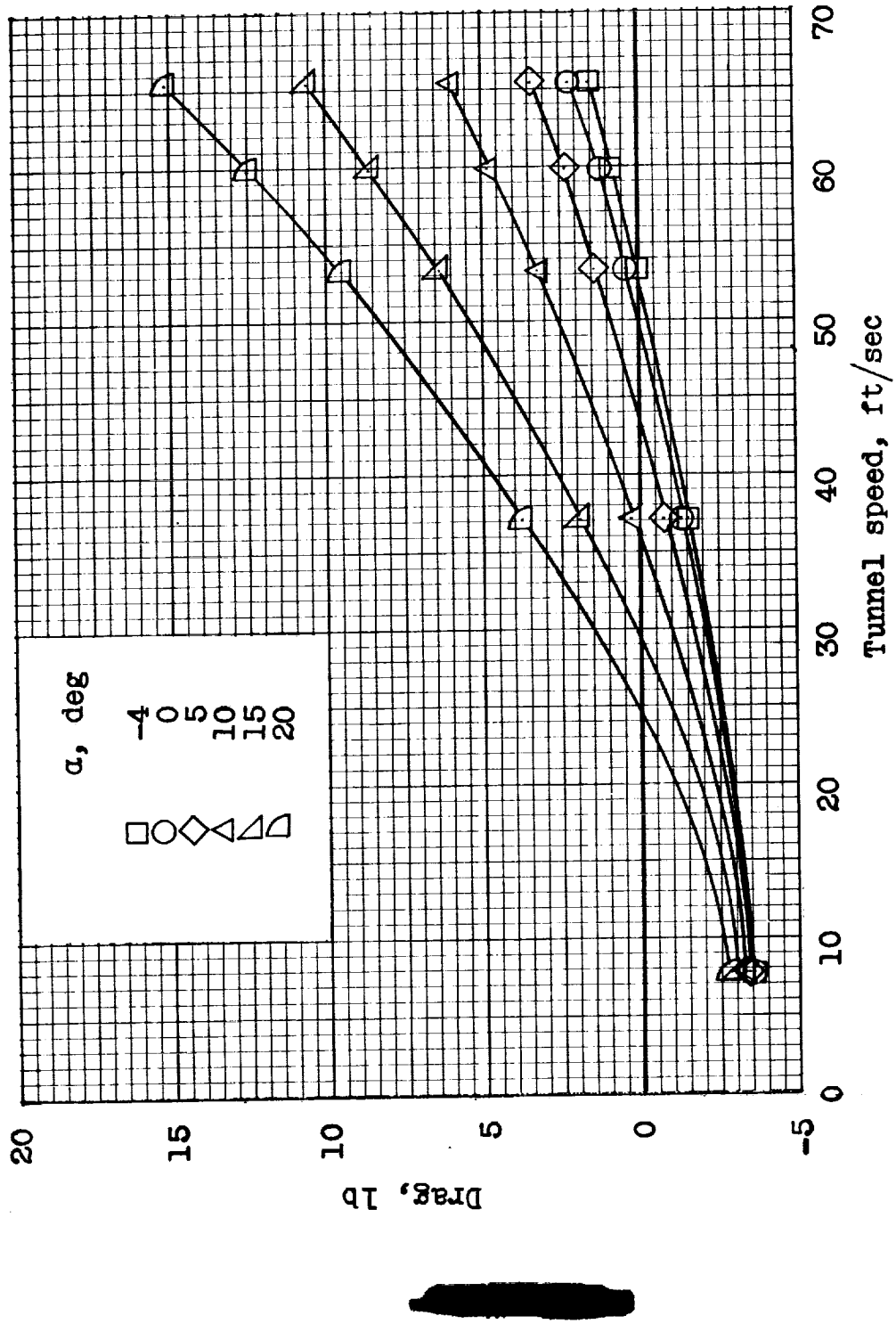

(b) $\Delta = 30^{\circ}$.

Figure 17.- Continued.

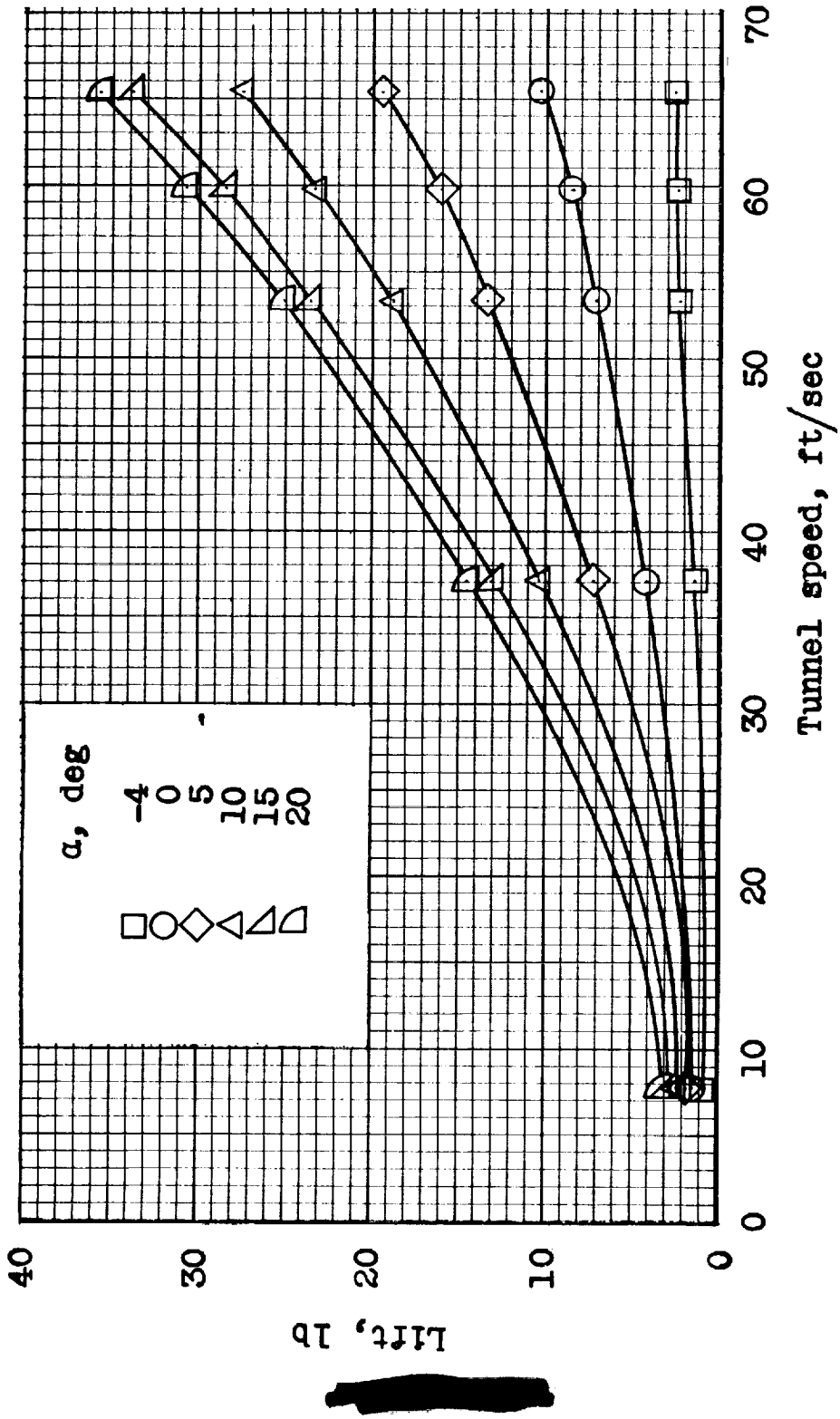

(b) Continued. $\Delta = 30^{\circ}$.

Figure 17.- Continued.

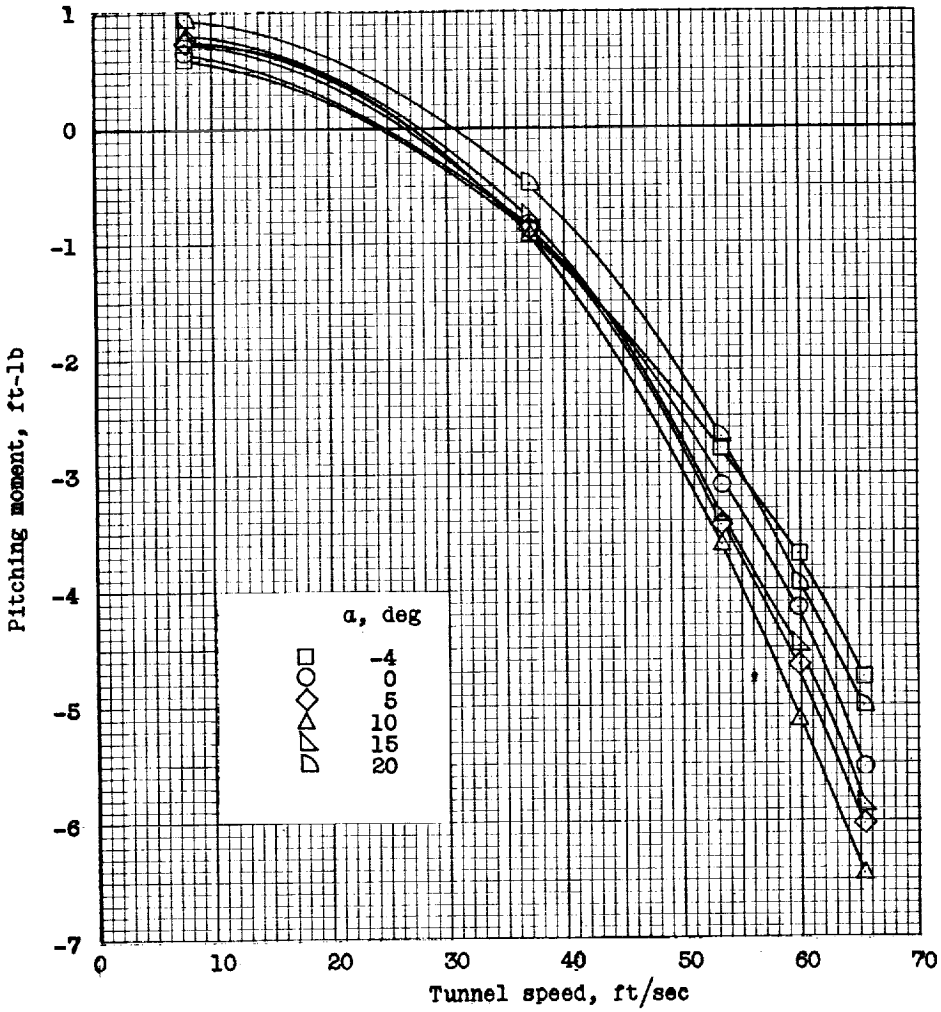

(b) Concluded. $\Delta = 30^{\circ}$.

Figure 17.- Continued.

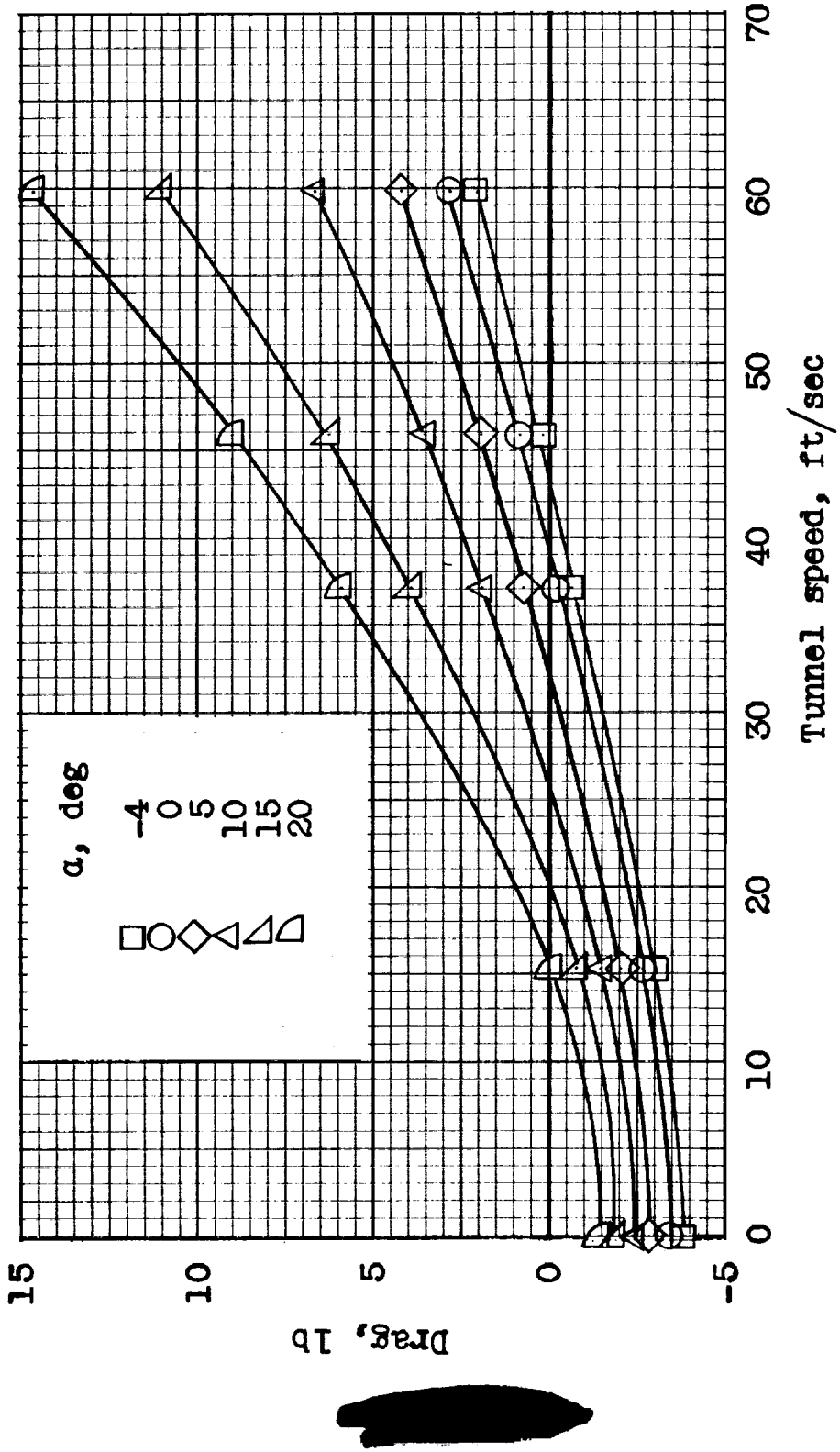

(c) $\Delta = 60^{\circ}$.

Figure 17.- Continued.

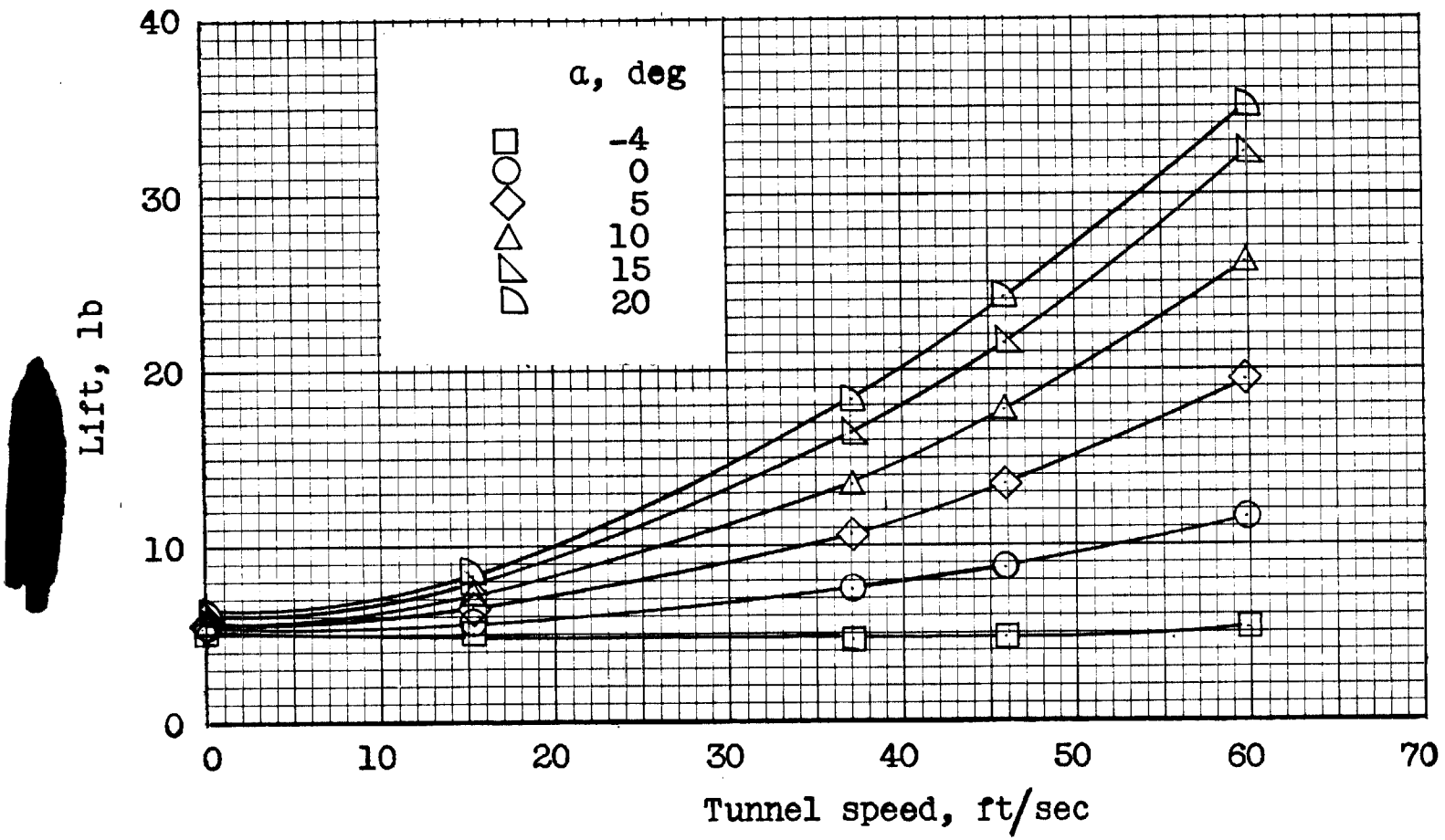

(c) Continued. $\Delta = 60^{\circ}$.

Figure 17.- Continued.

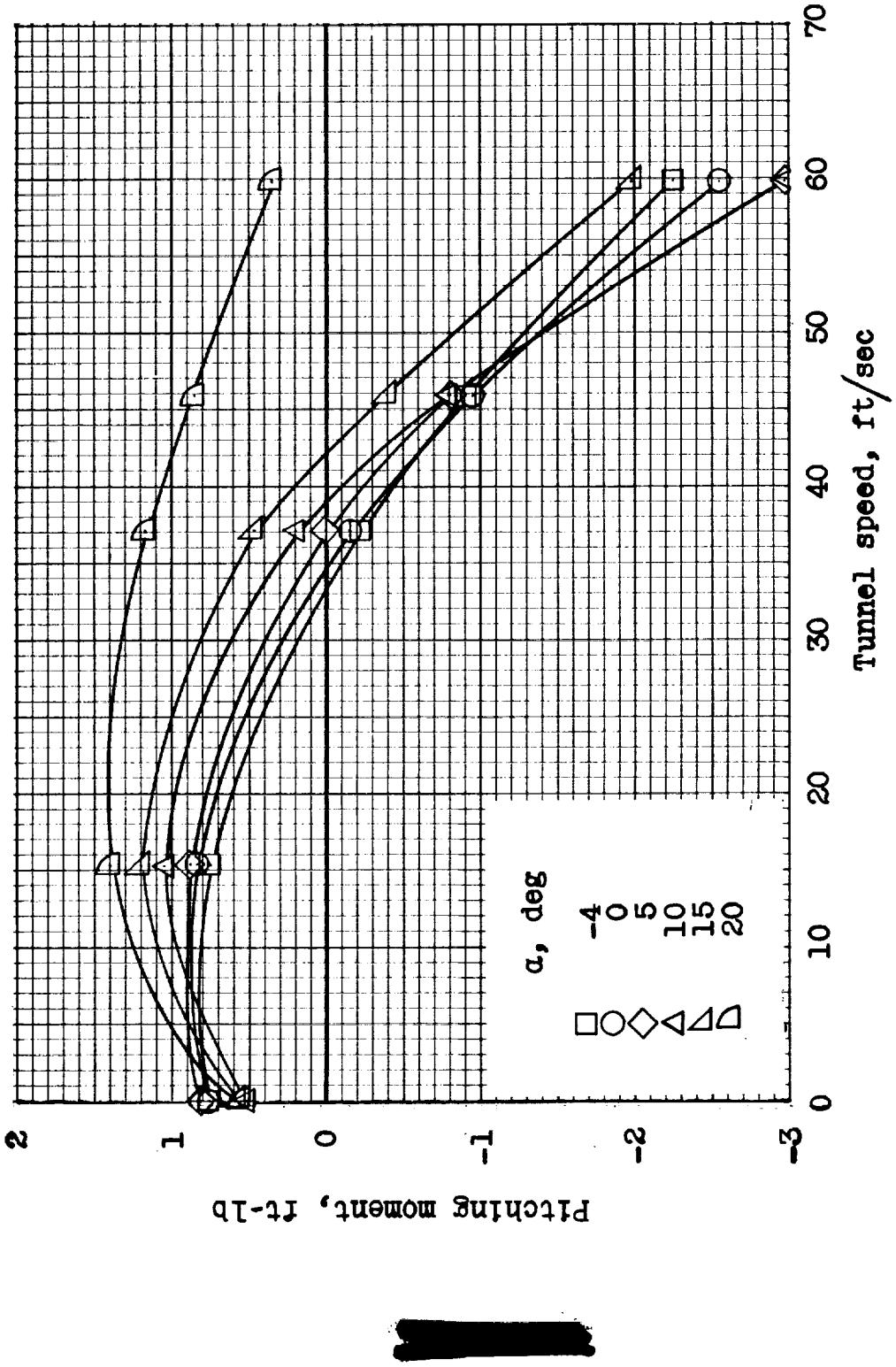

(c) Concluded. $\Delta = 60^{\circ}$.

Figure 17.- Concluded.

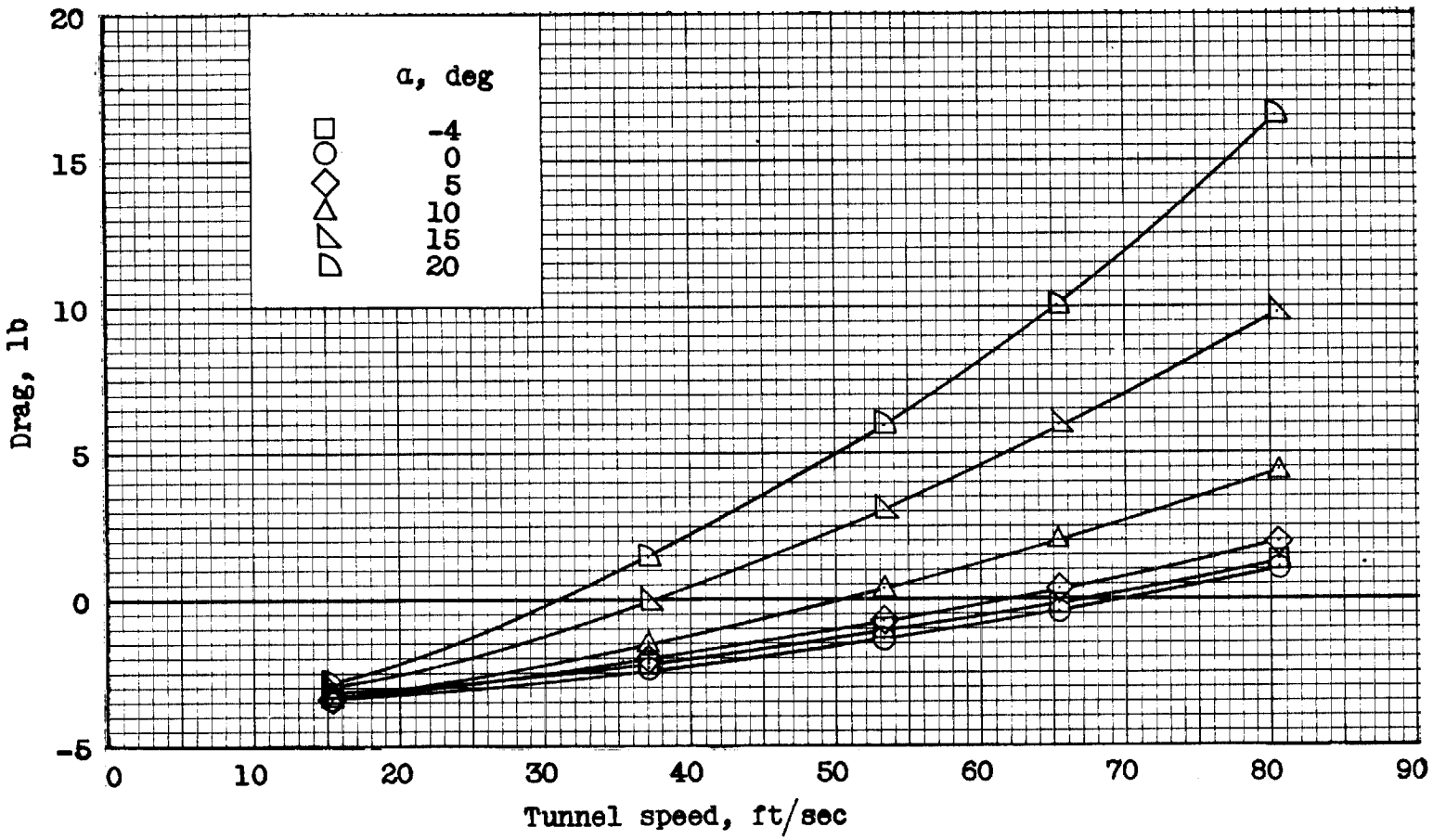

(a) $\Delta = 0^{\circ}$.

Figure 18.- Longitudinal force-test data for the model with $i_t = 10^{\circ}$ and $\delta_f = 0^{\circ}$. Referred to the wind axes.

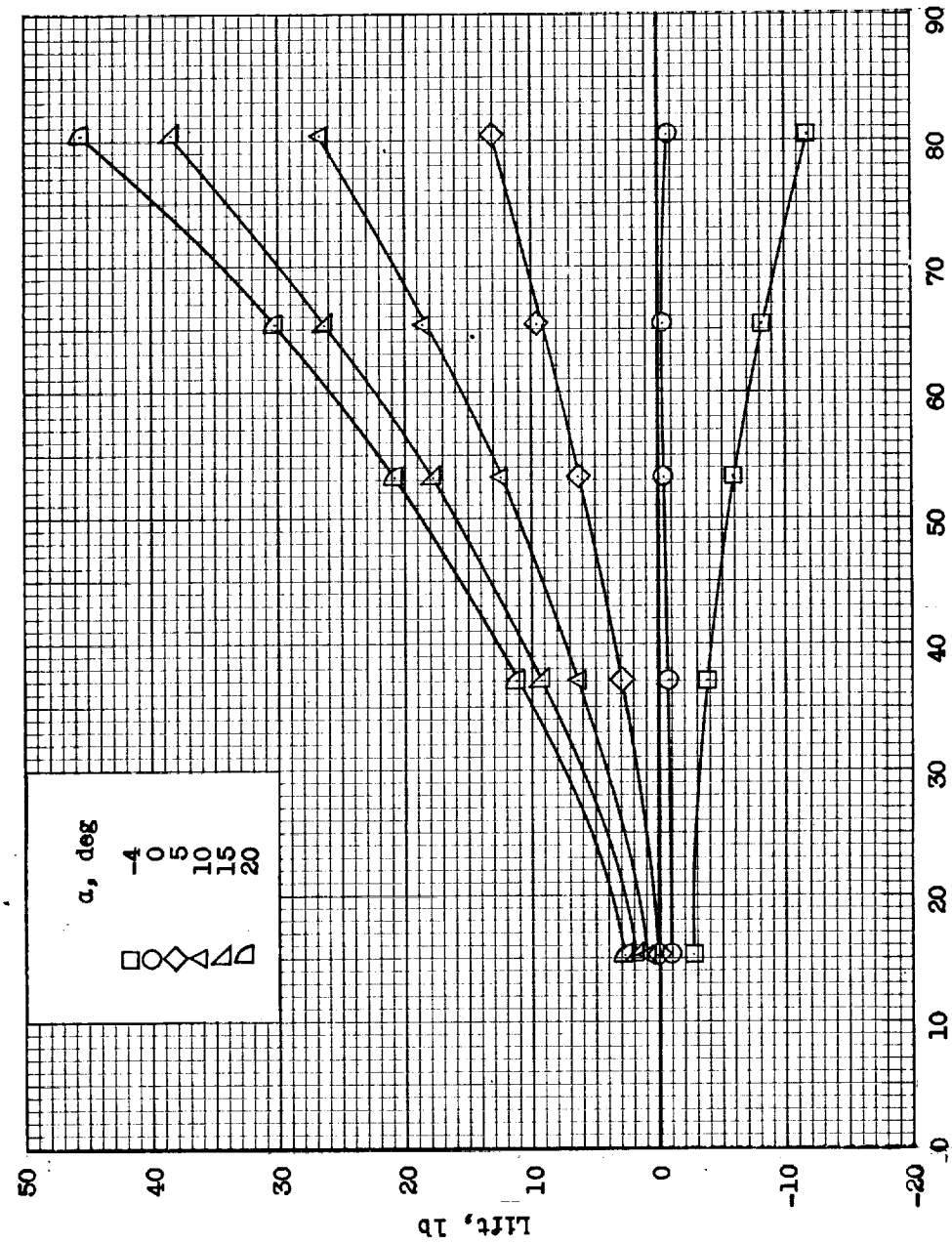

(a) Continued. $\Delta = 0^{\circ}$.

Figure 18.- Continued.

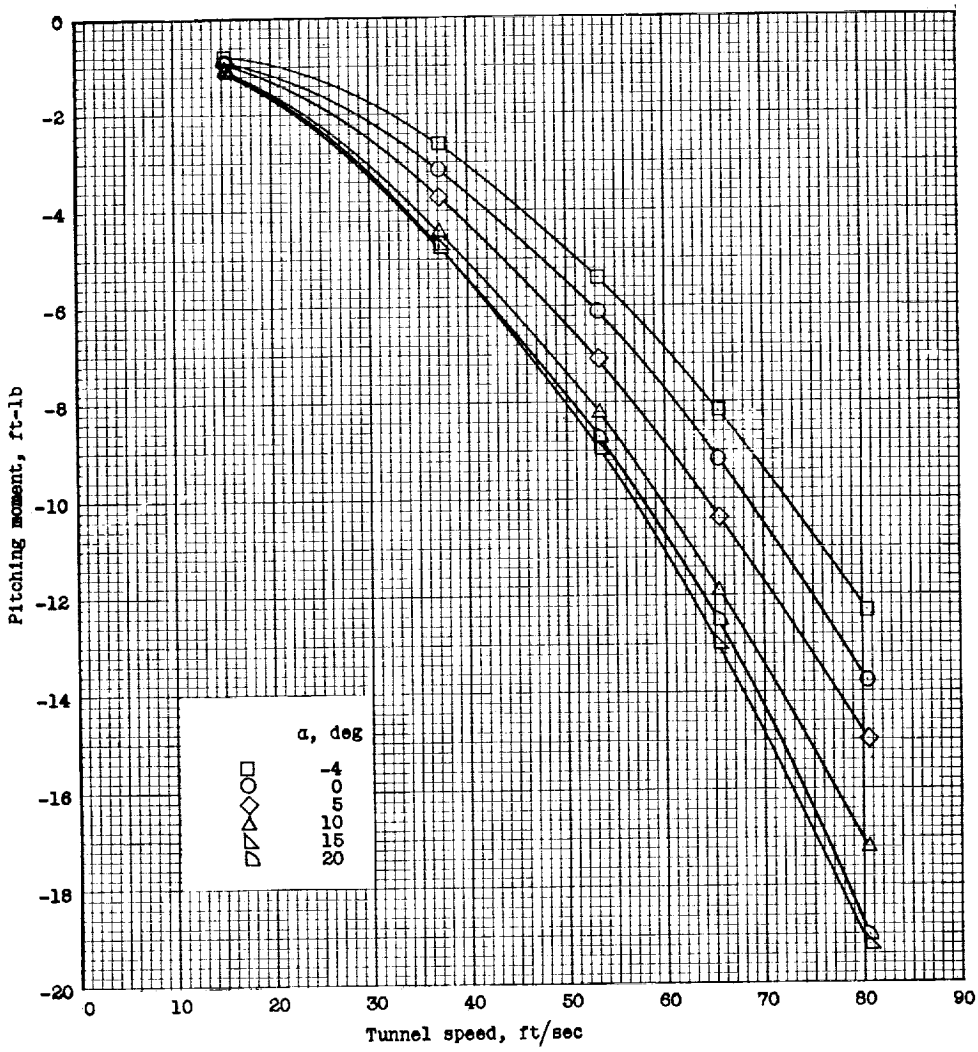

(a) Concluded. $\Delta = 0^{\circ}$.

Figure 18.- Continued.

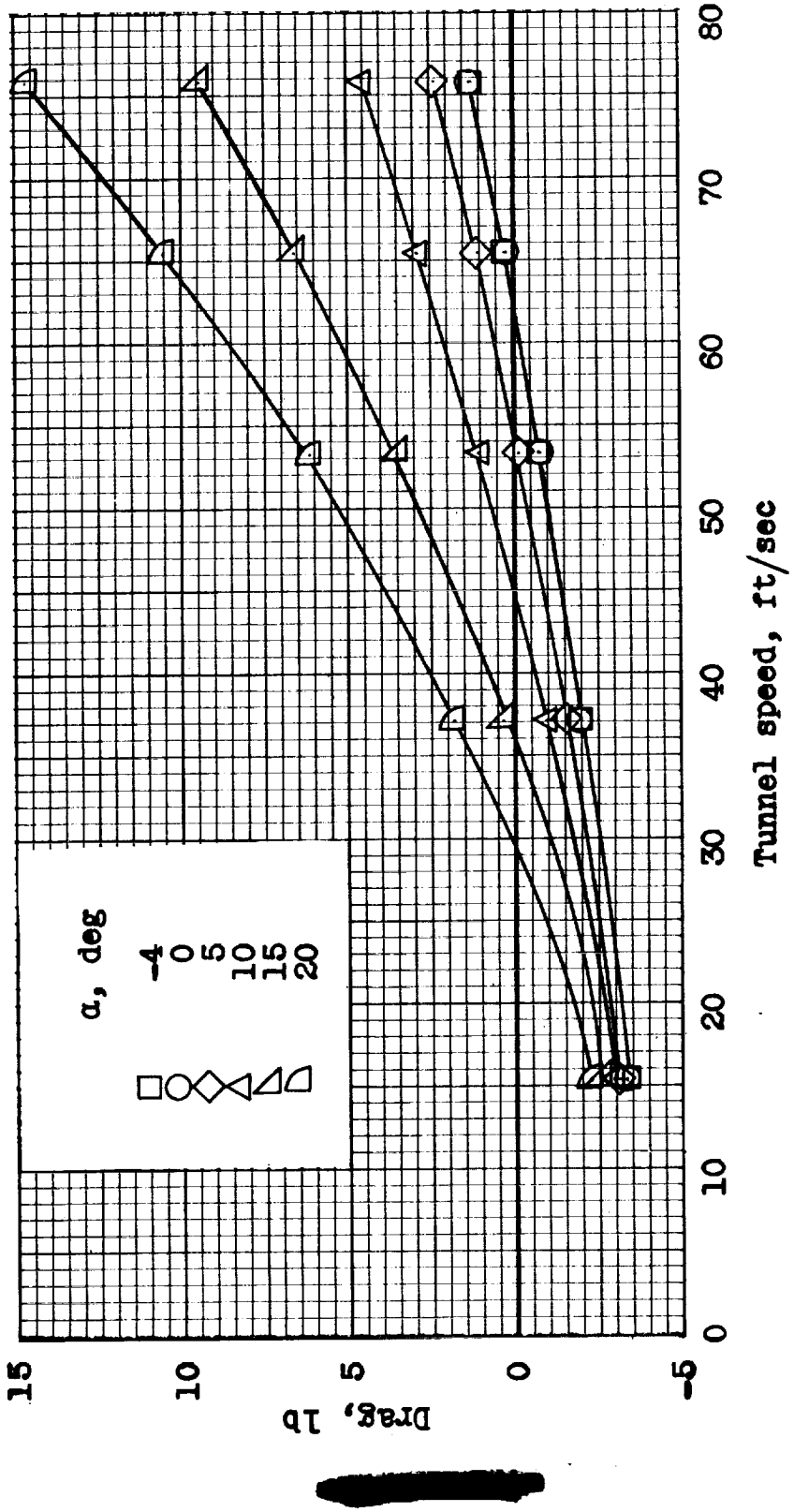

(b) $\Delta = 30^{\circ}$.

Figure 18.- Continued.

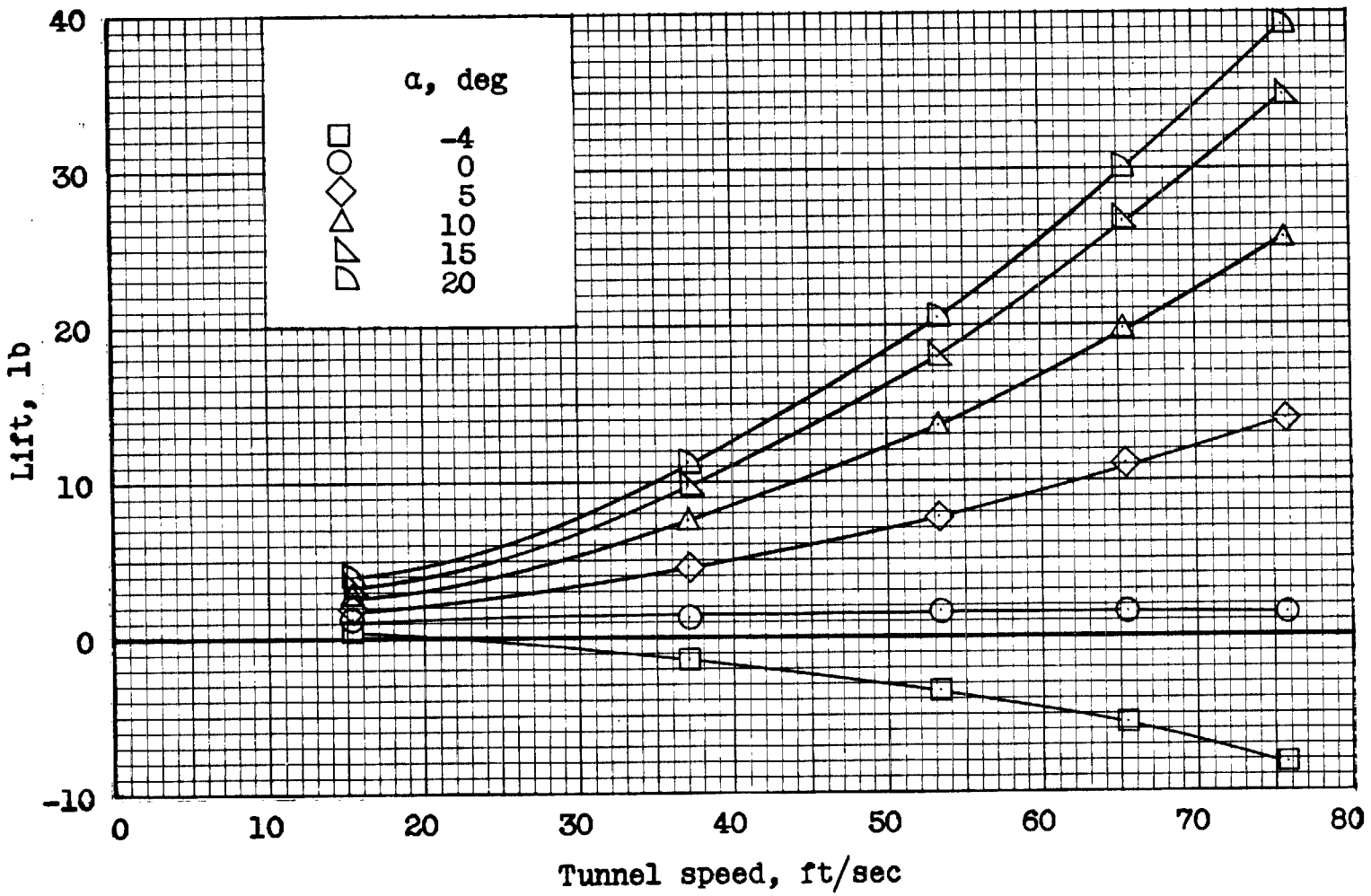

(b) Continued. $\Delta = 30^{\circ}$.

Figure 18.- Continued.

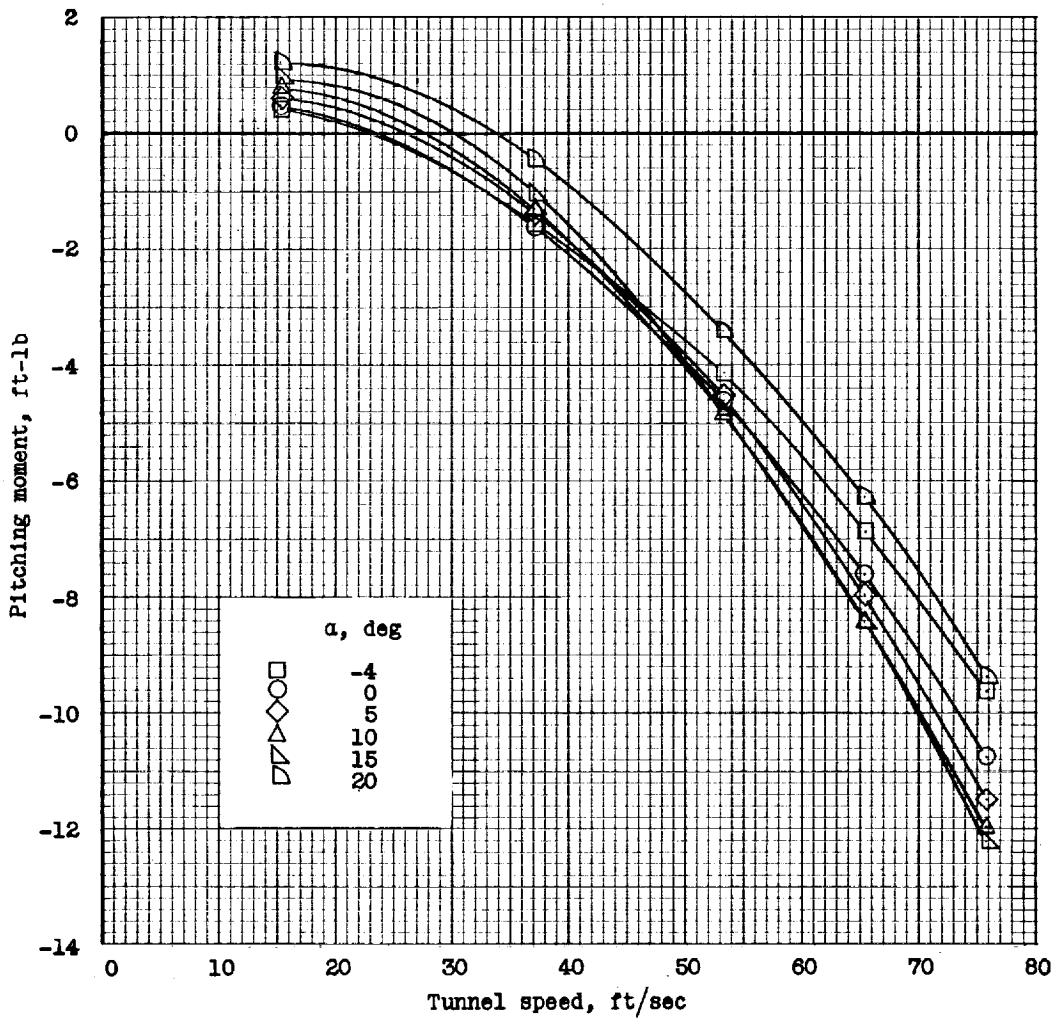

(b) Concluded. $\Delta = 30^{\circ}$.

Figure 18.- Continued.

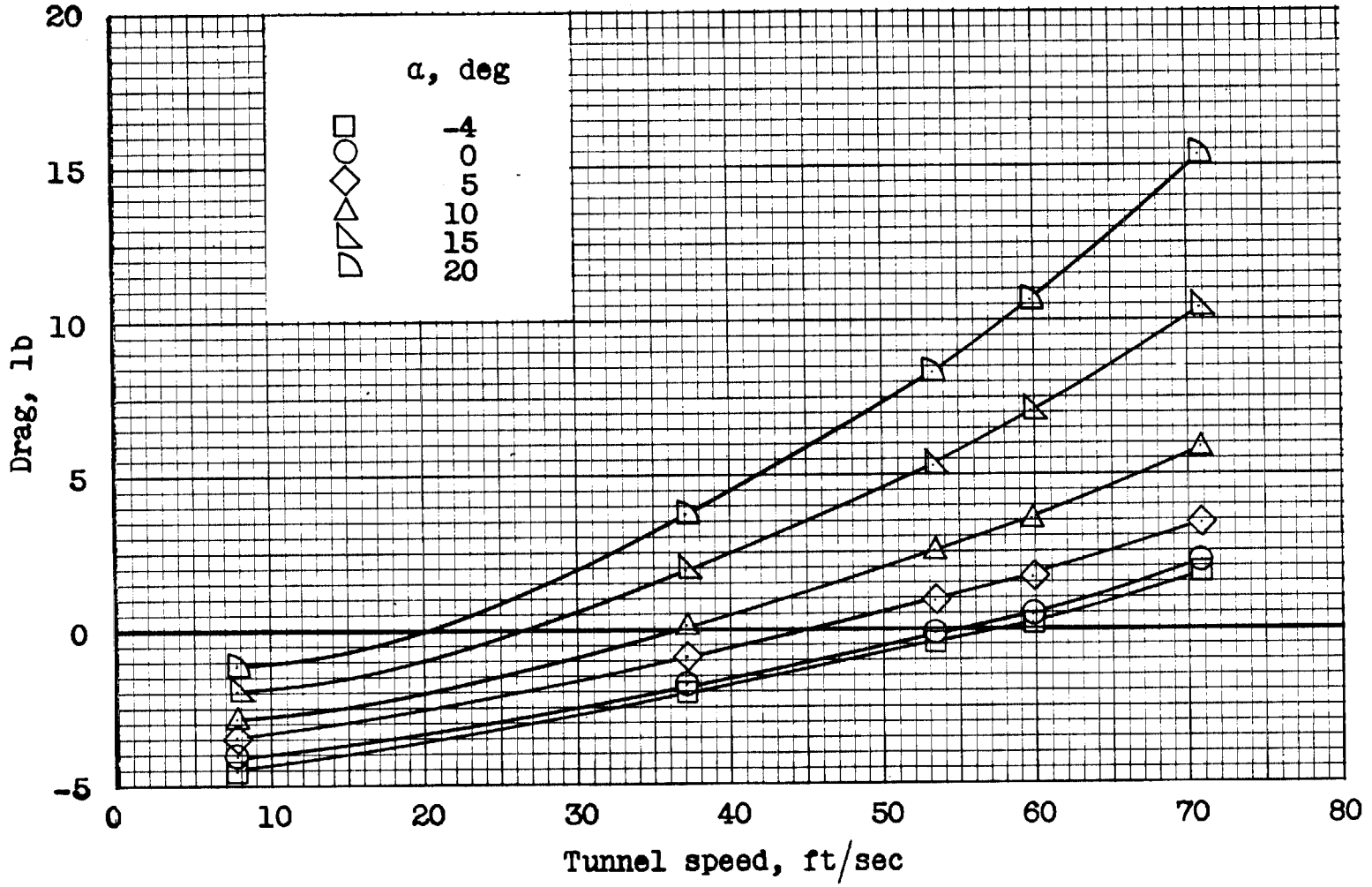

(c) $\Delta = 60^{\circ}$.

Figure 18.- Continued.

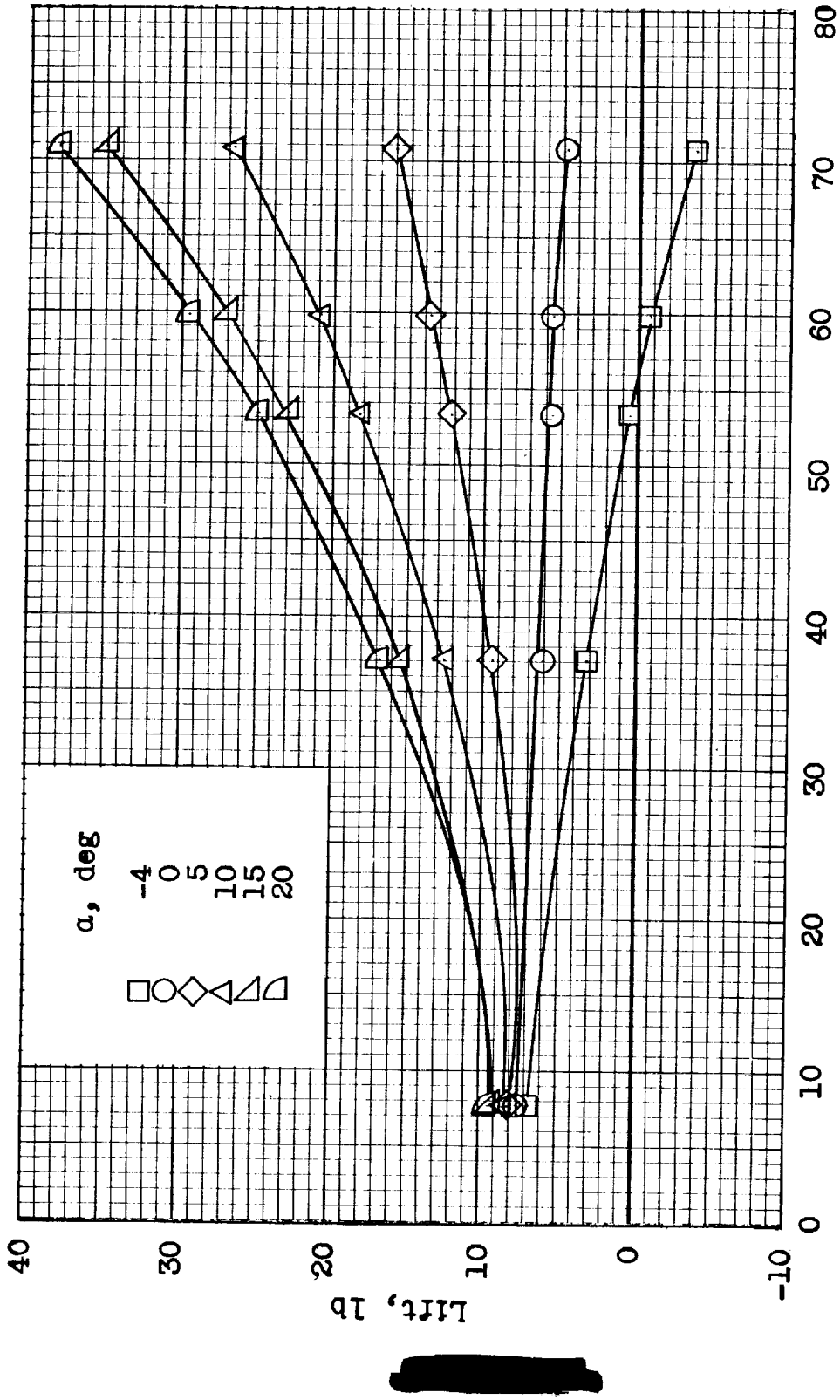

(c) Continued. $\Delta = 60^{\circ}$.

Figure 18.- Continued.

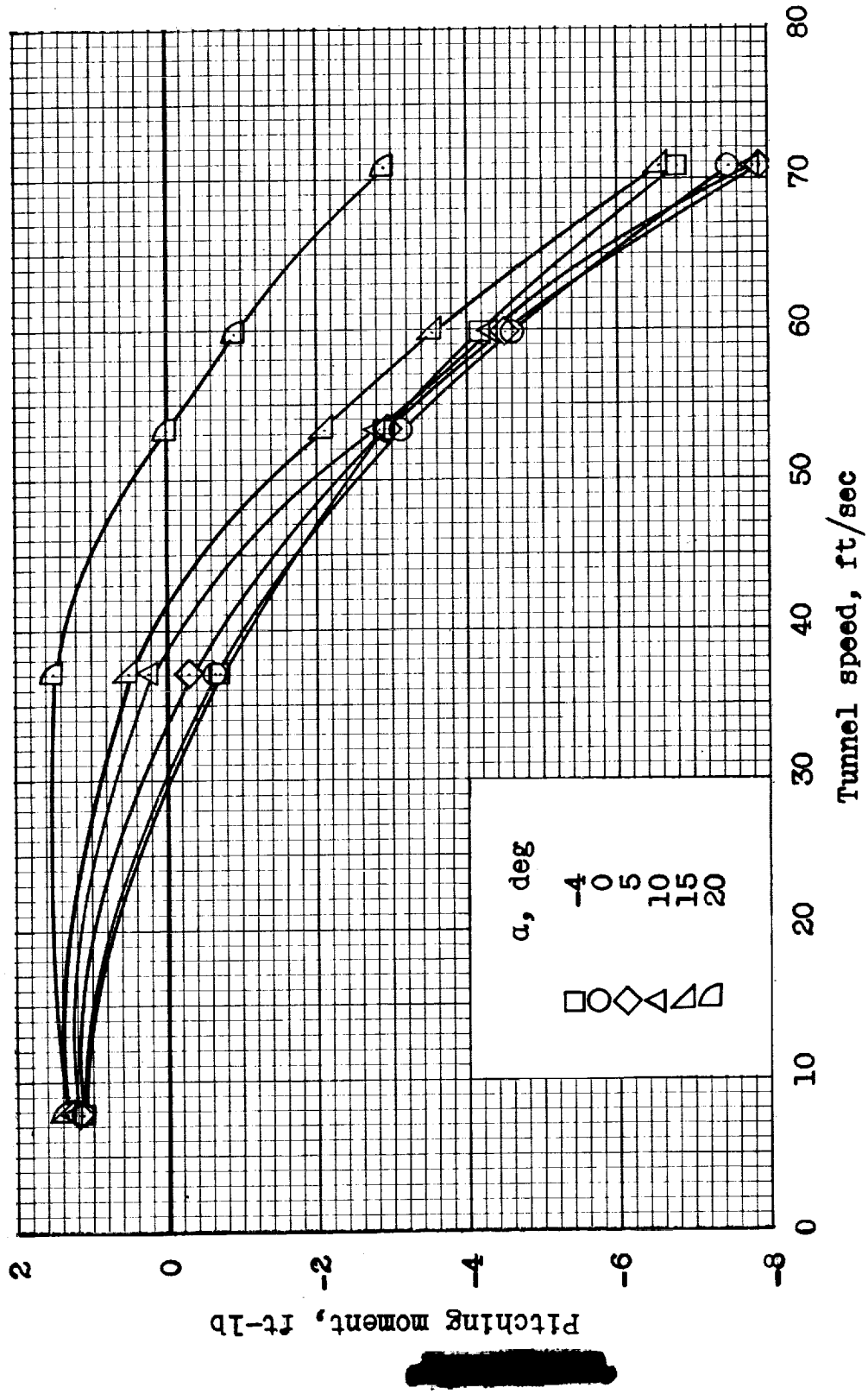

(c) Concluded. $\Delta = 60^{\circ}$.

Figure 18.- Concluded.

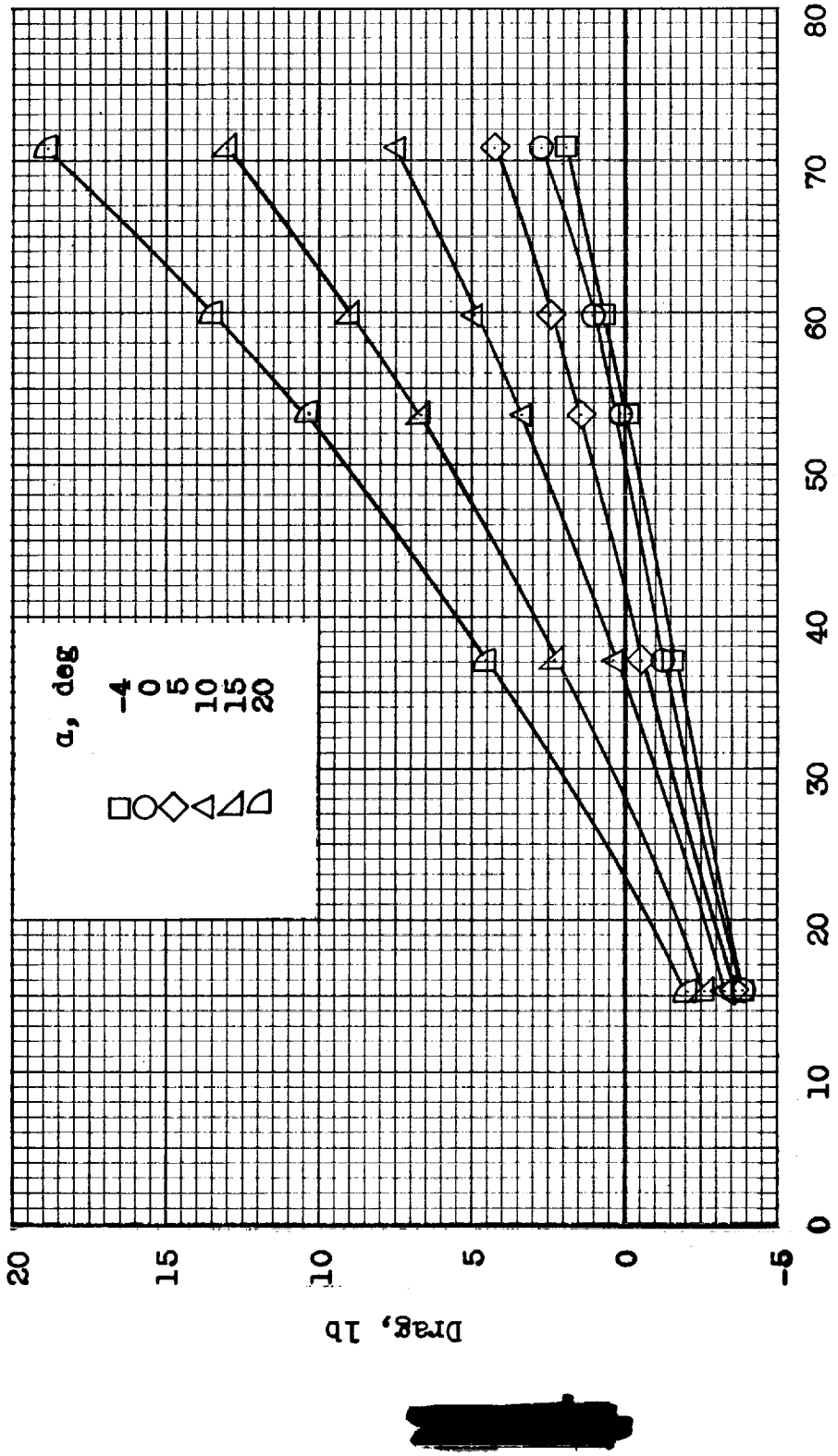

(a) $\Delta = 0^{\circ}$.

Figure 19.- Longitudinal force-test data for the model with the flaps deflected 50° and $i_t = 10^{\circ}$. Referred to the wind axes.

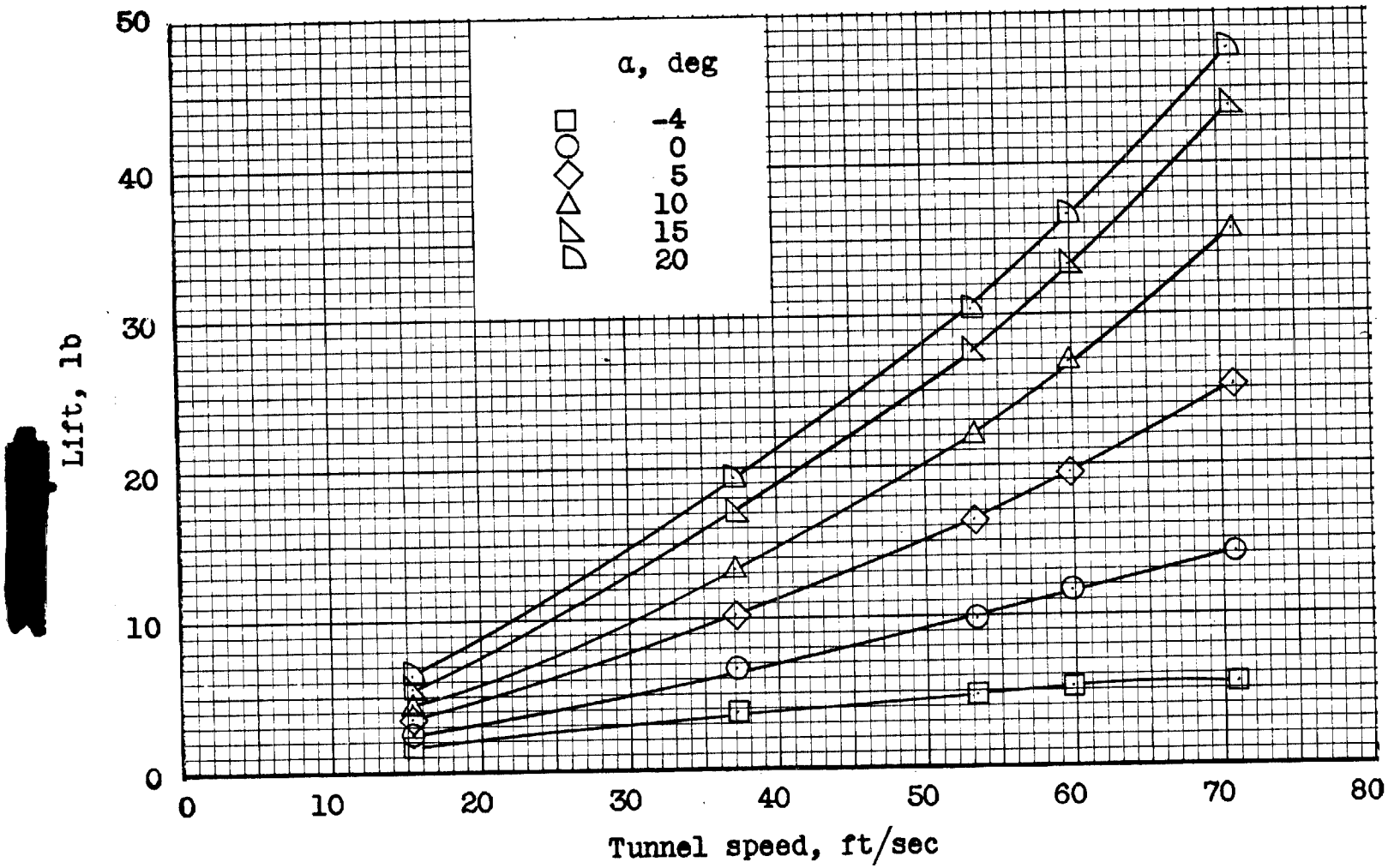

(a) Continued. $\Delta = 0^{\circ}$.

Figure 19.- Continued.

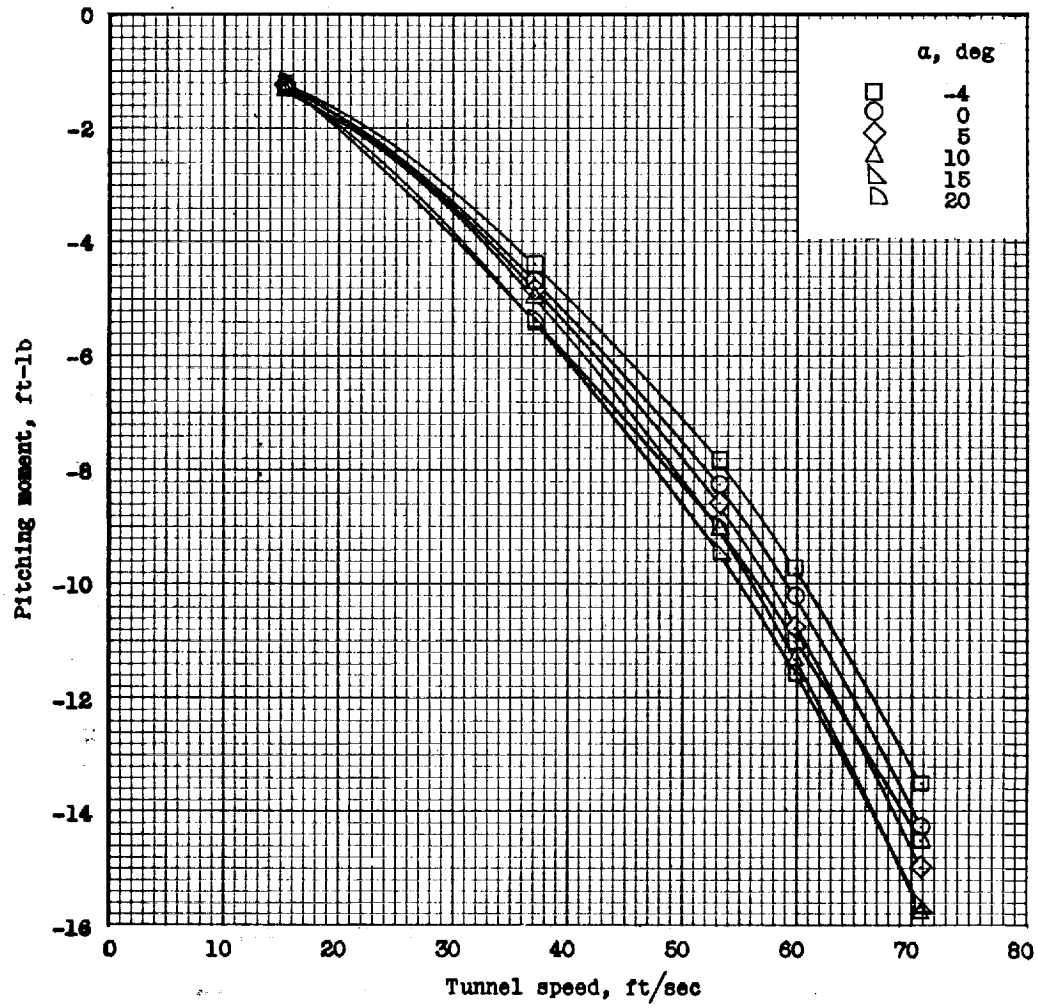

(a) Concluded. $\Delta = 0^{o}$.

Figure 19.- Continued.

[redacted]

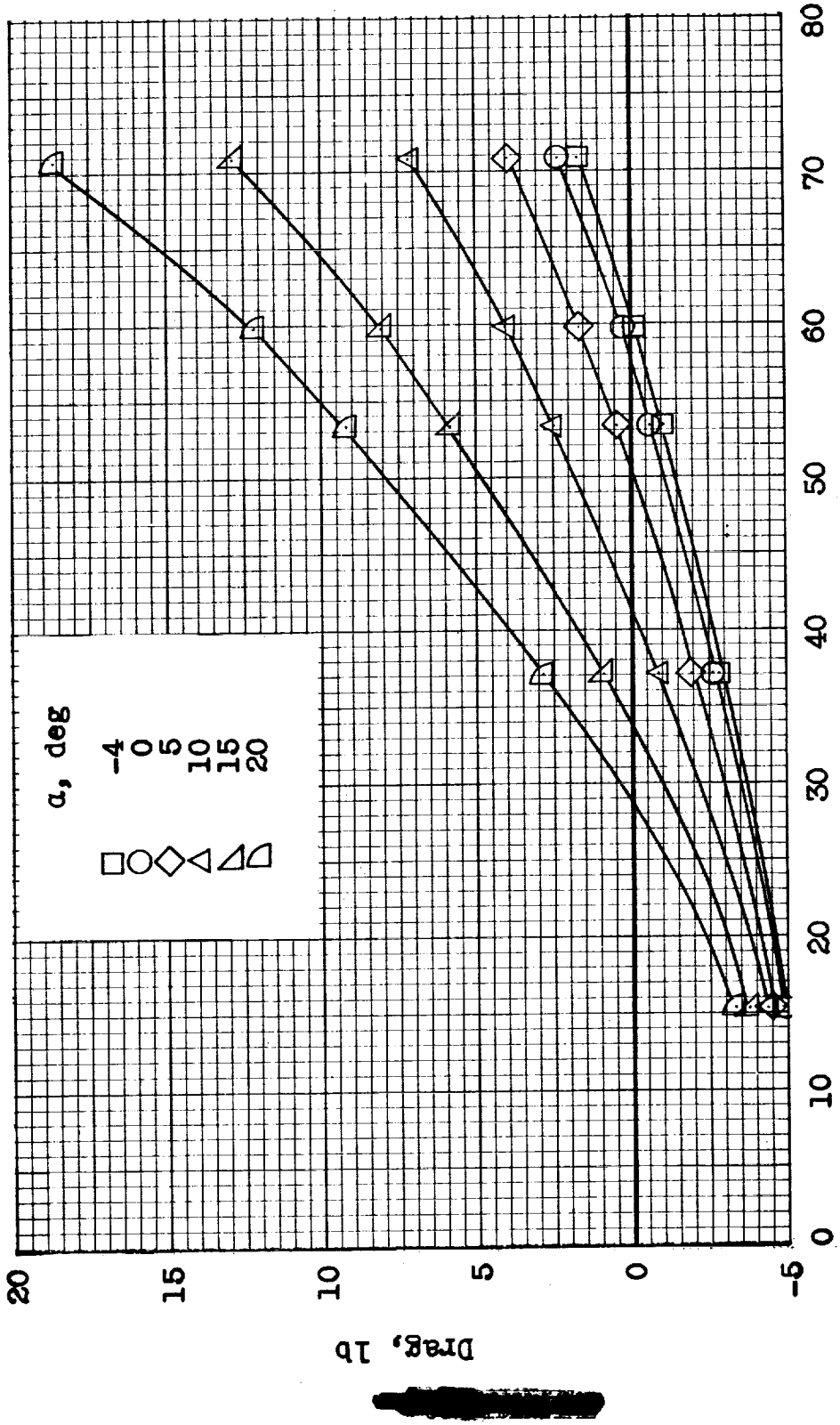

(b) $\Delta = 30°$.

Figure 19.- Continued.

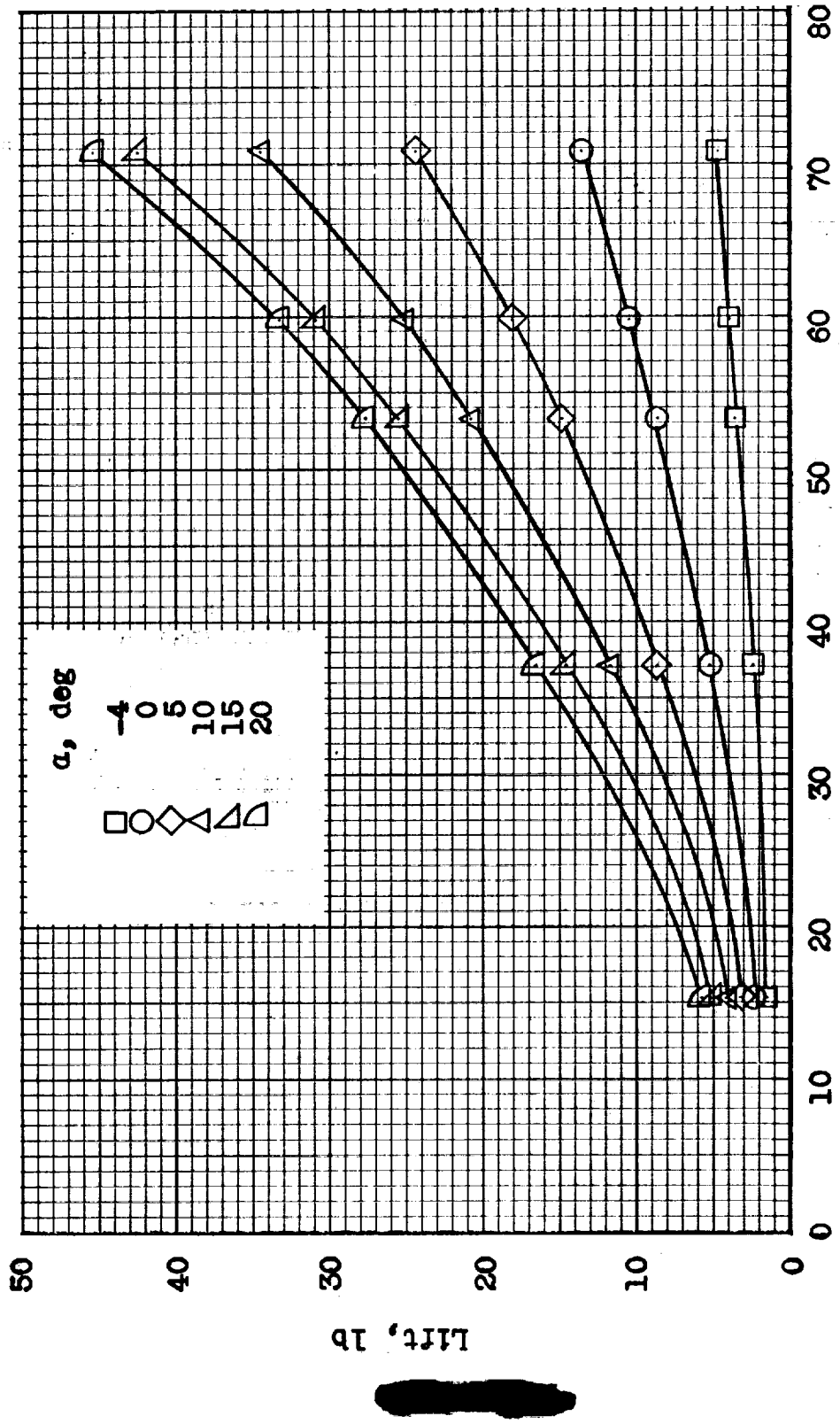

(b) Continued. $\Delta = 30^{\circ}$.

Figure 19.- Continued.

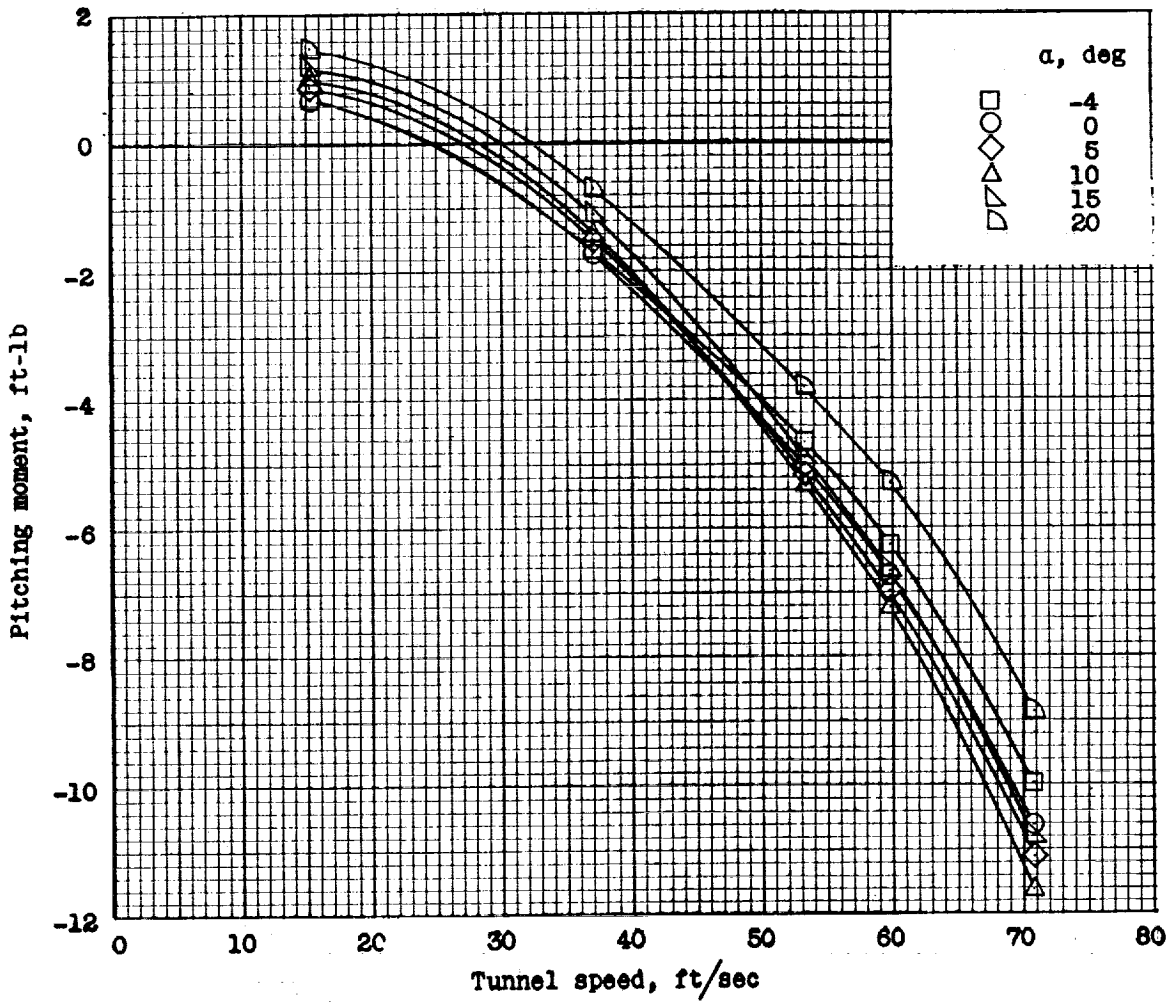

(b) Concluded. $\Delta = 30^{\circ}$.

Figure 19.- Continued.

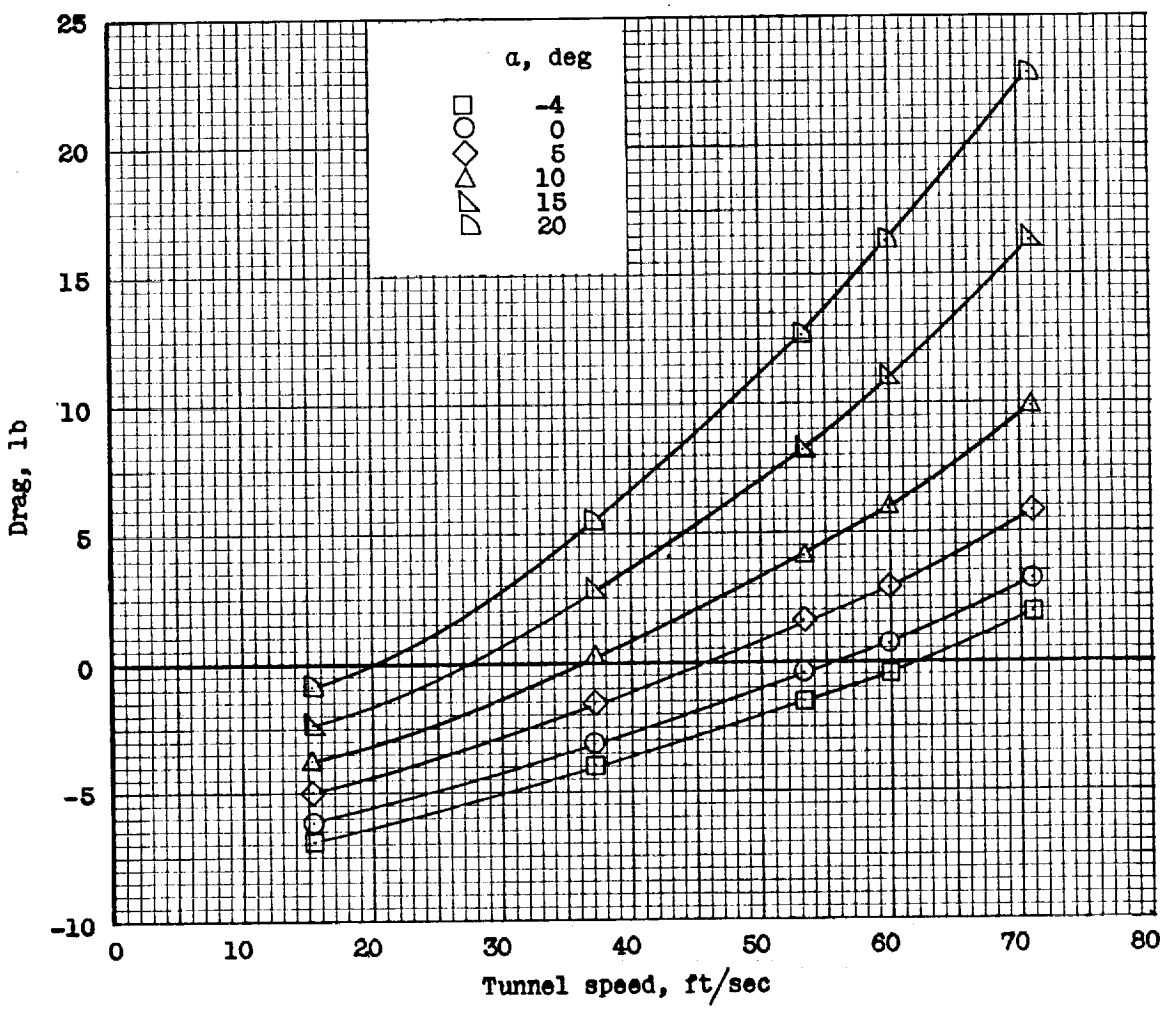

(c) $\Delta = 60^{\circ}$.

Figure 19.- Continued.

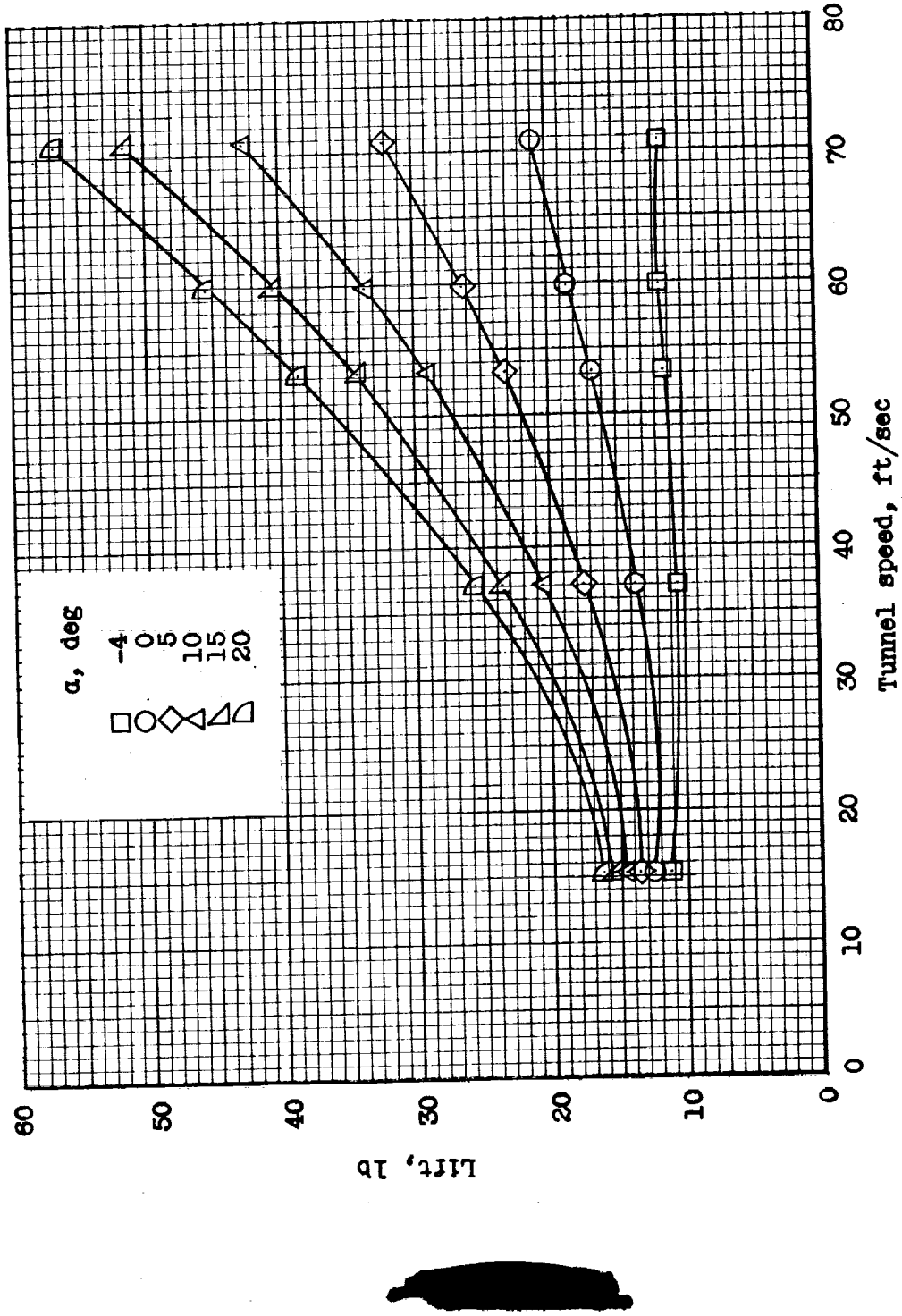

(c) Continued. $\Delta = 60^{\circ}$.

Figure 19.- Continued.

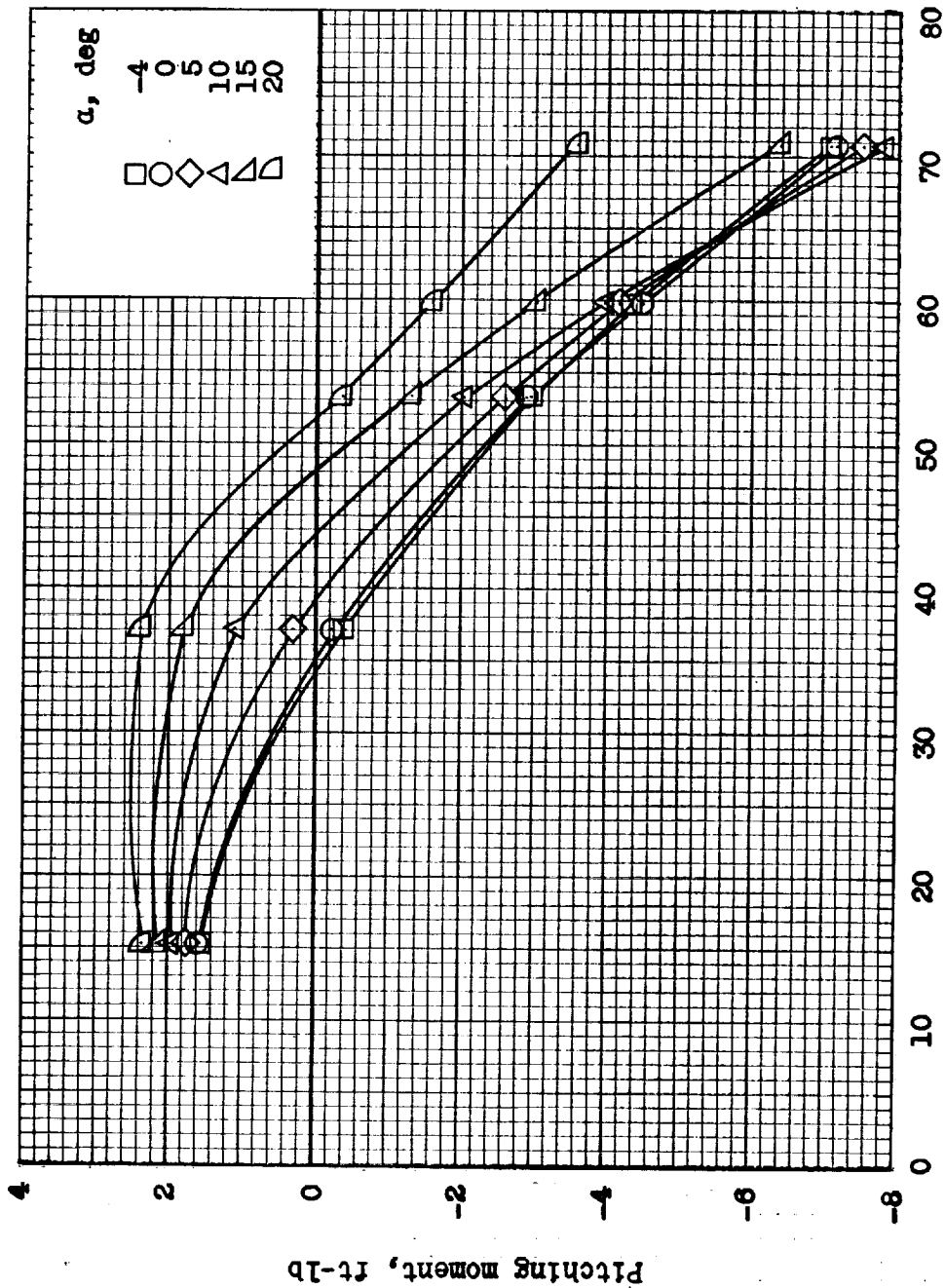

(c) Concluded. $\Delta = 60^{\circ}$.

Figure 19.- Concluded.

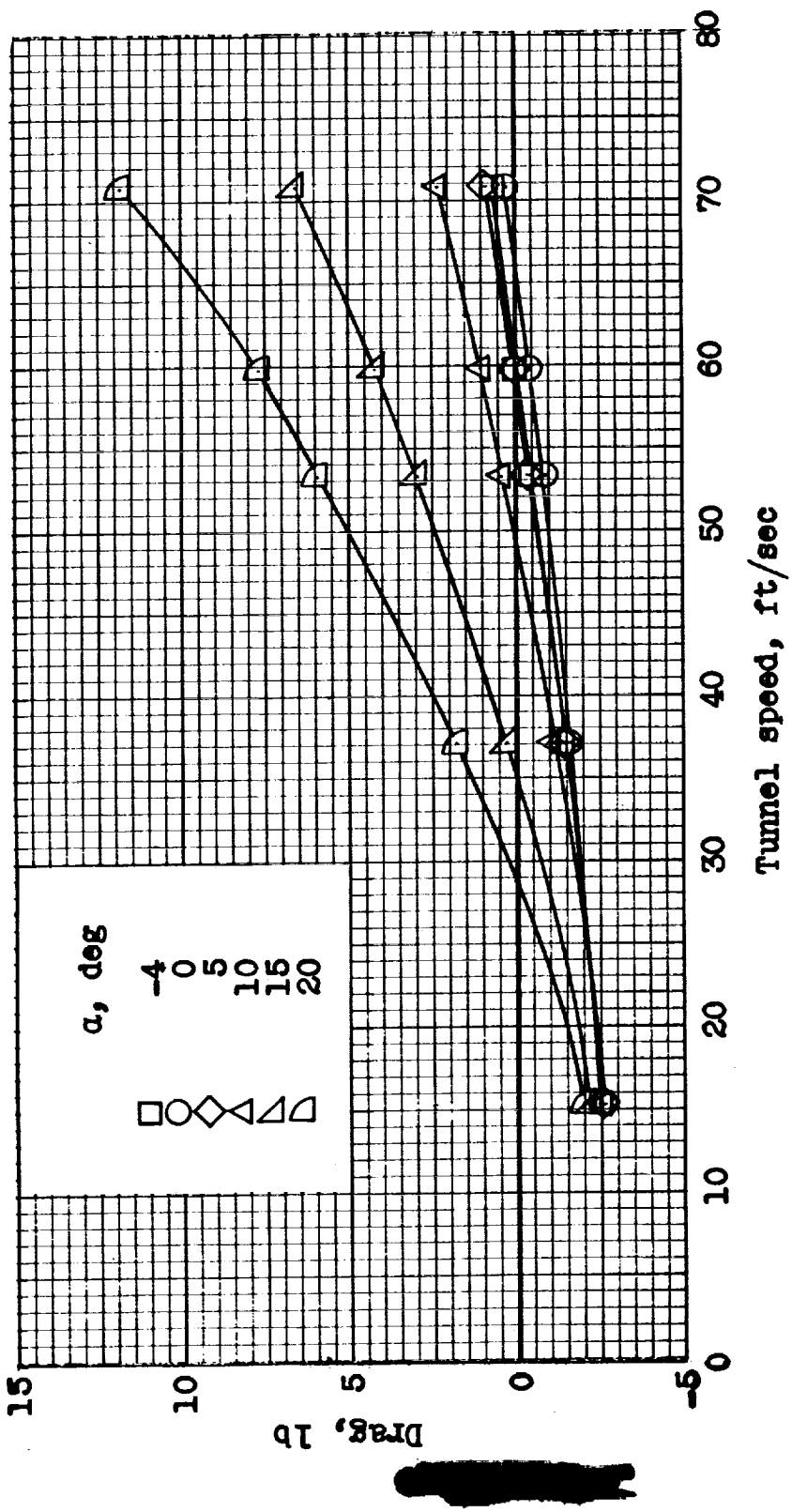

(a) $\Delta = 0^{\circ}$.

Figure 20.- Longitudinal force-test data for the model with a horizontal tail mounted low on the fuselage as suggested by the manufacturer. Referred to the wind axes. $i_t = 0^{\circ}$; $\delta_f = 0^{\circ}$.

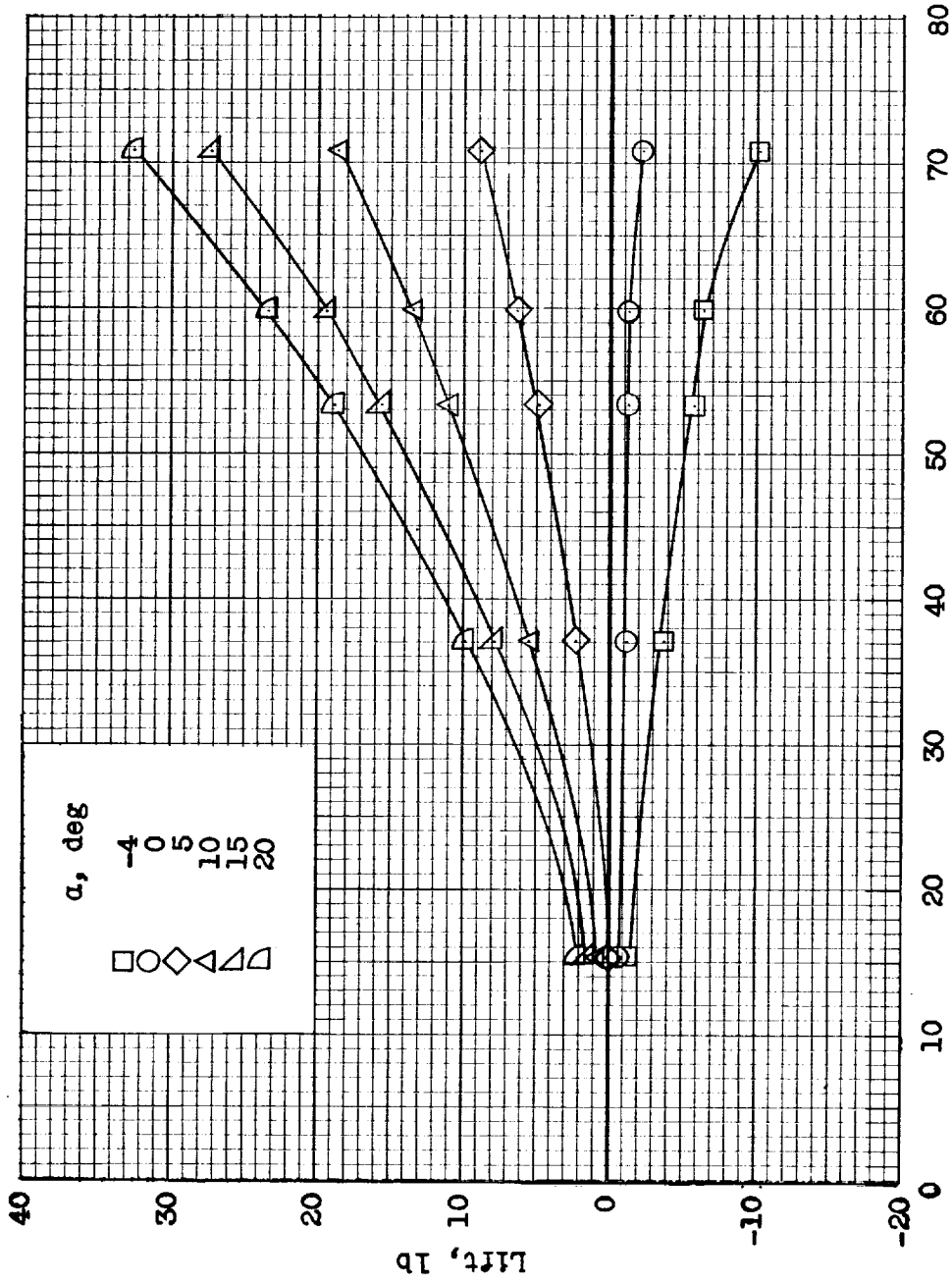

(a) Continued. $\Delta = 0^{\circ}$.

Figure 20.- Continued.

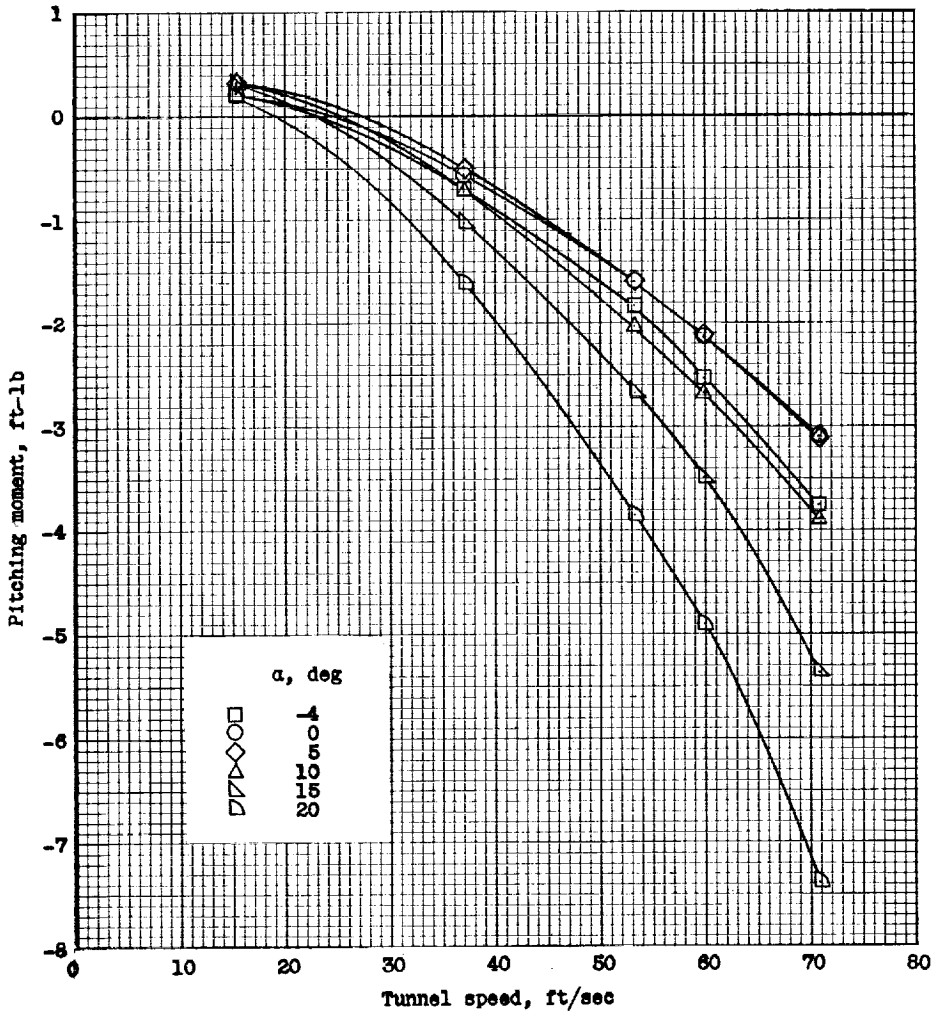

(a) Concluded. $\Delta = 0^{o}$.

Figure 20.- Continued.

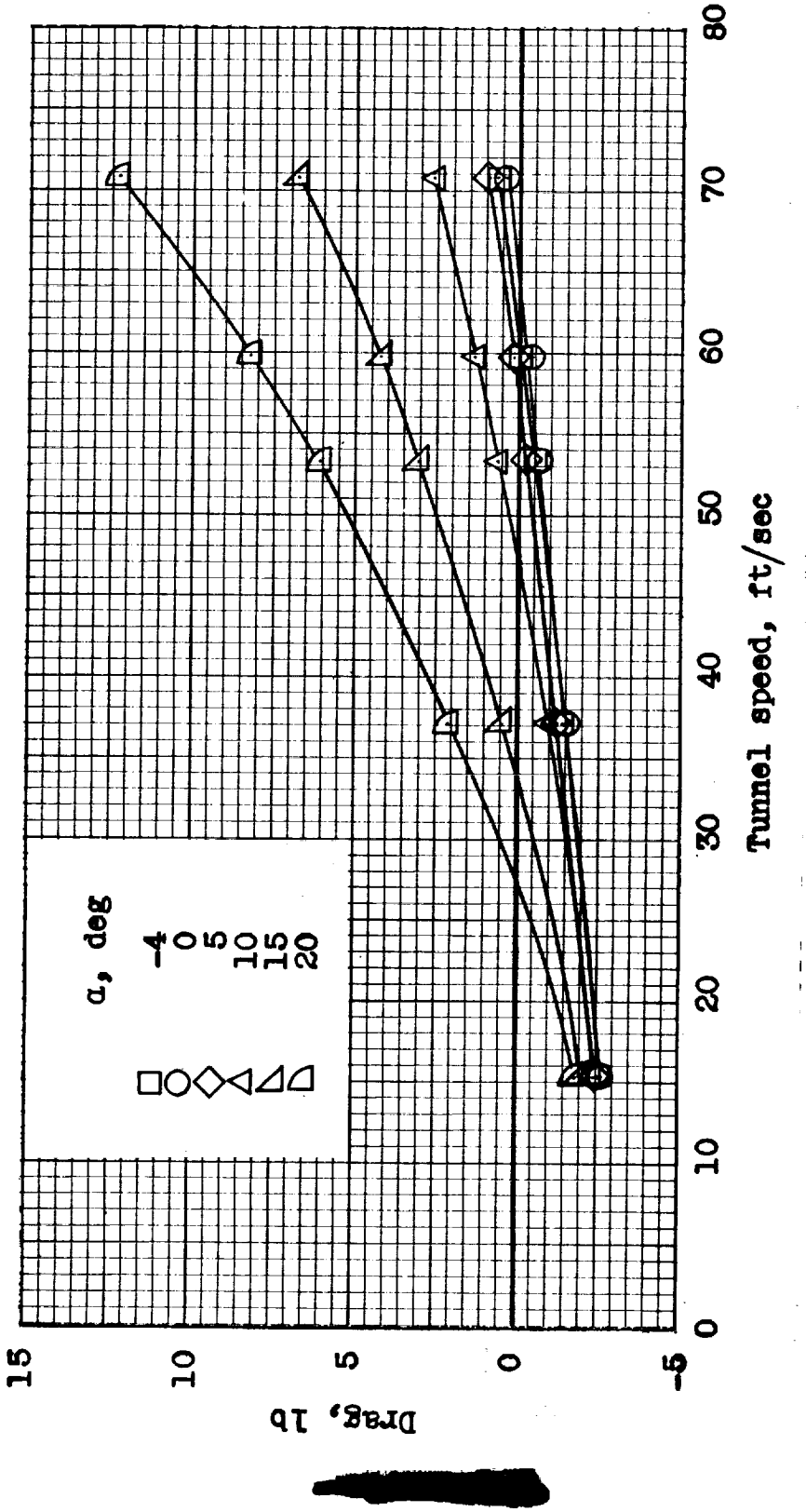

(b) $\Delta = 15^{\circ}$.

Figure 20.- Continued.

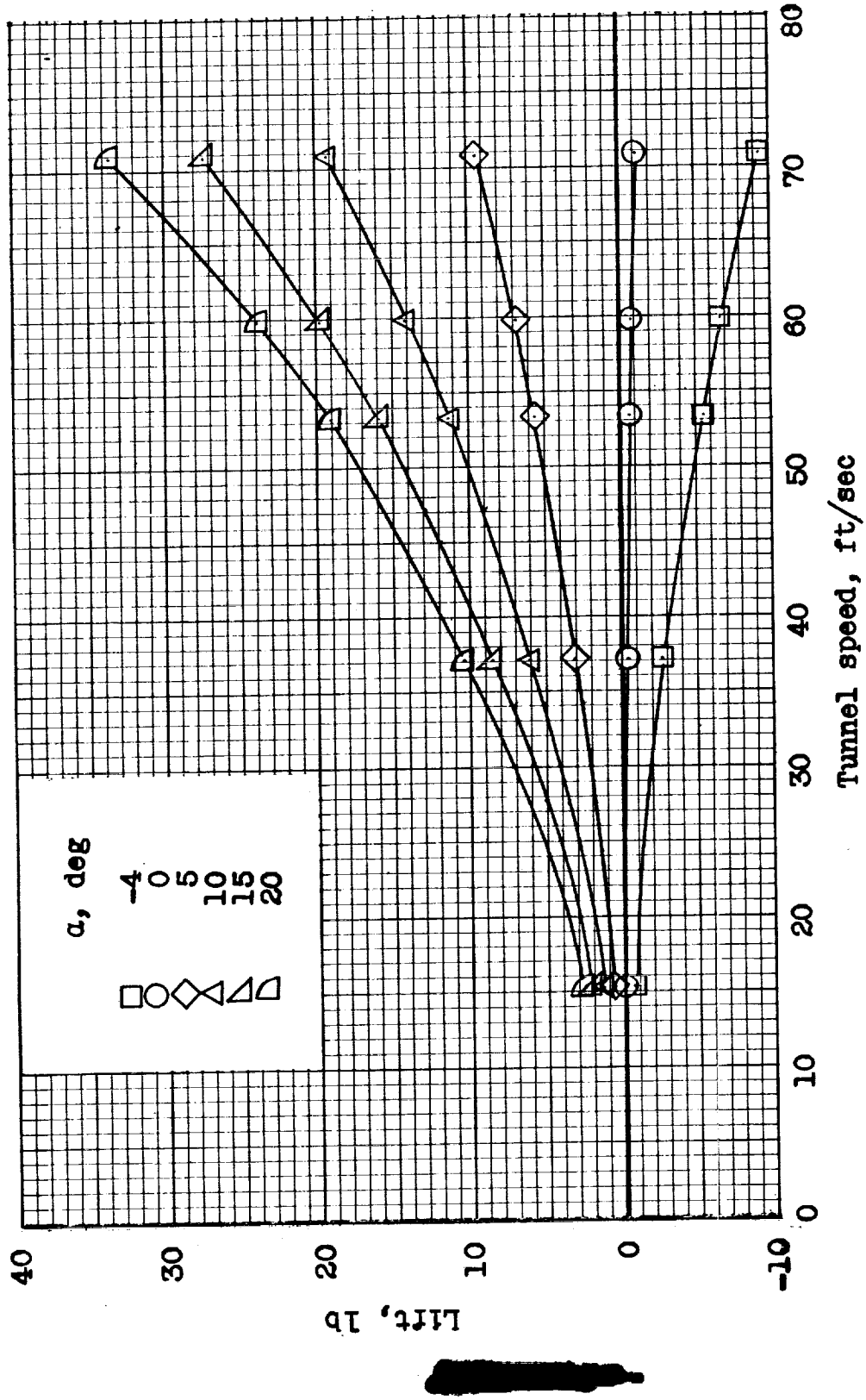

(b) Continued. $\Delta = 15^{\circ}$.

Figure 20.- Continued.

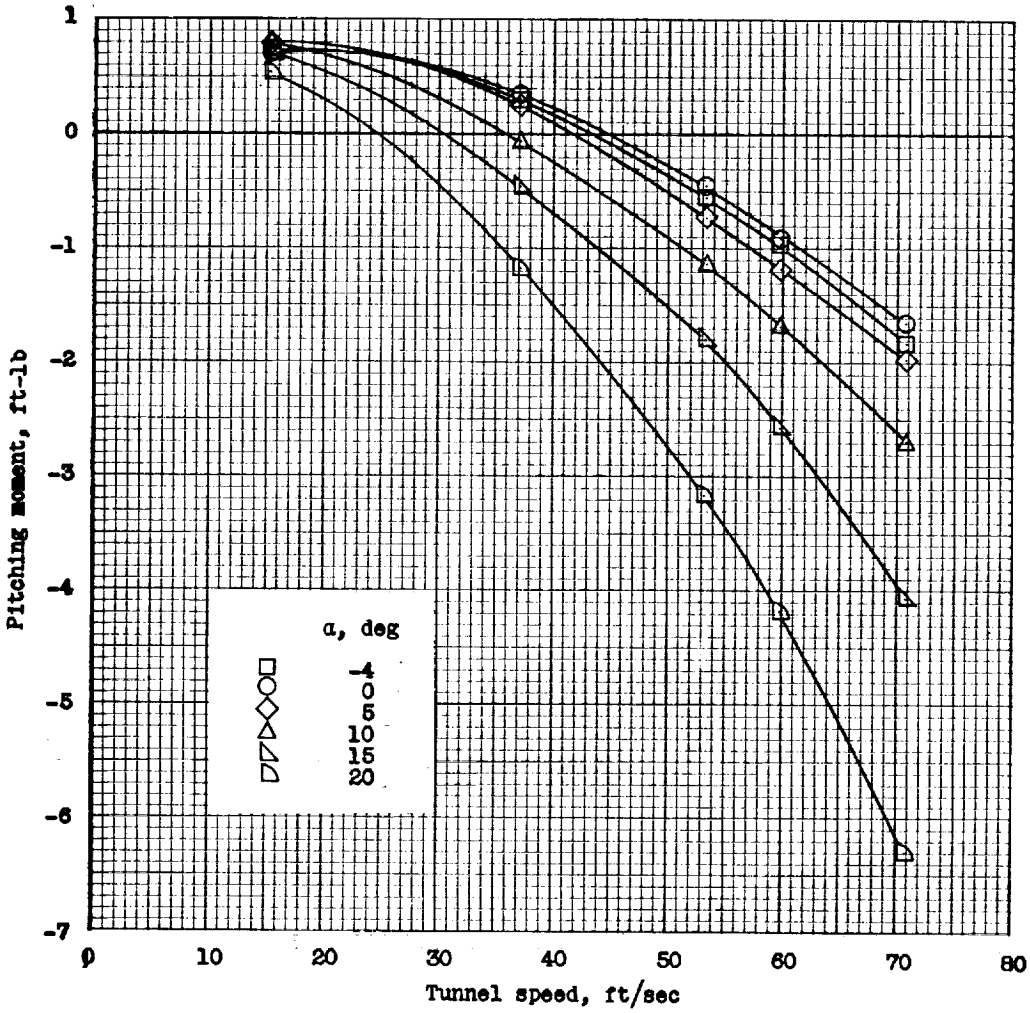

(b) Concluded. $\Delta = 15^{\circ}$.

Figure 20. - Continued.

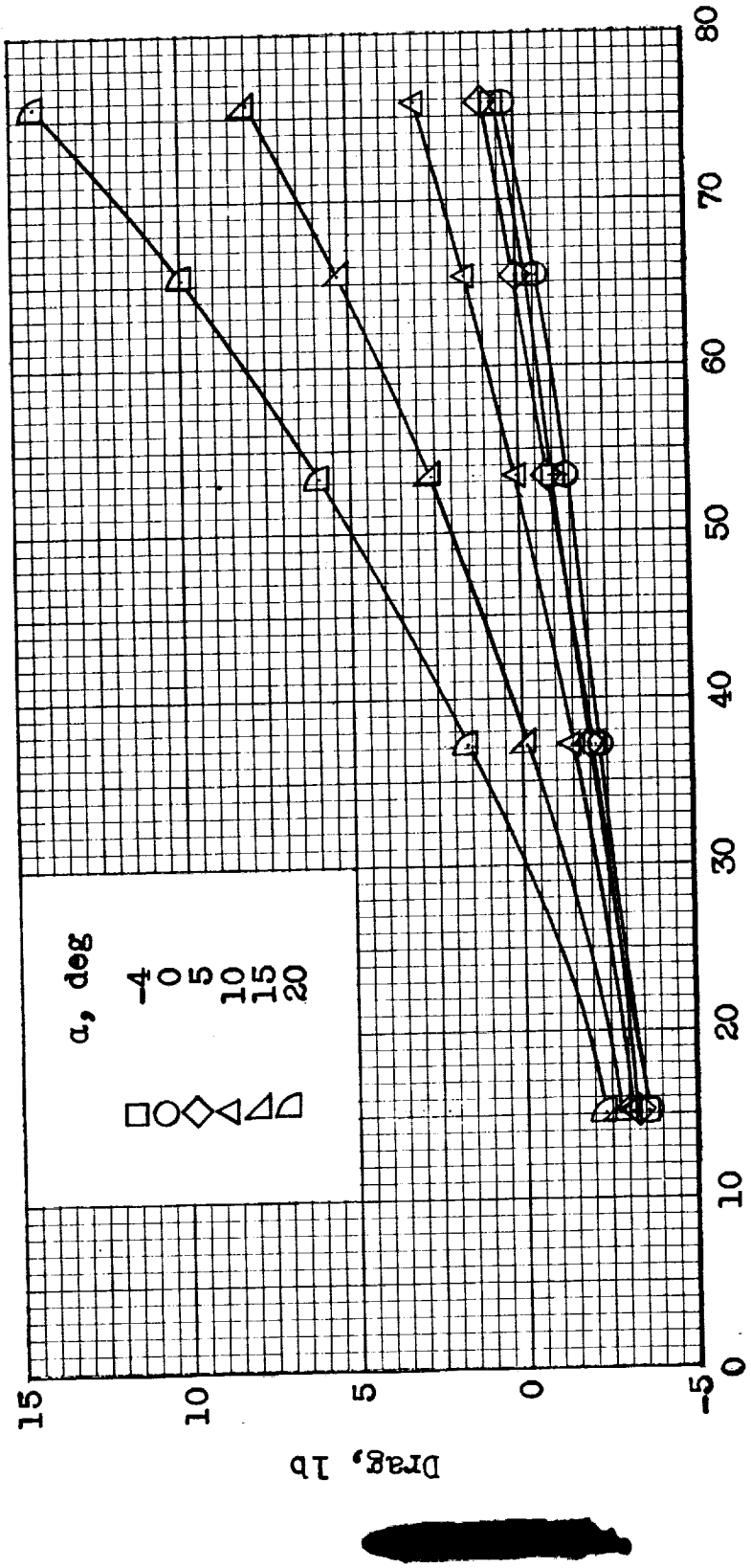

(c) $\Delta = 30^{\circ}$.

Figure 20.- Continued.

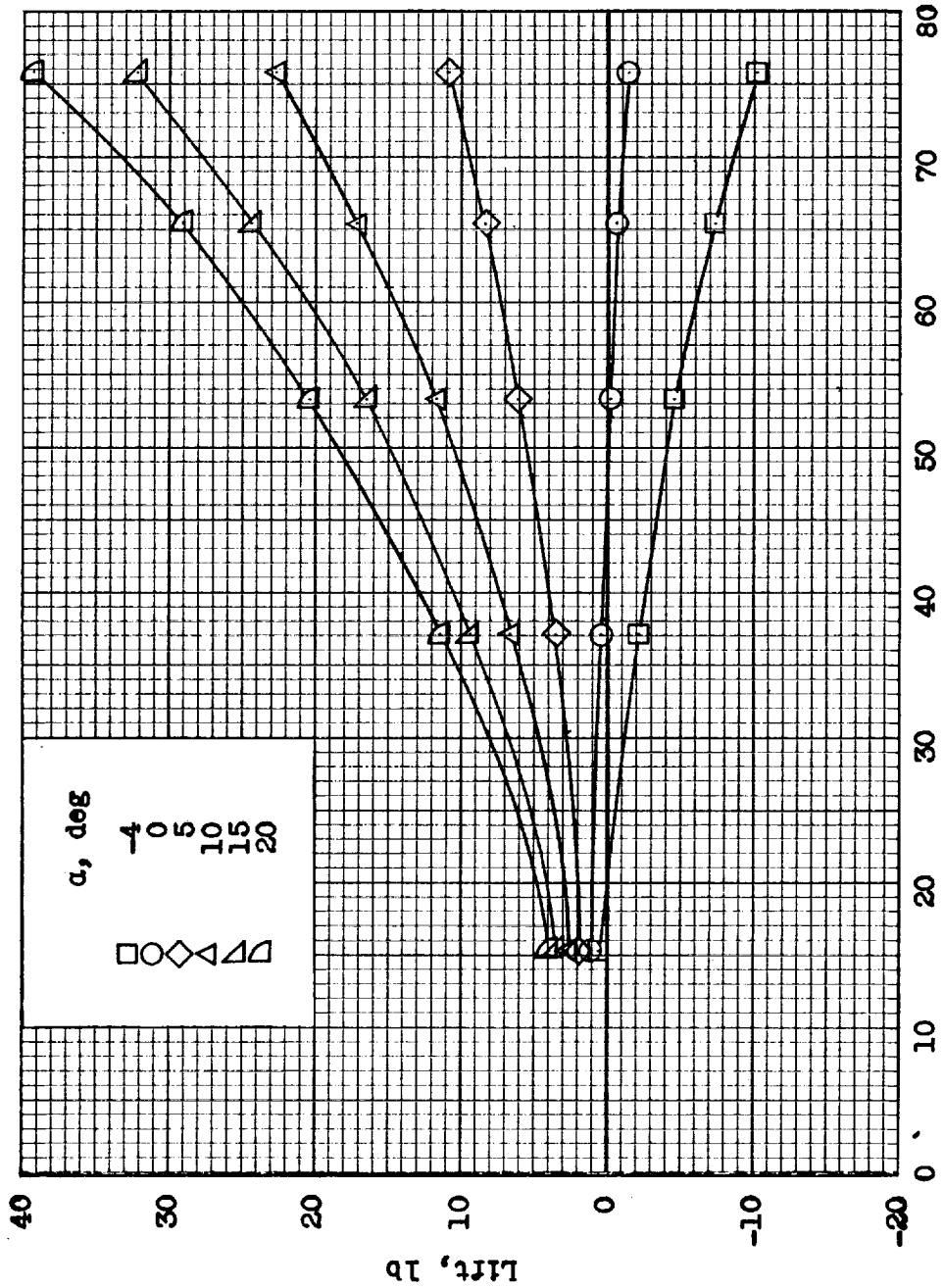

(c) Continued. $\Delta = 30^{\circ}$.

Figure 20.- Continued.

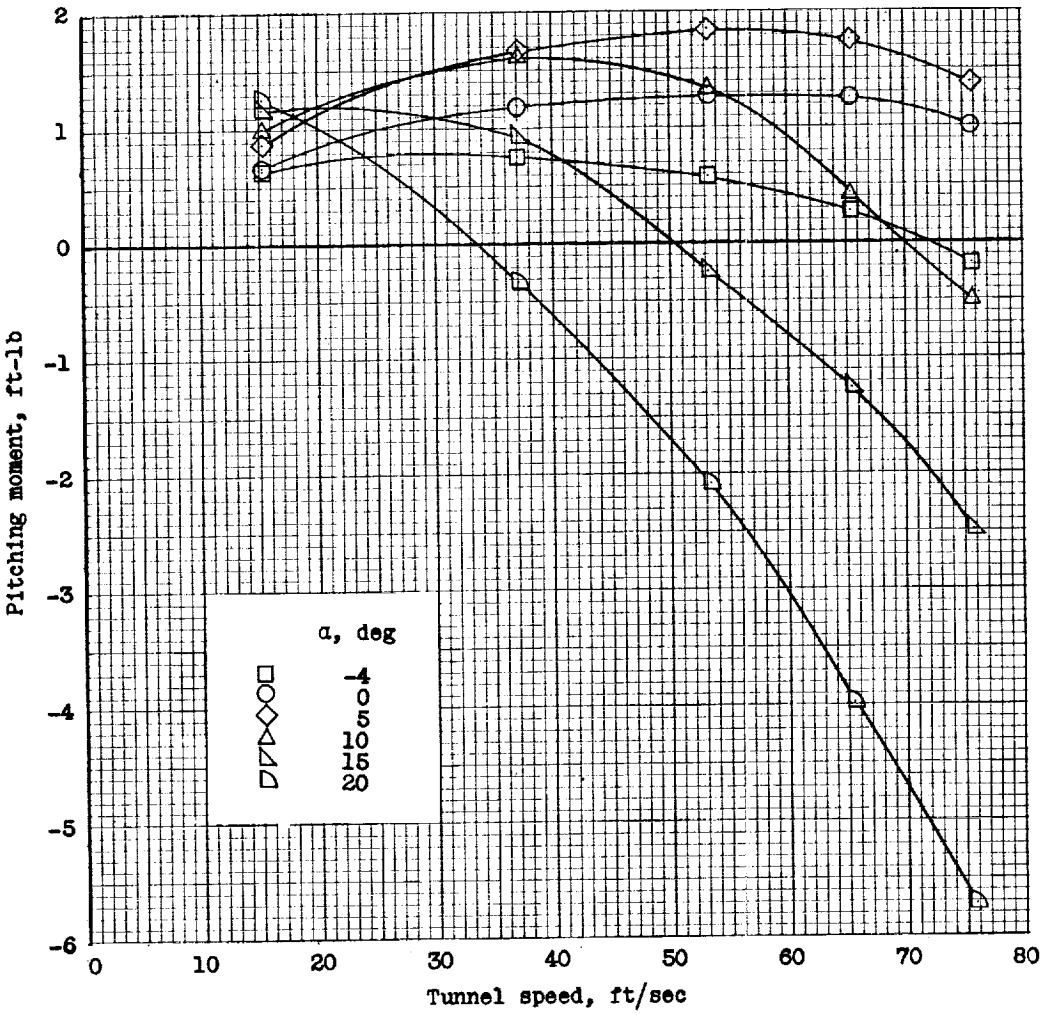

(c) Concluded. $\Delta = 30^{\circ}$.

Figure 20. - Continued.

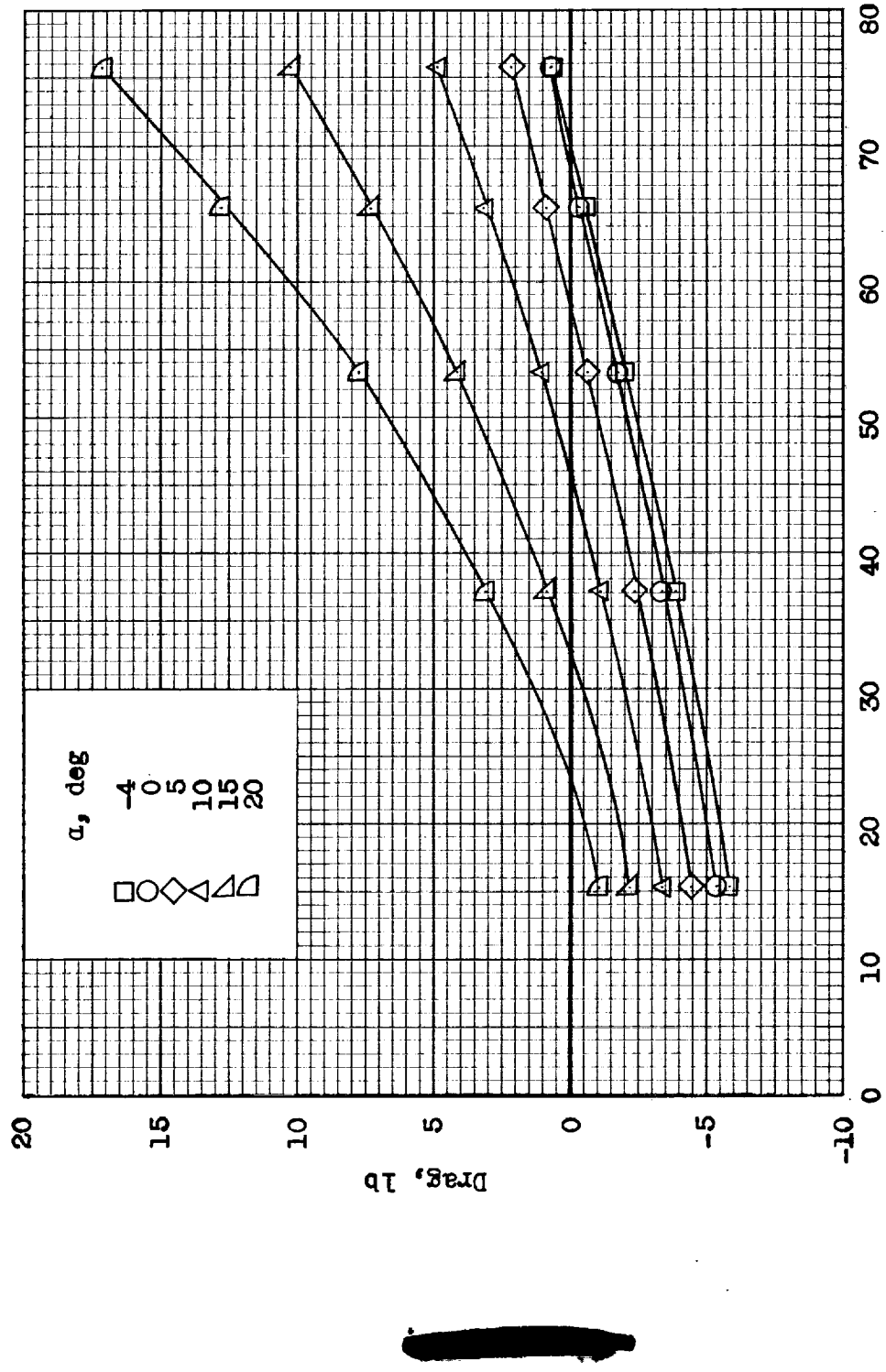

(d) $\Delta = 60^{\circ}$.

Figure 20. - Continued.

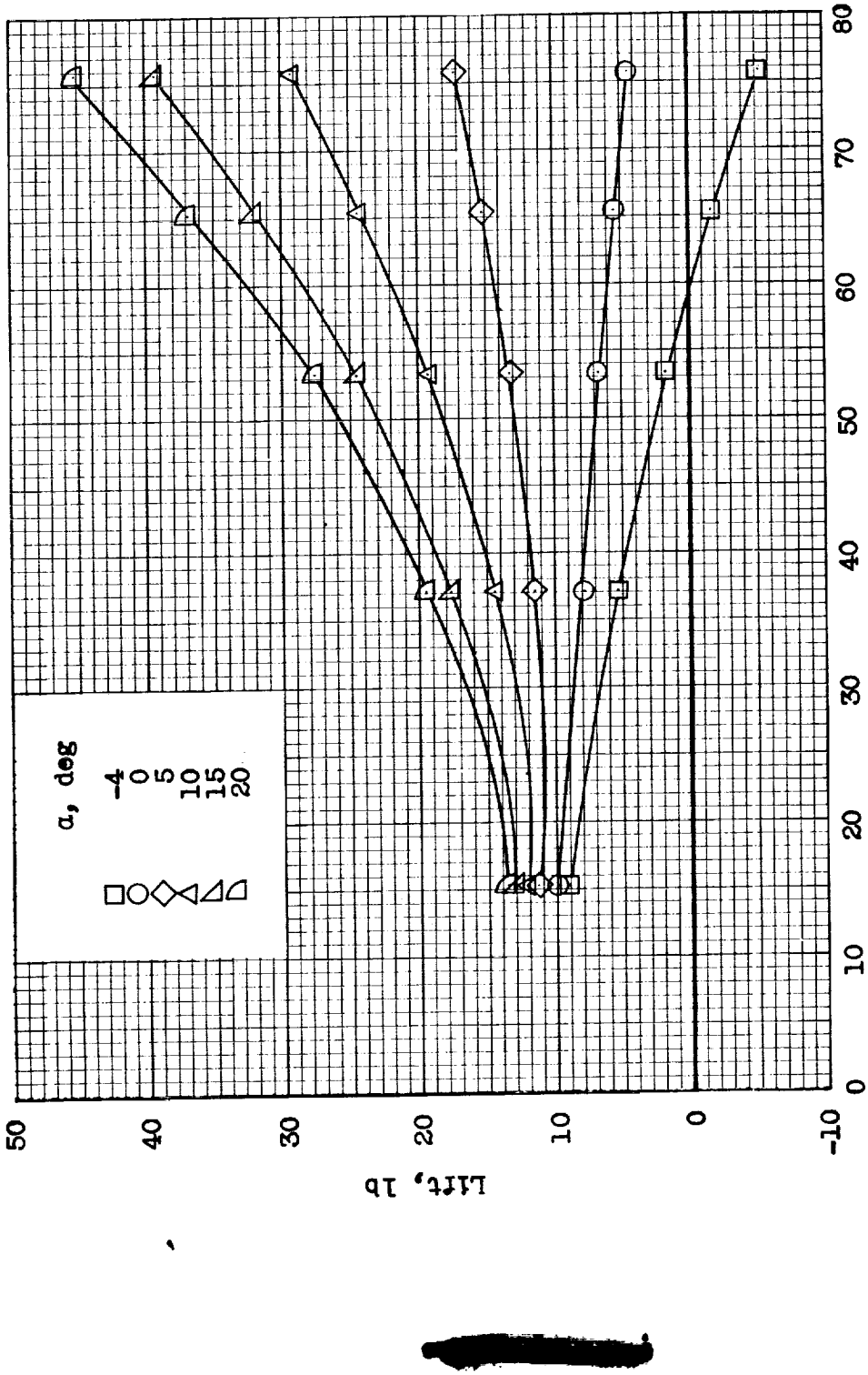

(d) Continued. $\Delta = 60^{\circ}$.

Figure 20.- Continued.

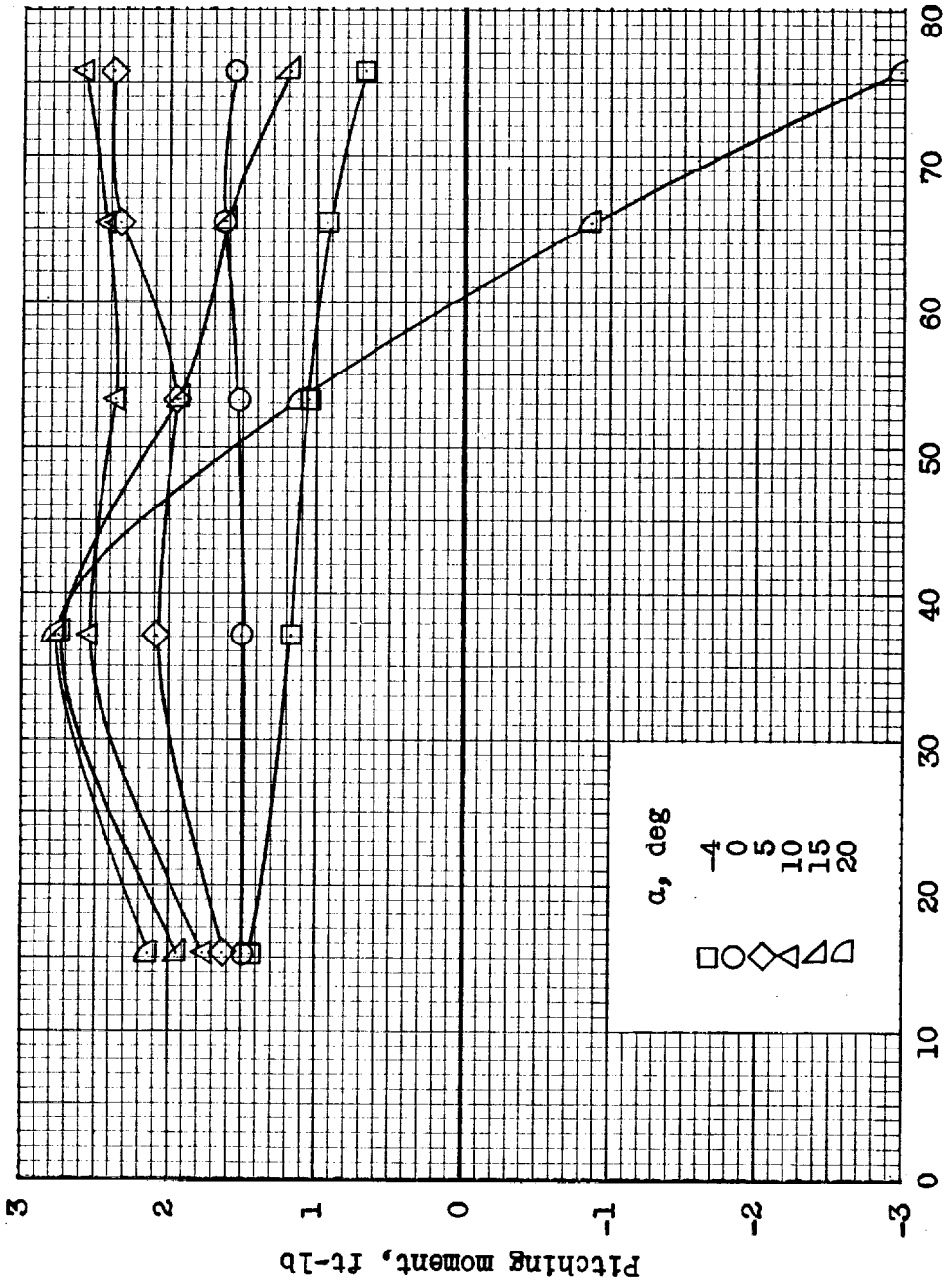

(d) Concluded. $\Delta = 60^{\circ}$.

Figure 20.- Concluded.

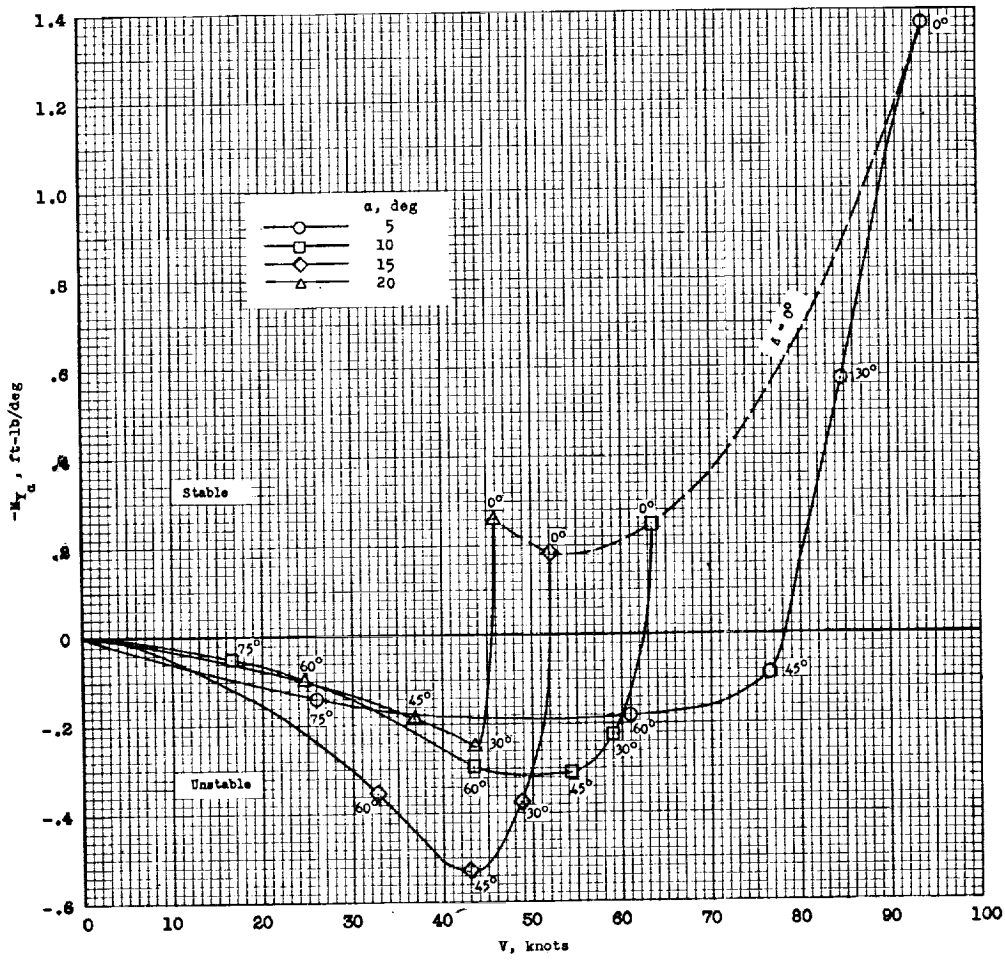

(a) $\delta_f = 0^\circ$.

Figure 21.- Variation of the static longitudinal stability of the model in transition flight. Data scaled to correspond to a model weight of 41 pounds. Referred to the wind axes.

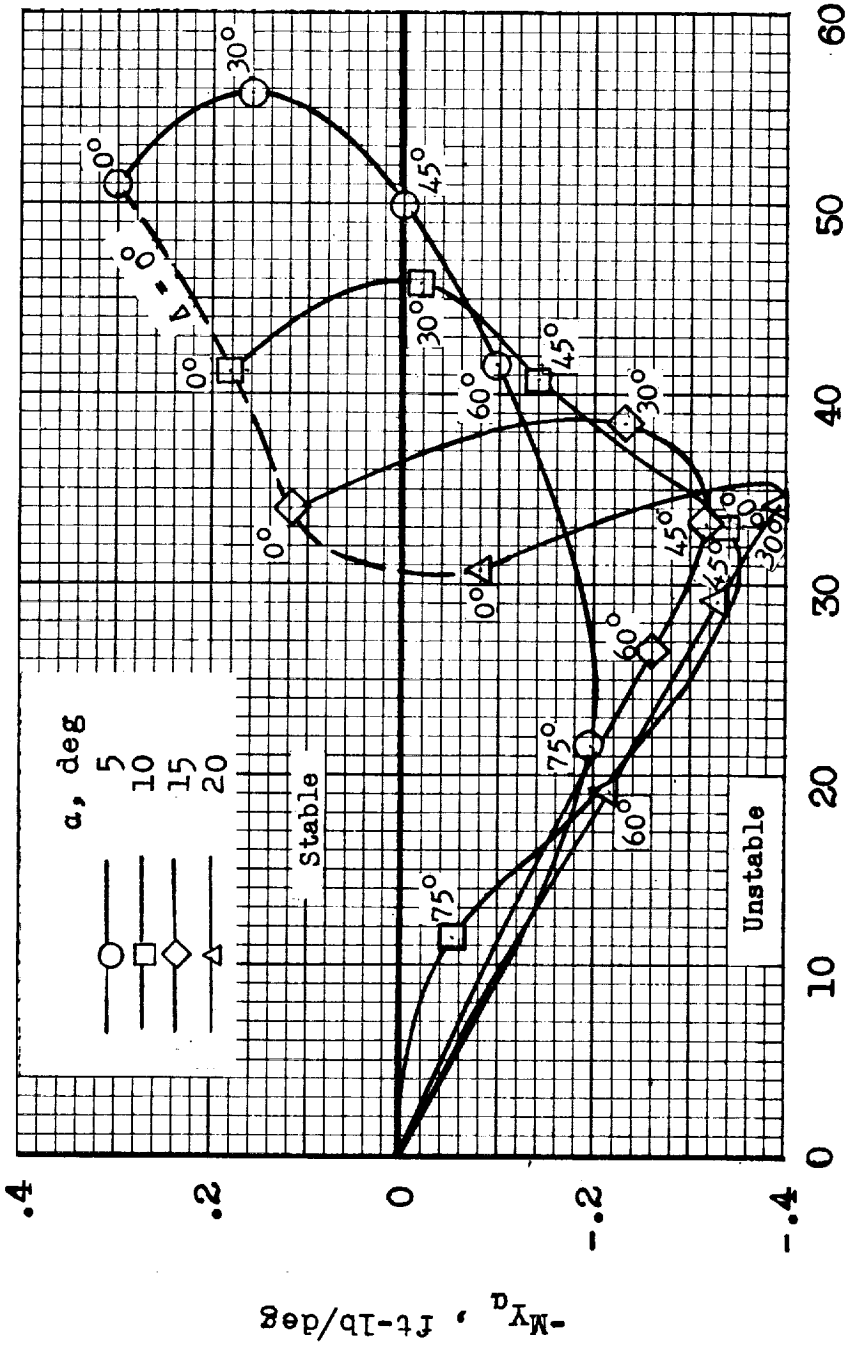

(b) $\delta_f = 50°$.

Figure 21.- Continued.

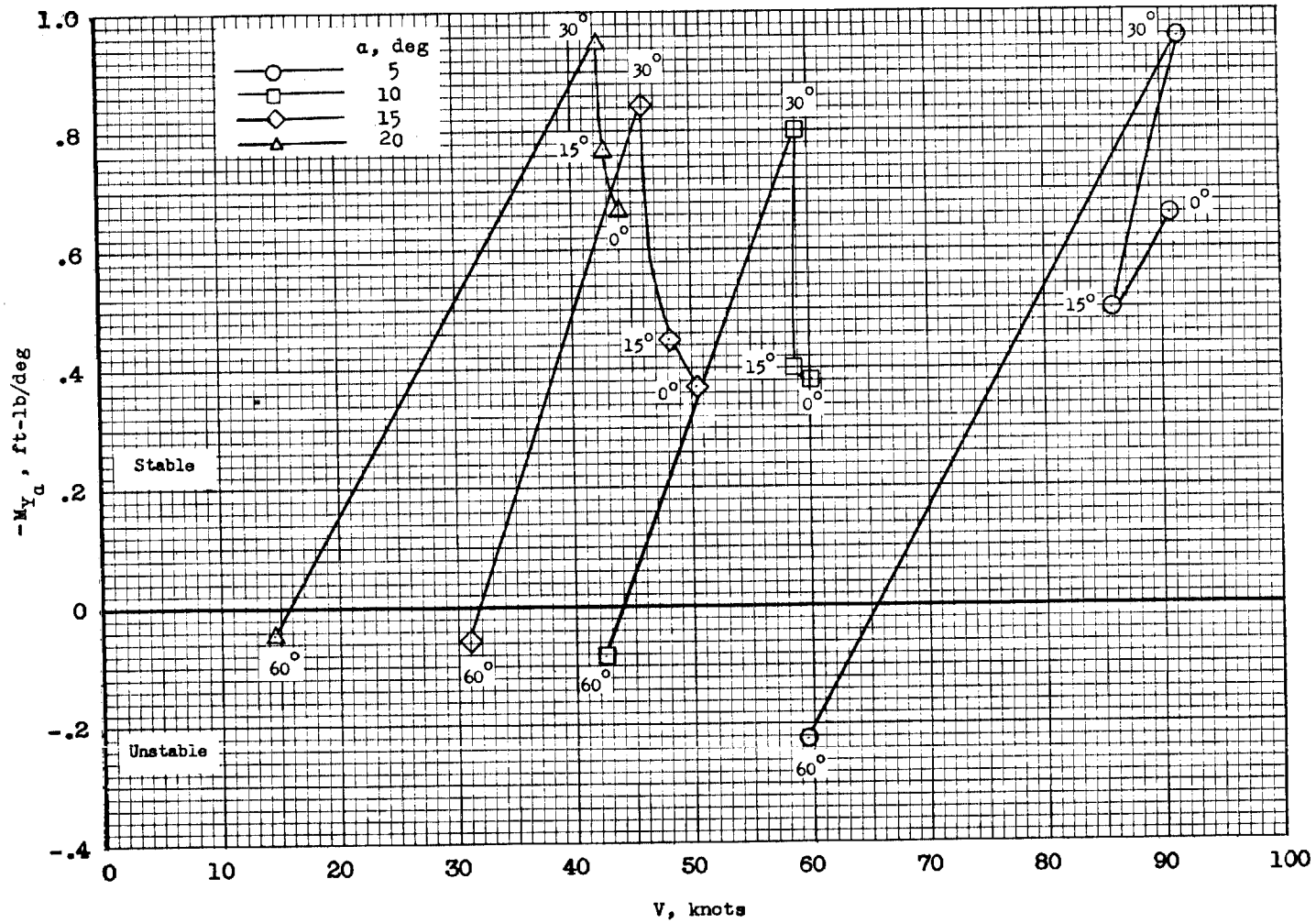

(c) Low horizontal tail, $\delta_f = 0^o$.

Figure 21.- Concluded.

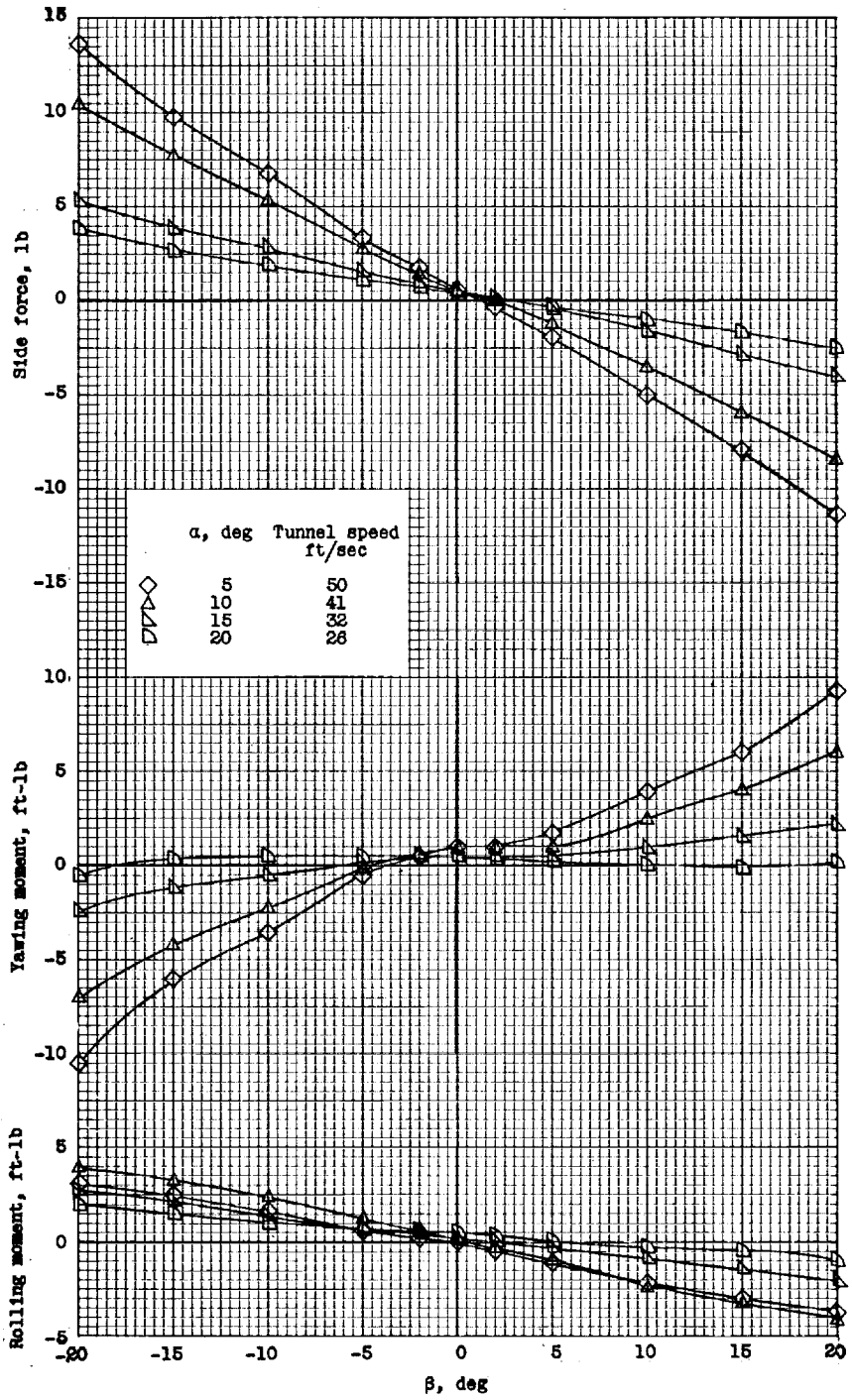

(a) $\Delta = 0^{\circ}$; $\delta_f = 0^{\circ}$.

Figure 22.- Basic lateral data. Referred to the body axes. $i_t = 0^{\circ}$.

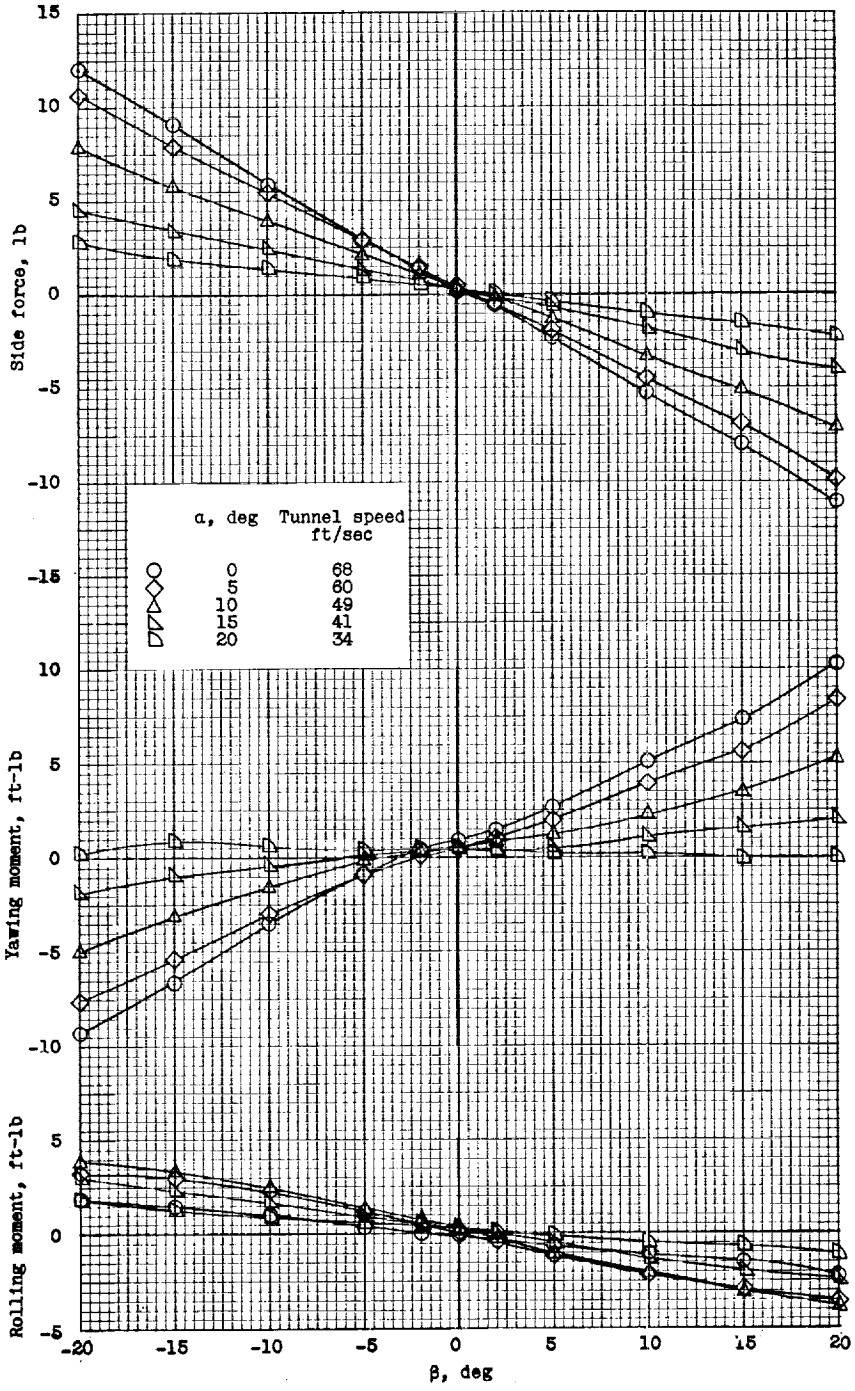

(b) $\Delta = 30^{\circ}$; $\delta_f = 0^{\circ}$.

Figure 22.- Continued.

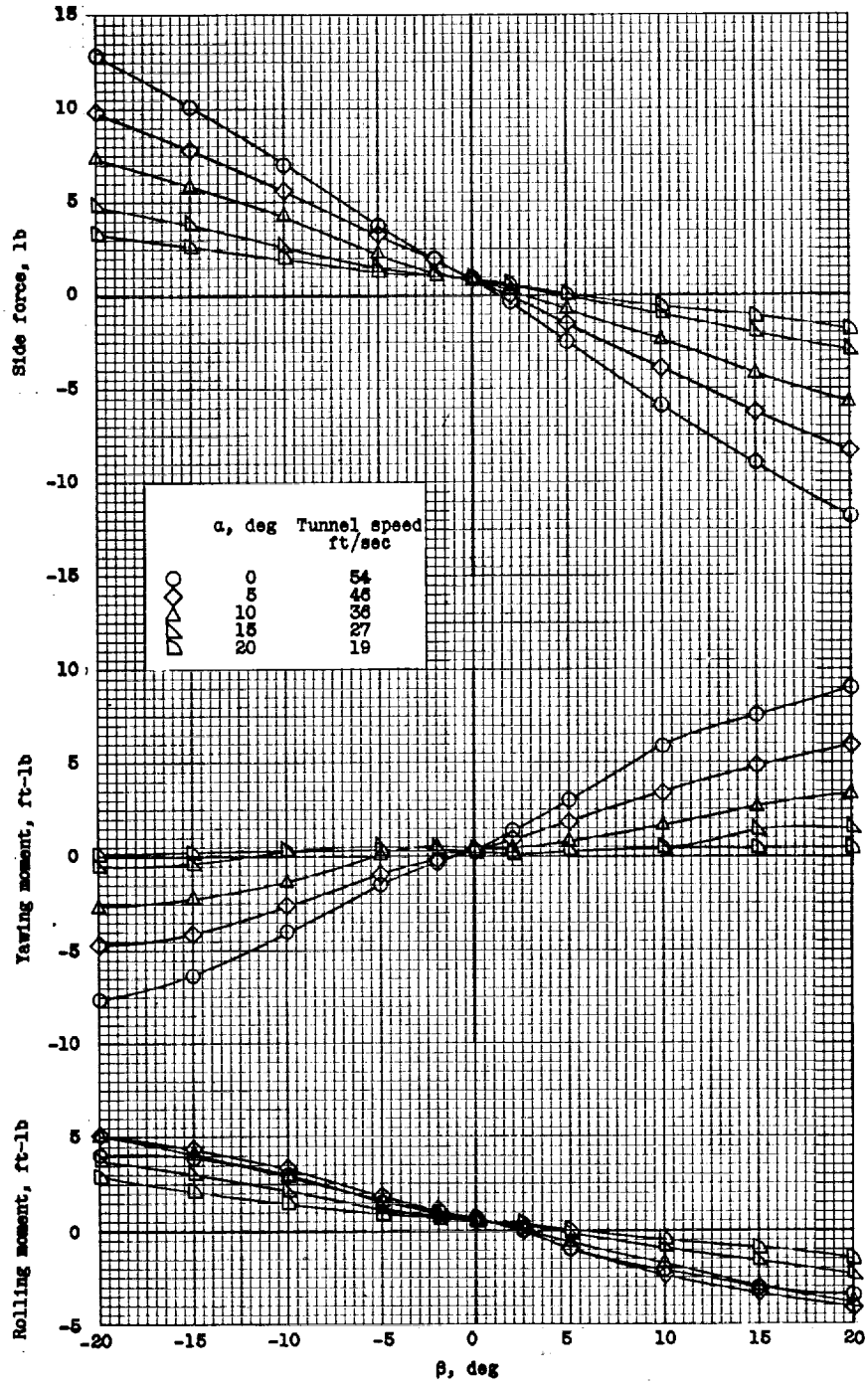

(c) $\Delta = 60^{\circ}$; $\delta_f = 0^{\circ}$.

Figure 22.- Continued.

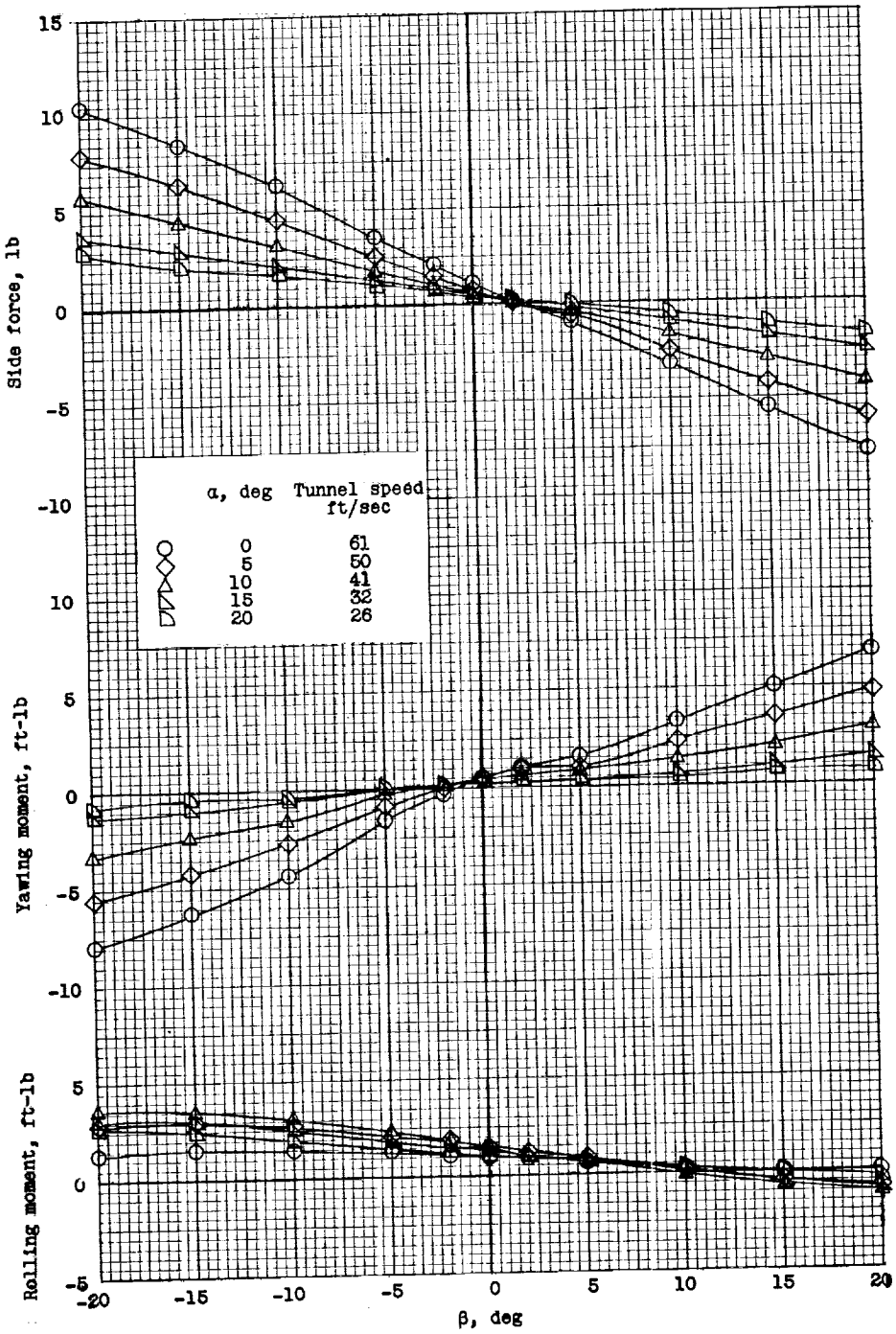

(d) $\Delta = 0^{\circ}$; $\delta_f = 50^{\circ}$.

Figure 22.- Continued.

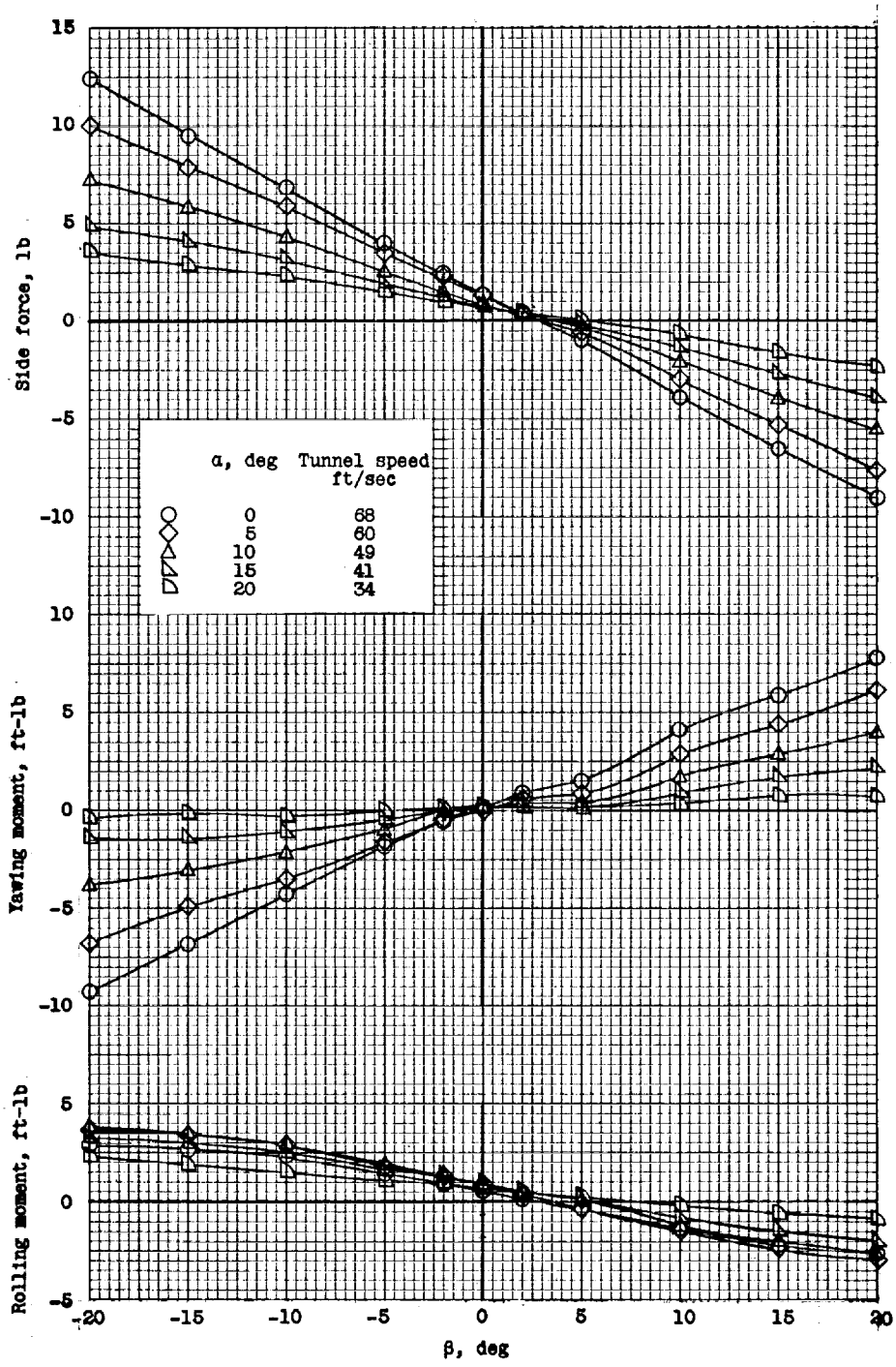

(e) $\Delta = 30^{\circ}$; $\delta_f = 50^{\circ}$.

Figure 22.- Continued.

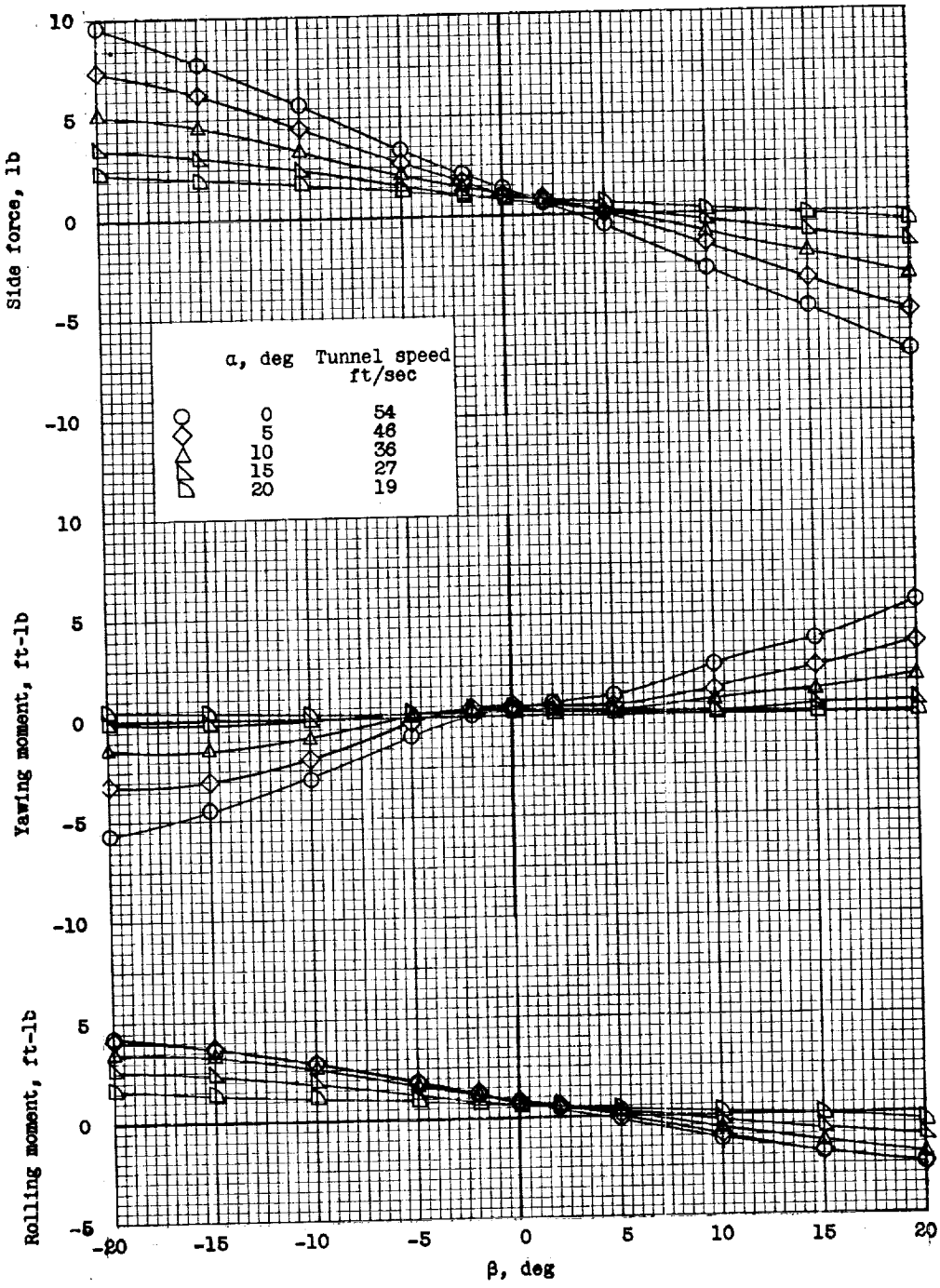

(f) $\Delta = 60^{\circ}$; $\delta_f = 50^{\circ}$.

Figure 22.- Concluded.

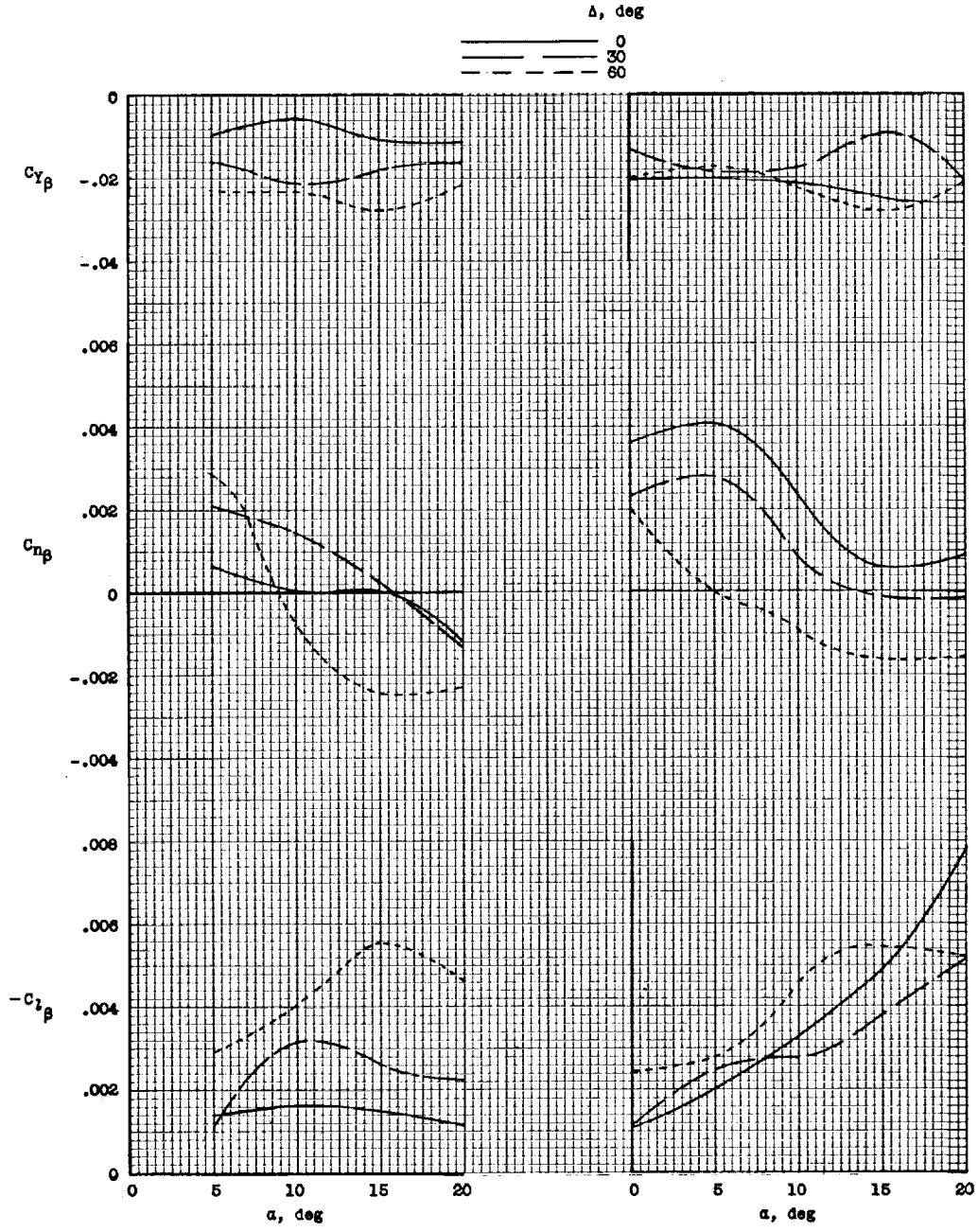

(a) $\delta_f = 0^\circ$.

(b) $\delta_f = 50^\circ$.

Figure 23.- Variation of static lateral stability derivatives with angle of attack. Data scaled to correspond to a model weight of 41 pounds. Referred to the body axes. $\beta = \pm 5^\circ$.

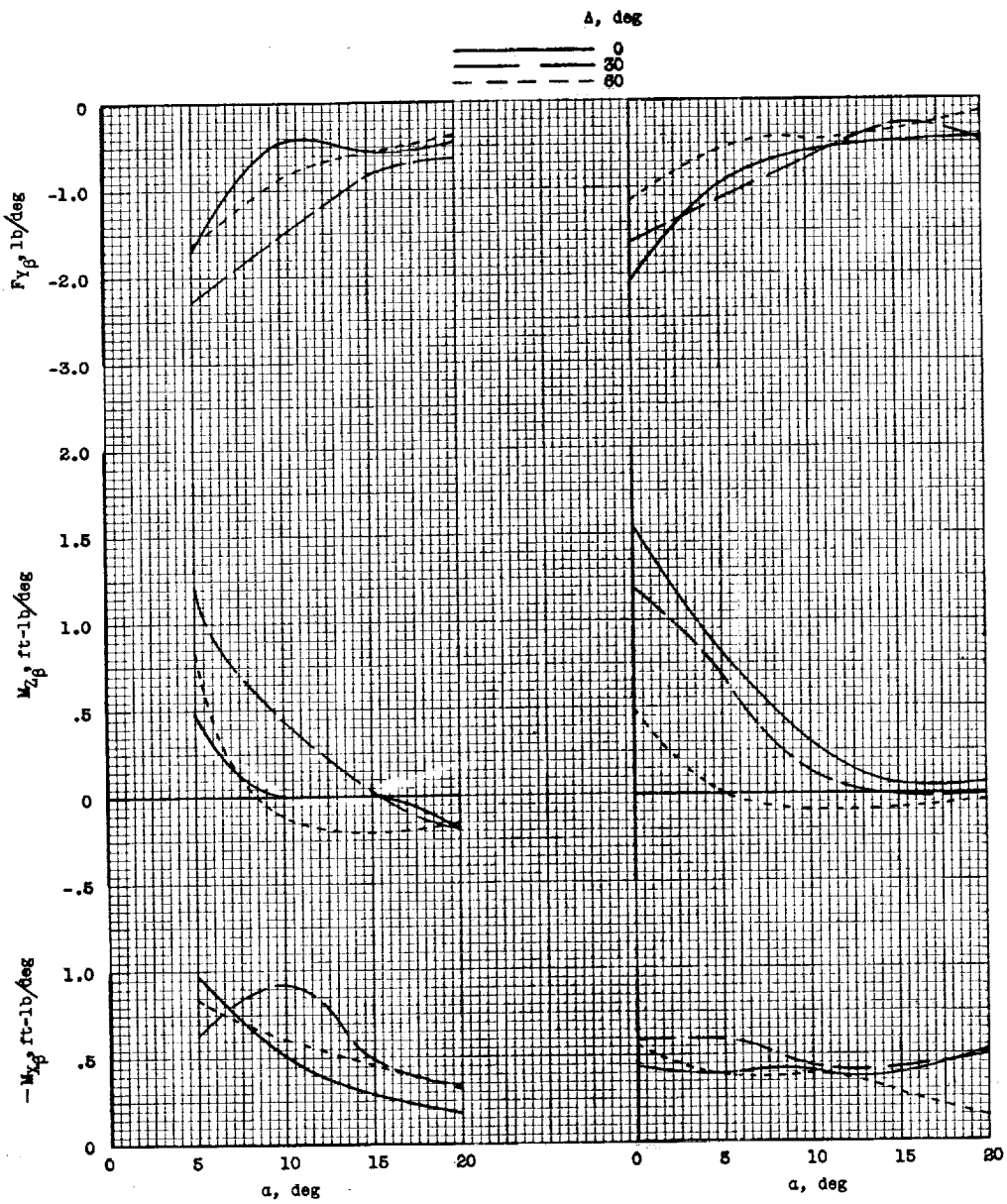

(c) $\delta_f = 0^\circ$.

(d) $\delta_f = 50^\circ$.

Figure 23.- Concluded.

[redacted]

NATIONAL AERONAUTICS AND SPACE ADMINISTRATION

TECHNICAL MEMORANDUM SX-531

for the

U.S. Air Force

FLIGHT TESTS OF A 1/6-SCALE MODEL OF THE HAWKER P 1127 JET VTOL AIRPLANE*

By Charles C. Smith, Jr.

ABSTRACT

The Hawker P 1127 airplane is a horizontal-attitude VTOL fighter with a single Bristol Siddeley BS 53 turbofan engine exhausting through four rotatable nozzles, two on each side of the fuselage, located beneath a swept wing mounted on top of the fuselage. The model could be flown successfully in hovering and transition flight although the jet-reaction roll control was somewhat weak and the model had a strong pitchup tendency in transition. Take-offs and landings (both VTOL and STOL) could be made smoothly and easily. In forward flight the model was longitudinally stable in the flaps-up condition but was neutrally stable with flaps down at the higher angles of attack.

*Title, [redacted]

[redacted]

[redacted]

[redacted]

A motion-picture film supplement, carrying the same classification as the report, is available on loan. Requests will be filled in the order received. You will be notified of the approximate date scheduled.

The film (16 mm, 15 min, B&W, silent) shows model in hovering flight, vertical take-offs and landings, transition flight, and short take-offs and landings.

Requests for the film should be addressed to the
National Aeronautics and Space Administration
Office of Technical Information and Educational Programs
Technical Information Division (Code ETV)
Washington 25, D.C.

NOTE: The handling of requests for this classified film will be expedited if application for the loan is made by the individual to whom this copy of the report was issued. In line with established policy, classified material is sent only to previously designated individuals. Your cooperation in this regard will be appreciated.

[redacted]

CUT

Date_____

Please send, on loan, copy of film supplement to NASA Technical Memorandum SX-531 (Film serial L-609)

_____

Name of organization

_____

Street number

_____

City and State

Attention *Mr._____

Title_____

(*To whom copy No. ___ of the Technical Memorandu was issued)

[redacted]

[redacted]

Place Stamp Here

National Aeronautics and Space Administration
Office of Technical Information and Educational Programs
Technical Information Division (Code ETV)
Washington 25, D.C.